Proceedings of the

SYMPOSIUM ON RECENT ADVANCES IN GEOTECHNICAL CENTRIFUGE MODELING

A symposium on Recent Advances in Geotechnical Centrifuge Modeling was held on July 18-20, 1984 at the University of California at Davis. The symposium was sponsored by the National Science Foundation's Geotechnical Engineering Program and the Center for Geotechnical Modeling at the University of California at Davis.

The symposium offered an opportunity for a meeting of the International Committee on Centrifuges of the International Society for Soil Mechanics and Foundation Engineering. The U.S. participants also met to discuss the advancement of the centrifuge modeling technique in the U.S. A request is being transmitted to the American Society of Civil Engineers to establish a subcommittee on centrifuges within the Geotechnical Engineering Division.

Proceedings of the

SYMPOSIUM ON RECENT ADVANCES IN GEOTECHNICAL CENTRIFUGE MODELING

A symposium on Recent Advances in Geotechnical Centrifuge Modeling was held on July 18-20, 1984 at the University of California at Davis. The symposium was sponsored by the National Science Foundation's Geotechnical Engineering Program and the Center for Geotechnical Modeling at the University of California at Davis.

The symposium offered an opportunity for a meeting of the International Committee on Centrifuges of the International Society for Soil Mechanics and Foundation Engineering. The U.S. participants also met to discuss the advancement of the centrifuge modeling technique in the U.S. A request is being transmitted to the American Society of Civil Engineers to establish a subcommittee on centrifuges within the Geotechnical Engineering Division.

TABLE OF CONTENTS

AMERICAN LITERATURE ON GEOTECHNICAL CENTRIFUGE MODELING 1931 - 1984

The earliest references in the American literature to centrifuge modeling were by Philip Bucky and his students at Columbia University from 1931 to 1949. The topics addressed were associated with mining engineering relating to mine roof design. Photo-elastic techniques were also introduced to the centrifuge technique at this time (Sinclair and Bucky, 1940). This work was followed by Louis Panek at the U.S. Bureau of Mines in College Park, Maryland, from 1949 to 1962. Panek was concerned with bolting systems for mine roof reinforcement.

Clark indicated awareness of the centrifuge technique in 1955 (Caudle and Clark, 1955) and developed a centrifuge at Missouri School of Mines, Rolla. A number of masters theses resulted between 1962 and 1970 that never reached technical journals or symposia (Chan, 1960 (MS); Esser, 1962 (MS); Haycocks, 1962 (MS); Gomah, 1963 (MS); Haas and Clark, 1970). Their work concerned stresses in mine openings, rock bolts, voussoir arches, photo-elastic study of slope stability, and lined and unlined cylindrical cavities. Wang et al. (1968) carried out tests utilizing photo-elastic models of rock beams.

The centrifuge technique was mentioned by Hubbert (Hubbert, 1937) in 1937. Also, mention was made of the technique by others (Caudle and Clark, 1955; Schuring and Emeri, 1964; Rambosek, 1964; Anderson and Reichenback, 1966; Shuring, 1966, U.S. Army, 1968), but actual research results were limited to the few indicated above, prior to 1970.

In 1969 Schofield introduced centrifuge modeling to the soil mechanics and foundation engineering literature in the English publication Advance (Schofield, 1969). This and activities at Cambridge University, Manchester University, and the Manchester Institute of Science and Technology (UMIST) influenced the growth of the technique in Europe. Later through funded research for the U.S. Army Corps of Engineers in Vicksburg, and a steady stream of sabbatical appointments at Cambridge University from 1975 and on Schofield influenced the growth of the technique in the U.S.

Another influence on the growth of centrifuge modeling in the soil mechanics field was the work of Oveson while on sabbatical leave at the University of Florida in 1971 and 1972. He tested the behavior of scaled models of cellular coffer dams over a range of scales and demonstrated the need for

centrifuge modeling. Also, he obtained a small surplus centrifuge which he modified for geotechnical use that still remains at the University of Florida under the direction of Townsend. Oveson used the centrifuge to study the bearing capacity of footings in sand that culminated later in his classic paper in Geotechnique in 1975.

In the decade of 1970-80 several developments occurred on the American scene. The use of centrifuge for modeling geophysical events and processes was carried to North America following the work of Ramberg in Swedan. Ramberg began his work in Chicago and later at the University of Connecticut where he proposed a high-g centrifuge for tectonic modeling. Lacking funding Ramberg returned to Swedan to carry out his work. However, Dixon in Canada using plastecine clay models studied the deformation in diapiric structures. (Dixon, 1974,1975). This was followed in 1980 and 1981 by research reports on modeling of tectonic development of Archean Greenstone Belts (Dixon and Summers, 1980,1981).

Several European scientists published centrifuge modeling results in the North American literature. Notable are Habib (1974) on shallow footings Waterways Experiment Station reports on River Bank Stability (1976), Atkinson and Potts (1977) on subsidence above shallow tunnels, Schofield (1978) on slope stability using the basket centrifuge, and, recently, Morris (1981) and Dickin and Leung (1983) on dynamic soil structure interaction and anchor plate pull-out respectively.

In 1976 Schmidt reported the first of a long series of results of explosive cratering data. The work of Schmidt and Holsapple has revolutionized the science of crater prediction at nuclear explosive levels and was accomplished by scale tests in the centrifuge at Boeing Company in Seattle, Washington, using small chemical explosives and impact of small projectiles at high velocities. (Schmidt, 1976,1978-1981; Holsapple, 1978-1984).

The results dramatically reduced the size estimates for craters formed by near-surface large-yield nuclear explosions and by planetary impact of large bodies. Because neither phenomenon can be tested at full scale, centrifuge simulation is the only alternative for obtaining an experimental data base. Estimates of crater sizes were reduced owing to the onset of a strength-gravity transition above which cratering efficiency decreases with size. Existing field data were too sparse and were conducted in far too diverse media to observe the phenomenon.

The application of these findings to Lunar and Planetary Science were pointed out by Gaffney (1978), Gaffney and Cheney (1983), and Gaffney, Brown, and Cheney (1983).

Scott (1977) entered the centrifuge literature in 1977 with cyclic and dynamic test on piles. This was followed in 1978 and on by work on modeling earthquake (Liu, Hagman, and Scott, 1978) and a general summary (Scott, 1978). Scott participated in a special preprint volume on Centrifuge Modeling of Geotechnical Problems at the ASCE National Convention in Atlanta, GA, in 1979 on pile tests and continued work reported in the XI Offshore Conference (Scott, 1979a,1979b). Scott's work on pile testing in the centrifuge was reported at the Stockholm Conference (Scott, 1981) and elsewhere (Scott, Ting, and Lee, 1982; Scott, Tsai, Steussy, and Ting, 1982).

The Scott-Morgan (1977) report on the "Feasibility and Desirability of Constructing a Very Large Centrifuge for Geotechnical Studies" was an outcome of a workshop on Geotechnical Centrifuge Modeling sponsored by the National Science Foundation at the California Institute of Technology in December 1975. This report has become a standard reference for many U.S. research proposals and results.

Scott has delved into many other projects on the centrifuge, some of which have been reported by his colleagues and students (Ortiz, Scott, and Lee, 1981) on forces on retaining walls, and (Prevost, Cuny, and Scott, 1981; Prevost, Cuny, Hughes, and Scott, 1981) on offshore gravity structures.

The special preprint volume on Centrifuge Modeling of Geotechnical Problems (1979) indicated the development of a geotechnical centrifuge research center at UC Davis with two small centrifuges in operation. Papers on modeling of lateral earth support (Shen, Kim, Bang, and Mitchell, 1979), overconsolidated clay slopes using a drum centrifuge (Fragaszy and Cheney, 1979), and simulation of earthquake motion (Arulanandan, Canclini, and Anandarajah, 1979), all coming from the UC Davis geotechnical group.

In the same specialty session Ko (1979) gave results he obtained on buried pipes and Townsend, Goodings, Schofield, and Al-Hussaini (1978) gave results of mine waste embankments utilizing in both cases the Cambridge University centrifuge.

Since that time Ko has developed a facility at UC Boulder and has produced a steady flow of results with his graduate students and colleagues

(Ferguson and Ko, 1981; Goble, Ko, and Houghnon, 1981; Kim and Ko, 1982; Ko, Azevedo, and Sture, 1982; Leung, Schiffman, Ko, and Pane, 1984; Gemperline and Ko, 1984; Ko, Dunn, and Simantob, 1984). The range of interest included cone penetrometers, piles, slopes, excavations in sand, footings on steep slopes, and effects of overtopping earth dams. These topics are addressed also in the following M.S. theses: Cargill, 1980; Ferguson, 1980; Houghnon, 1980; Kim, 1980 (Ph.D.); Croce, 1982; DePonati, 1982; Harrison, 1983; Manzoori, 1983; and Scully, 1983.

Townsend has developed the centrifuge at the University of Florida, Gainesville, that Oveson started, and is in the process at this date in building a second slightly more powerful centrifuge. His work has included bearing capacity of footings in sand, evaluation of the collapse of cavities (sink holes), and evaluation of sedimentation and consolidation characteristics of phosphatic waste clays. The latter is addressed by Bloomquist (1982 Ph.D. dissertation), Bertin (1978 M.S. thesis), McClimans (1984 M.S. report), Townsend and Bloomquist (1983), and Townsend and Israel (1983) reports.

The UC Davis group has also continued to produce research publications utilizing the two small centrifuges: swing bucket and drum (Cheney and Fragaszy, 1980; Cheney, 1981; Fragaszy and Cheney, 1981; Shen et al., 1981; Cheney and Oskoorouchi, 1982; Cheney and Brown, 1982; Shen et al., 1982; Arulanandan et al., 1981; Arulanandan and Anandarajah, 1983; Arulanandan et al., 1983; Bang and Shen, 1983; Cheney, Shen, and Ghorayeb, 1984).

During this same period the large man-rated centrifuge at NASA Ames Research Center was obtained for modification for geotechnical engineering research. This machine is designed to carry 6,000 lbs of soil payload (8,000 lbs with container) at 300 g's and at a radius of 30 feet. Details of this machine were presented by Cheney (1980). It will be the largest facility of its kind in the western world.

Early in 1984 the drive motor of the modified facility suffered a collapse of the thrust bearing of the motor rotor that caused extensive, although minor, damage to commutator bars and drive train.

Still other centers of geotechnical modeling have been developed. Sutherland et al. (1979) utilized the 25-foot radius Sandia Centrifuge at Albuquerque, New Mexico. Sutherland and his colleagues have carried out a number of tests for government agencies involving subsidence over coal mines

and stability of tailings dams (Sutherland, 1982; Sutherland et al., 1983,1983a; Sutherland et al., 1984).

Prevost at Princeton University has a small centrifuge and with his colleagues, has investigated the dynamic response of laterally loaded piles, buckling of a spherical dome, dynamic soil structure interaction, and subsurface wave reflections. (Prevost and Abdel-Ghaffar, 1982; Prevost et al., 1983; Prevost and Scanlan, 1983a,b; Cole, Scanlon, and Prevost, 1983a,b,).

In 1982 Goodings at the University of Maryland reported the work relating to the flow problem through and over waste embankments that was involved in her Ph.D. thesis at Cambridge and the Corps of Engineers, Waterways Experiment Station, Vicksburg. She has gained access to a small centrifuge at Goddard Space Flight Center near College Station and has produced several publications (Goodings, 1984a,b,c; Goodings and Schofield, 1984a,b). Her interest has progressed to boundary problems in reinforced soil structures (Santamarina and Goodings, 1984).

Whitman from MIT utilized the Cambridge Geotechnical Centrifuge to carry out basic tests in liquefaction. The first results were given by Whitman, Lambe, and Kutter (1981). Subsequently results were given by Whitman and Lambe (1982); Whitman, Lambe, and Akiyaina (1982); and Lambe and Whitman (1982).

Kutter accepted the position as Managing Director of the large centrifuge at NASA Ames Research Center after receiving his Ph.D. at Cambridge University and is now part of the UC Davis group. His M.S. thesis (1980) and his Ph.D. dissertation (1982) utilized the 'bumpy road' earthquake simulator that he developed at Cambridge. This work was presented in England (1982) and later in the U.S. (1983,1984a). A review of the costs of centrifuge construction was presented by Kutter in 1984a.

In 1982 Clark called together a workshop on "High Gravity Simulation for Research in Rock Mechanics" in hopes of raising interest in a large high-g machine for research in mining problems. Lade et al. (1981) published results at ISSMFE, Stockholm conference with Jessberger, Kabowske, and Jordan on modeling deep shafts, but rock mechanics centrifuge application is sparse to date.

The U.S. Air Force has shown increasing interest in centrifuge modeling of blast induced behavior (Nielson, 1983; Schmidt, Fragaszy, and Holsapple, 1981).

In the last few years there has been a blossoming of U.S. centrifuge activity. New centrifuges are being discovered and brought into play for example at Kirtland Air Force Base under the operation of the New Mexico Research Institute. Sterling at the University of Kentucky has built a 6,000 g-lb centrifuge for model landfill subsidence (Sterling and Ronayne, 1984). Ko at the University of Colorado, Boulder, has obtained funds for building an intermediate size centrifuge. At this writing there is high probability that there are some centrifuges that are being used that have been overlooked and papers presented that are not reported here. For this, apologies are extended.

The growth of the centrifuge as a research tool in the U.S. is phenomenal. The day will come when every well-equipped geotechnical research laboratory will include a centrifuge for model testing, and at that stage comprehensive reference lists such as this will be unfeasible.

REFERENCES

1931

Bucky, P.B. (1931), "Use of Models for the Study of Mining Problems," American Institute of Mining and Metallurgical Engineers, Technical Publication No. 425, pp. 3-28. February. New York

1934

Bucky, P.B. (1934), "Effect of Approximately Vertical Cracks on the Behavior of Horizontally Lying Roof Strata, Trans. Am. Inst. Min. and Met. Eng., Volume 109, pp. 212-229.

Bucky, P.B. and Fentress, A.L. (1934), "Application of Principles of Similitude to Design of Mine Workings, Trans. Am. Inst. Min. and Met. Eng., Volume 109, pp. 25-50.

1935

Bucky, P.B., Solakian, A.G. and Baldin, L.S. (1935), "Centrifugal Method of Testing Models," Volume 5, May, pp. 287-290.

1937

Hubbert, M.K. (1937), "Theory of Scale Models as Applied to the Study of Geologic Structures," Bulletin of the Geological Society of America, Volume 48, pp. 1459-1519.

1938

Bucky, P.B. and Taborelli, R.V. (1938), "Effects of Immediate Roof Thickness in Longwall Mining as Determined by Barodynamic Experiments," Trans. Am. Inst. Min. and Met. Eng., Volume 130, pp. 314-332.

1940

Bucky, P.B. and Taborelli, R.V. (1940), "Effects of Artificial Support in Longwall Mining as Determined by Barodynamic Experiment," Trans. Am. Inst. Min. and Met. Eng., Volume 139, pp. 211-224.

Bucky, P.B. (1940), "Stresses in Mine Working," Eng. and Min. Journal, Volume 141, November, pp. 33-36.

Sinclair, David and Bucky, P.B. (1940), "Photoelasticity and Its Application to Mine Pillar and Tunnel Problems," AIME Trans., Volume 139, pp. 225-252.

1949

Panek, L.A. (1949), "Design of Safe and Economical Arch Structures," Transactions of the American Institute of Mining and Metallurgical Engineers, Vol. 181, pp. 371-375.

Wright, F.D. and Bucky, P.B. (1949), "Determination of Room-and-Pillar Dimensions for the Soil-Shale Mine at Rifle, Colorado," Transactions of the American Institute of Mining and Metallurgical Engineers, Volume 181, pp. 352-359.

1952

Panek, L.A. (1952a), "Centrifugal Testing Apparatus for Mine-Structure Stress Analysis," Report of Investigations 4883, United States Department of the Interior, Bureau of Mines, June, 22 pp.

Panek, L.A. (1952b), "Centrifugal Testing Applied to the Design of Mine Structures with Special Reference to Roof Control," Proceedings of the Seventh International Conference of Directors of Safety in Mines Research.

1955

Caudle, R.D. and Clark, G.B. (1955), "Stresses Around Mine Openings in Some Simple Geologic Structures," University of Illinois Bulletin, Volume 52, Number 69, May, 41 pp.

1956

Panek, L.A. (1956a), "Theory of Model Testing as Applied to Roof Bolting," Report of Investigations 5154," United States Department of the Interior, Bureau of Mines, March, 16 pp.

Panek, L.A. (1956b), "Design of Bolting Systems to Reinforce Bedded Mine Roof," Report of Investigations 5155, United States Department of the Interior, Bureau of Mines, March, 16 pp.

Panek, L.A. (1956c), "Principles of Reinforcing Bedded Mine Roof and Bolts," Report of Investigations 5156, United States Department of the Interior, Bureau of Mines, March, 26 pp.

1961

Panek, L.A. (1961), "Use of Vertical Roof Bolts to Reinforce an Arbitrary Sequence of Beds," International Symposium on Mining Research, Univ. of Missouri, pp. 499-508.

1962

Panek, L.A. (1962a), "The Effect of Suspension in Bolting Bedded Mine Roof," Report of Investigations 6138, United States Department of the Interior, Bureau of Mines, 59 pp.

Panek, L.A. (1962b), "The Combined Effects of Friction and Suspension in Bolting Bedded Mine Roof," Report of Investigations 6139, United States Department of the Interior, Bureau of Mines, 31 pp.

1964

Rambosek, A.J. (1964), "A Centrifuge Designed to Study Two-Dimensional Transparent Photo-Elastic Models," Bureau of Mines Report of Investigations.

Schuring, D.J. and Emori, R.I. (1964), "Soil Deforming Processes and Dimensional Analysis," Proceedings of Society of Automotive Engineers' National Farm, Construction and Industry Machinery Meeting, September, pp. 485-494.

1966

Anderson, J.B. and Reichenbach, R.E. (1966), 76-Inch Diameter Centrifuge Facility, Naval Postgraduate School, Monterey, California NPS-TN-66T-4, September.

Schuring, D. (1966), "Scale Model Testing of Land Vehicles in a Simulated Low Gravity Field," Proceedings of the Automotive Engineering Congress, Detroit, Society of Automotive Engineers, January, pp. 1-8.

1968

U.S. Army Test and Evaluation Command (1968), Centrifuge Test Procedures, White Sands Missile Range, Material Test Procedure 5-2-586, February.

Wang, C.S., Boshkov, S.H. and Wane, M.T. (1968), "The Application of Barodynamic Photostress Techniques to the Study of the Behavior of Rock Beams Loaded by Their Own Weight," Ninth Symposium on Rock Mechanics, American Institute of Metallurgical Engineers.

1969

Johnson, S.W., et al. (1969), "Gravity and Atmospheric Pressure Effects on Crater Formation in Sand," Journal of Geophysical Research, Vol. 74, No. 20, pp. 4838-4850.

Schofield, A.N. (1969), "Laboratory Landslides," Advance, No. 7, October.

1970

Haas, C.J. and Clark, G.B. (1970), "Experimental Investigation of Small Scale Lined and Unlined Cylindrical Cavities in Rock-like Materials," University of Missouri School of Mining, Rolla, Missouri, Technical Report Number AFWL-TR-70-58, July, 191 pp.

1971

Davis, J.O. (1971), "Development of Large, High-Performance Centrifuges," SC-DR-710164, Sandia Laboratories, April, 62 pp.

1972

Rosenblad, J. Lyndon (1972), "Development of Rocklike Model Material," 10th Symposium on Rock Mechanics, pp. 331-361.

1973

Sharma, H.D. (1973), "Effect of Acceleration on Material Properties," Purdue University, Joint Highway Research Project, Report No. 24, September.

1974

Dixon, John M. (1974), "A New Method of Determining Finite Strain in Models of Geological Structures," Tectonophysics, Vol. 24, pp. 99-114.

Habib, P.A. (1974), "Scale Effect for Shallow Footings on Dense Sand," Journal of the Geotechnical Engineering Division, ASCE, Vol. 100, GTI, pp. 95-99.

1975

Dixon, John M. (1975), "Finite Strain and Progressive Deformation in Models of Diapiric Structures," Tectonophysics, Vol. 28, pp. 89-124.

Scott, F.E. (Compiler) (1975), "The Centrifuge Technique in Geotechnology Selected Papers," Calif. Inst. Tech., November.

1976

Schmidt, R.M. (1976), "A Centrifuge Cratering Experiment (Abstract)," Flagstaff Symposium on Planetary Cratering Mechanics, The Lunar Science Institute, Houston, 126 pp.

Waterways Experiment Station (1976), Verification of Empirical Criterion for River Bank Stability, Potomology Report 12-22, Vicksburg.

1977

Atkinson, J.H. and Potts, D.M. (1977), "Subsidence Above Shallow Tunnels in Soft Ground," Journal of the Geotechnical Engineering Division, ASCE, Vol. 103, GT4, April, pp. 307-325.

Schmidt, R.M. (1977), "A Centrifuge Cratering Experiment: Development of a Gravity-Scaled Yield Parameter," In Impact and Explosion Cratering, (D.J. Roddy, R.O. Pepin and R.B. Merrill, eds), Pergamon Press, New York, pp. 1261-1278.

Scott, R.F. and Morgan, N.R. (1977), "Feasibility and Desirability of Constructing a Very Large Centrifuge for Geotechnical Studies," National Science Foundation, March, 156 pp.

Scott, R.F. (1977), "Centrifuge Studies of Cyclic Laterial Load - Displacement Behavior of Single Piles," California Institute of Technology, Final Report to American Petroleum Institute.

Scott, R.F., Liu, H.P. and Ting, J. (1977), "Dynamic Pile Tests by Centrifuge Modelling," Proc. VI World Conf. on Earthquake Engineering, New Delhi, pp. 1670-1674.

1978

Gaffney, E.S. (1978), "Effect of Gravity on Explosion Craters," Proc. Lunar Planet. Sci. Conf. 9th, pp. 3831-3842.

Henderson, B.J., Schmidt, R.M. and Konicek, D.J. (1978), "Statistical and Dimensional Analysis of Crater Configuration (Abstract)," EOS (Trans. Am. Geophys. Union) 59, 245 pp.

Holsapple, K.A., Schmidt, R.M. and Dyrdahl, R.L. (1978), "Gravity Scaling Methods Applied to Crater Induced Ground Motions," Proceedings of the Nuclear Blast and Shock Simulation Symposium, San Diego, Defense Nuclear Agency Report, DNA 4797P.

Holsapple, K.A., Schmidt, R.M., and Dyrdahl, R.L. (1978), "Gravity Scaling Methods Applied to Crater Induced Ground Motions," Proc. of the Nuclear Blast and Shock Simulation Symposium, San Diego. Rep. DNA 4797P, Defense Nuclear Agency, Washington, D.C.

Holsapple, K.A. and Schmidt, R.M. (1978), "Subscale Modeling Using a Geotechnic Centrifuge," AGU Pacific Northwest Regional Meeting, University of Puget Sound, Tacoma, WA.

Liu, H.P., Hagman, R.L. and Scott, R.F. (1978), "Centrifuge Modelling of Earthquakes," Geophysical Research Letters, Vol. 5, No. 5, pp. 333-336.

Schmidt, R.M. (1978), "Centrifuge Simulation of the JOHNIE BOY 500 Ton Cratering Event," Proc., 9th Lunar Planet. Sci. Conf. pp. 3877-3889.

Schmidt, R.M. and Holsapple, K.A. (1978a), "Ottawa Sand Cratering Experiments in Centrifuge with Gravity Variation to 450 G's (Abstract)," EOS (Trans. AM. Geophys. Union) 59, 245 pp.

Schmidt, R.M. and Holsapple, K.A. (1978b), "Centrifuge Cratering Experiments I: Dry Granular Soils," Defense Nuclear Agency Report DNA 4568F, Washington, D.C.

Schmidt, R.M. and Holsapple, K.A. (1978c), "A Gravity-Scaled Energy Parameter Relating Impact and Explosive Crater Size (Abstract)," EOS (Trans. AM. Geophys. Union) 59, 1121 pp.

Schofield, A.N. (1978), "Use of Centrifuge Model Testing to Asses Slope Stability," Canadian Geotechnical Journal, Vol. 15, pp. 14-31.

Scott, R.F. (1978), "Modeling Summary," Proceedings ASCE Geotechnical Engineering Division, Specialty Conference, Earthquake Engineering and Soil Dynamics, June 19-21, Pasadena, pp. 1417-1424.

1979

Centrifuge Modeling of Geotechnical Problems (1979), ASCE National Convention, Atlanta, Georgia, October, Preprint No. 3786.

1. C.K. Shen, Y.S. Kim, S. Bang and J.F. Mitchell, "Centrifuge Modeling of a Lateral Earth Support".
2. R.J. Fragaszy and J.A. Cheney, "Drum Centrifuge Studies of Overconsolidated Slopes".
3. K. Arulanandan, A. Anandarajah and R.H. Bassett, "Centrifuge Testing in Geotechnical Engineering".
4. K. Arulanandan, J. Canclini and A. Anandarajah, "Simulation of Earthquake Motions in the Centrifuge".
5. H.Y. Ko, "Centrifuge Model Tests of Flexible, Elliptical Pipes".
6. F.C. Townsend, D.J. Goodings, A.N. Schofield and M.M. Al-Hussaini, "Centrifuge Modeling of Coal Waste Embankment Stability".
7. R.F. Scott, "Laterally Loaded Pile Tests in a Centrifuge".

Holsapple, K.A. (1979a), "Material Strength and Explosive Property Effects in Cratering and Ground Shock," Proceedings of the Sixth International Symposium of Blast Simulation, Cahors, France.

Holsapple, K.A. and Schmidt, R.M. (1979), "A Material Strength Model for Apparent Crater Volume," Proc. Lunar Plant. Sci. Conf. 10th., pp. 2757-2777.

Schmidt, R.M. (1979), "Simulation of Large Scale Explosive Cratering and Ground Shock Using a 600-G Geotechnic Centrifuge," Proceedings of the Sixth International Symposium of Blast Simulation, Cahors, France.

Schmidt, R.M. and Holsapple, K.A. (1979), "Centrifuge Crater Scaling Experiments II: Material Strength Effects," Defense Nuclear Agency Report DNA 4999Z, Washington, D.C.

Schmidt, R.M., Holsapple K.A. and Fisher, L.D. (1979), "Statistical-Dimensional Analysis: An Application to the Assessment of Crater Configuration," Defense Nuclear Agency Report DNA 4904F, Washington, D.C.

Schmidt, R.M., Holsapple, K.A. and Wauchope, C.R. (1979), "Nuclear Cratering: Why A Centrifuge?" Proceedings of the Strategic Structures Biennial Review, Defense Nuclear Agency - SPSS, SRI International, Menlo Park, CA 94025.

Schmidt, R.M., Watson, H.E. and Wauchope, C.R. (1979), "Projectile Density/Target Density Correlation for Impact Cratering in Dry Sand (Abstract)," EOS Trans. AM. Geophys. Union) 60, 871 pp.

Scott, R.F. (1979a), "Cyclic Lateral Loading of Piles, Analysis of Centrifuge," Research program for API OASAFR Project 13, Cal Tech.

Scott, R.F. (1979b), "Cyclic Static Model Pile Tests in a Centrifuge," XI Offshore Technology Conference, Paper OTC 3492, pp. 1159-1198.

Sutherland, H.J., Schmidt, R.A., Schuler, K.W., and Benzley, S.E. (1979), "Physical Simulations of Subsidence by Centrifuge Techniques," Proceedings of the 20th U.S. Symposium on Rock Mechanics, Society of Petroleum Engineers, Austin, Texas, pp. 279-286.

Townsend, F.C., Goodings, D.J., Schofield, A.N., and Al-Hussaini, M.M. (1979), "Centrifugal Modelling of Coal Waste Embankment Stability," Preprint ASCE Specialty Session on Centrifuge Modelling, Atlanta, Georgia, October.

1980

Cheney, J.A. (1980), "The Centrifuge as a Research Tool," Appendix E, Dam Safety Research Coordination Conference, Denver, Colorado, pp. 1-23, (invited paper).

Cheney, J.A. and Fragazy, R.J. (1980), "Short-Term Stability of Overconsolidated Clay Slopes," Proceedings International Symposium on Landslides (ISL 1980), New Delhi, pp. 149-155.

Clark, G.B. (1980), "Investigation of Effects of Sample Size and Compressibility Coefficients," Report for Lawrence Berkeley Laboratories, Contract #42932303, August, 173 pp.

Dixon, J.M. and Summers, J.M. (1979-1980), "A Centrifuge Model Study of the Tectonic Development of Archean Greenstone Belts," Geoscience Research Grant Program Summary of Research, Ontario Geological Survey MP93, pp. 58-71.

Holsapple, K.A. (1980), "The Equivalent Depth of Burst for Impact Cratering," Proc. Lunar and Planetary Sci. Conf. 11th, pp. 2379-2401, Pergamon Press.

Holsapple, K.A. and Schmidt, R.M. (1980a), "On the Scaling of Crater Dimensions 1," Explosive processes. J. Geophys. Res. 85, No. B12.

Holsapple, K.A. and Schmidt, R.M. (1980b), "A Subscale Simulation of Two 20-Ton Cratering Events (Abstract)," EOS (Trans. Am. Geophys. Union) 61, 1021.

Lambe, P.C. and Whitman, R.V. (1980), "Modelling Dynamic Ground Motions by Centrifuge - First Test Series," MIT Civil Engineering Research Report No. R80-40.

Schmidt, R.M. (1980), "Meteor Crater: Energy of Formation--Implications of Centrifuge Scaling," Proc. Lunar and Planetary Sci. Conf. 11th, pp. 2099-2128, Lunar and Planetary Institute, Houston.

Schmidt, R.M. and Holsapple, K.A. (1980a), "Theory and Experiments on Centrifuge Cratering," J. Geophys. Res. 85, No. 1, 235 pp.

Schmidt, R.M., Holsapple, K.A. and Piekutowski, A.J. (1980), "Centrifuge Simulation Study of the PRAIRIE FLAT Multi-Ring Crater (Abstract)," Conference on Multi-Ring Basins: Formation and Evolution, Lunar and Planetary Inst., Houston, Texas.

1981

Al-Hussaini, M.M., Goodings, D.J., Schofield, A.N. and Townsend, F.C. (1981), "Centrifugal Modelling of Coal Waste Embankments," ASCE, J. of The Geotechnical Division, Vol. 107 GT, April, pp. 481-499.

Arulanandan, K., Canclini, J. and Anandarajah, A. (1981), "Simulation of Earthquakes Motions in the Centrifuge," ASCE Journal of Geotechnical Engineering, Vol. 108, GT5, May, pp. 730-742.

Cheney, J.A. (1981), "Moderator's Report-Dynamic Excitation for Geotechnical Centrifuge Modeling," Proceedings International Conference on Recent Advances in Geotechnical Earthquake Engineering and Soil Dynamics, Vol. III, St. Louis, MO, pp. 1101-1104.

Dixon, J.M. and Summers, J.M. (1980-1981), "A Centrifuge Model Study of the Tectonic Development of Achean Greenstone Belts," Geoscience Research Grant Program Summary of Research, Ontario Geological Survey MP98, pp. 54-66.

Ferguson, K.A. and Ko, H.Y. (1981), "Centrifugal Modeling of the Cone Penetrometer," Proc. Symp. on Cone Penetration Testing and Experience, ASCE, St. Louis, pp. 108-123.

Fragazy, R.J. and Cheney, J.A. (1981), "Drum Centrifuge Studies of Overconsolidated Slopes," ASCE Journal of the Geotechnical Engineering Division, Vol. 107, No. GT7, pp. 843-858.

Goble, G.G., Ko, H.Y. and Houghnon, J.R. (1981), "Centrifugal Model Testing of Axial Pile Behavior," Report to Federal Highway Administration, University of Colorado.

Holsapple, K.A. (1981), "Coupling Parameters in Cratering," (abstract), EOS (Trans. Amer. Geophys. U.) 62, pp. 949.

Lade, N.V., Jessberger, H.L., Kakowski, E. and Jordan, P. (1981), "Modeling of Deep Shafts in Centrifuge Tests," International Conference on SMFE, Stockholm, Vol. 1, pp. 683-692.

Lambe, P.C. and Whitman, R.V. (1981), "Modelling Dynamic Ground Motions by Centrifuge - First Test Series," MIT Report R-80-40, Order No. 684 for Div. of Civil & Mech. Eng. and Appl. Sci. Directorate Nat. Sci. Found.

Morris, D.V. (1981), "Dynamic Soil-Structure Interaction Modelled Experimentally on a Geotechnical Centrifuge," Can. Geotech Jour., Vol. 18, No. 1, pp. 40-51.

Ortiz, L.A., Scott, R.F. and Lee, J. (1981), "Dynamic Testing of a Cantilever Retaining Wall," Report, Soil Mechanics Laboratory, CIT, Pasadena, CA.

Prevost, J.H., Cuny, B. and Scott, R.F. (1981), "Offshore Gravity Structures: Centrifugal Modeling," Journal of the Geotechnical Engineering Division, ASCE, Vol. 107, GT2, Feb., 125 pp.

Prevost, J.A., Cuny, B., Hughes, T.J.R. and Scott, R.F. (1981), "Offshore Gravity Structures: Analysis," Journal of the Geotechnical Engineering Division, ASCE, Vol. 107, GT2, Feb., 143 pp.

Prevost, J.H., Romano, J.D., Abdel-Ghaffar, A.M. and Rowland, R. (1981), "Dynamic Response of Laterally Loaded Piles in a Centrifuge," Proceedings ASCE/EMD Specialty Conference on Dynamic Response of Structures, Atlanta, GA, January, pp. 386-400.

Schmidt, R.M., Fragaszy, R.J., and Holsapple, K.A. (1981), "Centrifuge Modeling of Soil Liquefaction due to Airblast," Proc. of the Seventh International Symposium on Military Applications of Blast Simulation, Medicine Hat, Alberta, Canada, 4.2-1/4.2-18, 1981.

Schmidt, R.M., Fragaszy, R.J. and Holsapple, K.A. (1981), "Centrifuge Modelling of Soil Liquefaction Due to Airblast (Abstract)," Seventh International Symposium on Military Applications of Blast Simulation, Medicine Hat, Alberta, Canada.

Schmidt, R.M. and Holsapple, K.A. (1981b), Gravity scaling with centrifuge data: Minutes of the sixth meeting of DNA ad hoc cratering working group. RDA-TR-120004-001, Marina Del Ray, CA.

Schmidt, R.M. and Holsapple, K.A. (1981a), "An Experimental Investigation of Transient Crater Size (Abstract)," Lunar and Planetary Science XII, Lunar and Planetary Institute, Houston, TX, pp. 934-936.

Schmidt, R.M. (1981), "Scaling Considerations for Dynamic Experiments," International Conference on Recent Advances in Geotechnical Earthquake Engineering and Soil Dynamics, Vol. III. St. Louis, MO, April-May, pp. 1111-1113.

Schmidt, R.M. (1981), "Scaling Crater Time-of-Formation," (abstract), EOS (Trans. Amer. Geophys. U.) 62, No. 45, pp. 944.

Schmidt, R.M., Fragaszy, R.J., and Holsapple, K.A. (1981), "Centrifuge Modeling of Soil Liquefaction Due to Airblast," Proc. of the Seventh International Symposium on Military Applications of Blast Simulation, Medicine Hat, Alberta, Canada, 4.2-1/4.2-18.

Scott, R.F. (1981), "Pile Testing in a Centrifuge," Proc., Int. Conf. on Soil Mech. and Found. Eng. Summary, Stockholm, pp. 839-842.

Shen, C.K. et al. (1981), "An In Situ Earth Reinforcement Lateral Support System," Report No. 81-03, Department of Civil Engineering, UC Davis, Chapter 4, Centrifuge Model Study, pp. 31-51.

Whitman, R.V., Lambe, P.C. and Kutter, B.L. (1981), "Initial Results from a Stacked Ring Apparatus for Simulation of a Soil Profile," International Conference on Recent Advances in Geotechnical Earthquake Engineering and Soil Dynamics, Vol. III, St. Louis, MO, April-May, pp. 1105-1110.

1982

Akiyama, J. (1982), "Evaluation of Martin-Seed Simplified Procedure Using Data from Dynamic Centrifuge Tests," MIT Civil Engieering Research Report R82-28.

Cheney, J.A. and Oskoorouchi, A.M. (1982), "Physical Modeling of Clay Slopes in the Drum Centrifuge," Transportation Research Record 872, Washington, D.C.

Cheney, J.A. and Brown, R.K. (1982), "Modelling Foundation Elements for Structural Response to Earthquakes," Proc. of Conf. on Soil Dynamics and Earthquake Engineering, Southampton, July, pp. 409-418.

Clark, G.B. (1982), High Gravity Simulation for Research in Rock Mechanics Workshop, Colorado School of Mines, May 13-14.

Goodings, D.J. (1982), "Relationships for Centrifugal Modelling of Seepage and Surface Flow Effects on Embankment Dams," Geotechnique, Vol. 32, pp. 149-152.

Holsapple, K.A. and Schmidt, R.M. (1982), "On the Scaling of Crater Dimensions 2," Impact processes, J. Geophys. Res., , 87(B3), pp. 1849-1870.

Holsapple, K.A. (1982), "A Comparison of Scaling Laws for Planetary Impact Cratering: Experiments, Calculations, and Theory," (abstract). Lunar and Planetary Science XIII, 331-332, Lunar and Planetary Institute, Houston.

Holsapple, K.A. and Schmidt, R.M. (1982), "On the Scaling of Crater Dimensions-2: Impact Processes," J. Geophys. Res. 87(B3), pp. 1849-1870.

Housen, K.R., Schmidt, R.M., Holsapple, K.A., and Piekutowski, A.J. (1982), "Scaling of Explosion Crater Ejecta Velocities," (abstract), EOS (Trans. Amer, Geophys. U.) 63, No. 45, pp. 1020.

Kim, M.M. and Ko, H.Y. (1982), "Centrifugal Testing of Soil Slope Models," Transportation Research Record 872, pp. 7-15.

Ko, H.Y., Azevedo, R. and Sture, S. (1982), "Numerical and Centrifugal Modeling of Excavations in Sand," Deformation and Failure of Granular Materials (Edited by P.A. Vermeer and H.J. Luger), A.A. Balkema, Rotterdam, The Netherlands, pp. 609-614.

Kutter, B.L. (1982), "Deformation of Centrifuge Models of Clay Embankments Due to 'Bumpy Road' Earthquakes," Proc. of Conf. on Soil Dynamics and Earthquake Engineering, Southampton, July, pp. 331-350.

Lambe, P.C. and Whitman, R.V. (1982), "Scaling for Earthquake Shaking Tests on a Centrifuge," Proc. of Conf. on Soil Dynamics and Earthquake Engineering, Southampton, July, pp. 367-380.

Prevost, J.H. and Abdel-Ghaffar, A.M. (1982), "Dynamic Response of Laterally Loaded Piles and Pile Groups" Centrifugal Modeling," Proc. 2nd Int. Conf. Num. Meth. in Offshore Piling, Austin, TX, April.

Schmidt, R.M. (1982), "Dynamic Scaling Relationships for Impact Crater Formation," (abstract). Lunar and Planetary Science XIII, pp. 687-688, Lunar and Planetary Institute, Houston.

Schmidt, R.M. and Holsapple, K.A. (1982), "Estimates of Crater Size for Large-Body Impact: Gravity Scaling Results." Geological Society of America Special Paper 190, pp. 93-102.

Schmidt, R.M., Holsapple, K.A., and Housen, K.R. (1982), "Scaling of Dynamic Models: Cratering Phenomena." Proceedings of the Workshop on High Gravity Simulation for Research in Rock Mechanics. Colorado School of Mines, Golden, CO.

Schmidt, R.M., Fragaszy, R.J., and Holsapple, K.A. (1982), "Centrifuge Modeling of Soil Liqauefaction Due to Airblast." Proceedings of the Seventh International Symposium on Military Applications of Blast Simulation, Medicine Hat, Alberta, Canada, 4.2-1/4.2-18.

Scott, R.F., Ting, J.M. and Lee, J. (1982), "Comparison of Centrifuge and Full Scale Dynamic Pile Tests," Proc. of Conf. on Soil Dynamics and Earthquake Engineering, Southampton, July, pp. 299-310.

Scott, R.F., Tsai, C.-F., Steussy, D. and Ting, J.M. (1982), "Full-Scale Dynamic Lateral Pile Tests," Paper OTC 4203 Offshore Technology Conference, Houston, TX, May.

Shen, C.K., Kim, Y.S., Bang, S. and Mitchell, J.F. (1982), "Centrifuge Modeling of Lateral Earth Support," Journal of Geotechnical Engineering Division ASCE, GT, Sept., pp. 1150-1164.

Sutherland, H.J. (1982), "Centrifuge Simulation of the Subsidence over Coal Mines and the Stability of Tailing Dams," presented at High Gravity Simulation for Rock Mechanics Research Workshop, Colorado School of Mines, May, pp. 71-98.

Sutherland, H.J. and Rechard, R.P. (1982), Physical Modeling of Tailings Dams Using Centrifuge Simulation Techniques, Sandia Report SAND 82-1191, August.

Sutherland, H.J. and Schuler, K.W. (1982), A Review of Subsidence Prediction Research Conducted at Sandia National Laboratories, Proceedings of the Workshop on Surface Subsidence Due to Underground Mining, S.S. Peng and M. Harthill, eds., West Virginia University, Morgantown, WV, USA, pp. 1-14.

Whitman, R.V. and Lambe, P.C. (1982), "Liquefaction Consequences for a Structure," Proc. Soil Dynamics and Earthquake Engineering Conf., Southampton, pp. 941-949.

Whitman, R.V., Lambe, P.C. and Akiyama, J. (1982), "Consolidation During Dynamic Tests on a Centrifuge," ASCE National Convention, Las Vegas, NV, April.

Whitman, R.V. and Lambe, P.C. (1982), "Verification of Theoretical Method for Predicting Effect of Earthquakes on Foundations for Oil Storage Tanks," MIT Civil Engineering Research Report No. R82-24, prepared for Toa Nenryo Koago.

Whitman, R.V. and Lambe, P.C. (1982), "Liquefaction: Consequences for a Structure," Proceedings of Conference on Soil Dynamics and Earthquake Engineering, Southampton, July, pp. 941-949.

1983

Arulanandan, K. and Anandarajah, A. (1983), "Dynamic Centrifuge Modeling," Recent Advances in Engineering Mechanics and Their Impact on Civil Engineering Practice, Proceedings 4th Engineering Mechanics Division Specialty Conference ASCE/END, Purdue University, West Lafayette, IL, Vol. 1, pp. 626-629, (invited paper).

Arulanandan, K., Anandarajah, A. and Abghari, A. (1983), "Centrifuge Modeling of Soil Liquefaction Susceptibility," ASCE Journal of Geotechnical Engineering, Vol. 109, No. 3, pp. 281-300.

Bang, S. and Shen, C.K. (1983), "Soil Reinforcement in Soft Ground Tunneling," U.S. Department of Transportation Research Report DOT/RSPA/DMA-50/83/15, Chapter 5, Preliminary Centrifuge Model Tests, pp. 71-90.

Barton, Y.D., Finn, W.D.L., Parry, R.H.G. and Towhata, I. (1983), "Lateral Pile Response and P-y Curves from Centrifuge Tests," Proceedings of the Offshore Technology Conference, May, pp. 503-508.

Bradley, D.M., Townsend, F.C., Faqundo, F.E. and Davidson, J.L. (1983), Centrifuge Scaling Laws for Ground Launch Cruise Missle Shelter, Final Report Air Force Engineering and Services Laboratory ESL-TR-84-07, Tyndall Air Force Base, Florida, December.

Cheney, J.A. and Whitman, R.V. (1983), "Workshop for Development of Specifications for a Ground Motion Simulator for Centrifuge Modeling in Geotechnical Engineering," MIT Endicott House, Dedham, Mass., June.

Cole, C.J., Scanlon, R.H. and Prevost, J.A. (1983a), "On Dynamic Stress Wave Reflections in Centrifuge Soil Models," Earthquake Engineering and Structural Dynamics, September.

Cole, C.J., Prevost, J.H. and Scanlon, R.H. (1983b), "Dynamic Stres Waves Attenuation and Earthquake Simulation in Centrifuge Soil Models," Earthquake Engineering and Structural Dynamics, September.

Dickin, E.A. and Leung, C.F. (1983), Model Tests on Vertical Anchor Plates, J. Geotech. Engrg. Div., ASCE, Vol. 109, GT12, December.

Fragaszy, R.J., Voss, M.E., Schmidt, R.M., and Holsapple, K.A. (1983), "Laboratory and Centrifuge Modeling of Blast-Induced Liquefaction." Proceedings of the Eighth International Symposium on Military Applications of Blast Simulation, Spiez, Switzerland.

Gaffney, E.S. and Cheney, J.A. (1983), "Containment Science on a Centrifuge," in Proc. 2nd Symp. Containment of Underground Nucl. Expl., CONF-830882, Vol. 2, 365-378.

Gaffney, E.S., Brown, H.K., and Cheney, J.A. (1983), "Explosion Craters in Ice at Large Scaled Yields," (abstract). Lunar and Planetary Science XIV, pp. 233-234, Lunar and Planetary Institute, Houston.

Holsapple, K.A. (1983), "On the Existence and Implications of Coupling Parameters in Cratering Mechanics," (abstract). Lunar and Planetary Science XIV, pp. 319-320, Lunar and Planetary Institute, Houston.

Holsapple, K.A. and Schmidt, R.M. (1983), "On the Scaling of Crater Dimensions-3: Implications, of Coupling Parameters," in preparation to be submitted to J. Geophys. Res.

Housen, K.R. (1983), "Cratering Flow Fields: A General Form and the Z Model," (abstract). Lunar and Planetary Science XV, 377-378, Lunar and Planetary Institute, Houston.

Housen, K.R. (1983), Crater Ejecta Scaling Laws," (abstract). Lunar and Planetary Science XIV, pp. 333-334, Lunar and Planetary Institute, Houston.

Housen, K.R., Schmidt, R.M., and Holsapple, K.A. (1983), "Crater Ejecta Scaling Laws 1: Fundamental Forms Based on Dimensional Analysis." J. Geophys. Res. 88 (B3), pp. 2485-2499.

Kim, Y.S., et al. (1983), "Oil Storage Tank Foundation on Soft Clay," Proceedings VIII European Conference on Soil Mechanics and Foundation Engineering, Helsinki, Finland.

Kutter, B.L. (1983), "Geotechnical Centrifuges and Earthquake Simulator," Proc. 4th Eng. Mech. Div. Specialty Conference on Recent Advances in Eng. Mech., ASCE, Purdue University, pp. 621-625.

Lawver, J.E. and Carrier, W.D., III (1983), "Mathematical and Centrifuge Modeling of Phosphatic Clay Disposal Systems," Paper Presented at Spring Meeting, AIME, Atlanta, Georgia.

Leung, P.K., Schiffman, R.L., Ko, H.Y. and Pane, V. (1983), "Centrifuge Modeling of Shallow Foundation of Soft Soil," Offshore Technology Conference Paper.

Nielson, J.P. (1983), The Centrifuge Simulation of Blast Parameters, Air Force Engineering and Services Laboratory ESL-83-12, Tyndall Air Force Base, Florida, February.

Pane, V., Croce, P., Znidarcic, D., Ko, H.Y., Olsen, H.W. and Schiffman, R.L. (1983), "Effects of Consolidation on Permeability Measurements for Soft Clays," Geotechnique, 33, pp. 67-72.

Prevost, J.H., Billington, Di, Rowland, R. and Lim, C.C. (1983), "Buckling of a Spherical Dome in a Centrifuge," Experimental Mechanics, September.

Prevost, J.H. and Scanlan, R.H. (1983a), "Dynamic Soil-Structure Interaction: Centrifugal Modeling Report 83-SM-1, Department of Civil Engineering, Princeton University.

Prevost, J.H. and Scanlon, R.H. (1983b), "Dynamic Soil-Structure Interaction-Centrifuge Modeling," International Journal of Soil Dynamics and Earthquake Engineering, February.

Schmidt, R.M. (1983a), "Strength-Gravity Transition for Impact Craters in Wet Sand," (abstract). Lunar and Planetary Science XIV, pp. 666-667, Lunar and Planetary Institute, Houston.

Schmidt, R.M. (1983b), "Centrifuge Quarter-Space Cratering Results: A Gravity Criterion for Kinematic Similarity," (abstract). EOS (Trans. Amer. Geophys. U.) 64, No. 45, 747 p.

Schmidt, R.M., Holsapple, K.A., and Housen, K.R. (1983), "Optimum Depth of Burst Cratering: Strength-Gravity Transition Identified," (abstract). EOS (Trans. Amer. Geophys. U.) 64, No. 18, 255 p.

Schmidt, R.M. and Piekutowski, A.J. (1983), "Development of the Quarter-Space Technique for Cratering Experiments on a Centrifuge," (abstract). Lunar and Planetary Science XIV, pp. 668-669, Lunar and Planetary Institute, Houston.

Sutherland, H.J. (1983), Physical Simulations of Hole Closure in Deep Ocean Sediment, Sandia Report SAND 83-0988, June.

Sutherland, H.J., Hommert, P.J. Taylor, L.M. and Benzley, S.E. (1983), Subsidence Prediction for Two USC Projects, In Situ, in publication.

Sutherland, H.J., Rechard, R.P. and Heckes, A.R. (1983), Physical Modeling of Marginally Stable Tailings Dams Using Centrifuge Simulation Technqiues, Sandia Report SAND 83-2227, February.

1984

Cheney, J.A., Shen, C.K. and Ghorayeb, F. (1984), "Fault Movement: Its Potential Damage to Embankment Dams," Proceedings, World Conference on Earthquake Engineering, San Francisco, CA.

Ferguson, F.A. and Ko, H.Y. (1984), "Application of Centrifuge Modeling to Cone Penetrometer Technology," paper to be presented at Conference on Applications of Centrifuge Modeling to Geotechnical Design, Manchester University.

Gemperline, M.C. and Ko, H.Y. (1984), "Centrifugal Model Tests for Ultimate Bearing Capacity of Footings on Steep Slopes in Cohesionless Soils," paper to be presented at Conference on Applications of Centrifugal Modeling to Geotechnical Design, Manchester University, April.

Goodings, D.J. (1984a), "Geotechnical Centrifuge Modelling," Proc. 21st Annual Meeting of the Society of Engineering Science, V., Blacksburg, VA, October.

Goodings, D.J. and Schofield, A.N. (1984a), "Centrifuge Modelling of Slope Failures in Champlain Sea Clay," Proc. IV International Symposium on Landslides, September.

Goodings, D.J. (1984b), "Relationships for Modelling Water Flow in Geotechnical Centrifuge Models," Applications of Centrifuge Modelling to Geotechnical Design, Manchester, U.K., April.

Goodings, D.J. and Schofield, A.N. (1984b), "Centrifugal Modelling of Slope Failures in Ottawa Area Champlain Sea Clay," Canadian Geotechnical Journal.

Goodings, D.J. (1984c), "Geotechnical Centrifuge Modeling of Soil Erosion," Transportation Research Record, January.

Holsapple, K.A. (1984), "On Crater Dynamics: Comparisons of Results for Different Target and Impactor Conditions," (abstract). Lunar and Planetary Science XV, pp. 367-368, Lunar and Planetary Institute, Houston.

Holsapple, K.A. and Schmidt, R.M. (1984), "On the Scaling of Crater Dimensions-3: Implications of Coupling Parameters," (in preparation). To be submitted to J. Geophys. Res.

Housen, K.R. (1984), "Cratering Flow Fields: A General Form and the Z Model," (abstract). Lunar and Planetary Science XV, pp. 377-378, Lunar and Planetary Institute, Houston.

Ko, H.Y., Dunn, R.J. and Simantob, E. (1984), "Study of Embankment Performance During Overtopping and Throughflow," Report to U.S. Army Corps of Engineers.

Kutter, B.L. (1984a), "Earthquake Deformation of Centrifuge Model Banks," ASCE, Journal of Geotech. Eng. Div., V110, No. 12, December.

Kutter, B.L. (1984b), "NGC Facility and Trends in Cost of Centrifuges," Proceedings of Symposium on Recent Advances in Geotechnical Centrifuge Modeling, Davis, CA, July.

Santamarina, J.C. and Goodings, D.J. (1984), "Centrifuge Modelling of Foundation and Adjacent Soil Effects of Reinforced Soil Structures," Parts I & II, ASCE J. of Geotechnical Engineering.

Schmidt, R.M. (1984), "Transient Crater Motions: Saturated Sand Centrifuge Experiments," (abstract). Lunar and Planetary Science XV, pp. 722-723, Lunar and Planetary Institute, Houston.

Schmidt, R.M. and Holsapple, K.A. (1984), "Explosively Generated Water Waves," (abstract). EOS (Trans. Amer. Geophys. U.) 65, No. 16, 221.

Schmidt, R.M., Holsapple, K.A., and Housen, K.R. (1984), "Gravity Effects in Cratering," draft report, DNA 001-82-C-0301, Defense Nuclear Agency, Washington, D.C.

Sutherland, H.J., Taylor, L.M., Benzley, S.E. (1984), "Physical and Numerical Simulations of Subsidence in Fractured Shale Strata," Proceedings, 10th Annual Underground Coal Gasification Symposium, August 12-15, Williamsburg, VA.

Sutherland, H.J., Hecks, Albert A. and Taylor, L.M. (1984), Physical and Numerical Simulations of Subsidence above High Extraction Coal Mines, Sandia Report SAND83-1191C, March.

Whitman, R.V. (1984), "Experiments with Earthquake Ground Motion Simulation," Proc. Symposium on the Application of Centrifuge Modelling to Geotechnical Design, University of Manchester, England, April 1984.

THESES

1960

Chan, S.M.C. (1960), "Physical Properties Tests of Rock, Centrifugal Tests, and the Design of Mine Openings," M.S. Thesis, University of Missouri School of Mines, Rolla, Missouri.

1962

Esser, R.H.K. (1962), "A Model Study of the Application of Roof Bolts Under Unsymmetrical Loading Conditions," M.S. Thesis, University of Missouri School of Mines, Rolla, Missouri.

Haycocks, C. (1962), "Mechanics of a Voussoir Arch," M.S. Thesis, University of Missouri School of Engineering, Rolla, Missouri.

1963

Gomah, Aly H. (1963), "Application of Photoelasticity to the Stability of Slopes," M.S. Thesis in Mining Engineering, University of Missouri School of Mining, Rolla, Missouri.

1978

Bertin, Y. (1978), "A Centrifuge Study of the Collapse of Hemispherical Cavities in Soil," M.S. Thesis, University of Florida, Gainesville, Florida.

1979

Fragaszy, R.J. (1979), "Drum Centrifuge Studies of Overconsolidated Clay Slopes," Ph.D. Thesis, University of California, Davis.

Morris, D.V. (1979), "The Centrifugal Modelling of Dynamic Soil-Structure Interaction and Earthquake Behavior," Ph.D. Thesis, Cambridge University.

1980

Anandarajah, A. (1980), "Centrifuge Modeling of Earthquake Response of Soil Embankments," M.S. Thesis, University of California, Davis.

Cargill, K.W. (1980), "Centrifugal Modeling of Transient Water Flow in Earth Embankments," M.S. Thesis, University of Colorado.

Ferguson, K.A. (1980), "Centrifugal Modeling of the Quasi-Static Cone Penetrometer," M.S. Thesis, University of Colorado.

Gillogley, E. (1980), "Centrifuge Testing to Study the Mechanism of Hydraulic Fracture," M.S. Thesis, University of California, Davis.

Houghnon, J.R. (1980), "Centrifugal Modeling of Axially Loaded Piles," M.S. Thesis, University of Colorado.

Kim, M.M. (1980), "Centrifugal Model Testing of Soil Slopes," Ph.D. Thesis, University of Colorado.

Kim, Y.S. (1980), "Centrifuge Model Study of a Lateral Earth Support System," M.S. Thesis, University of California, Davis.

Kutter, B.L. (1980), "Behavior of Embankments Under Dynamic Loading," M.Phil. Thesis, Department of Engineering, Cambridge University.

1981

Heidari, M. (1981), "Centrifugal Modelling of Earthquake Induced Liquefaction in Saturated Sand," M.Phil. Thesis, Cambridge University.

Oskoorouchi, A. (1981), "Drum Centrifuge Modeling of Overconsolidated Clay Slopes," Ph.D. Thesis, University of California, Davis.

1982

Abghari, A. (1982), "Centrifuge Modeling of Soil Liquefaction," M.S. Thesis, University of California, Davis.

Bloomquist, D.C. (1982), "Centrifuge Modeling of Large Strain Consolidation Phenomena in Phosphatic Clay Retention Ponds," Ph.D. Dissertation, University of Florida (University Microfilm ROD83-13610).

Coles, C.K. (1982), "Centrifuge Models of a Spile-Reinforced Tunnel," M.S. Thesis, University of California, Davis.

Croce, P. (1982), "Evaluation of Consolidation Theories by Centrifugal Model Tests," M.S. Thesis, University of Colorado.

1983

Ghorayeb, F. (1983), "Centrifugal Modeling of Foundations on Collapsible Soils," M.E. Thesis, University of California, Davis.

Ryan, W.F. (1983), "Centrifuge Testing of Model Piles in Sand," M.S. Report, University of Florida.

Townsend, F.C. and Bloomquist, D.G. (1983), "Centrifugal Model Evaluation of Cap Enhanced Consolidation of Kingsford Waste Clays," EIES Report for IMC Corp., Bartow, Florida.

Townsend, F.C. and Israel, D.L. (1983), "Centrifugal Model Evaluation of Consolidation Characteristics of Waste Phosphatic Clays," EIES Report for Occidental Chemical Co., White Springs, Florida (also Israel's M.S. Report).

1984

Brown, R.K. (1984), "Centrifuge Modeling of Machine Foundations," M.S. Thesis, University of California, Davis.

Kim, Y.S. (1984), "Centrifuge Model Study of an Oil Storage Tank Foundation," Ph.D. Thesis, University of California, Davis.

McClimans, S.A. (1984), "Centrifugal Model Evaluation of the Consolidation Behavior of Sand/Phosphatic Clay Mixes," M.S. Report, University of Florida.

Zenaidi, J. (1984), "Predicting Pore Pressures Under Strip Loading During Dynamic Centrifuge Tests," S.M. Thesis, Department of Civil Engineering, MIT, Cambridge, Massachusetts.

THE CENTRIFUGE AS AN AID TO THE DESIGNER

William H. Craig, University of Manchester, U.K.

The centrifuge in the recently renamed Peter W. Rowe Laboratory at the University of Manchester has been used since its commissioning in 1971 for a wide range of studies, many of which have been allied to site-specific design projects, [Craig and Rowe (1981), Rowe (1983) and Craig (1984)]. For more than a decade this centrifuge has been the machine with the largest purpose-designed geotechnical payload capacity operating in the Western world - 3.5 tonnes to 120 g (structure capable of sustaining 3.5 tonnes to 200 g with more powerful drive system). The philosophy of the Manchester group has been that whilst operating within the limitations of a university environment (as are all three major U.K. centrifuges), such a machine with its unique capabilities should, and can be made available for use in design studies.

If real engineering design problems are to be tackled using centrifuge techniques then the machine and its support team and facilities must be capable of responding within a time period which is acceptable to the overall design team. The centrifuge may fulfill a number of roles; those often quoted include :

(a) determination of mechanisms,
(b) parametric studies,
(c) validation of numerical analyses,
(d) prototype response prediction.

The time span involved will depend on the individual project and the role of the particular model, but there may be need to be a capability to respond to major new initiatives within months rather than years, and to design changes within days or weeks, if the centrifuge is to contribute to the continuous feedback process of design studies. Examples of the way in which a centrifuge has been used in major projects where all the above roles have been described by Rowe and Craig [(1976, 1978, 1980)].

As a university-based machine, the Manchester centrifuge has been supported by

(a) academic staff,

(b) established (permanent) technician and engineering staff,

(c) research students,

(d) contract staff.

Of necessity, academic staff have committments other than to the centrifuge - they are part-timers. Research students whose outlook has both an established target (a higher degree) and a finite time-span, are generally full-time, but this must include significant time spent in literature reviews, analysis and computation. They are in a sense mission-orientated but the restrictions, in the U.K. system at least, make them unsuitable for on-line design projects. We have had, at times, the full time support of one technician dedicated to the centrifuge and the part time support of three other established technicians in the University Soil Mechanics Laboratories - the latter also support teaching and other research. In order to sustain project-orientated activity and major design studies it has been necessary to employ continuously one additional engineer and one or two technicians over the last ten years. The whole group has operated within a single building with addditional backing from the greater resources of a major university department. In order to maintain a viable level of activity with continuity of employment for non-established staff, a contract turnover of around $150,000 per annum has been required.

The Manchester machine can be seen as a forerunner of the latest generation of centrifuges being designed and constructed in a number of countries. The machines have capital investments in excess of $\$10^6$. Such sums are generally put up by organisations funded directly or indirectly by government and it seems reasonable to suppose that the centrifuges are intended to respond to the needs of major designs in the national and international engineering context. In brief, the billion dollar project should be able to gain useful access to the million dollar machine. This requires, in addition to the bare machine, a support structure which can accept the challenges as and when they arise.

REFERENCES

CRAIG, W.H. (1984) : Modelling for site specific prototypes. Proc.Symp. on Application of Centrifuge Modelling to Geotechnical Design, University of Manchester, pp 473-489.

CRAIG, W.H. & ROWE, P.W. (1981) : Operation of a geotechnical centrifuge from 1970 to 1979. Geotechnical Testing Journal, Vol 4, pp 19-25.

ROWE, P.W. (1983) : Use of large centrifugal models for offshore and nearshore works. Geotechnical Aspects of Coastal and Offshore Structures. ed. Yudhbir & A.S. Balasubramaniam, pub. Balkema, Rotterdam, pp 21-33.

ROWE, P.W. & CRAIG, W.H. (1976) : Studies of offshore caissions founded on Oosterschelde sand. Conf. on Design and Construction of Offshore Structures, pp 49-55, Inst. of Civil Engineers, London.

ROWE, P.W. & CRAIG, W.H. (1978) : Predictions of caisson and pier performance by dynamically loaded centrifugal models. Symp. on Foundation Aspects of Coastal Structures, Paper IV.3, pp 1-16.

ROWE, P.W. & CRAIG, W.H. (1980) : Application of models to the prediction of offshore gravity platform foundation performance. Int.Conf. on Offshore Site Investigation, pp269-281, Graham & Trotman, London.

NGC FACILITY AND TRENDS IN COST OF CENTRIFUGES

B. L. Kutter
Department of Civil Engineering
University of California, Davis

THE NGC FACILITY

The National Geotechnical Centrifuge is the largest capacity centrifuge of its type in the Western World. Located at NASA Ames Research Center at Moffett Field, California, the NGC will be open for use by any bona-fide researcher. The capabilities and acceleration goals of the machine are listed in Tables 1 and 2. Figure 1 shows an isometric view of the machine. Several pieces of the data acquisition system and sample preparation equipment of the NGC have been acquired. The data acquisition system consists of a DEC LSI 11/23 computer with an ADAC "Direct Memory Access" analog to digital converter (which digitizes 100,000 data points per second), a plotter, printer, terminal, and an onboard signal conditioning system. A 35 mm camera, two video cameras and high speed movie cameras are available. Bins, hoppers, an overhead crane, and a soil delivery system have also been acquired.

Construction of this large centrifuge was made possible by a grant from NSF along with hardware and engineering support from NASA Ames Research Center. NASA provided an obsolete manned motion simulation centrifuge which could be modified for geotechnical research. It was possible to use the rotunda, slip rings, drive motor, and power supply from the old centrifuge, which greatly reduced the required costs.

After reaching 35 g accelerations in several separate runs, the drive motor thrust bearing failed and caused significant damage. The bearing was carrying loads well within its capacity, but improper lubrication caused a premature failure. Presently, funding is being sought to carry out the repair and completion of the centrifuge.

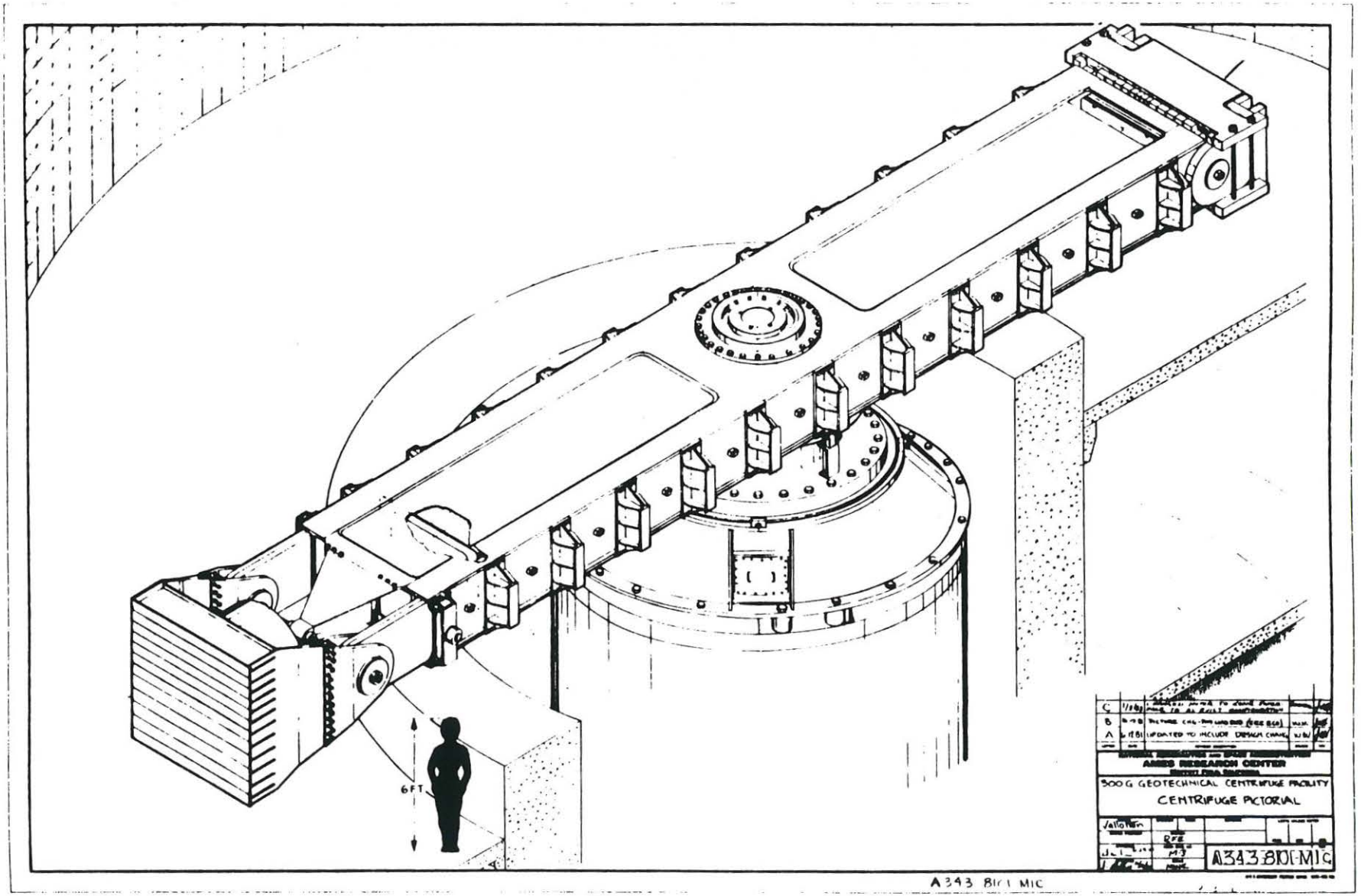

FIGURE 1. Isometric View of the National Geotechnical Centrifuge

Achievement of a 300 g acceleration capability will require significant architectural modifications to improve the aerodynamics of the rotunda in order to reduce power requirements. This may include lowering the ceiling, reducing the radius and smoothing the walls of the centrifuge chamber. Our analyses show that faring the centrifuge arm would be difficult and would only provide secondary reductions in power requirements. Streamlining the arm results in an increase in the relative velocity between the arm and the air so that the power requirements are not reduced in proportion to the reduction in the drag coefficient as may be intuitively expected.

TABLE 1

NGC Capabilities

Payload Capacity	6,000 lb	2,700 kg
Allowable Out-of-Balance Mass (at 300 g)	600 lb	270 kg
Radius to Platform Surface	30 ft	9.2 m
Platform Dimensions	6 x 7 ft	1.8 x 2.2 m
Platform Area	42 ft^2	4.0 m^2

TABLE 2

Acceleration Goals

35 g	achieved December 1983
70 g	goal for February 1984 not achieved due to bearing failure
100 g	can be achieved after bearing repair
300 g	requires aerodynamic modification
2000 g-ton	100 g, 20 ton payload requires new platform and swinging counterweight

The free body diagram in Figure 2 shows the tensile force, F, at the centerline opposing the inertia force of the payload (Nw), and the inertia force on half the arm ($\frac{N}{2}\frac{W}{2}$). The center of gravity of half of the arm in the free body diagram is assumed to be at D/4, where the centripetal acceleration is N/2. Equilibrium gives:

$$F = (\frac{N}{2}\frac{W}{2} + wN) \tag{1}$$

$$F = (w + \frac{W}{4})N \tag{2}$$

where W is the weight of the arm. The minimum cross-sectional area of the arm is related to this force by the allowable tensile stress, σ_{all}

$$F = \sigma_{all}A \tag{3}$$

Eliminating F from (2) and (3) we obtain

$$\sigma_{all}(A) = (w + \frac{W}{4})N \tag{4}$$

We can then multiply both sides by $D\gamma$ giving

$$\sigma_{all}(AD\gamma) = (w + \frac{W}{4})ND\gamma \tag{5}$$

where D = length of arm, γ = unit weight of metal, and $AD\gamma$ is simply the weight of the arm, W. Solving equation (5) for W gives

$$W = \frac{w}{\frac{\sigma_{all}}{ND\gamma} - \frac{1}{4}} \tag{6}$$

This relation indicates that a centrifuge of uniform cross-section approaches infinite weight as $\frac{\sigma_{all}}{ND\gamma}$ approaches $\frac{1}{4}$. For typical high-strength

steel, $\gamma = 500\ lb/ft^3$ and $\sigma_{all} = 30{,}000\ lb/in^2$. The critical value of ND, when the denominator becomes zero, can be determined from

$$\frac{30{,}000\ lb/in^2}{ND\ (500\ lb/ft^3)} = \frac{1}{4} \tag{7}$$

$$ND = 414{,}720\ in \tag{8}$$

for a 30' radius (720" diameter), the critical g-level is N = 576. Again, assuming $\sigma_{all} = 30{,}000$, and $\gamma = 500\ lb/ft^3$, if the model dimension is to be no larger than one-tenth of the diameter, there is a limiting prototype dimension D_p that can be simulated on the centrifuge:

$$D_p = \frac{ND}{10} = \frac{414{,}720"}{10} = 3{,}456\ ft \tag{9}$$

Equation (6) assumes that all the steel in the centrifuge structure acts in pure tension. In reality, a major portion of the centrifuge mass is required to hold the centrifuge up under the 1 g loading of earth's gravity. However, the design of the NGC and other recently designed machines use a scheme that separates the primary centrifugal loads from the 1 g down loads. Centrifugal loads are taken almost in pure tension of straps. Equation (6) probably provides a reasonable estimate of the required weight of tension straps for centrifuges where the centrifugal tension and the 1 g bending loads are de-coupled. However, for all centrifuges the weight determined from equation (6) may be approximately proportional to the actual required arm weight. The equation does serve to indicate the trends in centrifuge weight which in turn can be assumed to be roughly proportional to centrifuge cost.

To obtain a consistent comparison between the costs of three hypothetical centrifuges, let us assume the characteristics listed in Table 3. To approximately account for the fact that the tensile members will be subject to loads other than pure tension, the allowable tensile stress in Table 3 has been reduced to 20,000 psi instead of 30,000 psi as used in the above calculations.

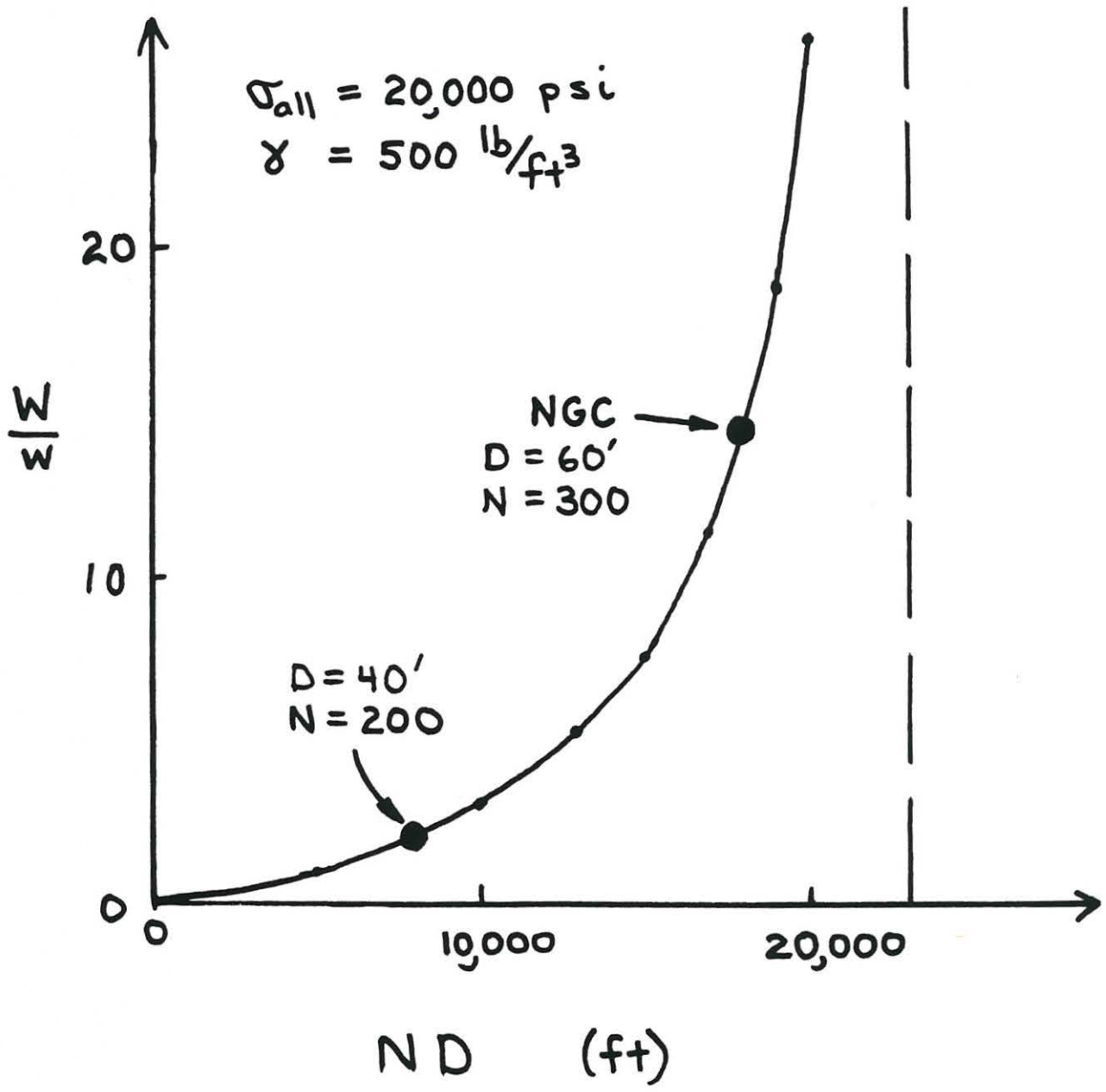

FIGURE 3. Relation Between the Ratio of Arm Weight to Payload Weight and Centrifuge Diameter According to

$$\frac{W}{w} = \frac{1}{\frac{\sigma_{all}}{ND\gamma} - \frac{1}{4}}$$

TABLE 3

Centrifuge	I	II	III
Payload Weight, w (lb)	4,000	6,000	40,000
Centrifuge Acceleration N (g)	200	300	100
Centrifuge Diameter, D (ft)	40	60	60
Density of Structural Material, γ $(\frac{lb}{ft^3})$	500	500	500
Allowable Tensile Stress σ_{all}(ksi)	20	20	20
$\frac{ND\gamma}{\sigma_{all}}$	1.39	3.125	1.04
$W = \frac{w}{\frac{\sigma_{all}}{ND\gamma} - \frac{1}{4}}$ (lb)	8,521	85,700	50,600

The final row in Table 3 indicates that the tension straps for centrifuge II (a 900 g-ton machine) would weigh an order of magnitude more than for centrifuge I (the 400 g-ton machine). Part of the reason for this dramatic increase in centrifuge weight is that centrifuge II is approaching the theoretical limit where, as $\frac{ND\gamma}{\sigma_{all}}$ approaches 4, the centrifuge weight approaches infinity. It is recognized that the selected values of γ and σ_{all} can be altered for various centrifuge designs, but the trends in cost indicated by Table 3 should be valid. Figure 3 illustrates the dramatic rate of increase of centrifuge weight as the factor ND increases.

Power Requirements

Since a large centrifuge requires more power than a smaller one, costs are expected to increase. Consider an element of area dA of the cross-section

of the arm where dA = hdr and h is the thickness of the arm. The torque dT required to push this element through the air is

$$dT = rdF \tag{10}$$

where r is the radius to the element and dF is the drag force on the element:

$$dF = C_D \rho V^2 dA \tag{11}$$

where C_D is the drag coefficient, ρ is the air density, and V is the relative velocity between the arm and the air. If V is assumed to be a constant factor k times the absolute arm velocity,

$$dF = C_D \rho \ (k^2 \omega^2 r^2) \ h \ dr \tag{12}$$

$$T = (C_D \rho \omega^2 k^2 h) 2 \int_0^R r^3 dr \tag{13}$$

$$T = (C_D \rho \ k^2 h) \ \frac{\omega^2 R^4}{2} \tag{14}$$

The power, P, required is simply ωT

$$P = C_D \rho h k^2 \ \frac{\omega^3 R^4}{2} \tag{15}$$

$$P = C_D \rho h k^2 \ (\omega^2 R)^{1.5} \ R^{2.5} \tag{16}$$

which (if C_D, ρ and k are constant) is proportional to what we shall call a power index, P.I.

$$P.I. = hN^{1.5} R^{2.5} \tag{17}$$

where N is the g level. We can again compare hypothetical machines as in Table 4.

TABLE 4

Centrifuge	I	II
Arm Thickness, h	2'	3'
Arm Radius, R	20'	30'
g-Level, N	200	300
P.I.	1.0×10^7	7.7×10^7

The 900 g-ton machine would require approximately eight times more power than the 400 g-ton machine. This factor of eight will cause a similar increase in the costs of the drive motor, power supply, wiring, and architectural treatment to reduce power requirements.

SUMMARY

The calculations in this paper indicate that the weight of a centrifuge increases disproportionately with an increase in the ratio $\frac{NDY}{\sigma_{all}}$. The calculations show that to support the centrifugal loads alone in a machine similar to the NGC at 900 g-tons would require almost ten times as much steel as a smaller radius 400 g-ton machine. Power related costs were also shown to increase by approximately a factor of eight when increasing the capacity from 400 to 900 g-ton and increasing the radius from 20 to 30 feet.

In the initial conceptual stages of the NGC it was realized that the machine may cost about $10 million to build from scratch. Modification of the existing NASA facility allowed considerable savings. NASA has provided the buildings, the drive motor, a power supply, a large slip ring unit, and a large amount of engineering support. This has enabled the facility to nearly reach 100 g capability at a fraction of the cost of starting from nothing. It is important for the geotechnical community to take advantage of the significant contributions made by NASA. It may never again be possible to obtain such a large centrifuge at such a low cost.

THE L.C.P.C. CENTRIFUGE

J.-F. CORTE Head Geotechnical and Soil Mechanics Division # 2
Laboratoire Central des Ponts et Chaussées (France)

Centrifugal testing for geotechnical studies has been practised in France at the Laboratoire Central des Ponts et Chaussées (L.C.P.C.) since 1975. However the experimentations had to be run on the facilities of the Commissariat à l'Energie Atomique (C.E.A.) which were designed for defense applications. In 1980 a proposal to build a new large centrifuge, entirely devoted to geotechnical studies, was accepted and the L.C.P.C. centrifuge should be in operation by the end of 1984.

The main characteristics which define the capacity of this machine are summarized in Table 1.

distance to platform surface		5.50 m
maximum acceleration at 5m radius		200 G
maximum payload	at 100 G	2 000 kg
" "	at 200 G	500 kg
maximum package dimensions	length	1.40 m
	width	1.10 m
	height	1.50 m
run up time to 100 G		180 s

Table 1. L.C.P.C. Centrifuge capacity

THE CENTRIFUGE

The centrifuge was designed by ACUTRONIC Corporation from the specifications defined by L.C.P.C. for performance and operation of the machine. The design of the mechanical parts aimed at avoiding complex states of stresses for a good understanding of all the efforts in the most highly strained regions. Moreover to limit the uncertainties in ageing brought by the manufacturing process, all parts are free from welding except the platform and the bearing support. Figure 1 shows a general view of the centrifuge and its drive unit.

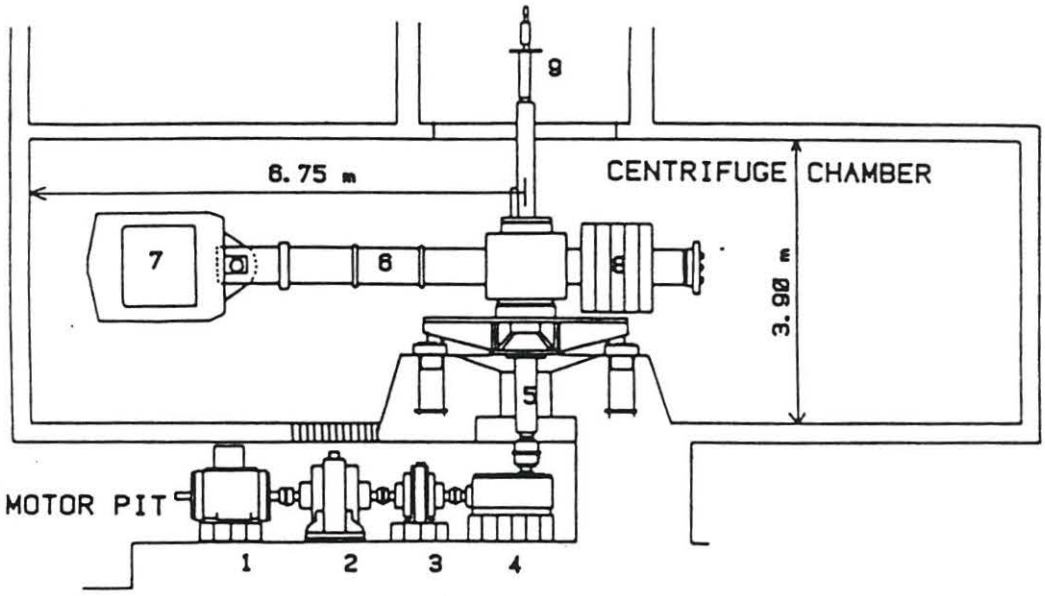

1. AC MOTOR
2. EDDY CURRENT CLUTCH
3. EDDY CURRENT BRAKE
4. GEAR BOX
5. DRIVING SHAFT
6. ROTOR ARM
7. COUNTERWEIGHTS
8. SWINGING BASKET
9. SLIPRING STACK

Figure 1. L.C.P.C. Centrifuge. Machine and drive unit

The swinging basket

Its design had to conciliate antagonistic objectives : low mass, high rigidity and large openings allowing easy access to the model package and photographic observation of the rear face of the model in flight. (Figure 2). Finite element analyses were made to improve the design.

The platform has a honeycomb welded structure ; its stiffness limits the deflection to less than 1 mm under maximum load. The swing arms are machined from steel plates 100 mm thick.

In order to reduce aerodynamic forces, the swinging basket is covered with fairings designed from model tests with a small centrifuge at a 1/19 scale.

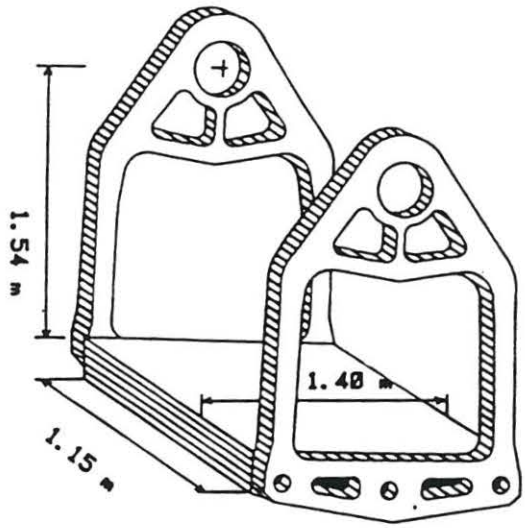

Figure 2. Swinging basket without its fairings

The rotor and its support

The rotor arm is dissymetrical to reduce power requirements (Figure 3). It is made from two cylindrical solid blanks of steel (0.50 m in diameter, 6.50 m long, mass 6800 kg).

On the basket side the bars are bored to reduce their weight and are machined to support the sperical bearing of the swinging basket. The opposite portion is threaded for the displacement of the counterweights.

These two cylinders are fixed to the central box by four compression rings. The rotor is connected to the vertical driving shaft by a diaphragm.

The counterweights are made of five cast iron plates of 3500 kg each. The balance is adjusted by displacement along the threaded portion of the arm.

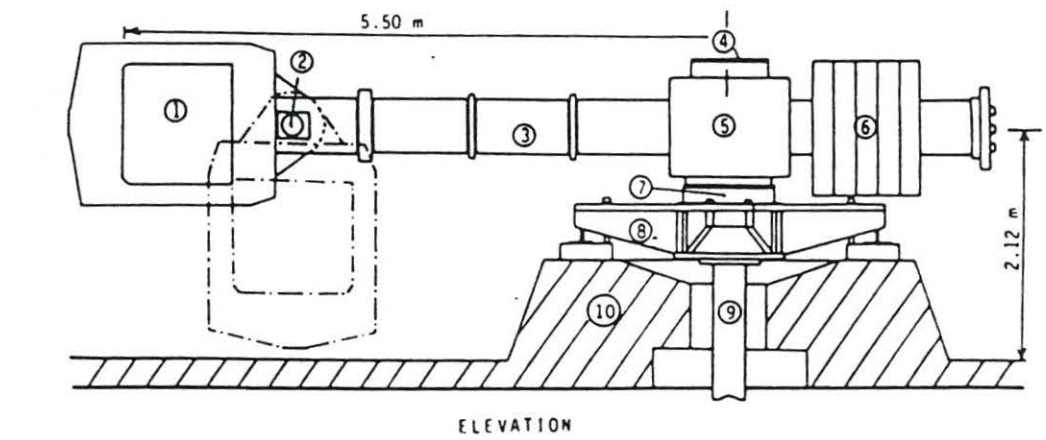

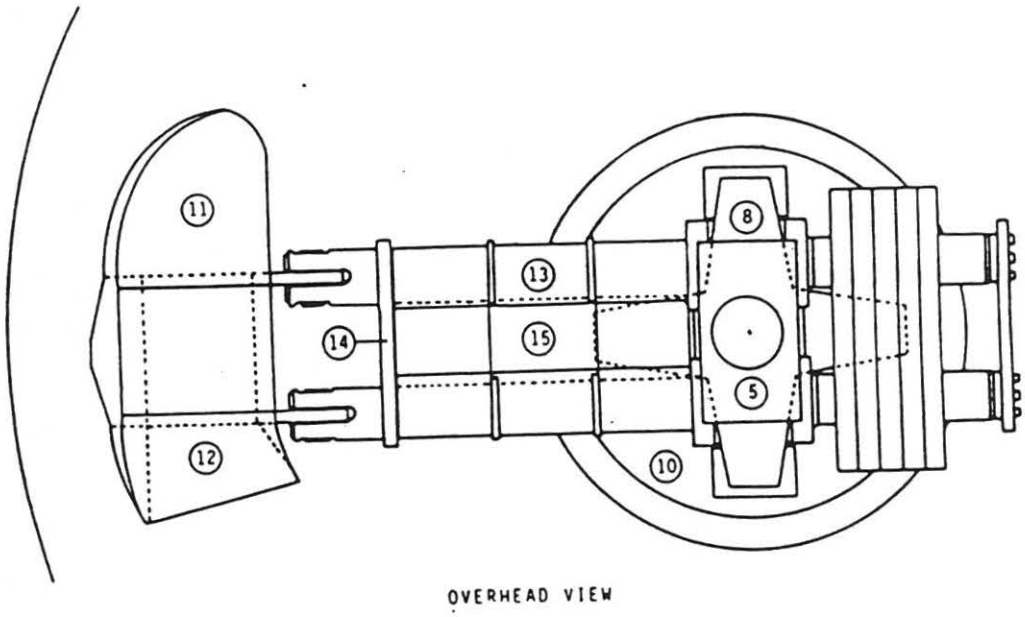

1. Swinging basket
2. Spherical bearing
3. Rotor arm
4. Diaphragm
5. Central driving box
6. Counterweight
7. Bearing shaft
8. Support
9. Driving shaft
10. Concrete base
11. Basket front shroud
12. Basket rear shroud
13. Arm tube
14. Brace
15. Hinged lid cover

Figure 3. Elevation and overhead drawings of the L.C.P.C. Centrifuge

The hollow bearing shaft carries three roller bearings. The radial forces act on two barrel-shaped roller bearings placed symmetrically with respect to the medium plane of the rotor. The gravity load is carried by a third taper roller bearing placed underneath. The bearing shaft is welded to a four-arm base.

To drive unit

The drive system consists of four elements : a constant speed electric motor, an eddy current clutch, an eddy current brake and a gear box. This solution has been selected mainly because it generates a minimum of electric interferences.

The A.C. motor has two speeds for better efficiency and lower running costs. Its characteristics are given in table 2.

number of poles	4	6
rotating speed at full load	1 480	985 rpm
nominal power	410	170 kW
efficiency at full load	94	94,8 %
nominal torque	2 645	1 650 Nm
maximum torque	4 760	5 110 Nm

Table 2. Characteristics of the dual speed motor

DATA ACQUISITION SYSTEM, OBSERVATION AND OPERATION ON THE MODEL

Data acquisition

Different lines are provided to transfer data exchanges between the model mounted on the swinging platform and the control room, via sliprings. Two different configurations are available (Figure 4).

In the first case, a 100 channel H.B.M. acquisition chain is fixed on the rotor near the central shaft. Analog signals from the transducers placed on the model are sampled, digitized and stored. The results are then transmitted to the computer in the control room via a IEEE 488 line with HP-IB extender via only one high frequency slipring. The acquisition frequency is about 20 channels/s.

In the second configuration the analog signals transit directly via the 100 low noise sliprings to analog recorders in the control room. The twenty coaxial lines have a bandwidth of more than 10 Mg Hz, and the eighty two-conductors armored lines can transmit signals of 1 Mg Hz.

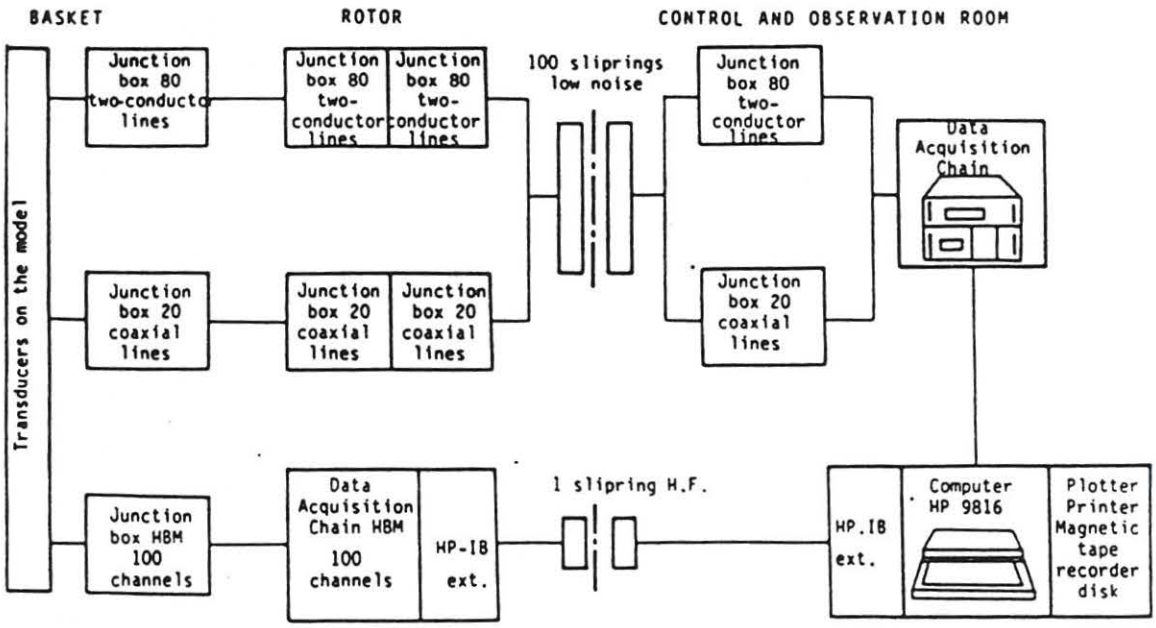

Figure 4. Organization of the data acquisition system

Observation of the model

Three television cameras are used : two survey the centrifuge chamber, the third one is fixed on the rotor arm and gives a continuous overhead view of the model.

The rear face of the model can also be photographed in flight from a small room adjacent to the centrifuge chamber.

Operations on the model

Various tools and equipments to load foundations, to build embankments or to excavate in flight are presently under study.

Electric energy is supplied to equipments mounted on the model or on the rotor arm by five power sliprings (3 phases, 1 neutral, 1 earth). Six rotary joints (two high pressure 20 MPa, four low pressure 1 MPa) are also available for the command of hydraulic or pneumatic devices.

Figure 5 shows the general arrangement of the service lines.

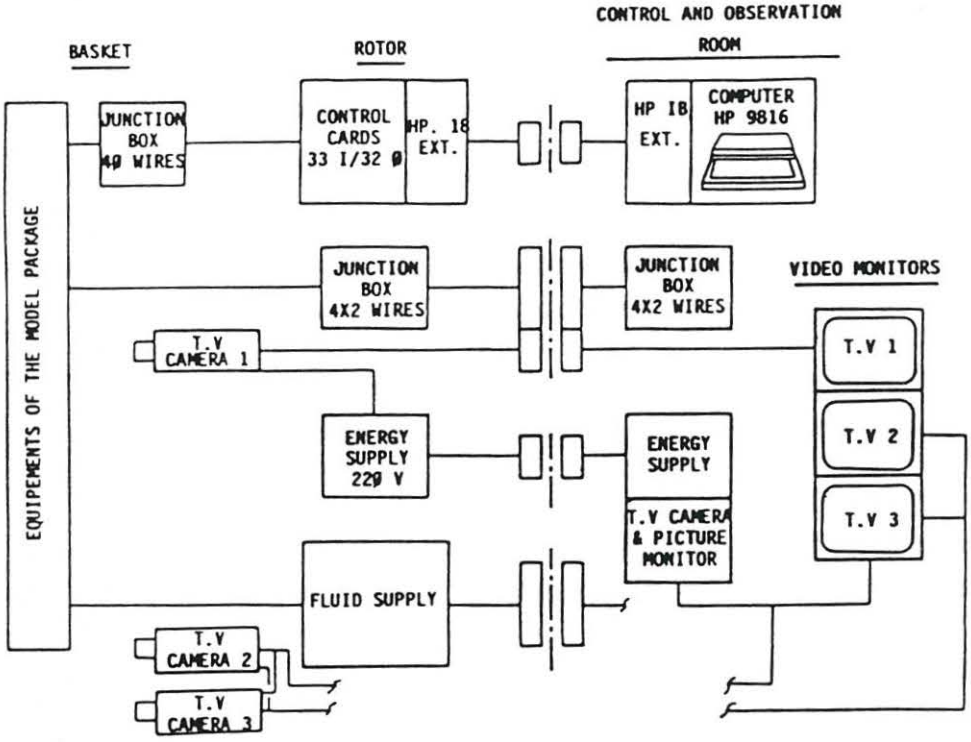

Figure 5. Service lines for observation an operations on the model in flight

THE CENTRIFUGE BUILDING.

The centrifuge is built on the Nantes Center site of the L.C.P.C. in a special building shown by Figure 6. For a convenient use all the facilities have been placed together : from the soil preparation laboratory to the centrifuge chamber ; these rooms are also at the same level. The centrifuge chamber which houses the rotor is 13.5 m in diameter and almost 4 m high. For safety, the reinforced concrete wall is surrounded by an embankment 6 m thick.

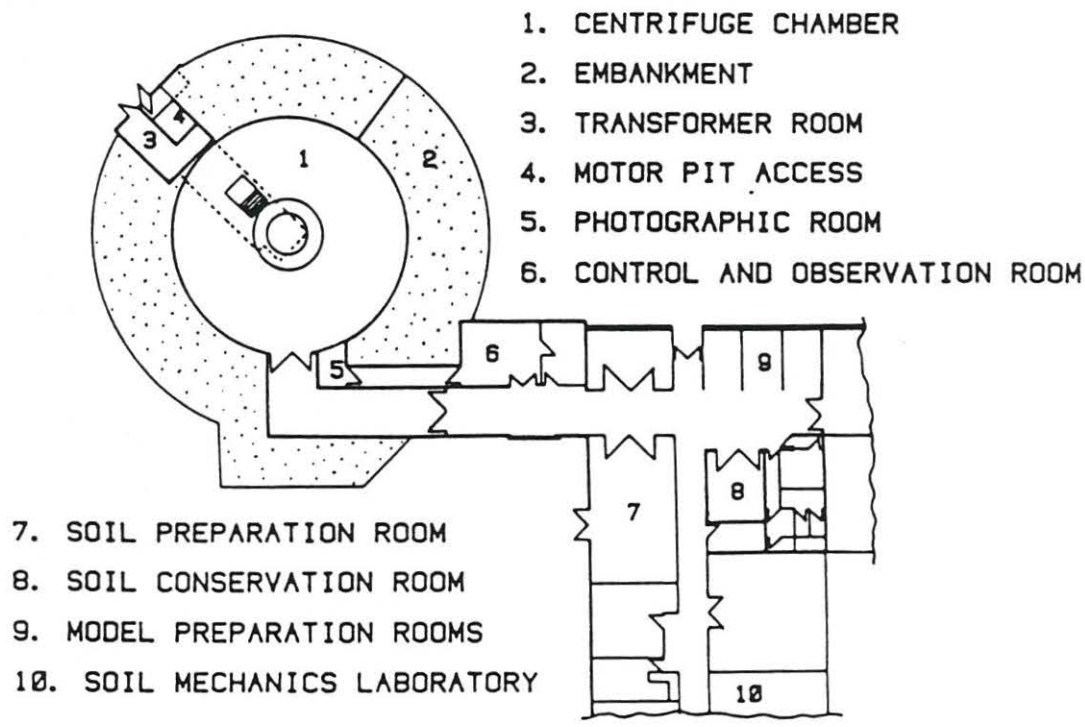

Figure 6. L.C.P.C. centrifuge facilities

ABSTRACTS I

THE PHRI GEOTECHNICAL CENTRIFUGE

by

M. Terashi
M. Kitazume
H. Tanaka

Port and Harbour Research Institute
Yokosuka, Japan

ABSTRACT

A large scale centrifuge was installed in the Port and Harbour Research Institute, Ministry of Transport for geotechnical studies in the March of 1980. Various data acquisition system including photo-instrumentation and surrounding facilities were completed in the following two years. This is the largest centrifuge among four active ones existing in Japan (i.e., Osaka City University, Tokyo Institute of Technology, Chuo University, and PHRI).

In the article, details of the centrifuge, current research projects and scope of the future are described with brief comment on the already published test results. A summary of major specifications is listed is Table I.

Paper included in the Proceedings of International Symposium on Geotechnical Modeling, in Tokyo, in April of 1984.

TABLE I

Major Specifications

Maximum acceleration (G)	115
Diameter of rotating arm (mm)	9650
Maximum effective radius (mm)	3800
Maximum number of rotation (rpm)	185
Space of swinging platform (mm)	1600x1600
Maximum payload (kg)	2710
Maximum G-tons	300
Main motor (kW)	400
Electric slip rings (poles)	80
Rotary transformer (kVA)	5.2
Number of hydraulic joints (ports)	10
Total weight of the centrifuge (t)	87

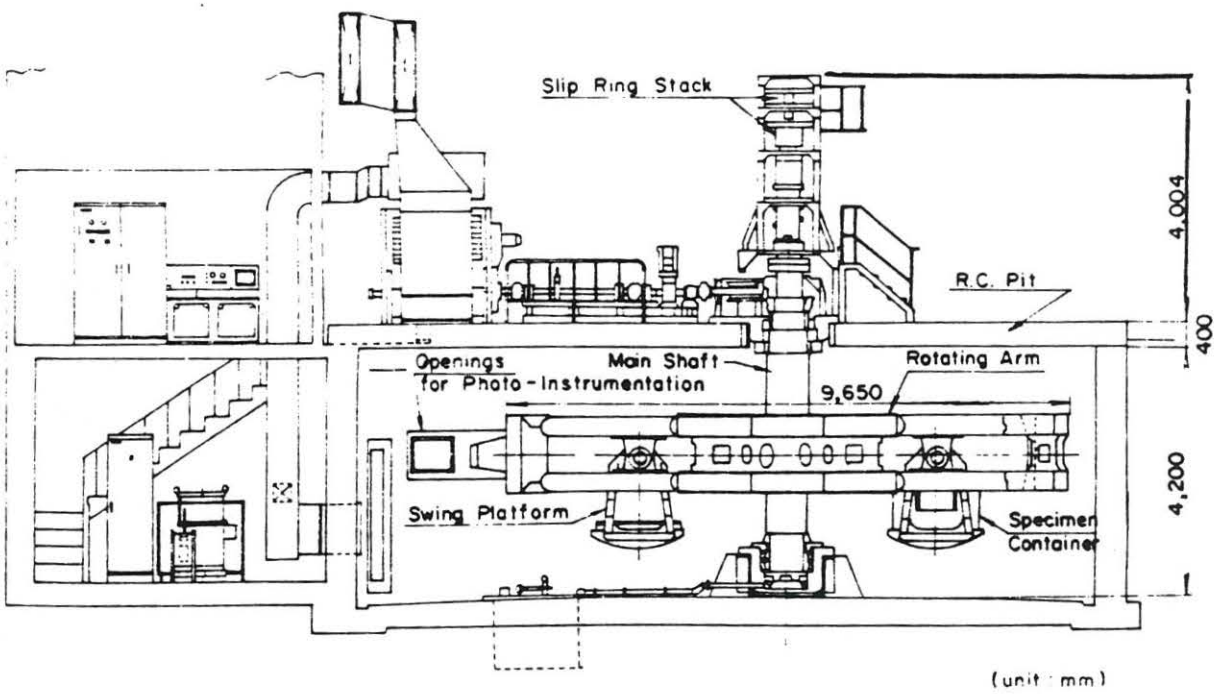

FIGURE 1. PHRI Geotechnical Centrifuge

DESIGN CHARACTERISTICS OF THE BOCHUM GEOTECHNICAL CENTRIFUGE AND POSSIBLE FIELDS OF RESEARCH

Hans L. Jessberger
Ruhr-University, Bochum

ABSTRACT

1. Design Characteristics

At the end of 1983 the Deutsche Forschungsgsgemeinschaft (DFG) granted funds for the Bochum Geotechnical Centrifuge. The centrifuge is now under construction and it is planned to have it in operation in the summer of 1985. Figure 1 shows the design principles with the following details:

- Swinging buckets
- Effective radius to the platform: 4.125 m
- Platform area: 1.25 x 1.25 m. In one direction the area is expandable to 2 m
- Payload: 2,000 kg
- Maximum acceleration: 250 g which gives a capacity of 500 g tons
- The centrifuge is driven by 3 hydraulic motors with a maximum power of 400 KW
- The aggregates are located in a separate room beside the centrifuge
- There will be a circular pit with an inner diameter of 9.50 m. The centrifuge building is partly inground placed on hard rock
- The slipring tower has 120 low current sliprings, 6 high current sliprings, 12 sliprings for water, air and chilled brine, and 1 slipring for LN_2 as coolant

The centrifuge is located adjacent to an existing building of an abandoned coal mine (Figure 2 and 3). This building has a large hall in which several soil mechanics test machines are in operation. There is also a test pit inside the hall. The free height to the crane is 6 m.

The ground plan (Figure 3) shows the arrangement of the centrifuge related to the already existing soil mechanics laboratory of about 500 m^2 area. In the center of this area is a cold room which can be cooled down to -20°C.

The centrifuge building is located outside of the Ruhr-University campus but within walking distance. Heavy equipment is transported between campus and centrifuge by car which needs about 5 km.

2. Intended Fields of Research

The design of the centrifuge allows to simulate the conditions in 300 m depth of the prototype or to investigate the behavior of a prototype with a horizontal length of 500 m.

The centrifuge is equipped with a device to cool or heat models. It is possible to change the temperature field during flight by cooling down to -196°C or by heating up to +200°C.

In the following intended fields of research are summarized:

a) Frozen soil engineering
   - Frozen soil supporting inground opening such as shafts, tunnels, etc.
   - Buried LNG storage tanks

b) Cold regions engineering
   - Simulating of frost heave and thaw effects on pipe lines
   - Thaw consolidations
   - Stability of slopes in permafrost

c) Ice engineering
   - Impact of flowing ice sheets and ice islands on structures
   - Shafts or tunnels in a deforming ice shelf in the Antarctica

d) Research projects in relation to mining activity

- Deep shafts
- Tunnels and galleries
- Open pit mining
- Caverns in salt rock for nuclear waste disposal schemes

e) Transfer of 1 g dynamic test results to flying models

- Impact loading - dynamic consolidation
- Cyclic loading using open and partly drained systems

PART II

QUASI-STATIC APPLICATIONS

EVALUATION OF A CONSTITUTIVE MODEL FOR SOFT CLAY USING THE CENTRIFUGE

BY

R.Y.K. Liang, E.C. Tse, M.R. Kuhn, & J.K. Mitchell
Department of Civil Engineering
University of California, Berkeley

Prepared For The Symposium on
Recent Advances In Geotechnical
Centrifuge Modeling

held at the
Center for Geotechnical Modeling
University of California, Davis

July 1984

ABSTRACT: A general constitutive model has been formulated which may provide a rational method for prediction of the time-dependent performance of embankments on soft clay foundations, with due consideration for creep effects during the undrained, consolidation, and fully drained stages. Tests on embankment type soil structures are being performed on the U.C. Davis Schaevitz Centrifuge to measure the time-dependent pore pressure and deformation behavior for comparison with predictions made using the constitutive model. This paper inlcudes descriptions of the building, testing, and monitoring of the centrifuge models. The results of the centrifuge tests are compared with predictions made using a simplified form of the constitutive model.

Centrifuge testing is valuable for investigating the accuracy and usefulness of new soil behavior models, particularly in the absence of or as a supplement to detailed field records. The unique conditions imposed by the centrifugal environment, such as stress history, stress path, geometry, and curved "gravity" field can be properly accounted for in numerical analyses. Further, careful model preparation minimizes the uncertainty concerning the value and spatial variation of soil properties.

INTRODUCTION

A general time-dependent constitutive model considering the combined effects of creep and hydro-dynamic consolidation of soft clays was formulated by Kavazanjian and Mitchell (1977, 1980). Later, Bonaparte (1981) extended the model to acount for plane strain conditions and other important factors including anisotropy and creep pore pressure response. The model has been shown to predict well the results of triaxial and plane strain tests, using various stress paths, on both remoulded and undisturbed San Francisco Bay mud. Moreover, the model was successfully used to make blind predictions as a part

of the NSF/NSERC workshop held in Montreal (Kavazanjian et al., 1980). The true capability of the model for use in more complicated field problems has yet to be evaluated, however. Field loading situations represent much more complex geometric and stress conditions than are the case for laboratory specimens subjected to uniform boundary loadings. Thus, to evaluate more fully the usefulness of the model, centrifuge model testing and well-documented field case studies are helpful. This paper describes a centrifuge test program, still in progress, that is designed for this purpose.

The centrifuge provides a controlled environment in which prototype structures can be studied as scaled-down models, while preserving the stress states required to develop the appropriate soil properties. Table 1 lists some advantages and limitations of centrifuge testing for geotechnical studies. Although the modelling of actual structures may be uncertain, the conditions imposed by the centrifugal environment, such as stress history, stress path, curved gravity field, and boundary constraints, can be readily accounted for by treating the test as a real event and incorporating these conditions in analysis procedure. Thus, centrifuge testing is well suited for the study of deformation and failure phenomena and for the evaluation of constitutive models.

CONSTITUTIVE MODEL

The time-dependent constitutive model proposed by Kavazanjian and Mitchell (1977) has been updated over a period of several years to account for various factors affecting the behavior of clays. A current version of the model which has been coded into a finite element computer program SPIN2D was developed by Borja (1984). Only the principles of this formulation are described herein; details can be found in Borja (1984).

The constitutive model is applicable for "wet" clays (i.e. normally consolidated to lightly overconsolidated) of low to medium sensitivity. Deformation is separated into two components: time-independent (or immediate) and time-dependent (or delayed) as suggested by Bjerrum (1973). The time-independent, immediate component assumes an elasto-plastic, strain-hardening material that follows the Modified Cam Clay yield surface and the associative flow rule developed by Roscoe and Burland (1968). The time-independent deviatoric behavior is modeled by projecting the Modified Cam Clay model into the deviatoric stress-strain (q-γ) plane and assuming it to take on a hyperbolic shape.

For the time-dependent delayed component, the model assumes that both the Modified Cam Clay yield surface and the associative flow rule can be used to generate the delayed strain rate tensor. The validity of this assumption has been shown by laboratory test results obtained by Bonaparte (1981). Two approaches for generating the creep strain rate tensor are used. The first is to use the conventional volumetric creep equation for secondary compression and to scale it using the Modified Cam Clay yield surface and the associative flow rule. The second is to use the deviatoric creep function of Singh and Mitchell (1968) and similarly to scale it as above. For brevity, the first approaches is called "C_α scaling" and the second "SM scaling".

Consideration of time-dependency requires that the yield surface expand not only as a result of increase in stress (as in conventional strain-hardening plasticity) but also due to increase in time, i.e. quasi-preconsolidation or aging. The time-state relationship is described by two age variables. The volumetric age t_v is evaluated by determining how far in the void ratio e direction a state point is from the immediate state boundary surface in e-p'-q space. On the other hand, the deviatoric age t_{dev} is obtained by determining

the distance of a state point in the shear strain γ direction from the immediate deviatoric stress-strain curve in the q-γ plane.

A total of 11 soil parameters, as listed in Table 2, is required. The parameters can be determined from conventional triaxial laboratory tests as shown in the table and, in principle, only two triaxial tests are needed to generate them. An isotropically consolidated undrained triaxial compression (ICU) test with pore pressure measurement can be used to determine all parameters except the Singh-Mitchell creep parameters. The Singh-Mitchell parameters can be obtained from a single-multiple increment creep test using the superposition procedure outlined by Singh and Mitchell (1968). In practice, however, additional test results would be desired to improve confidence in the values obtained.

CENTRIFUGE EXPERIMENTS

Several models of a sand embankment on a clay foundation were tested using the U.C. Davis Schaevitz centrifuge. This centrifuge has a radius of approximately 3 ft and an allowable payload of 10,000 LB-G, as described by Houston (1978). During the centrifuge tests, both deformations and pore pressures were measured to provide data for comparison with numerical predictions.

Materials - A kaolinite clay of low plasticity was chosen as the foundation material because of its relatively high permeability and the consequent shorter time required for consolidation. Classification properties of the material are: specific gravity, 2.61, liquid limit 34%, platic limit 12%, plasticity index, 22%. It contains 25% sand size, 40% silt size and 35% clay size particles by weight and is classified as (CL) in the Unified System.

Series of triaxial tests (ICU) and undrained creep tests (ICUC) were performed to determine the required model parameters. The values of the parameters obtained from the results of these tests are listed in Table 2.

Monterey 0 sand was used to construct the embankment and a drainage blanket. The properties of this sand have been well documented by Lade (1971) and are summarized in Table 2.

Model Geometry - The models consisted of a drainage boundary at the bottom, a layer of soft clay foundation overlain by a saturated sand blanket, and the sand embankment,as shown in Fig. 1. Because of space limitations, only half of a symmetrical embankment and foundation system was modelled.

Apparatus - A strong box with inside dimensions of 16-1/2 in. x 8 in. in plan x 12 in. in height was built to contain the model. A transparant plexiglas plate was used as one of the side walls of the box to enable side viewing of the sample container during testing. The other walls were aluminum plates lined with teflon to minimize side friction and adhesion. Similarly, a thin layer of silicon grease was spread on the plexiglas for the same purpose. The box was sufficiently rigid to maintain plane strain conditions in the model.

Model Construction - The model's clay foundation was prepared by press consolidation of a thoroughly mixed slurry (initial water content w_i = 90%) in the model container. A 4 psi consolidation pressure was used to produce a clay cake that was sufficiently strong for later installation of measurement sensors. The top sand blanket was constructed by deposition of sand under water followed by static densification to a specified void ratio. The sand embankment was built inside a template in layers.

Instrumentation - Pore pressures developed in the foundations were measured with five miniature semiconductor pressure transducers (manufactured by Entran,

EPB-125 Series). The stainless filters were secured by heat shrinkable plastic tubing on top of the transducer diaphragm to filter soil particles. Care was exercised to properly de-air the transducer before inserting it into the clay foundation.

The transducers were installed as follows. First, horizontal holes in the foundation clay were drilled by a auger. The holes were then backfilled with thin slurry that was injected using a long syringe. This was followed by insertion of a de-aired transducer. Each transducer was oriented with its pressure sensitive area parallel to the direction of acceleration forces to minimize any effects the centrifugal forces might have on its response. In a calibration test using only water in the model box, transducer sensitivity proved constant over the test G range.

Deformations in the foundation clay were determined by a photographic method. Through an angled mirror arrangement, a remote-control camera mounted on the centrifuge arm recorded movements of plastic marker beads implanted on clay surface in a 1 in x 1 in grid pattern. The coordinates of markers on each photo negative were digitized and stored using a comparator. Deformations that occurred between any two frames could then be calculated using a data reduction program (Britto, 1980).

Test Procedure - After construction of the model and installation of instruments, the model container was placed in the swing-up basket. Both static and dynamic balance were established before activating the centrifuge.

The centrifuge test consists of two stages, as schematically shown in Fig. 2. The first stage, called the re-initialization stage, was intended to re-establish the past maximum consolidation pressure on the foundation material. The second stage was used to further load the clay. The length of Stage I was

purposesly chosen to be long enough to ensure full dissipation of all excess pore pressure before commencing the loading stage.

TEST PROGRAM AND RESULTS

At the time of writing, two series of centrifuge model tests have been performed: (I) a series of tests on models having the same geometry and loading conditions, and (II) a series of modeling of model tests. Detailed descriptions of the test program are given by Mitchell and Liang (1984). The results from these tests were evaluated using a simplified version of the constitutive model and a computer program, CON2D, originally developed by Chang and Duncan (1977). As the analysis using the SPIN2D computer program to evaluate Series II tests has not yet been completed, only the results of Series I tests are presented herein for comparisons with predictions using the complete constitutive formulation.

The measured pore pressures of two transducers during Stage II are shown in Fig. 3; Stage II began 84 minutes after the start of Stage I. The observed vertical settlements at two representative locations in the foundation clay are plotted against time and shown in Fig. 4.

ANALYSIS AND COMPARISONS

Fig. 1 shows the mesh and boundary conditions used to represent the model for finite element analysis. The acceleration-time history of the centrifuge test was reproduced in the FEM computations. The clay soil was represented in the finite element mesh by quadrilateral elements, each with nine displacement nodes and four pore pressure nodes (Q9P4 elements); whereas, the sand blanket and embankment were represented with nine displacement node quadrilateral elements (Q9P0 elements). The sand embankment and drainage layer were modeled

in progress to explore other possible causes of the observed discrepencies. Nevertheless, the model accurately described the time-dependent deformations. It is also apparent that creep does play a significant role in the magnitude of these deformations, as may be seen by comparing the curves for analyses with and without creep in Fig. 4. The differences between the analysis that did not account for creep deformation and the analysis that included creep by C_α scaling can be as high as 25% to 30%.

CONCLUSION

A time-dependent constitutive model which considers the combined effects of creep and hydro-dynamic consolidation is being evaluated by comparing centrifuge test results with numerical FEM predictions. Three sets of analysis have been performed: two of them considered creep strains (SM scaling and C_α scaling) and one in which the creep strain effect was neglected. The results of the comparisons suggest that:

1) For relatively permeable and low plasticity clay materials, creep does not play a significant role in pore pressure response. Analyses that either used SM scaling or neglected creep altogether, provided very satisfactory predictions.
2) Creep strains are significant contributions to the total time-dependent deformations. For the kaolinite tested, C_α scaling analysis provided a better prediction of consolidation deformations; whereas, SM scaling analysis seemed to underpredict the rate of creep strains and thus the total deformations.
3) The constitutive model underestimates immediate deformations but predicts long-term delayed deformations well.

4) Overall, the agreement between the predicted and observed behavior was good, thus adding further support to the concept of summed immediate and delayed deviatoric and volumetric components that are computed using readily determined soil properties.

5) Centrifuge testing proved to be a viable tool for studying predictive models of soil behavior.

ACKNOWLEDGEMENT

This work was supported by the National Science Foundation under Grant Number CEE-8203563. This support is gratefully acknowledged. The writers thank Professor James A. Cheney and Professor C. K. Shen of the University of California at Davis for their assistance during the experimental work; and Professor Edward Kavazanjian, Jr. and Dr. Ronaldo Borja of Stanford University for developing the FEM program used in this investigation.

TABLE 1

ADVANTAGES AND LIMITATIONS OF CENTRIFUGE TEST

Advantages:

* Boundary conditions (both deformation and drainage) are well defined.
* Spatial variations and uncertainties of material properties can be minimized by careful model preparation.
* The effects of various stress histories, stress paths, and geometry conditions can be easily studied.
* Time-dependent problems such as consolidation can be studied in a short period of time.
* Measurement of responses such as deformation and pore pressure variations are easy and accurate.

Limitations:

* Careful model construction procedure are required to simulate the prototype structure.
* The gravity field in the centrifuge is radial and the vertical stress distribution deviates from a straight line stress distribution.
* Boundary restraints may distort the actual behavior of the model.

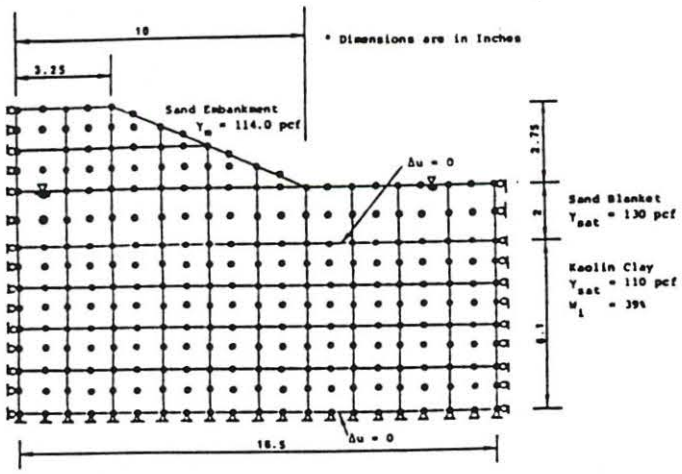

Fig. 1 Model Configurations

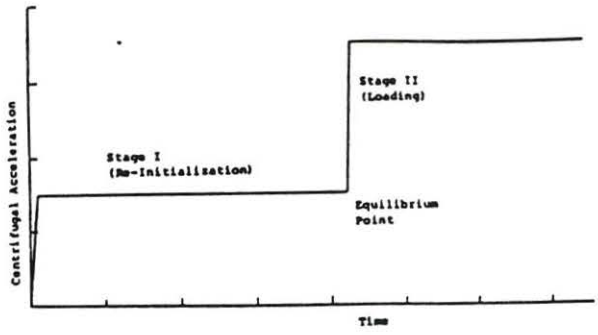

Fig. 2 Centrifuge Testing Procedure

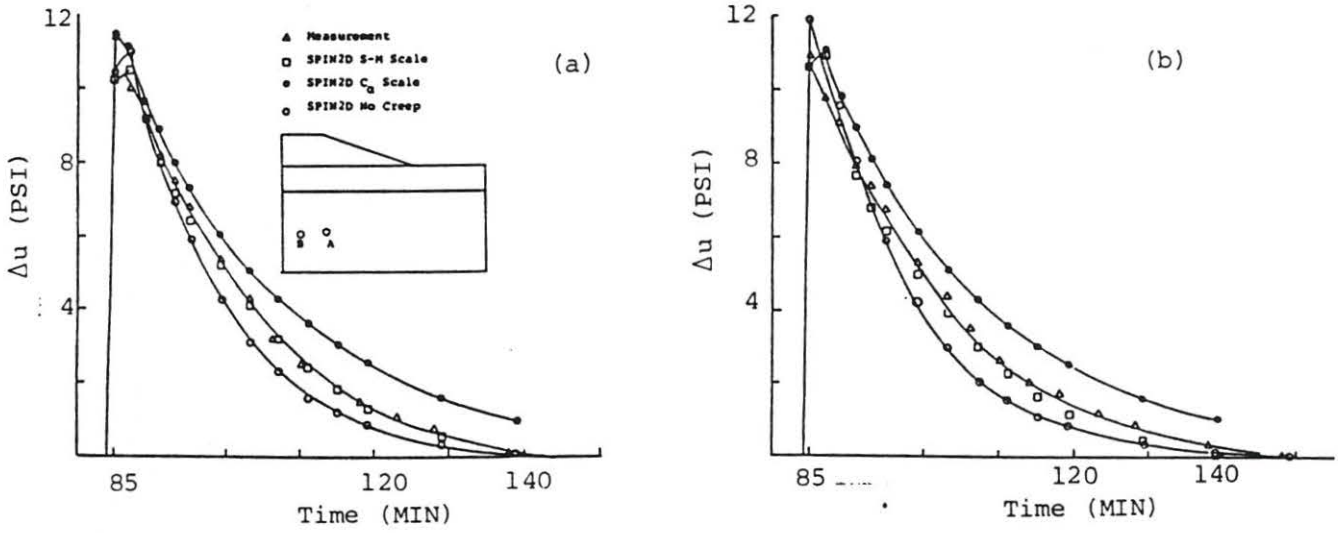

Fig. 3 Comparisons of Pore Pressure Response

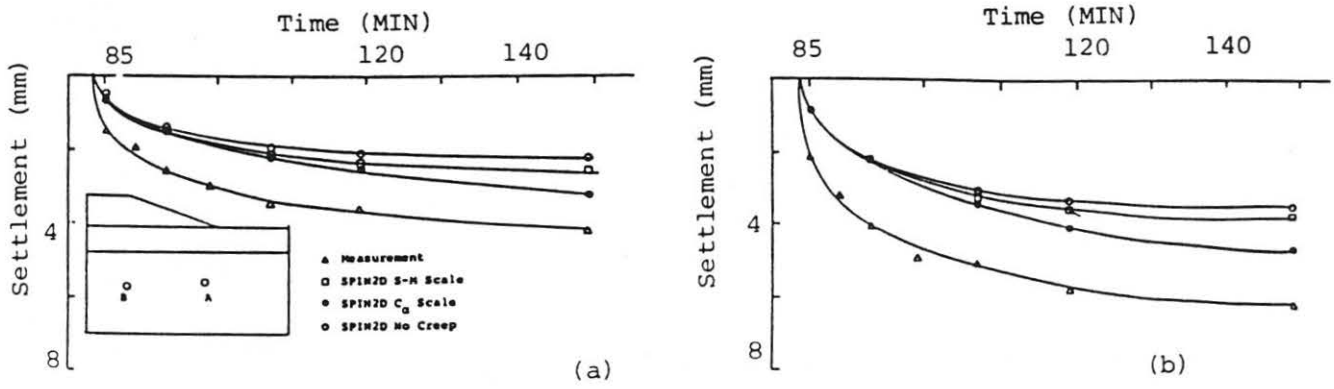

Fig. 4 Comparisons of Vertical Settlement

"Centrifugal Modeling of Subsidence of Landfill Covers"

by

Harry J. Sterling
Assistant Professor of Civil Engineering
University of Kentucky
Lexington, Kentucky 40506-0046

Michael C. Ronayne
Graduate Student
University of Kentucky

Volume reduction and settlement of wastes in controlled and uncontrolled burial sites may result in subsidence of the soil cover system. Following subsidence, water flow through the cover may rise dramatically due to piping through tension cracks in the cover and ponding over depressed areas. This water, which becomes contaminated, can then pose a hazard to the local groundwater if leakage through the bottom liner system takes place. The design and construction of cover systems which reduce the adverse effects of subsidence is an important step in reducing the potential for groundwater contamination.

A centrifugal modeling procedure for laboratory study of landfill cover subsidence was developed at the University of Kentucky in an EPA-sponsored investigation of the hydrologic integrity of multi-layered landfill covers under stable and subsidence conditions. During the summer of 1983, funds from the study were used to construct a 1.14 m (3.75 ft) radius centrifuge capable of accelerating a 27 kg (60 lb) sample to 100 G's. Two field scale landfill covers were constructed in central Kentucky and serve as prototypes for the centrifugal modeling.

The prototypes' 61 cm (24 in.) thick cover layer is modeled in the laboratory at 1/24 scale. While being accelerated, the clay model layer is supported on a 28.5 cm (11.5 in.) diameter, rigid aluminum disk within a cylindrical container constructed of aluminum and plexiglass. Several molds have been formed to simulate depressions (and thus subsidence) of various amounts. These depressions simulate cavities ranging from 0.61 m to 4.9 m (2 to 16 feet) in diameter. The mold is beneath the model layer and connected to the aluminum disk. The container is equipped with a gauge to determine the magnitude of subsidence with time.

The testing procedure consists of: 1) preparing the 28.5 cm (11.5 in.) diameter, 2.5 cm (1 inch) thick model cover layer to a specified moisture content and compaction density; 2) selection and placement of a mold into the cylindrical container; 3) filling the depression in the mold with lead shot and then placing the model layer on it; 4) measuring the surface profile of the clay layer; 5) placing lead shot onto the top of the model layer to simulate other soil layers above it; 6) attaching the container and a counterweight to opposing arms of the centrifuge; 7) accelerating the specimen to 24 G's and maintaining this acceleration for a period of time sufficient to allow the excess pore pressures to dissipate; 8) simulating subsidence by releasing (using a solenoid valve) the lead shot in the depression of the mold; 9) measuring, with the gauge, the movement of the clay layer surface with time; 10) decelerating the container; 11) removing the container; 12) taking a profile of the surface; and 13) photographing both sides of the specimen and taking samples for determination of the soil's properties. The studies are being conducted to investigate the effects of soil moisture content and density, soil composition, soil chemistry, and cavity diameter on subsidence.

RECENT ADVANCES IN GEOTECHNICAL CENTRIFUGE MODELING

Center for Geotechnical Modeling

University of California, Davis

July 18-20, 1984

A Centrifuge Modeling Procedure for Landfill Cover Subsidence

by

Harry J. Sterling[1] and Michael C. Ronayne[2]

Department of Civil Engineering

University of Kentucky

Lexington, Kentucky 40506-0046

EPA Grant No. CR-810431-02

ABSTRACT

Trench cover subsidence has been a common and damaging form of landfill cover failure. It results from void filling and volume reduction of buried waste materials and takes the form of depressions, tension cracks, and potholes in landfill covers. Following subsidence, water flow through the affected cover may rise dramatically due to tension crack seepage, ponding over depressed areas, and direct flow through potholes. Water that reaches the waste material will become contaminated and may threaten ground and surface water supplies if leakage occurs through the surface cover or the bottom liner system.

This paper describes a geotechnical centrifuge and an experimental procedure, that were developed at the University of Kentucky, for testing scale model landfill cover systems under subsidence conditions. The study was part of an EPA sponsored investigation of the hydrologic response of multi-layered landfill covers. Two field scale cover systems, consisting of 2 ft layers of compacted clay, sand, and topsoil, were constructed, and modeled in the laboratory at 1/24 scale. A 1.14 m (3.75 ft) radius, swinging bucket centrifuge, capable of accelerating 27 kg (60 lb) samples to 100 G's, was designed and built for the study. The effects of subsidence were reproduced by forming cavities beneath model covers during centrifugation.

Initial model tests have been conducted with the silty clay soil that was used to construct the prototype clay layer. The sand and topsoil layers were assumed to provide no resistance to subsidence and were modeled by a lead shot surcharge. Preliminary data has been collected for: (1) the largest (critical) cavity diameter that can be spanned by model clay layers compacted at moisture contents below, equal to and above optimum; (2) the time to cover failure (cracking or collapse) when the critical cavity diameter is exceeded; (3) qualitative estimates of the degree to which cracking vs. plastic flow of the clay layer occurs when the critical cavity diameter is exceeded; and (4) predicted behavior of the test plots under subsidence conditions.

---

1 Assistant Professor of Civil Engineering, University of Kentucky, Lexington.

2 Research Graduate Assistant, Dept. of Civil Engineering, University of Kentucky, Lexington.

INTRODUCTION

Subsidence

Proper design, construction and performance of a surface infiltration barrier (trench cover system) is integral to a properly functioning waste landfill. However, buried waste materials do not typically provide a stable support structure for the overlying cover. Many trench cover failures have been attributed to subsidence of the waste materials. Three cover subsidence responses have been observed:

- area subsidence - settlement of the entire trench cover
- slumps - local cover depressions
- sinkholes - vertical erosion channels

After subsidence, water flow through the cover may rise dramatically, due to tension crack piping, ponding, and direct flow through potholes. Water that reaches the waste material will become contaminated and can threaten local ground and surface water supplies if leakage occurs through the surface cover or the bottom liner system.

This paper describes an apparatus and test procedure that were developed for modeling trench cover slump subsidence in a multi-layer system with a compacted clay infiltration barrier. The goals of the study were to predict the behavior of two, full-scale trench covers under subsidence conditions and to gain a better understanding of the slumping phenomenon for application to the design of subsidence resistant trench covers.

The functions of solid and hazardous waste trench covers as determined by the Office of Solid Waste, U.S. EPA, are outlined in Table 1.

Cover designs vary considerably, but the following methods of infiltration control are common to all designs: 1) reduction of surface soil permeability, and 2) grading and other methods of runoff diversion. Under ideal conditions, isolation of the waste from surface water infiltration should continue indefinitely. However, cover performance in the field may be much different than predicted, due to the inherent variability, instability, and behavioral uncertainties of the materials involved. In addition, cover failure can result from attack by weather, erosion, waste materials, water and gas movements, construction and maintenance vehicles, plants, animals, and subsidence of the waste layer. (Skryness, 1982)

The most common and often the most damaging of the failure mechanisms mentioned above is the inability of cover systems to adjust to short- and long-term subsidence of the underlying waste and backfill materials. Volume change of the trench fill and the resultant slumping, cracking, or collapse of the trench cover is shown in Figure 1. Subsidence may breach cover integrity and jeopardize cover performance in each of the areas enumerated in Table 1. The most damaging effects of subsidence are significantly increased infiltration rates due to ponding and crack formation, direct exposure of the waste cell to precipitation and surface runoff, release of contaminants, and accelerated degradation of the disposal site. (Skryness, 1982)

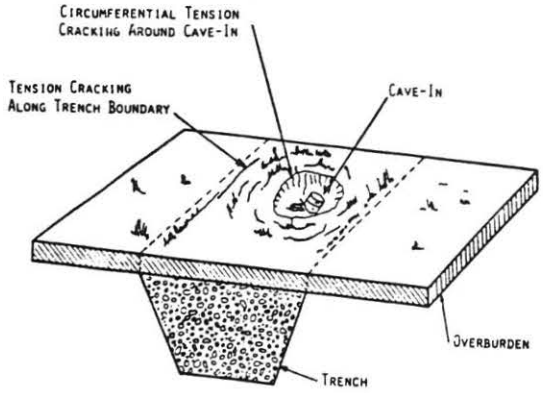

Figure 1. Trench cover slump failure

Effective trench covers are difficult to construct and maintain. Constructing a trench cover to withstand subsidence while still functioning effectively as an infiltration barrier is an even more difficult task. Several approaches to this problem have been suggested. However, problems exist with each of the proposed schemes, and there are many uncertainties about the short and long-term ability of any cover system to

Table 1. Functions of solid and hazardous waste trench covers (Lutton, 1979)

- Control moisture infiltration and final cover erosion
- Preserve slope stability and resist cracking
- Control potentially harmful gas movement and noxious odors
- Minimize settlement and maximize compaction
- Minimize fire hazard potential
- Minimize vector breeding areas and animal attraction
- Resist cold climate deterioration and operational difficulties
- Minimize wind erosion and dust generation and blowing material
- Provide sightly appearance to the landfill operation.
- Provide for vegetative growth.
- Dewater solid waste

withstand subsidence. Few of the concepts have been tested, either in the laboratory or in the hostile environment of a waste disposal facility. Considering the fact that subsidence has been the most common mechanism of trench cover failure to date, a definite need exists for continued research in this area.

Prototype Study

The U. S. Environmental Protection Agency, through its Municipal Environmental Research Laboratory's Solid and Hazardous Waste Research Division, has addressed this need by sponsoring several projects which seek to define, measure, and develop solutions to the problems associated with landfill subsidence. In August 1982, EPA allocated funds to the University of Kentucky for a project entitled, "Demonstration and Evaluation of the Hydrologic Effectiveness of a Three Layer Landfill Cover Under Stable and Subsidence Conditions". The objective of this project was to design, construct, and monitor a series of full-scale, multi-layer cover cells under stable and subsidence field conditions, in order to evaluate their performance as infiltration barriers. To duplicate the effects of slumping subsidence on the cover cells, a system for creating sub-surface cavities beneath the covers was included in the design. Since little quantitative documentation of cover behavior under subsidence conditions was available, the project also included a laboratory investigation of this phenomenon.

The prototype structures for the laboratory study were three multi-layer cover test plots that were constructed at Tyrone, Kentucky on property leased from Kentucky Utilities Company by the Department of Agricultural Engineering. Each plot was subdivided into three cover cells. Figure 2 shows the plan view of the field cover plots. A cross section through a typical cover cell is illustrated in Figure 3. The plots were constructed in three layers: a bottom 2 ft layer of compacted clay that served as the primary infiltration barrier, a 2 ft sand drain layer, and a 2 ft topsoil, vegetative surface layer. Both cover systems were constructed over a 3 ft sand bed. Soil auger pipes were incorporated in the sand beds. After a 2 to 3 year monitoring period under stable conditions, cover subsidence will be induced by augering material from the underlying sand beds. The initial goal of the laboratory study was to investigate the effects of augered cavity size, and initial soil moisture content of the clay barrier layer, on the nature and effects of subsidence.

Selection of Centrifugal Modeling

The main force which results in slumping is the soil cover self-weight. Centrifugal model testing was selected for this study because it is the only laboratory procedure which can reproduce the effects of gravity in a reduced-scale model (Al-Hussaini,1976). The use of centrifugal soil modeling is becoming an accepted method for verifying laboratory soil parameters, geotechnical design assumptions and safety factors (Townsend and Bloomquist, 1983). It has also been applied to complex problems of soil response, for which acceptable solutions have yet to be developed. (Al-Hussaini, 1976)

The basic concept of centrifuge modeling is to create a scale model that is similar in geometry, material properties, and boundary conditions, to the full-scale prototype, and to subject the scale model to a radial acceleration via centrifugation such that the increase in self-weight stresses in the model matches those at corresponding points in the prototype. If the model dimensions are scaled by a factor 1/n as compared to the prototype dimensions, then an acceleration field of n times the acceleration of gravity is required for stress similarity between model and prototype. (Cheney, 1982)

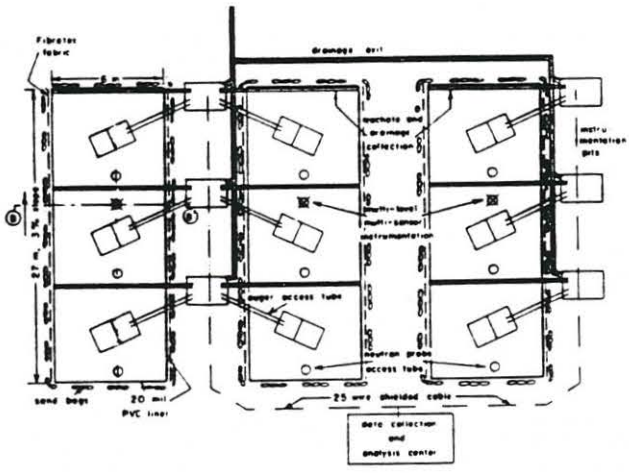

Figure 2. Plan view of prototype cover plots

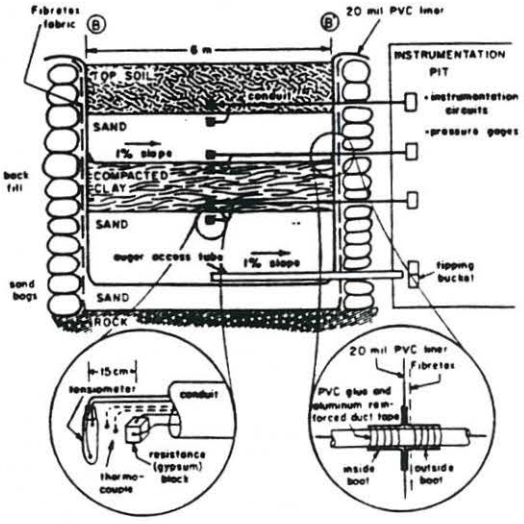

Figure 3. Cross sectional view of a prototype cover cell

the slab. Design of the centrifuge support frame was based on compatibility with this system. Available lab area limited the maximum diameter for the complete centrifuge assembly to 12'. Both 110 V and 220 V electric power is available, as are high pressure air and water lines. The lab has a complete workshop which is useful for constructing, maintaining and modifying the centrifuge.

The centrifuge was conceived as a horizontal rotating arm mounted on a vertical drive shaft powered by an electric motor. The design and construction of the centrifuge was broken down into six basic sub-units:

- sample container and counterweight
- rotating arm
- power supply, transfer, control system
- structural frame
- sand bag wall and protective housing
- data collection and slip-ring assembly

Project funding was limited. Therefore, a major design goal was to build a simple device, using stock parts and materials. Figure 4 shows a cross sectional view of the complete apparatus.

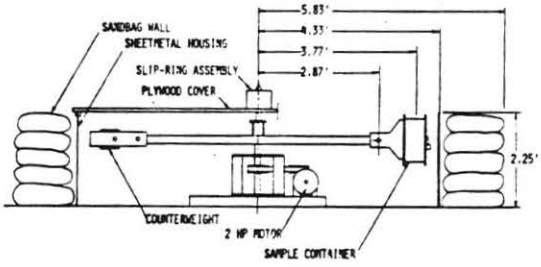

Figure 4. Cross section of centrifuge

Sample Container and Counterweight

The main features of the centrifuge sample container are illustrated in Figure 5. Container design was based on the model size limitations imposed by centrifugation as well as on the following conditions:

- The minimum clay layer thickness was 0.5", based on workability.
- Field cover cells were composed of 2' of compacted clay, 2' of sand and 2' of topsoil.
- Field cover cells were 20' wide.
- Augering was expected to create inverted, cone shaped cavities beneath the field cover cells.
- Kahle and Rowlands (1981) reported that most subsidence features at the Sheffield, Illinois low-level radioactive waste landfill were 12' in diameter or less.

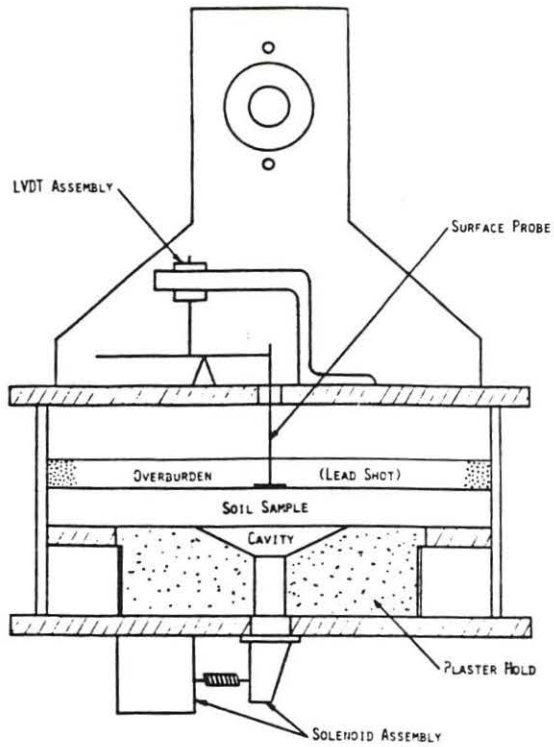

Figure 5. Centrifuge sample container

Consideration of these factors led to the selection of a 1/24 model scale and a maximum prototype cavity diameter of 12' for model construction. Circular models were used, to preserve the radial symmetry of the prototype sand cavities. The sand and topsoil layers of the prototype cover system were assumed to provide no resistance to collapse, acting only as a surcharge to the clay layer, and were modeled as a layer of lead shot having the same weight as the equivalent depths of the two soil layers. Model covers were supported over cavities that were initially filled with lead shot. Subsidence was reproduced by emptying the cavities in flight. At 1/24 scale, the prototype cover was modeled as a 1" thick clay layer, surcharged by 0.5" of lead shot. The maximum cavity diameter was 6".

A 12" diameter plexiglas cylinder housed the model and allowed for photography and visual observation of the sample. The cylinder was 6" in height, to accommodate a base plate, clay layer, and lead shot surcharge, and to allow for other model configurations. The base plate assembly supported the clay sample and was sized to fit snugly within the plexiglas tube. The unit was designed to simplify the process of creating different diameter cavities beneath the model clay layer. The assembly consisted of an aluminum ring, a plexiglas ring, and a plaster disk. The aluminum and plexiglas rings were bolted to the lower aluminum base plate with the plaster disk resting inside the rings. A conical subsidence cavity and shot removal hole were milled in the plaster disk. Two,

1/2" x 14" diameter aluminum plates enclosed the container. A groove, of the same diameter and width as the plexiglas cylinder, was machined into each plate and served to lock the cylinder into position. An o-ring in each groove served to cushion the plexiglas/aluminum contact. A mounting bracket, which allowed the cylinder assembly to swing freely from the centrifuge arm, was bolted to the top plate. A linear voltage displacement transducer (LVDT) was mounted to the top plate for data collection purposes. A 7/8", lead shot release hole, was drilled through the bottom plate. Activation of a spring-loaded solenoid gate opened the hole and allowed the lead shot to fly out of the subsidence cavity in the plaster disk.

The sample container mounted to one arm of the centrifuge; a counterweight mounted to the other arm. Rotational balance required that the sample container and the counterweight to be of equal mass and that the centers of mass of both, be equidistant from the center of rotation. To meet these requirements, the counterweight's mass could be easily changed. Two, steel plates form the basic structure of the counterweight. Fourteen steel plates, weighing approximately 5 pounds each, were used for gross balancing. As many plates as necessary could be bolted together to counterbalance the sample container. Fine balance was achieved by adding extra washers and nuts to the counterweight.

Rotating Arm

A 2" square, cold-rolled, 1018 steel bar was used as the rotating arm of the centrifuge. The length of the arm was determined by the spacial limitations of the Structural Engineering Laboratory. The largest possible length was desired, in order to minimize the deviation of the radial centrifuge force field from the essentially parallel gravitational force field of the Earth. Allowing for the permanent fixtures in the laboratory (counters and cabinets), walkways, a protective sandbag wall around the centrifuge, and the grid locations of the tie-down system, a 6.0' arm length was selected.

A 1.0" diameter hole was drilled through each end of the bar. The sample container and the counterweight were connected to opposite ends of the arm with 1.0" diameter x 9.0" long steel bars that were passed through the two flange bearings in each mounting bracket and the hole in the rotating arm. Each bar was bolted to the arm to prevent the sample container and the counterweight from moving laterally due to drag forces.

A slot was milled into the bottom center of the arm to receive the drive shaft. Thus, a mechanical connection was created between the two components. A 5/8" bolt, passed through a hole in the arm and screwed into a threaded center hole in the drive shaft. The self-weight of centrifuge arm, the sample container, and the counterweight assembly (approximately 250 pounds) also acted to hold the two pieces together.

Power Supply, Transfer and Control System

Calculations based on a radius of 3.75' indicated that 2 HP was required to balance the aerodynamic drag forces at a maximum speed of 280 rpm. Accordingly, a 2 HP, 1750 rpm, DC electric motor coupled to a 5:1 worm gear speed reducer was used to power the apparatus.

A gearbelt system transferred power from the gear reducer to the centrifuge drive shaft. This drive system has several safety and performance advantages over a direct, belt, chain, or gear drive. Slippage does not occur at normal loads with this system, since power is transmitted by positive engagement of belt teeth with pulley grooves instead of by friction. As a result, little heat was generated during operation, and drive-shaft bearing loads are reduced due to the low belt tension that is required. In the event of a motor or bearing failure, the gearbelt will slip and lessen the risk of personal injury and/or destruction of the apparatus.

The drive shaft was fabricated from a 1.5" diameter, 14" long, solid bar of cold-rolled 1018 steel. A keyseat was milled into the shaft to provide a positive connection with the gearbelt pulley. Parallel flats were cut into the upper sides of the shaft and hole was drilled into the top end of the shaft and tapped to receive the 5/8" bolt. These two features allowed the top end of the drive shaft to be inserted into the rectangular slot in the bottom of the rotating centrifuge arm, and the two units to be securely bolted together. The drive shaft was supported in the structural frame by two, 1.5" bore, self-aligning, relubricatible, wide inner ring ball bearings.

The centrifuge payload velocity (acceleration) was regulated by a solid state speed control unit, which could operate both manually and automatically. In the manual mode, the operator used a potentiometer to directly vary the motor speed. In the automatic mode, the required angular speed was input to the control unit, which then accelerated the centrifuge to this speed at a preselected linear rate. A light emitting diode panel, which displayed the centrifuge speed in rpm, and a feedback circuit which limited speed fluctuations, were available in both modes. The controller also allowed for direct input and output via a microcomputer system.

Support Structure

The supporting structure for the centrifuge consisted of a square base frame which tied the other system components together and a box frame that supported the drive shaft.

The drive shaft support frame was constructed of two, 0.5" steel plates, and four pieces of 3x3 structural tubing. The two plates were drilled to receive the 1.5" bore drive shaft bearings, which were bolted down

at the center of each plate. Four pieces 0.625" diameter threaded rod, which passed through the top plate, the steel tubes, and the bottom plate, served to tie the drive shaft support frame together and to secure it to the base frame.

The base frame was 40.0" square and was constructed of structural tubing in a nine-square grid pattern. The center square had 15" long sides that corresponded to the dimensions of the drive shaft support frame. Holes were drilled through the four outside corners, and the frame was secured to the floor using the existing structural tie-down system and connectors. Rubber strips were cemented to the bottom of the frame to dampen vibrations generated by the centrifuge.

The electric motor and gear reducer were bolted to a 0.5" steel plate, which was also bolted to the base frame. The motor, reducer, and plate moved as a single unit. In this way, the gearbelt could be removed or installed without changing the motor/reducer shaft alignment.

Slip Ring Assembly

Thirteen circuits (including the centrifuge frame) were available for signal transfer to and from the centrifuge payload. A two circuit slip ring assembly, unsuitable for precise data collection, was used to activate the solenoid. A ten circuit assembly was available for more sensitive applications. Four circuits were used to power and receive data from the LVDT in this study.

Protective Housing

For safety reasons, a 12 ft. diameter sand bag barrier wall was constructed around the centrifuge. A 9 ft. diameter x 27 in. high, sheet metal housing and a plywood cover were constructed inside the sand bag wall to reduce the wall drag coefficient and to reduce the centrifuge "fan" action. The plywood cover was hinged to allow access for model testing and centrifuge maintenance. The ten circuit slip ring assembly mounted to the cover.

EXPERIMENTAL PROCEDURE

Data Collection

The data recorded for each test is listed below.

- model scale factor
- centrifuge speed
- radius to the sample container's centroid
- cavity geometry
- number of blows for clay layer compaction
- clay layer weight
- clay layer moisture content values
- lead surcharge weight
- initial and subsided elevations of points on the surface of the clay layer
- time allowed for pore pressure dissipation
- midpoint subsidence of the clay layer
- photographs of the subsided clay layer
- qualitative description of the test

Surface elevation measurements were made with a dial-gauge. A template was temporarily attached to the test capsule, and used to locate the points to be measured. It was made from a 15" square sheet of plexiglas, with dial-gauge guide holes drilled on 0.5" centers in a 23 x 23 grid pattern. Each hole was identified by a set of reference coordinates.

During each test, subsidence was recorded by monitoring the mid-point deflection of the soil layer. The LVDT mounted on the top plate of the sample container was used to convert the movement of a surface displacement probe into a voltage that was linked to a strip chart recorder via the slip ring assembly. Physical connection between the LVDT and the probe was made with a balanced lever, which minimized the additional load applied to the soil surface. The elapsed time and the LVDT output as read from a voltmeter, were written down on the chart record at regular time intervals during the test and when rapid changes in deformation were observed.

Preparation of the Soil

Representative samples of the soil used to construct the prototype clay barrier layers were obtained from the field site and transported to the laboratory, where they were air dried and broken into fragments. Pieces of rock larger than 0.5" in diameter were picked out by hand during this process. The soil was further broken up by passing it through a crushing machine. It was then passed through a No. 4 U. S. standard sieve and stored in 5 gal. plastic buckets.

Prior to testing, a quantity of soil was weighed out and a moisture content determination made for the material. The volume of water needed to increase the soil moisture content to a selected value was calculated. Tap water from the Kentucky River, the source of water applied to the field plots, was added to the soil. Blending of the soil and water was accomplished by hand mixing. The soil was then returned to the plastic buckets. To minimize subsequent moisture loss, a wet rag was also placed in each bucket. The soil was allowed to cure for at least 48 hours before testing to allow time for uniform water distribution among the soil particles.

Compaction of Soil Specimens

The compaction mold for the clay slab was made of a 0.5" thick x 11.5" diameter aluminum plate that was bolted to a 14" square x 1.5" thick steel base plate. Before preparing a new soil specimen, the plexiglas tube from the centrifuge testcapsule was slipped down over the aluminum plate to form the mold's side wall. The inside of the compaction mold was lightly coated with a commercial vegetable oil spray, to prevent soil from sticking to the sides and base of the mold. The quantity of soil needed for a particular test configuration (see Table 5) was then weighed out from storage and imme-

The motor speed was incremented at a constant, predetermined rate, to accelerate the payload from the initial 5 rpm rotational speed to that required for the test. The final centrifuge speeds and the corresponding start-up time intervals for each test configuration are listed in Table 5. The required speed was maintained for 5 minutes to assure that the soil layer and the other components were fully seated in the test capsule. Power to the motor was then cut off. After the centrifuge came to rest, the cover was reopened. The LVDT input and output voltages were readjusted. The chart recorder was checked for a zero reading. The housing cover was closed and the centrifuge was brought up to the required speed in the same manner as before.

The test capsule was accelerated for 60 to 120 minutes to allow for the dissipation of excess pore pressure. The chart recorder speed was increased. The solenoid was activated, releasing the lead shot and forming the cavity beneath the soil specimen. The chart recorder speed was reduced after a period of 5 minutes or after rapid changes in LVDT output were no longer observed. Acceleration was continued until collapse of the clay layer was indicated or until the operator decided to terminate the procedure. Power to the motor was then cut off. After the centrifuge came to rest, the cover was reopened and both payloads were removed.

Post-test Procedures

The test capsule was disassembled, the deflection probe removed, and the lead shot emptied from the cylinder. The template sheet was reattached and a final set of surface elevation measurements were taken. The soil specimen was removed from the cylinder and weighed. Photographs were taken of the upper and lower surfaces of the specimen as well as of any unusual features that were observed. A description of the sample's post-test condition was written down. Four samples were removed from the specimen for moisture content determination.

RESULTS AND DISCUSSION

Description of Soil

Model tests have been carried out using soil from the prototype clay barrier layers. The material was a silty, inorganic clay (CH). Table 6 lists some properties of this material.

Behavior of Model Clay Layers

To date, centrifuge model tests have been conducted in which the clay layer moisture content (w) and the subsidence cavity diameter were varied. Preliminary findings from these tests are summarized below.

Three responses were common to all tests.

- Small displacements were recorded for every test as the centrifuge was brought up to speed. These initial drops have been attributed to the re-seating of the movable components in the sample container with increased acceleration.
- During the pore pressure dissipation period, rapidly decreasing rates of displacement were observed during all tests. This behavior was probably caused by consolidation of the clay layer.
- Measurable subsidence of all clay layers was recorded at the instant of cavity formation. For dry soils and/or small cavities, the magnitude of subsidence was small. No apparent changes in the clay layers were visible. For wet soils and/or large cavities, immediate collapse resulted.

The design moisture content of the prototype clay barrier layers was 27% (2% above optimum). Test results for model layers compacted at 27% moisture and undermined by a range of cavity diameters are shown in Figure 6.

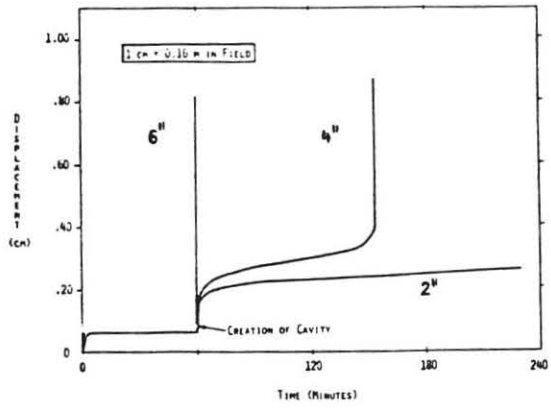

Figure 6. Model subsidence response at optimum moisture content

Table 6. Properties of Soil Used in Centrifuge Studies

Optimum moisture content (standard Proctor)	25 %
Maximum dry density (standard Proctor)	98 pcf
Percent sand	25 %
Percent silt	37 %
Percent clay	38 %
Specific gravity	2.82
Liquid limit	57 %
Plastic limit	26 %
Plasticity index	31 %

All 6 inch cavity tests (12 ft field equivalent) at 27% moisture content resulted in immediate failure of the clay layer (total collapse with severe cracking). All 2 inch cavity tests (4 ft field equivalent) were stable, showing no evidence of cracking or collapse during the periods of acceleration. Tests with 4 inch cavities (8 ft field equivalent) exhibited the full range of subsidence behavior. As a result, 4 in. cavities were used in most tests.

Results from 4 inch cavity tests, for moisture contents ranging from 26.7% to 28.7%, are illustrated in Figure 7. The curves in Figure 7 indicate that clay layer subsidence behavior is highly sensitive to the moisture content at compaction.

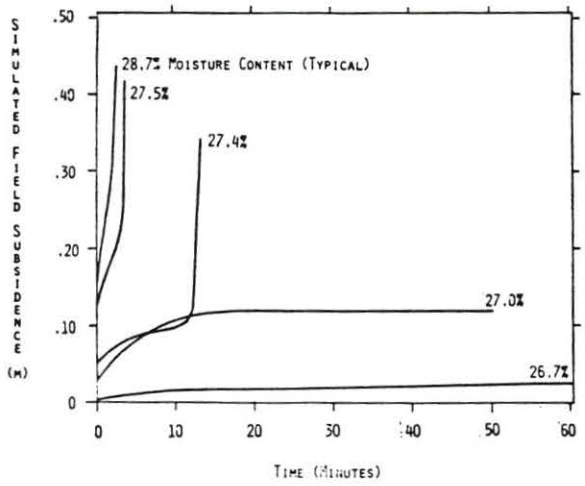

Figure 7. Model subsidence response with 4 inch diameter cavities

The observed subsidence behavior of model covers undermined by 4 in. diameter cavities is summarized below:

- Initial subsidence was recorded at the sample midpoint in all cases. Values ranged from 0.02 in (.04 ft field equivalent) at 4.5% below optimum to 0.125 in (0.25 ft) at 4.5% above optimum.
- For moisture contents below optimum, subsidence tended to occur without cracking and without visible slumping.
- For moisture contents greater that optimum but less than 2% above optimum, clay layers tended to remain stable following cavity formation. However, radial cracking of the lower surfaces, circumferential cracking of the upper surfaces, and slumping was observed.
- For moisture contents greater that 2% above optimum but less that 2.4% above optimum, collapse tended to occur after a period of slow deformation.
- For moisture contents greater than 2.4% above optimum, rapid collapse tended to occur immediately after cavity formation.

CONCLUSION

The severe problems which hazardous waste landfill sites have experienced due to trench cover subsidence dictate that methodologies be developed to better understand this phenomenon. This study was initiated to develop a laboratory procedure for examining these processes. Centrifugal model testing was determined to be the best experimental technique for small-scale studies, primarily because of its ability to duplicate the forces and resultant stresses which lead to failure in the field. The scope of this work was limited to clay layers subjected to "slump", a type of subsidence characterized by localized void spaces beneath the cover.

Pending verification of test results, this experimental methodology will be used to:

- estimate the largest cavity that can be spanned by a given trench cover
- estimate the time to cover failure when this cavity diameter is exceeded
- estimate the degree of subsidence cracking and slumping for application to infiltration studies
- develop recommendations for subsidence resistant landfill cover designs
- investigate the influence of other parameters on subsidence
- investigate the physical mechanisms of subsidence

BIBLIOGRAPHY

Al-Hussaini, M. M., "Centrifuge Model Testing of Soils: A Literature Review", U. S. Army Engineer Waterways Experiment Station, Vicksburg, Mississippi, 1976.

Cheney, J. A., "An Introduction to Geotechnical Centrifuge Modeling", Proc. Recent Advances in Geotechncial Centrifuge Modeling, University of California, Davis, 1982.

Kahle, R., and Rowlands, J., Evaluation of Trench Subsidence and Stabilization at Sheffield Low-Level Radioactive Waste Disposal Facility, Final Report, October 15,1980 - March 30, 1981, NUREG/CR-2101.

Lutton, R. J., Regan, G. L., Jones, L. W., Design and Construction of Covers for Solid Waste Landfills, U.S. Army Waterways Experiment Station, Vicksburg, Ms., August, 1979, EPA-600/2-79-165.

Skryness, R., "Overview of Design Considerations for Effective Trench Covers", Proc. Symposium on Low-Level Waste Disposal. Facility Design, Construction, and Operating Practices. Washington, D.C. September 29-30, 1982. NUREG/CP-0028

Townsend, F. C. and Bloomquist, D. G., "Geotechnical Centrifugal Modelling and University of Florida Experiences", Report, University of Florida, Department of Civil Engineering, Gainesville, 1983.

Symposium on Recent Advances in Geotechnical Modeling
University of California at Davis 19-20 July 1984

CENTRIFUGE PREDICTION OF EGRESS SYSTEM PERFORMANCE

R.M. Schmidt, N.E. Funston, V.T. Webbeking, K.R. Housen, K.A. Holsapple and M.E. Voss

Boeing Aerospace Company, M/S 13-20, Seattle, WA 98124

Hard silo basing requires missile canister egress through a layer of blast-compacted soil debris on the order of 15 to 20 feet thick. This is analogous to the pull out of a shallow soil-anchor for the 16-foot canister closure under consideration. Anchor design formulae have been developed by numerous investigators over the past 25 years; see attached references, especially the literature search by Gurtowski (1984). All of these results are based upon laboratory model test data and in some cases are supported with finite element code analysis. A common conclusion is that break-out mode and maximum load depend greatly upon soil strength properties. Recently, Ko (1982) suggested that the modeling fidelity of subscale egress could be improved by conducting laboratory tests on a centrifuge, and performed a suite of tests using a typical Yuma desert soil.

The work described here is an application of the centrifuge technique as a prediction method in the design of a full-scale field demonstration test to be conducted in March of 1985. Two approaches to the egress problem were employed.

In the first approach, five generic soil types were used in an attempt to determine egress load in terms of soil properties. For each soil type, direct shear tests were conducted to estimate strength properties, as a function of dry density and moisture content (Godlewski, 1984). Maximum loads required for egress were measured for various scaled debris depths. The centrifuge data were cast in nondimensional form and used in a step-wise second order polynomial regression analysis. This provided a design prediction equation in terms of measured or estimated soil properties, which can be used for system studies. This equation is still under development; however a preliminary version based upon specific results (discussed below) of just three density variations of the Engineering Test Bed (ETB) soil is shown in Fig. 1. Here, F is the peak load observed during egress; ρ, c and ϕ are the soil density, cohesion and friction angle; g is gravitational acceleration; h is debris depth and d is closure diameter.

FIGURE 1
CORRELATION OF LOAD COEFFICIENT WITH AVE SHEAR STRESS

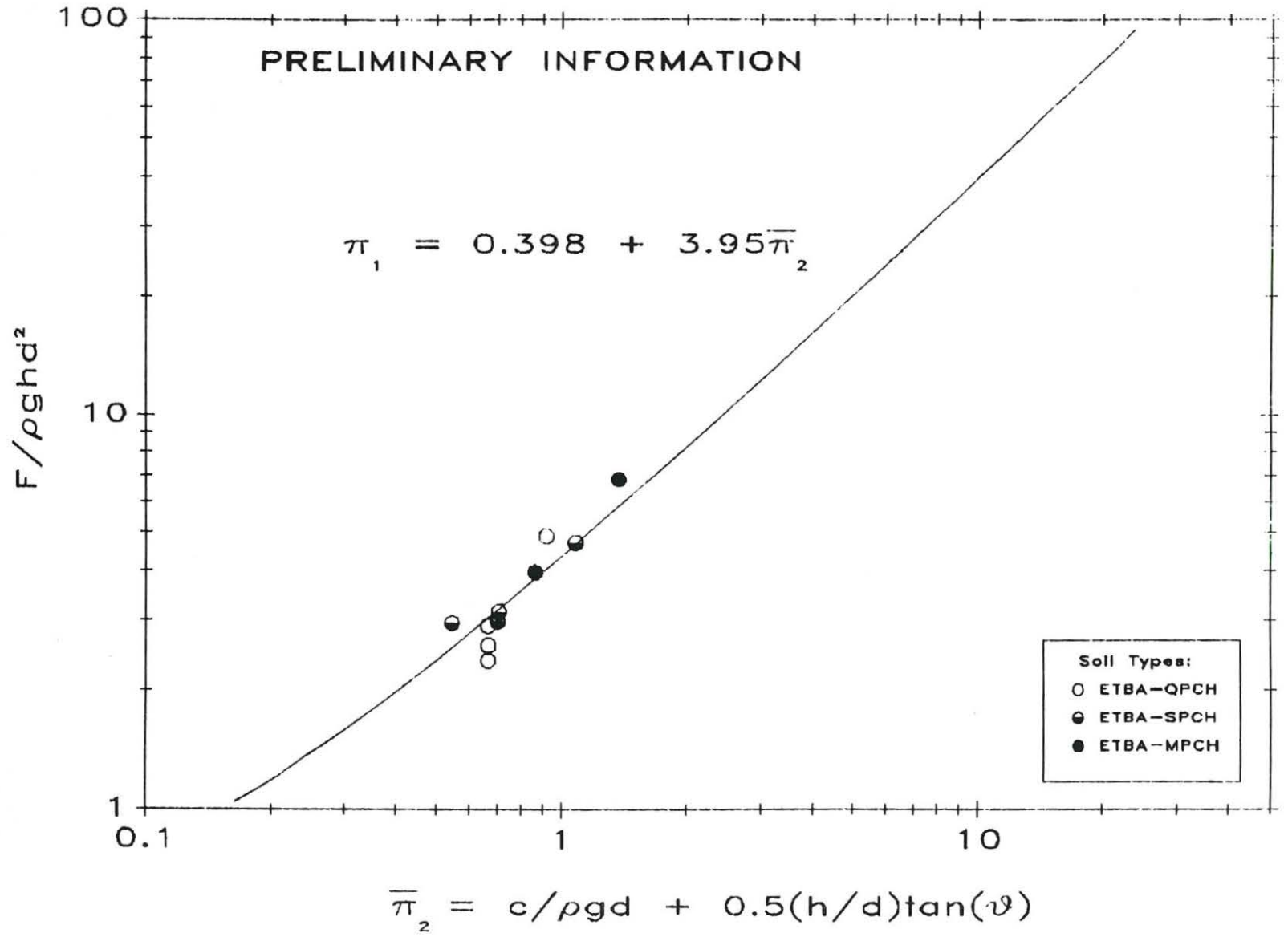

The second approach was to use the centrifuge model to directly simulate the anticipated field event using an "identical" soil. The success of this method depends upon the fidelity of the soil model representing the debris embankment to be placed in field. Here, samples of the actual ETB soil were obtained from DOE pit 400. The nominal field condition is to place this soil at a density corresponding to the standard Proctor (ASTM D698-78).

Load histories from a model of the model test are compared in Fig. 2. The result from test 37A-9ED is for a 4-inch diameter model closure run at 64G. It can be compared to the result from test 43A-OED, which is for a 2-inch diameter model run at 128G. Peak scaled loads are in good agreement, however load decay with time is more rapid for the larger closure. This is attributed to a grain-size effect that governs the rate at which material falls through the emerging rupture gap in the soil around the closure. Both models were run at a constant strain rate corresponding to a full scale velocity of 12 inches/second.

To examine the range of loads that can be expected due to extremes in soil placement, centrifuge tests were conducted at three different densities, all at the same moisture content, nominally 5%. The three curves shown in Fig. 3 are for soil densities that correspond to modified Proctor (MP) compaction (ASTM D1557-78), standard Proctor (SP), and "quarter" Proctor (QP) using an energy of compaction equal to 25% of the standard Proctor. The left ordinate shows the pressure in the actuator corresponding to the total load as shown on the right. The curves are based upon a least squares fit to the ETB data using the values for soil mechanical properties measured by Godlewski (1984). A typical value for one standard deviation in the region of 15-foot debris depth is approximately 50 psi. Reproducibility of the centrifuge results is on the order of 5%. This plot provides the current best estimate for the upcoming full-scale field test.

REFERENCES

Balla, A. (1961) "The Resistance to Breaking Out of Mushroom Foundations for Pylons," **Proceedings of the 5th International Conference on Soil Mechanics and Foundation Engineering,** Paris, France, Vol. 1, 569-576.

Clemence, S.P. and Veesaert, C.J. (1977) "Dynamic Pullout Resistance of Anchors in Sand," **Proceedings of the International Symposium on Soil Structure Interaction,** University of Roorkee, 389-397.

Davie, J.R. and Sutherland, H.B. (1977) "Uplift Resistance of Cohesive Soils," **Journal of the Geotechnical Engineering Division, ASCE,** Vol. 103, No. GT9, 935-951.

12:07:40 13-SEP-84

FIGURE 2: MODEL-OF-MODEL LOAD HISTORIES
(Closure Tare Weight Excluded)

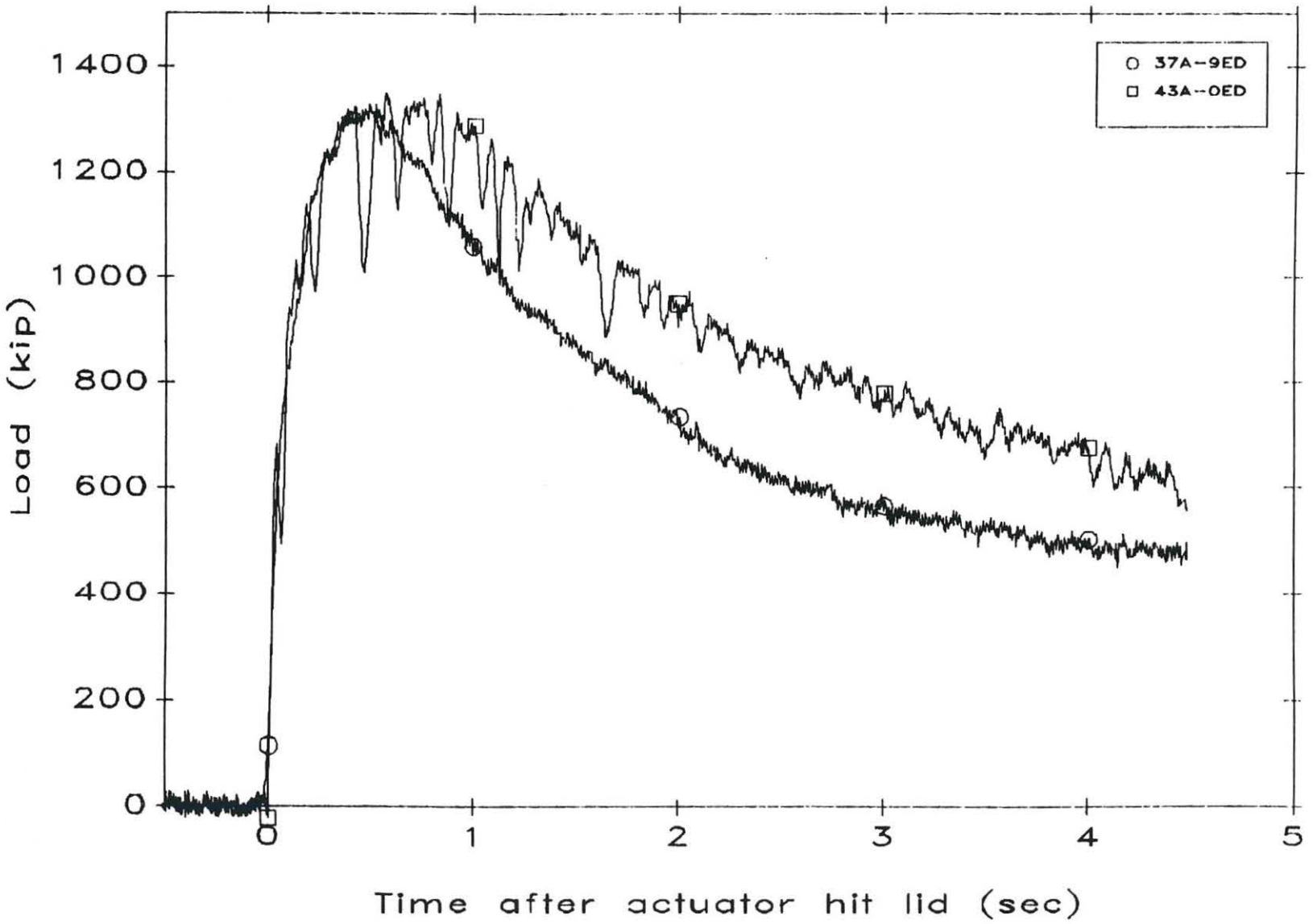

FIGURE 3

CENTRIFUGE PREDICTION OF ETB EGRESS LOADS VS DEPTH

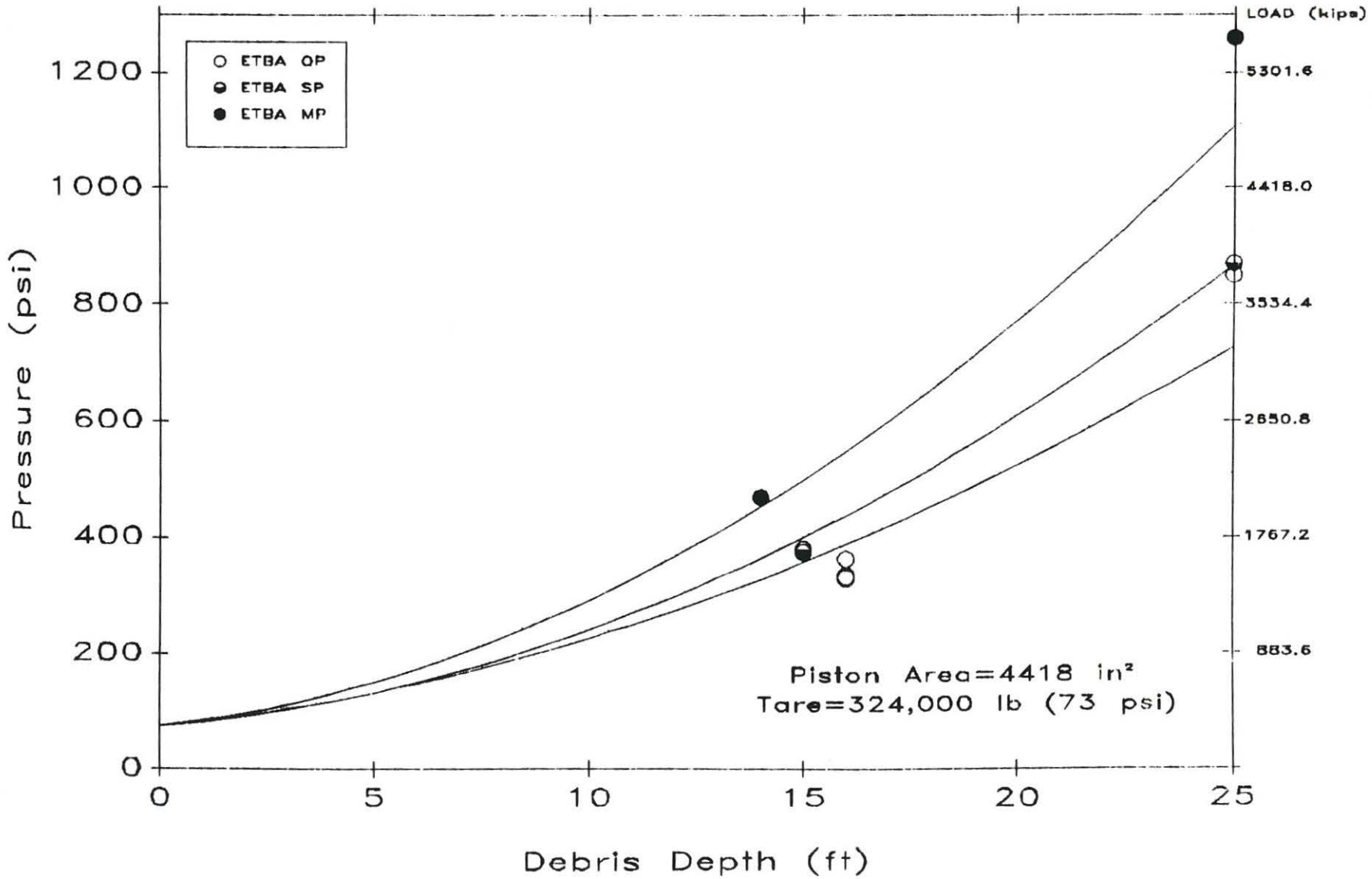

Godlewski, P. (1984) "Debris Characterization Study, Test No. HV12-T1C, Centrifuge Model Test Program." Shannon & Wilson, Inc. report to the Boeing Aerospace Company, Seattle, Washington.

Gurtowski, T.M. (1984) "Breakout Loading Study Engineering Test Bed Demonstration Project, Test No. HV11-T3." Shannon & Wilson, Inc. report to the Boeing Aerospace Company, Seattle, Washington.

Ireland, H.O. (1963) Discussion of "Uplift Resistance of Transmission Tower Footings," by Edward A. Turner; **Journal of the Power Division, ASCE,** Vol. 89, No. P01, 115-118.

Ko, H.Y. and Ni, C.K. (1982), "Experimental Egress Load Determination," report to Martin Marietta Corporation, Contract No. R9H2-393613.

Mariupol'skii, L.G. (1965), "The Bearing Capacity of Anchor Foundations," **Soil Mechanics and Foundation Engineering,** No. 1, Jan.-Feb., 26-37.

Matsuo, M. (1967) "Study on the Uplift Resistance of Footings," **Soil and Foundation,** Japan, Vol. 7, No. 4, 1-37.

Meyerhof, G.G. and Adams, J.J. (1968) "The Ultimate Uplift Capacity of Foundations," **Canadian Geotechnical Journal,** Vol. 5, No. 4, 224-244.

Mors, H. (1959) "The Behavior of Mast Foundation Subjected to Tensile Forces," **Bautechnick,** Vol. 36, No. 10, 367-378.

Rowe, R.K. and Davis, E.H. (1982a) "Behavior of Anchor Plates in Clay," **Geotechnique,** Vol. 32, No. 1, 9-23.

Rowe, R.K. and Davis, E.H. (1982b) "Behavior of Anchor Plates in Sand," **Geotechnique,** Vol. 32, No. 1, 25-41.

Vesic, A.S. (1971) "Breakout Resistance of Objects Embedded in Ocean Bottom," **Journal of the Soil Mechanics and Foundations Division, ASCE,** Vol 97, No. SM9, 1183-1205.

An investigation of the Bearing Capacity of Footings under eccentric and inclined loading on Sand in a Geotechnical Centrifuge

by R. G. James* and H Tanaka†

* Assistant Director of Research, Cambridge University Engineering Dept.

† Senior Research Engineer, Port & Harbour Research Institute, Yokosuka, Japan

Abstract

The results of centrifuge model tests on the behaviour of flat and conical footings on dense sand are reported and compared with the standard bearing capacity formulae for veritcal, horizontal and eccentric loading.

Introduction

The work reported in the paper is part of an SERC research program conducted at the C.U.E.D. in relation to the behaviour of conical foundations (spuds) of Jack-up platforms. This program covers the behaviour of plane circular footings and conical footings on sand and on thin layers of sand overlying soft clay - however the results reported here will be mainly confined to the behaviour of flat circular footings on sand under inclined and eccentric loading.

The practical situation of a jack-up rig that one is attempting to model is illustrated in Fig. 1. That is the jack-up rig is floated onto the drilling site, the legs are lowered to the sea bed raising the platform (hull) above the sea surface and then preloading the foundations (spuds) by ballasting the hull with water.

The ballast (preload) is then removed prior to commencing drilling operations during which the foundations may be subjected to environmental forces such as wind, wave and tidal current, as well as the vertical self weight forces of the rig. This results in the footings being subject to vertical and horizontal forces P_v and P_h and to a moment M. A typical spud foundation is illustrated in Fig. 2. Although in the past many research workers have investigated the bearing capacity problem, e.g. Terzaghi, Meyerhof, Brinch-Hansen, Ticof Muhs and Weiss and many others.

The majority of this work has been conducted with small scale model footings at comparatively low stress levels thus the standard formulae involving bearing capacity factors in common use, quoted below in equation 1 have in general only been validated with data based on such models, there being very little data at sizes and stress levels appropriate to prototype scale footings and of course very little indeed appropriate to conical based footings.

$$q = S_c\, C\, N_c + S_q\, D\, N_q + \tfrac{1}{2}\, S_\gamma\, \gamma\, B\, N_\gamma \qquad (1)$$

where q is the vertical bearing capacity stress,

S_c, S_q, S_γ are footing shape factors

N_c, N_q, N_γ are the bearing capacity factors

for cohesion, surcharge, and self-weight respectively, and vary exponentially with the angle of internal friction ϕ,

C is the soil cohesion D is the depth of overburden and B is the breadth or diameter of the footing.

Typically S_c, S_q and S_γ have values of 1 for strip footings 1.2, 1, 0.4, respectively for square footings and 1.2, 1, 0.6 respectively for circular footings.

For the case of eccentric and inclined loading of strip footings on sand equation 1 is often modified as shown in equation 2 below.

$$q = \left(1 - \frac{2e}{B}\right)\left(1 - \frac{2\alpha}{\pi}\right)^2 \gamma D N_q + \left(1 - \frac{2e}{B}\right)^2 \left(1 - \frac{\alpha}{\phi}\right)^2 \tfrac{1}{2}\gamma B N_\gamma \qquad (2)$$

where e is the eccentricity at the point of action of the force on the base of the foundation measured from the centreline of the foundation and α (which must be less than ϕ) is the inclination of the force to the vertical (see fig. 3).

If such equations are to be of use for the case of full scale spud foundations then they need to be validated at appropriate stress levels for both flat and conical based footings.

The aim of this paper is to provide some of the data for such validations by presenting data from centrifuge model tests at stress levels more appropriate to full-scale footings. In addition data on the load displacement behaviour under eccentric and inclined loads will also be presented.

The Test Program

In view of the sparsity of data at different stress levels for flat based footings most of the tests were conducted with flat based circular footings. The program of tests that has been achieved so far is summarized in Table I.

The tests about to be described below were conducted on the Cambridge 10 m diameter Geotechnical centrifuge.

The tests covered vertical, horizontal and eccentric loading of 50, 75 and 100 mm diameter flat footings and vertical loading of a 120 mm diameter conical footing with an apex angle of 120° on dense Leighton Buzzard sand (BS 14/25).

Four sand specimens were prepared by pouring with voids ratios in the range of 0.47 to 0.49.

The footings were made from a duralumin alloy with a good quality machined finish giving a coefficient of friction with the Leighton Buzzard sand in the region of 0.20.

The loading system is illustrated in Fig. 4 and had a capacity of about 10 kN (≈ 2000 lb) vertically and 2.5 kN (≈ 500 lb) horizontally. Photographs of the apparatus may be seen in Fig. 5.

The tests were conducted at g levels covering the range 10 to 60 g. Thus in the case of the 50 mm diameter model footing this corresponded to prototype diameters in the range 0.5 to 3.0 metres.

The sand specimen container was 762 mm x 762 mm square in plan with a depth to the base of the sand of about 200 mm. (Bricks were placed in the bottom of the specimen container in order to reduce the amount of sand required to prepare a specimen). Due to the relatively restricted capacity of the loading system it was not always possible to fail a footing at the planned g level, as a consequence in many cases multi-stage tests were conducted, i.e. having yielded a specimen - say at 40 g and also having reached the maximum capacity of the loading system the load would be removed and the g level then reduced to say 20 g, and the footing reloaded to yield. Subsequently the g level may again be reduced to say 10 g and the footing again reloaded to yield and then eventually to failure. Typical loading paths are shown in Fig. 6.

Some Typical Results

Vertical loading

Initially it was necessary to explore the effects of stress level or the so-called scale effect. This was most easily achieved by considering the results obtained from tests S1, S3 and S2, which were conducted on 100, 75 and 50 mm diameter footings respectively. These footings were brought to failure at 1 g, 10g and 60 g, corresponding to footing prototype diameters of 01. m, .75 m and 3.0 m, respectively. In order to appreciate the very marked scale effects these results are presented in Fig. 7 as N_γ and N_γ* plotted against $Bn\gamma$ where N_γ* is given by $q = 0.5\ \gamma B N_\gamma$* and $S_\gamma N_\gamma = N_\gamma$*, B is the footing diameter, n is the number of gravities and γ the soil unit weight at 1 g. S_γ is taken as 0.6 for a circular footing. Also indicated in this figure for comparative purposes are the results of Terashi et al (1984) and King et al (1984).

All of the results indicate a very marked scale effect and in the case of the present authors' results going from a 0.1 m diameter footing to a 3 m diameter footing reduces the N_γ values by a factor of 3 which corresponds to a reduction of ϕ of about 6°.

Since the restricted capacity of the loading system did not allow a satisfactory modelling of models at failure, such modelling of models was restricted to investigating load displacement behaviour. Load displacement results from the same three tests, i.e. S1, S3 and S2 carried out at 30, 40 and 60 g i.e. corresponding in each case to a 3.0 metre diameter prototype are presented in Fig. 8 in prototype terms.

If the modelling were perfect then instead of three slightly different curves that can be seen in the figure, there would only be one. Thus at first sight it appears that the world of geotechnical centrifuge modelling is indeed an imperfect one, however there are reasons why one might expect the curves to be slightly different. The main reason is possibly the influence of the boundaries of the container and in particular the influence of the depth of the sand layer (h_s) which was only .195 m which is comparable with the footing diameters, i.e. for model footing diameters of .1, .075 and .05 m the depth to footing diameter ratio ($^{h_s}/_B$) is 1.95, 2.60 and 3.9 respectively. Plots of the vertical stiffness $\bar{K}_v$ (where $\bar{K}_v = {}^{q_v}/_{(\frac{dv}{B})}$ and is

B times the slope in Fig. 8) against depth/diameter ratio h_s/B for first loading and reloading are shown in Fig. 9. It is evident that for both first loading and reloading that as the depth/diameter ratio decreases the soil foundation is apparently stiffer. Also indicated in this figure are curves based upon an elastic solution (Poulos & Davis 1968) allowing for the influence of a rigid base at finite depth. It therefore seems that the majority of the discrepancy between the three curves in Fig. 8 may be accounted for by the influence of the base of the sample container box. It is also apparent that in order to obtain a 'perfect' modelling of models it may be desirable to correctly scale the container as well as the model!

In respect of tests performed with eccentric and inclined loading some typical results (tests S7 and S8) are shown in Figs. 10(a) (b) (c). Three parameters are plotted in each figure against horizontal displacement, viz, the ratio of horizontal stress to vertical stress, the vertical displacement, and the rotation of the footing.

It is evident from the curves of q_h/q_v versus horizontal displacement that the behaviour is not precisely symmetric, however since positive values of eccentricity and inclination are smaller when plotting the data only the positive side of the loading loop will be considered. Fig. 11 shows the failure enveloped for horizontal load at zero eccentricity. Also presented are the data of Ticof (1977) and Muhs & Weiss (1973). The two bounding curves to the Ticof data are for $\frac{P_v}{P_v*} = \left(1 - \frac{\alpha}{\phi}\right)^2$ where $\alpha = \tan^{-1}\left(\frac{Ph}{P_v}\right)$ (3)

where P_v* is the vertical load capacity (P_v) at zero horizontal load (P_h) and zero eccentricity.

ϕ has been taken as 49° and 40° .

The line through the authors' data i.e. $\delta = 11.3°$ represents a reasonable lower limit to the centrifuge data obtained at 20 and 40 g. It is evident that most of these data points lie on the sliding limit of the envelope however the point at $P_v/P_{v*} = 0.5$ is at the changeover point to vertical bearing capacity failure as evidenced by the direction of the displacement vector.

Note that the footings used by James & Tanaka had a max δ value of about 11.3° corresponding to a friction coefficient of 0.2 whereas Ticof used rough sandpaper on the base of his footings allowing him to develop much larger δ values.

Fig. 12 is similar to Fig. 11 but now includes data and a failure envelope for the case of an eccentricity of 15 mm (footing diameter 75 mm $\therefore \frac{e}{B} = 0.2$).

The failure enveloped at e = 15 mm has been obtained from

$$\frac{P_v}{P_v^*} = \left(1 - \frac{2e}{B}\right)^2 \left(1 - \frac{\alpha}{\phi}\right)^2 \qquad (4)$$

and has been evaluated for $\phi = 40^\circ$. - Again most of the data points lie in the sliding failure range however the displacement vectors at $\frac{P_v}{P_v^*} = .25$ and .345 indicate a changeover into the vertical failure mode.

Thus from the present data, albeit very limited, it appears that the failure envelope defined by $\frac{P_v}{P_v^*} = \left(1 - \frac{2e}{B}\right)^2 \left(1 - \frac{\alpha}{\phi}\right)^2$ for eccentric and vertical load seems conservative, provided the lower portion of the envelope is cut off by the line $\frac{P_h}{P_v^*} = \frac{P_v}{P_v^*} \tan \delta$ ~

The validity of the eccentricity yield locus i.e. $\frac{P_v}{P_v^*} = \left(1 - \frac{2e}{B}\right)^2$ is of course supported by the findings of many other workers and here in Fig. 13, Fig. 17 of Terashi et al (1984) is reproduced, demonstrating clearly that this expression is a reasonable lower limit estimate.

Conical Footing Results

Typical results of the tests on the 120 mm diameter conical footing are shown in Fig. 14.

The hollow circles are for the total vertical load P against vertical displacement and the solid black circles are the average vertical stress q* i.e. $q^* = P/A_s$ where A_s is the area of a plane section through the cone at the level of the sand surface.

There is a difficulty on the centrifuge in establishing the complete loading displacement relationship for a cone since with a simple experimental arrangement it is necessary to start the test with an initial vertical embedment of the cone of some 20 to 30 mm, which

in prototype terms say for a 100^{th} scale model could represent 2.0 to 3.0 metres! In order to circumvent this problem multistage tests were performed, i.e. the cone was penetrated at 40 g from .0205 m to .0215 m (at which displacement the full capacity of the loading system was reached). This is plotted in prototype terms in Fig. 15 on the curve labelled 40 g, i.e. upto a load of about 3.5 MN the displacement remains steady at .82 m (.0205 x 40), then yield occurs and the vertical displacement increases to 1.1 m (.0275 x 40) at which point the cone is unloaded and the centrifuge acceleration reduced to 20 g thus in effect giving us a smaller prototype cone at a smaller embedment. That is the 20 g penetration test now commences at a vertical embedment of .55 m (.0275 x 20) yield occurs at about 2.0 MN vertical load and the displacement increases to 0.6 m (.03 x 20). The cone is now unloaded and the procedure repeated at 10 g. Each time yield is reached we may consider that we are back on the virgin loading curve and thus the dashed line in this figure may be considered as the virgin load dispalcement curve for such a cone. The 60 g curve on the righthand side of the figure was obtained from the results of Silva Perez (1983). The chain dotted line in this figure is calculated employing experimentally determined N_γ values from the flat footing tests and is for the equivalent flat footing, i.e. treating the plane section of the cone level with the soil surface as a surface footing. It is apparent for this particular case that the cone has approximately $\frac{1}{4}$ the capacity of the equivalent flat plate.

Conclusions

Initial exploratory centrifugal testing of circular footings on sand indicate a very strong dependence of the self weight bearing capacity factor N_γ on stress level. The failure locus given by the expression $\frac{P_v}{P_v^*} = \left(1 - \frac{2e}{B}\right)^2 \left(1 - \frac{\alpha}{\phi}\right)^2$ appears to be conservative however the lower portion of the yield locus must be cut off by a straight line $\frac{P_h}{P_v^*} = \frac{P_v}{P_v^*} \tan\delta$ where $\tan\delta$ is the coefficient of friction between the footing and the sand.

Modelling of Models with respect to the load displacement behaviour of a 3.0 m diameter prototype flat footing gave a "satisfactory" correlation. Initial results for conical footings indicate that in this particular case, i.e. a 120° cone angle and $\delta \simeq 11°$ the vertical bearing capacity is about ¼ of that of the equivalent flat plate at the surface.

Acknowledgements

The Authors wish to thank the S.E.R.C. for providing funds, the Engineering Department for providing faiclities, there colleagues for assistance and encouragement, the P.R.H.I. of Yokosuka, Japan for enabling H Tanaka to spend a year at the C.U.E.D., and Professor J. A. Cheney of Davis University, California, who organized the Geotechnical centrifugal modelling symposium at which this paper was presented. Finally we extend our thanks to Reveria Wells for typing the manuscript.

References

Hansen, Bent, (1976) Modes of failure under inclined eccentric loads, Proc. of the first Int. Conf. Behaviour of off-shore structures, Vol. 1, pp 488-500.

Hansen, Brinch (1970) A revised and extended formula for bearing capacity, Bulletin, No. 28, The Danish Geotechnical Institute, pp 5-11.

King, G. J. W. et al. (1984) The development of a medium-size centrifugal testing facility. The application of centrifuge modelling to geotechnical design. Edited by Craig, W. H., University of Manchester, pp 25-46.

Meyerhof, G. G. (1953) The bearing capacity of foundations under eccentric and inclined loads, Proc. 3rd Int. Conf. Soil Mech. Foun. Eng., Vol. 1, pp 440-445.

Muhs, H and Weiss, K. (1973) Inclined load tests on shallow strip footings, Proc. 8th Int. Conf. Soil Mech. Foun. Eng., Vol. 1, Part 3, pp 173-179.

Perez, A. S. (1982) Conical footings under combined loads, M Phil thesis, University of Cambridge.

Poulos, H. G. and Davis, E. H. (1974) Elastic solutions for soil and rock mechanics, John Wiley and Sons. Inc.

Terashi, M. et al (1984) Bearing capacity of sand under eccentric load, Unpublished.

Terzaghi, K. (1943) Theoretical soil mechanics, Wiley.

Ticof, J. (1977) Surface footings on sand under general planar loads, Ph.D. thesis, University of Southampton.

Test No.	Footing type *)	dia.of footing (mm)	e	preload (MN/m^2)	ground No.	void ratio	unit weight (kN/m^3)	loading **)
S-1	F	100	0	0	1	0.489	17.87	V
S-2	F	50	0	0	1	0.489	17.87	V
S-3	F	75	0	0	2	0.487	17.89	V
S-4	F	75	10	2.2 e=0	2	0.487	17.89	V E
S-5	F	75	20	2.3 e=0	3	0.490	17.85	V E
S-6	C	120	0	0	3	0.490	17.85	V
S-7	F	75	0	0	4	0.471	18.08	V H
S-8	F	75	15	1.8 e=15mm	4	0.471	18.08	VHE

*) F = Flat footing
C = Conical footing

**) V = vertical loading
E = eccentric loading
H = horizontal loading

TABLE I - SAND TESTS

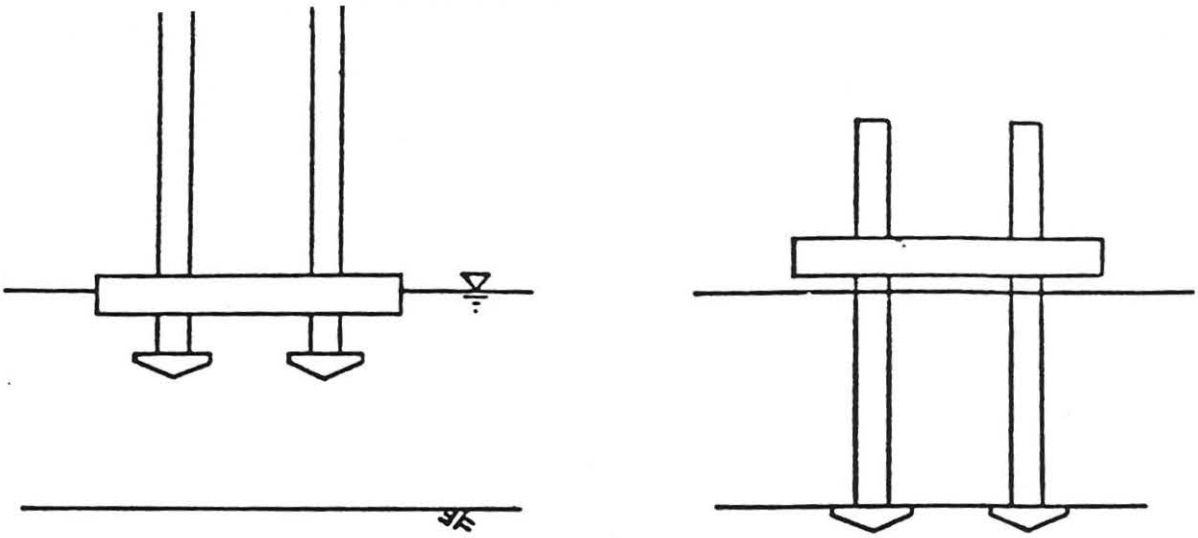

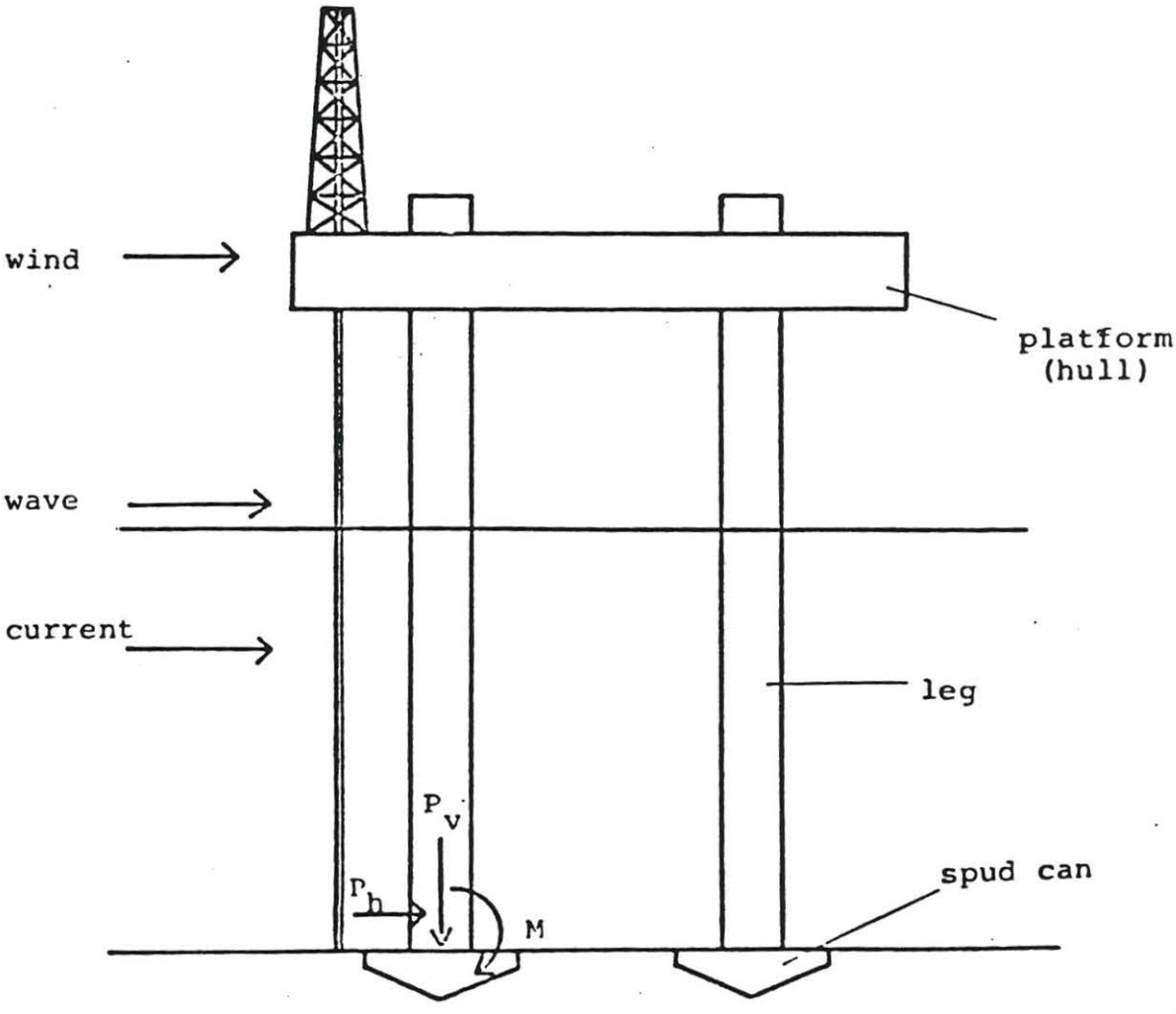

Fig. 1 jack-up rig

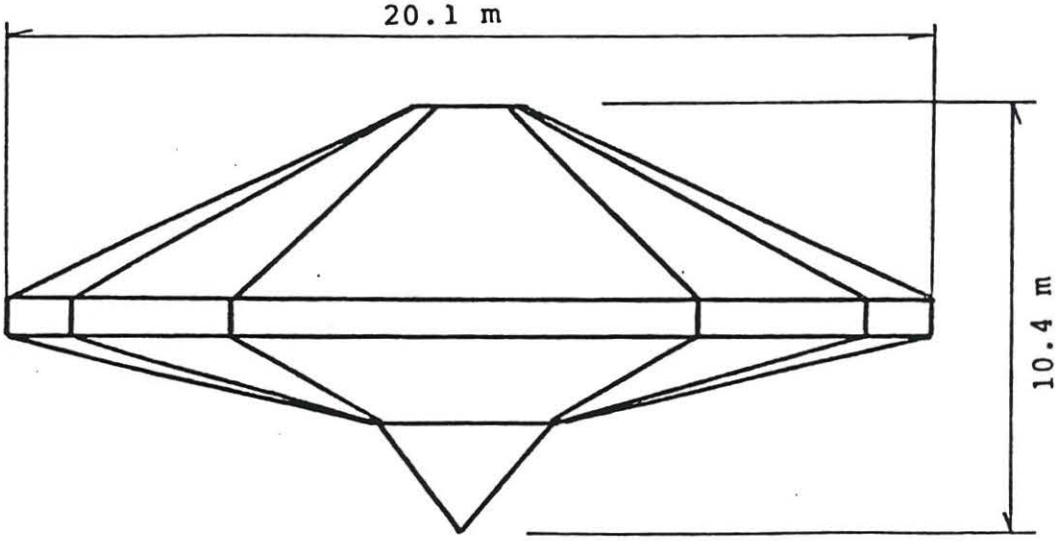

Fig. 2 spud can of jack-up rig

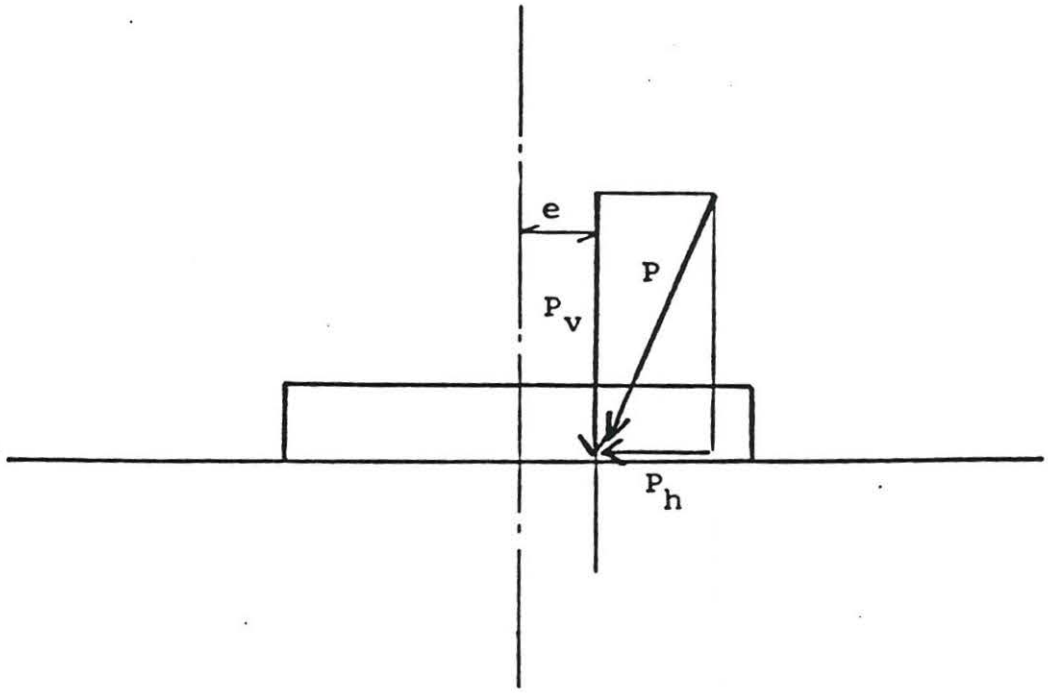

Fig. 3 eccentric and inclined load

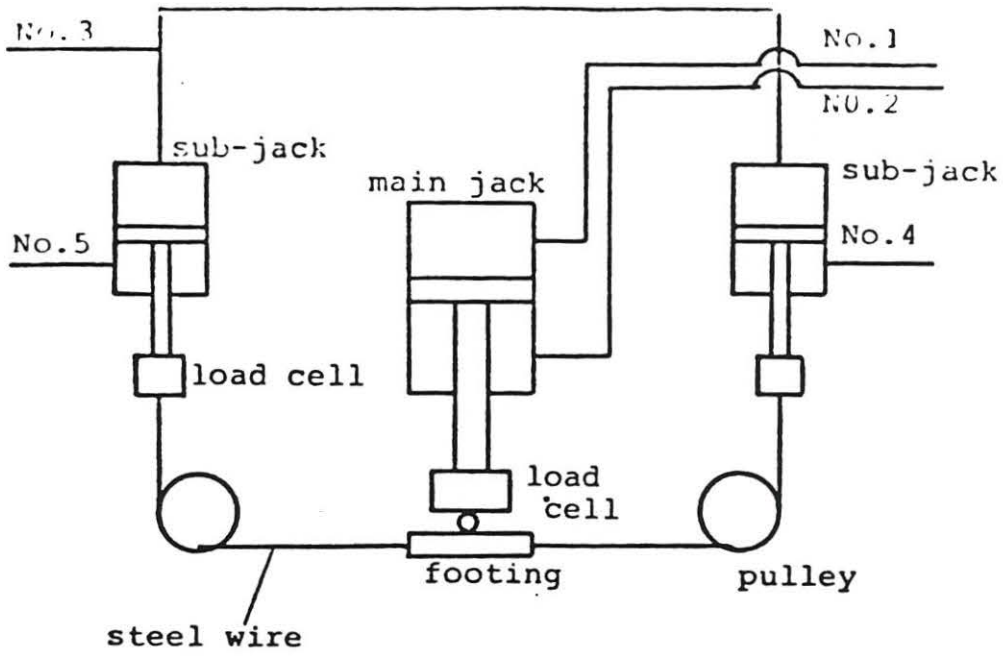

Fig. 4 . conceptual illustration of loading apparatus

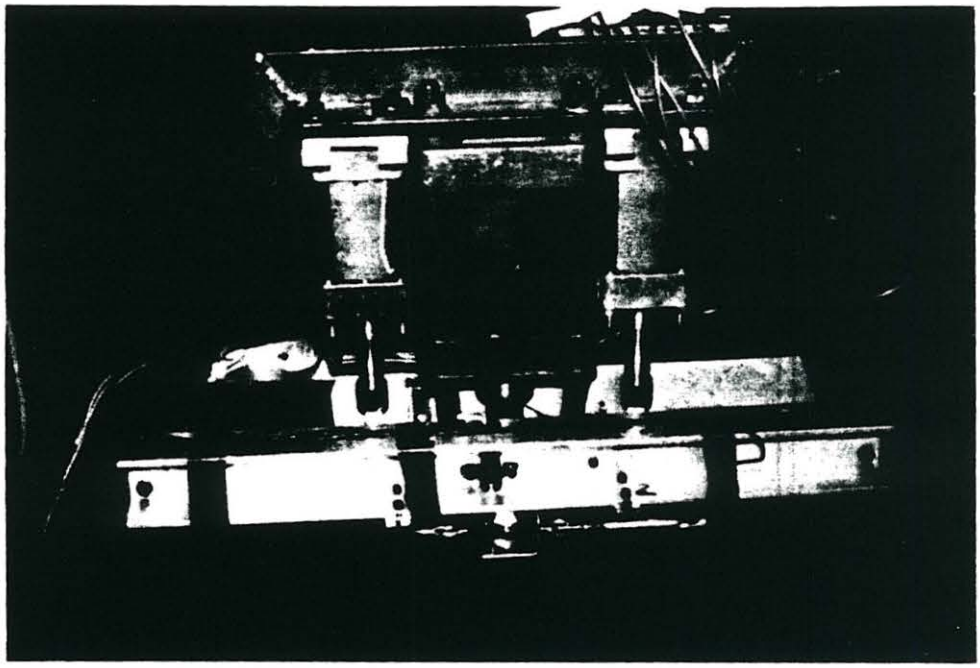

Fig. 5. Photographs of the footing apparatus

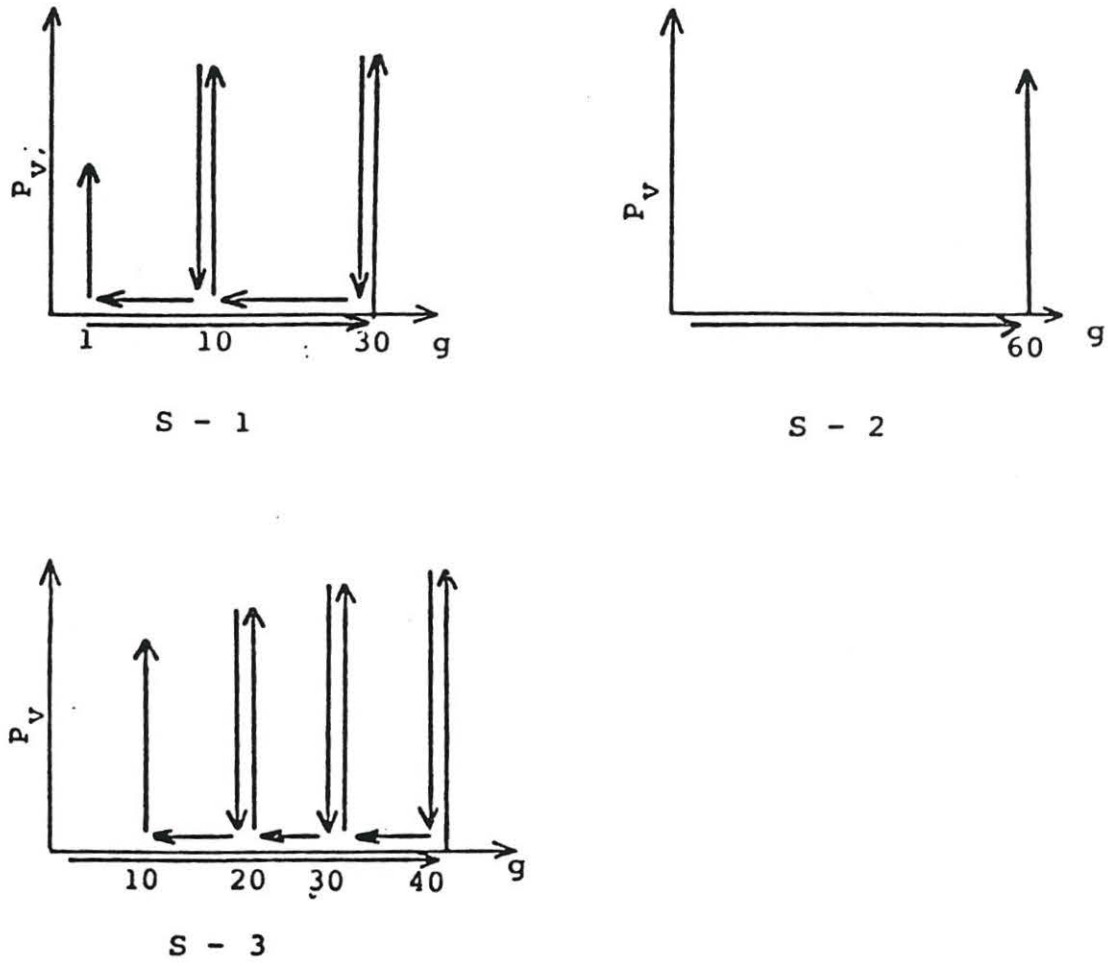

Fig. 6(a) loading path in tests S1 - S3

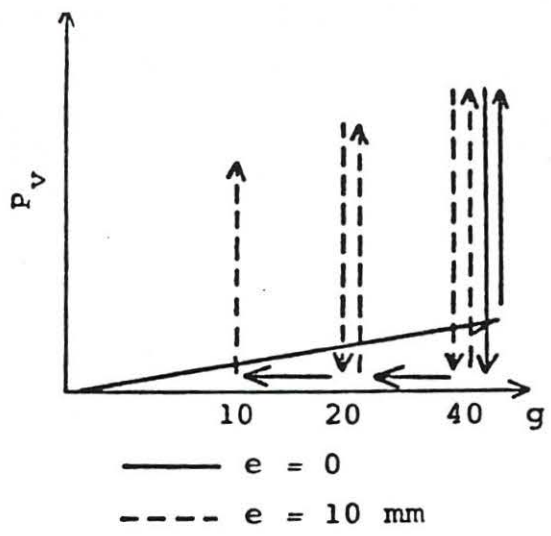

S - 4

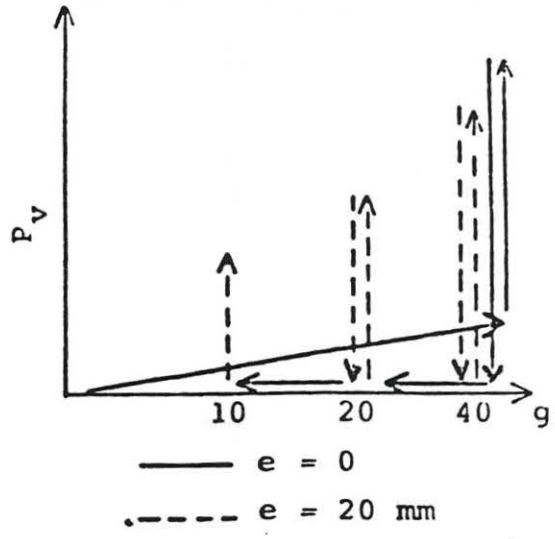

S - 5

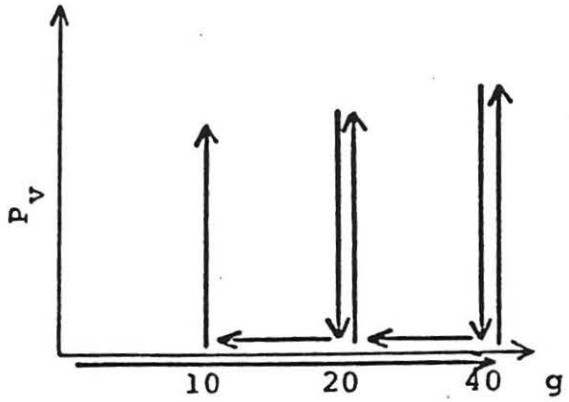

S - 6

H horizontal loading

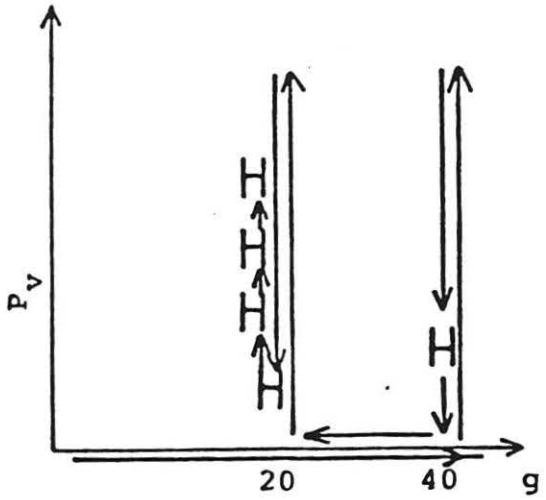

S - 7

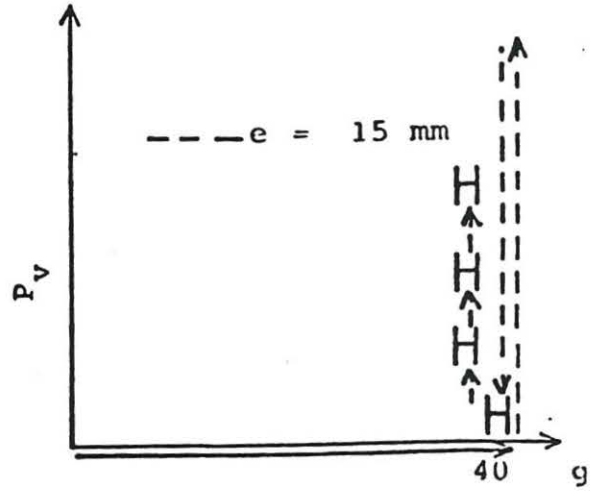

S - 8

Fig. 6(b) loading path in tests S4-S8

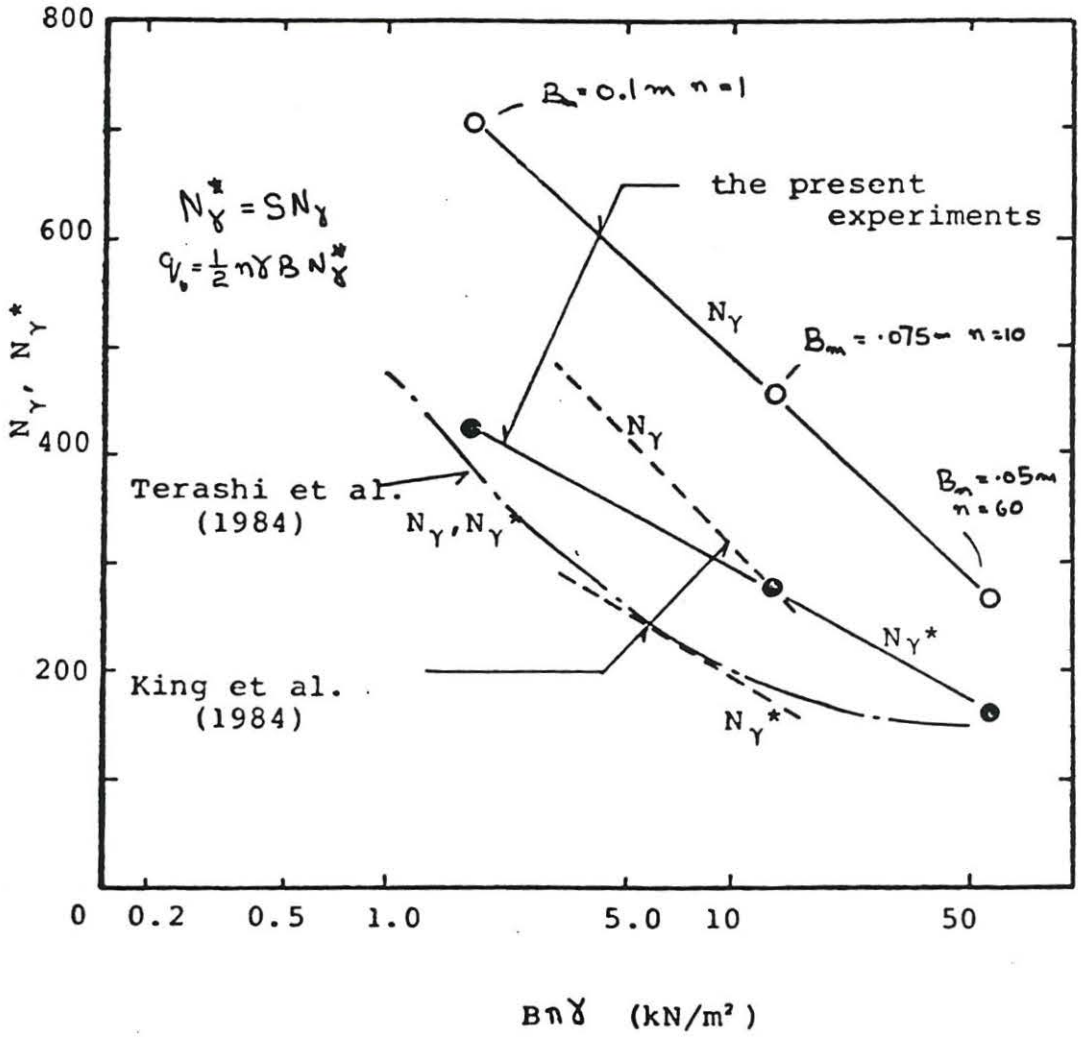

Fig. 7 influence of 'size effect' on bearing capacity factor N_γ

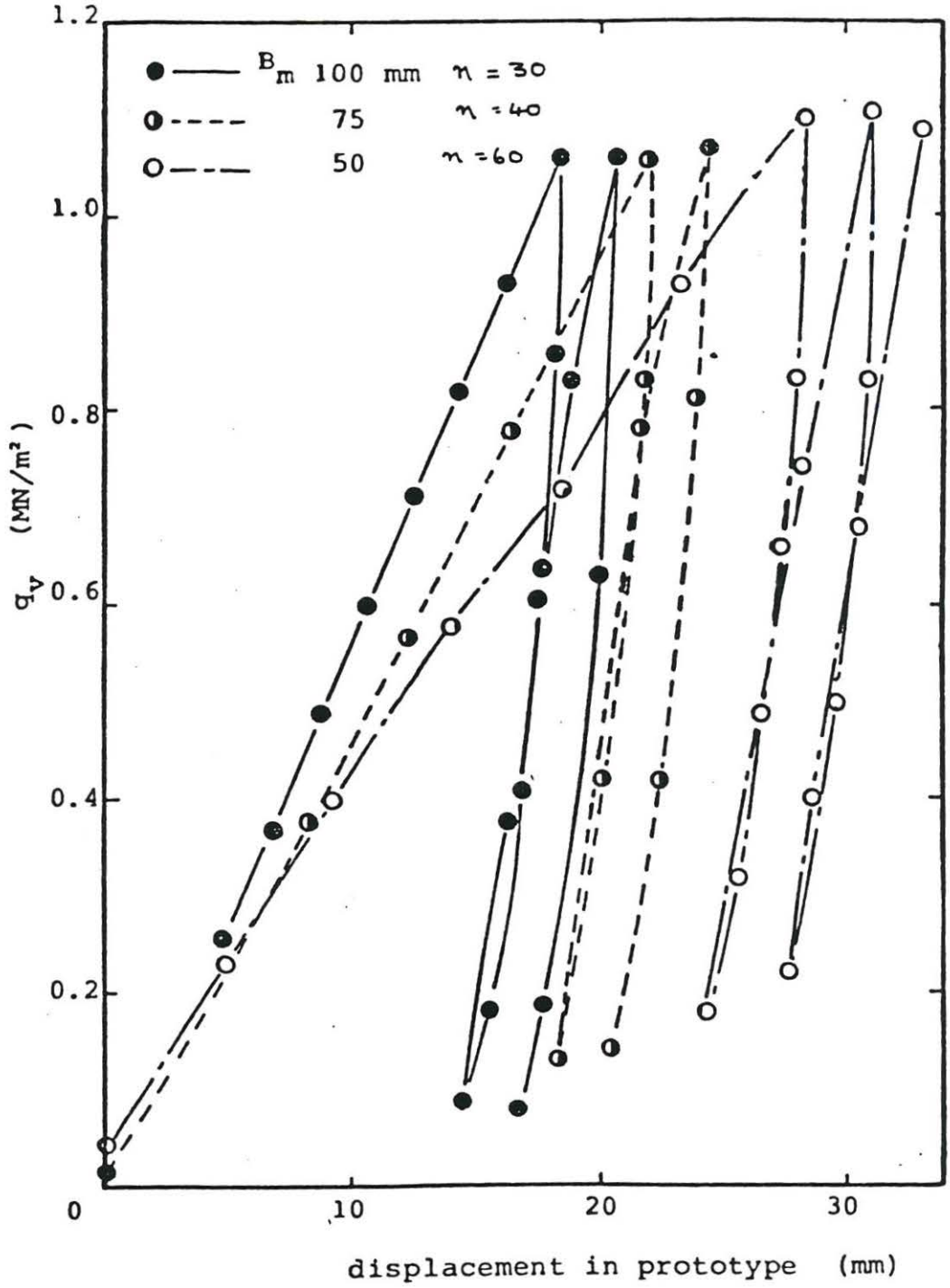

Fig. 8 modelling of models of bearing capacity on sand

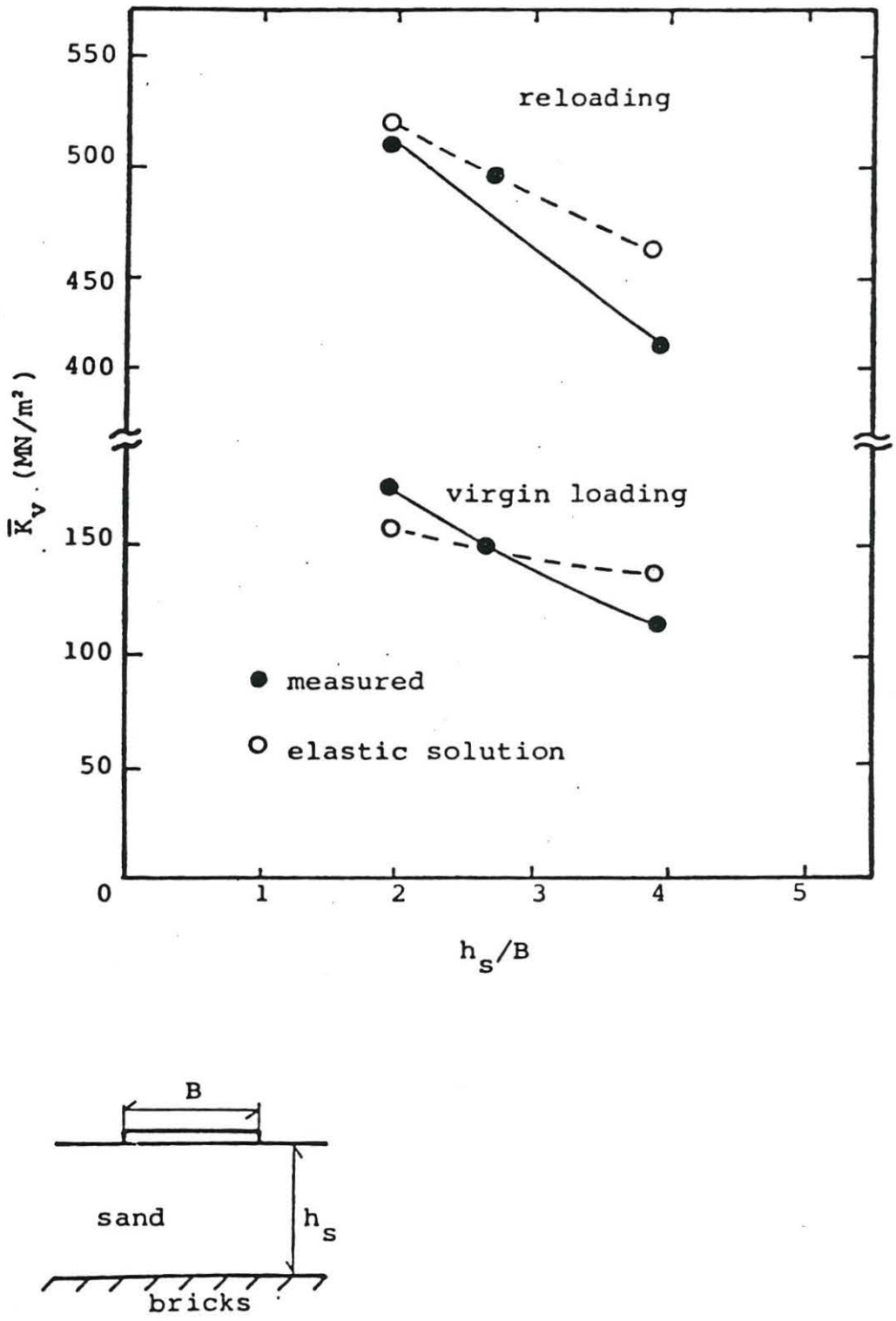

Fig. 9 influence of the existence of hard layer on coefficient of subgrade reaction

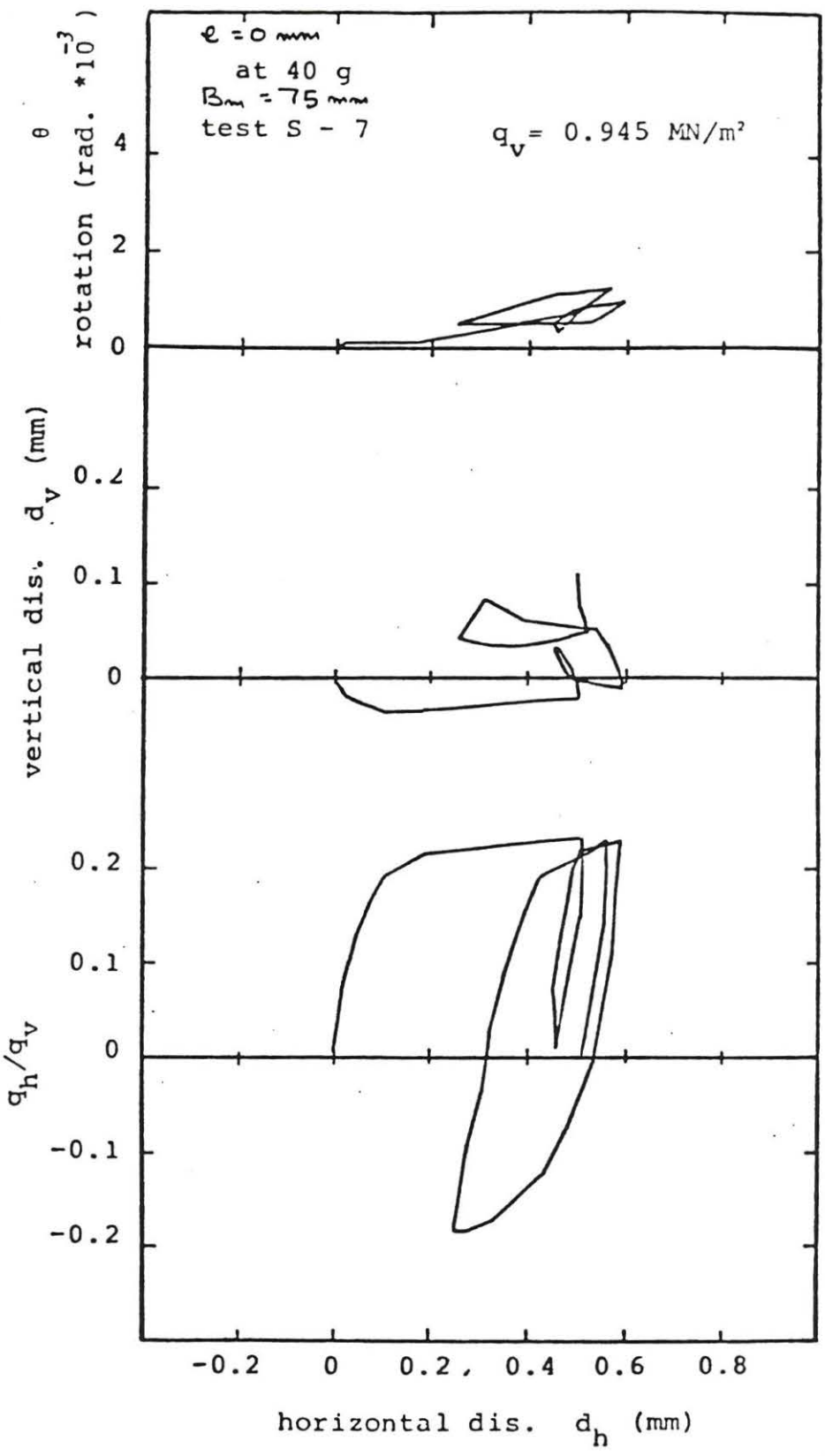

Fig. 10 (a) behaviour of footing under horizontal load no eccentricity

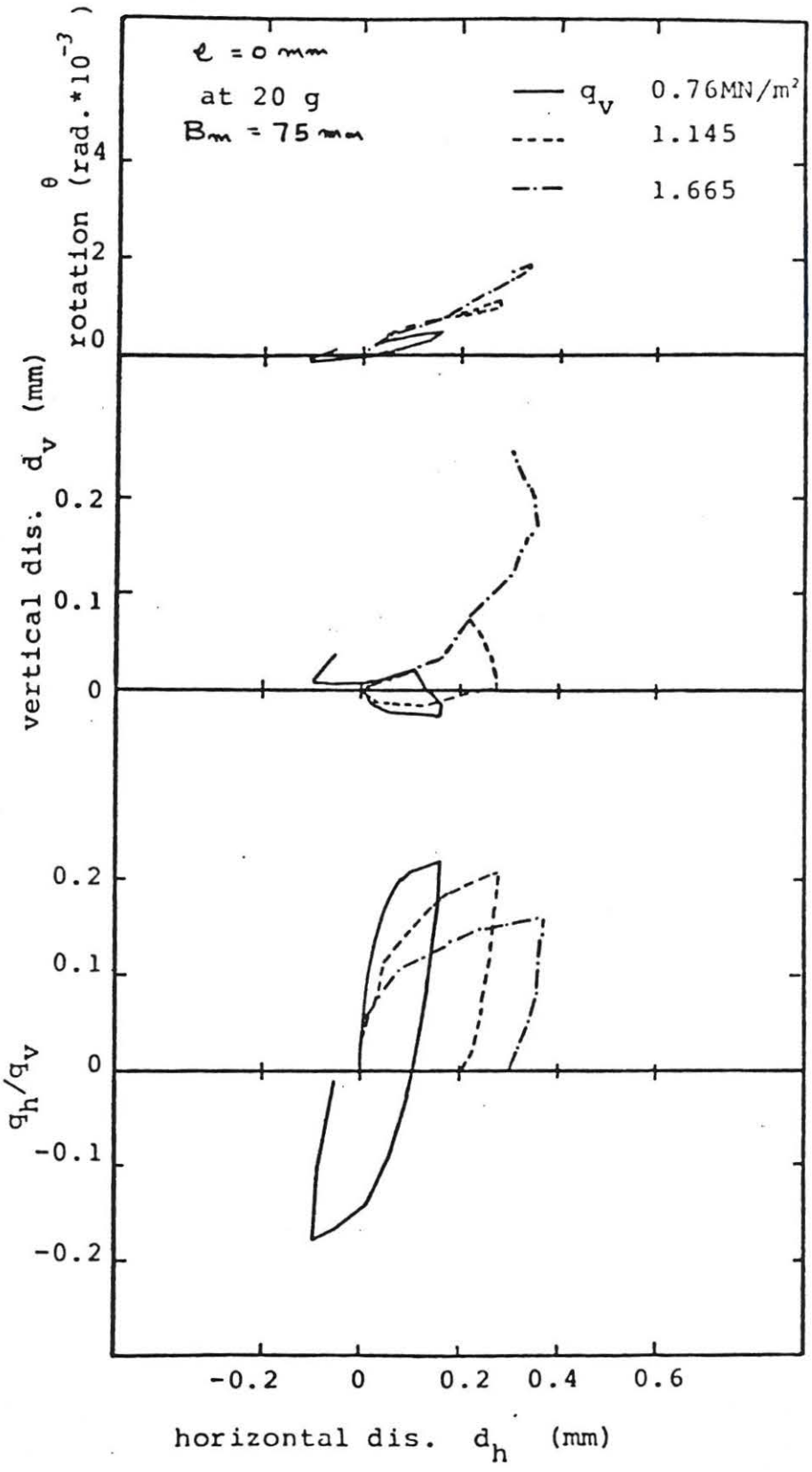

Fig. 10 (b) behaviour of footing under horizontal load no eccentricity

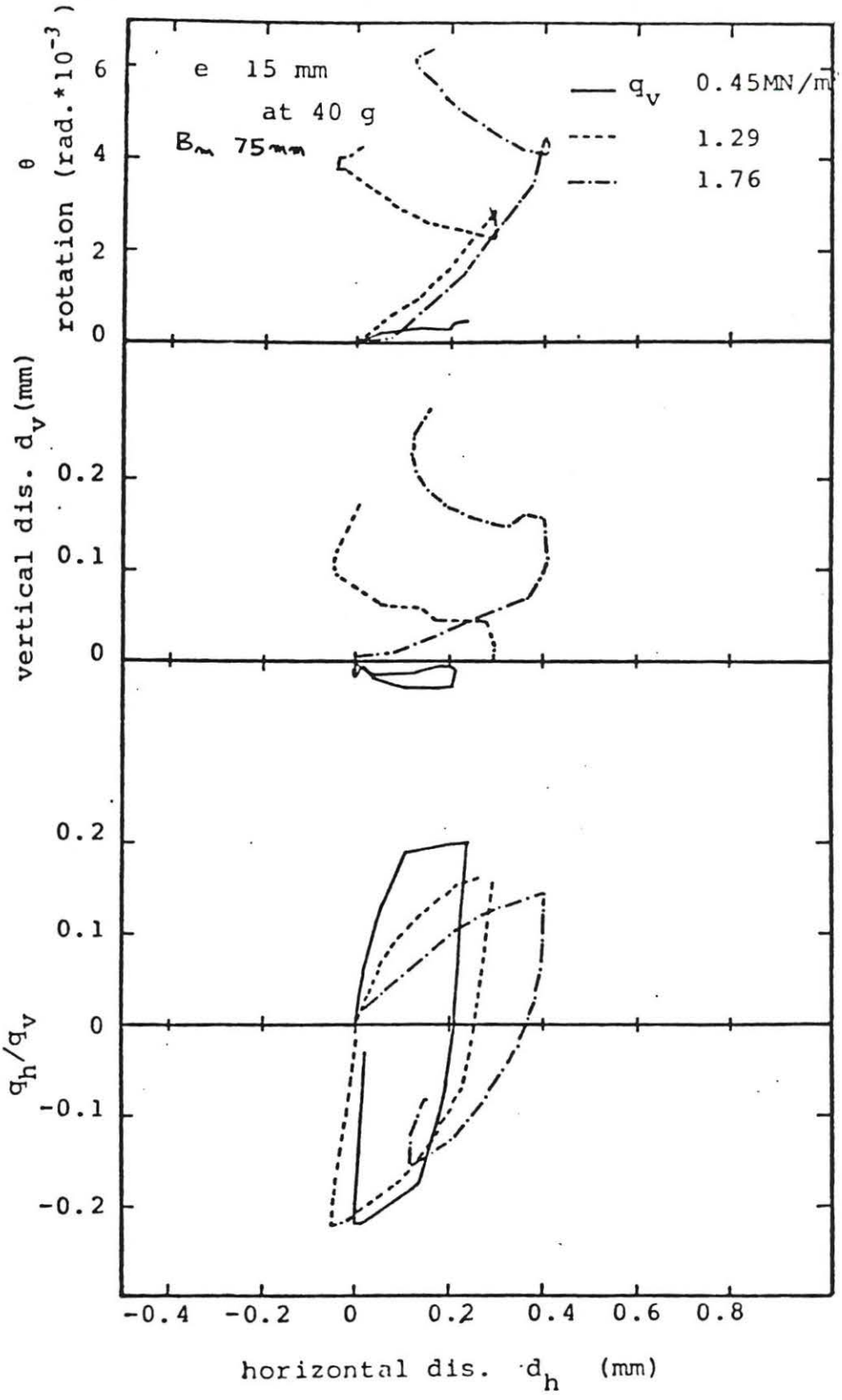

Fig. 10 (c) behaviour of footing under horizontal load eccentricity is 15 mm

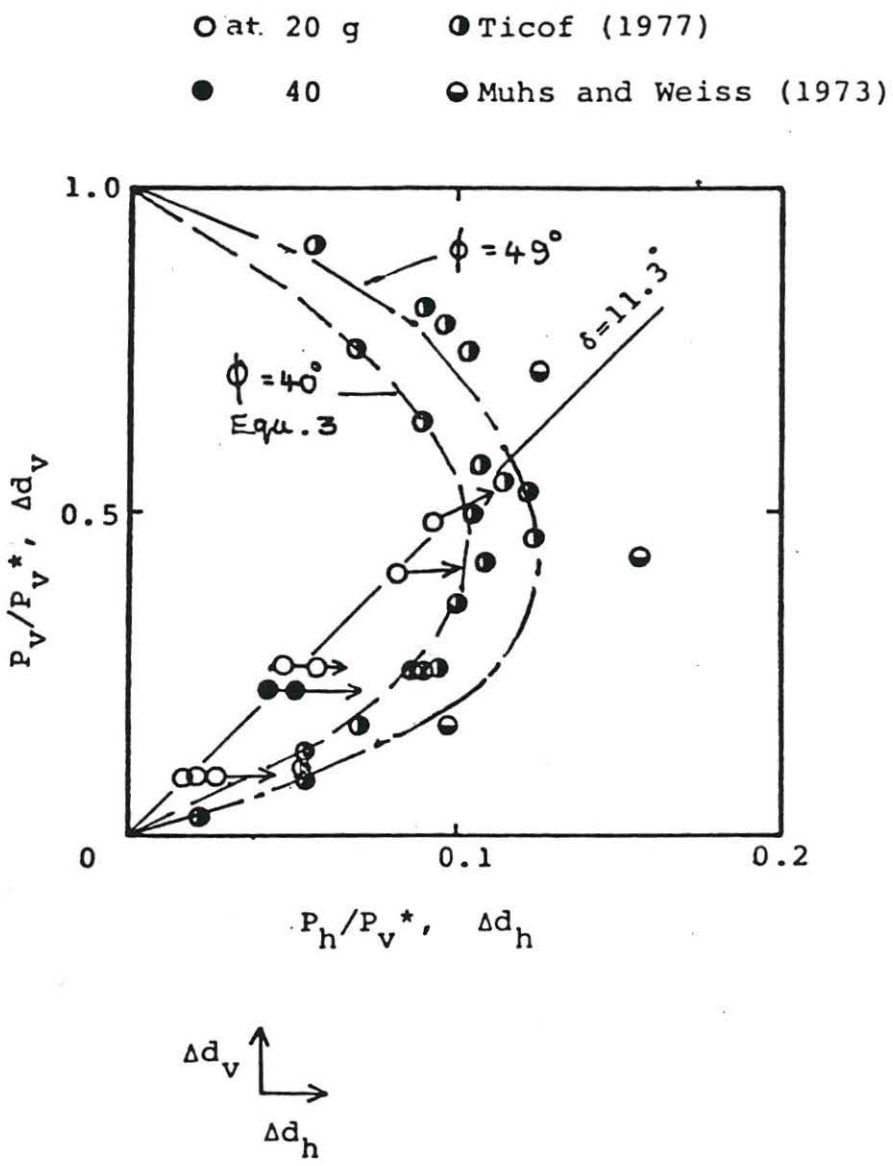

Fig. 11 failure envelope of horizontal load
no eccentricity

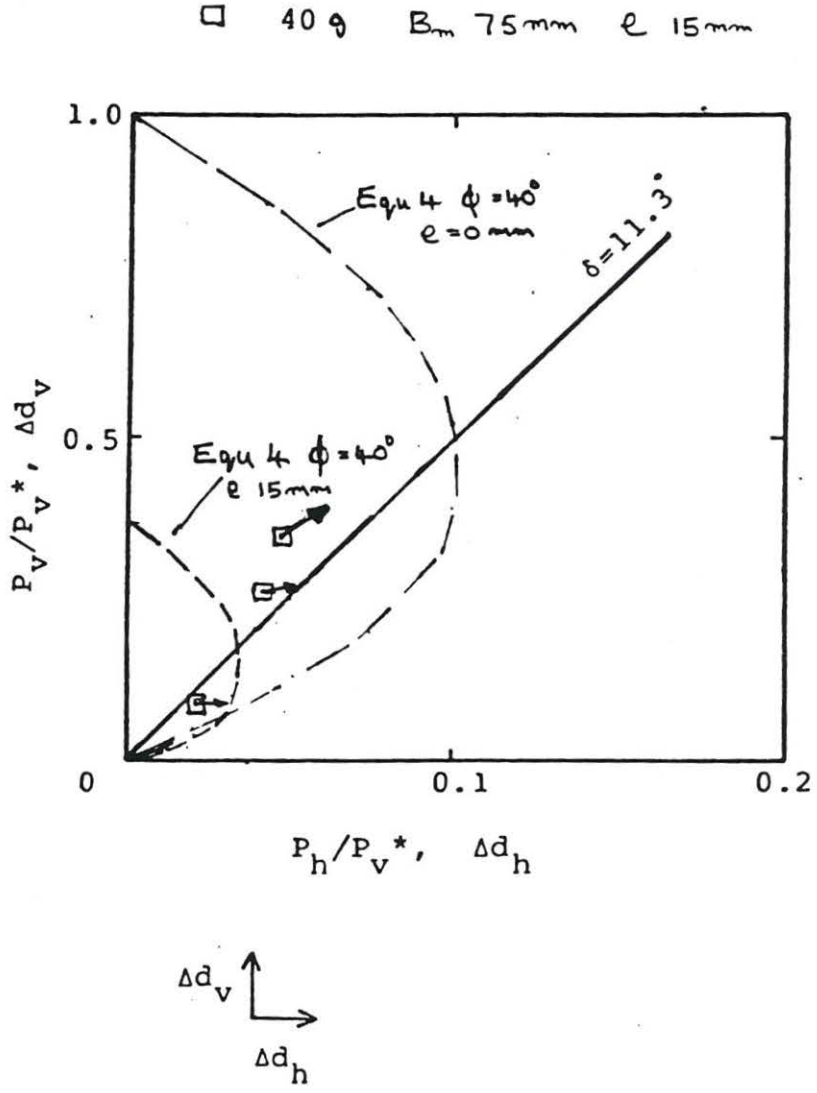

Fig. 12 failure envelope of horizontal load, eccentricity 15 m.m.

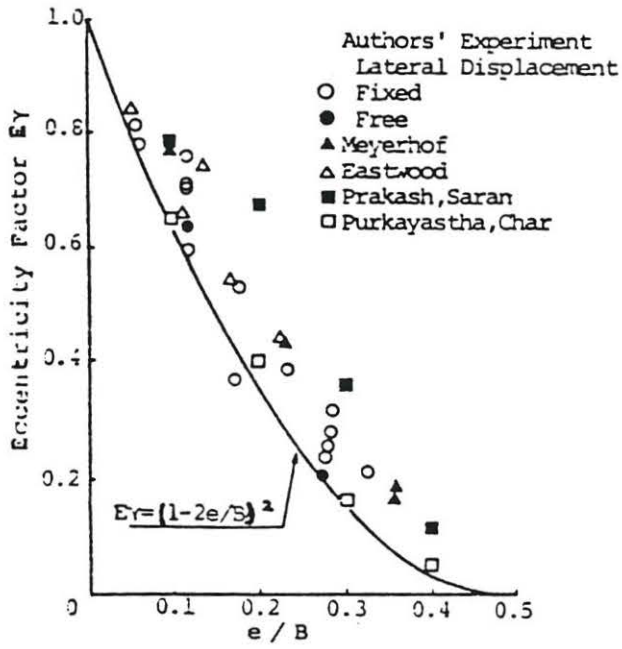

Fig. 17 Ey vs e/B

FIG. 13 ECCENTRICITY FAILURE 'LOCUS' (TERASHI et AL 1984)

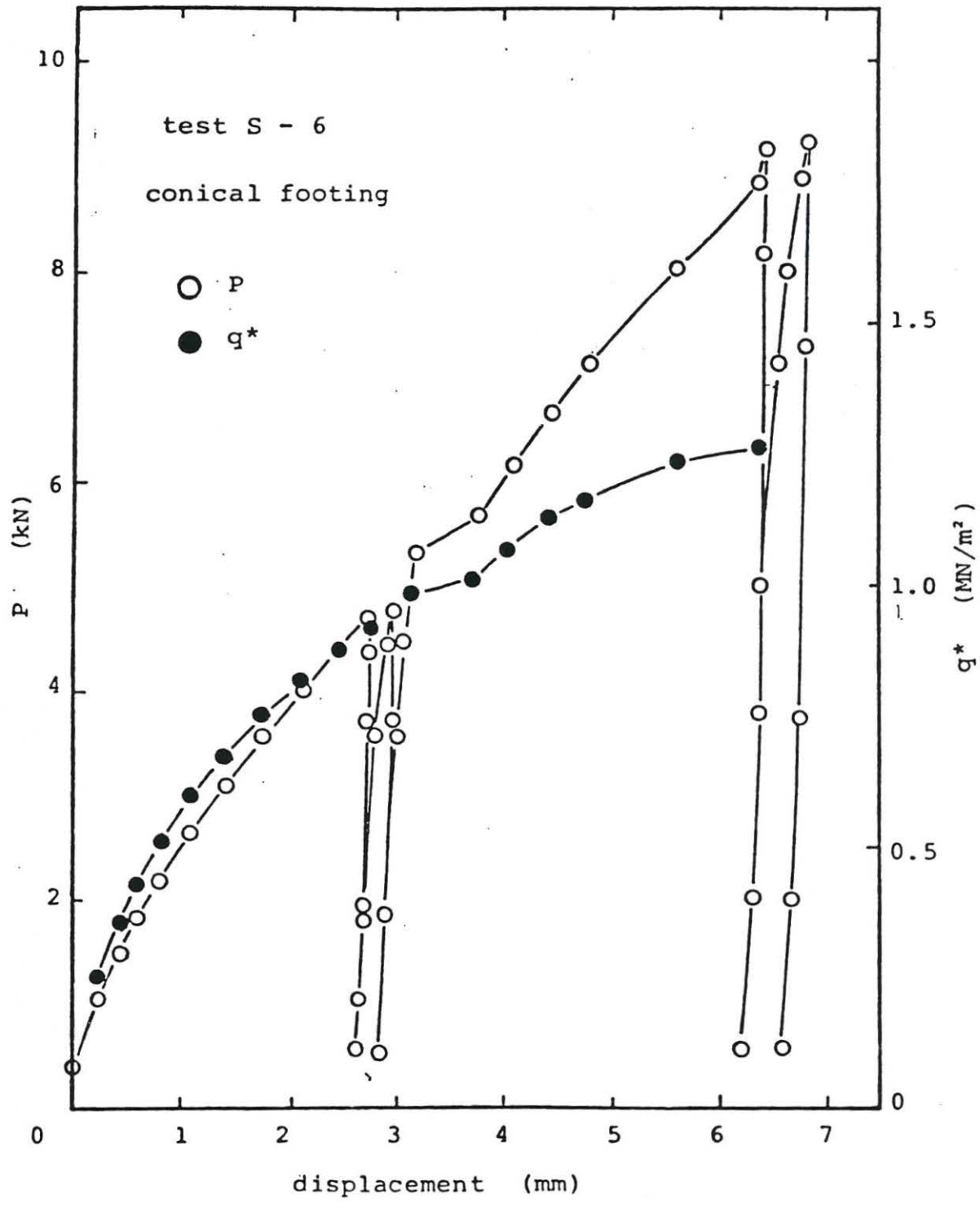

Fig. 14 relationships between force and displacement conical footing

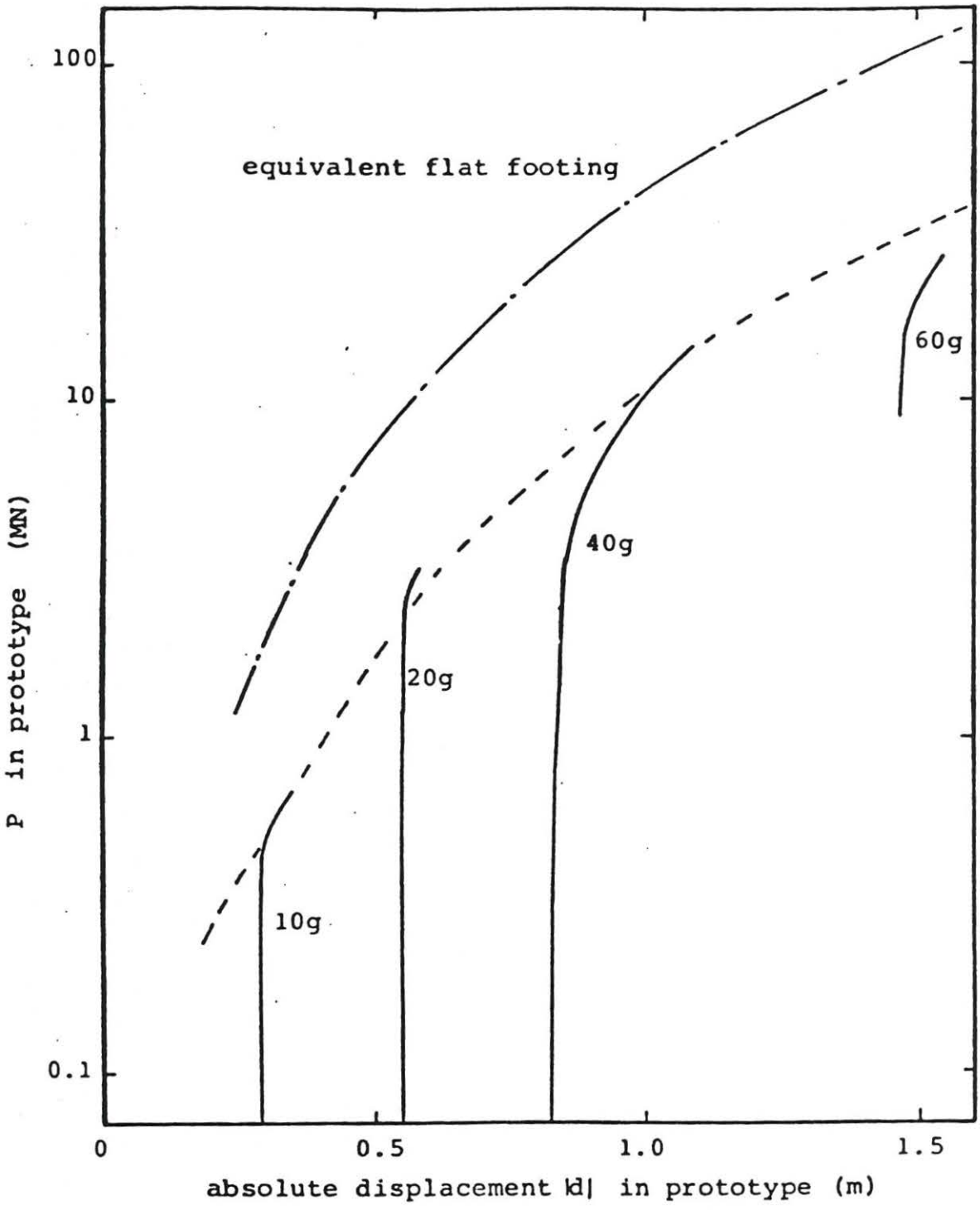

Fig. 15 relationships between force and absolute displacement in conical footing

ANALYTICAL AND CENTRIFUGE STUDIES ON LATERALLY LOADED SINGLE PILES

V. S. Chandrasekaran
Professor of Civil Engineering
Indian Institute of Technology
Bombay, India.

K. R. Kulkarni
Professor of Civil Engineering
Indian Institute of Technology
Bombay, India.

G. J. W. King
Senior Lecturer in Civil Engineering
The University of Liverpool
Liverpool, U.K.

Presented at the International Symposium on
Recent Advances in Geotechnical Centrifuge Modelling
University of California, Davis, USA
18-20 July, 1984.

S Y N O P S I S

A semi-analytical approach based on harmonic representation of displacements in the circumferential direction and finite element discretisation of the medium in the radial and vertical direction has been used to develop dimensionless parameters for the analysis of laterally loaded single piles. Parameters are given for piles embedded in half-space in which the elastic modulus is either constant or proportional to depth.

Results of centrifuge tests on laterally loaded single piles embedded in medium dense dry sand are compared with those computed using subgrade reaction and elastic continuum models. It is observed that the elastic theories are applicable at deflection levels of less than about one-half to one per cent pile diameter.

1. Introduction

Analysis of piles subjected to lateral loads is commonly carried out by replacing the soil support either by a spring bed or by an elastic continuum. The spring bed model has been studied by many investigators and has been refined to consider variations of horizontal subgrade reaction with depth (e.g. Reese and Matlock 1957, Davisson and Gill 1963). For cohesionless soil it is considered adequate to assume that the horizontal subgrade reaction is proportional to depth and based on field and laboratory data, several recommendations have been made in regard to the value of the proportionality constant n_h (Terzaghi 1955, Reese et al 1974, Davisson and Sulley 1970). Procedures for considering the non-linear behaviour of soil have also been introduced in this model through the use of p-y curves.

Solutions based on continuum model were first obtained by Poulos (1971) using Mindlin's solution for horizontal load within a homogeneous half-space. Recently the boundary element method (Banerjee and Davis 1978) has been applied to the problem of laterally loaded piles. In these approaches arbitrary inhomogeneity in the soil deposit cannot be considered. The finite element method based on harmonic representation of displacements in circumferential direction can be used for analysing a pile subjected to a lateral load. Randolph (1981) used linear strain triangular elements and proposed simple expressions for analysing flexible piles.

In the first part of the present paper dimensionless

parameters based on finite element analysis are presented in simple form for analysing the behaviour of flexible piles in homogeneous elastic half-space and in a half-space in which the elastic modulus is proportional to depth.

In the second part of this paper results of lateral load tests on single piles carried out in a centrifuge are presented and discussed with a view to identify some of the main trends in the pile behaviour.

2. Parametric Study on Long Piles

In many instances it may be expedient to assume that the modulus of elasticity of soil either remains constant with depth or has a value proportional to depth. For both of these situations the results of the analysis may be conveniently presented using simple dimensionless influence factors. Here results of a parametric study for long piles is presented. The effect of variation of Poisson's ratio of the soil is also investigated.

Homogeneous Medium

Consider a pile as shown in Fig. 1 subjected to a horizontal load P_t and a moment M_t. When the soil medium is homogeneous it is convenient to define a characteristic length T given by

$$T = \sqrt[4]{\frac{EI}{E_s}} \qquad \ldots (1)$$

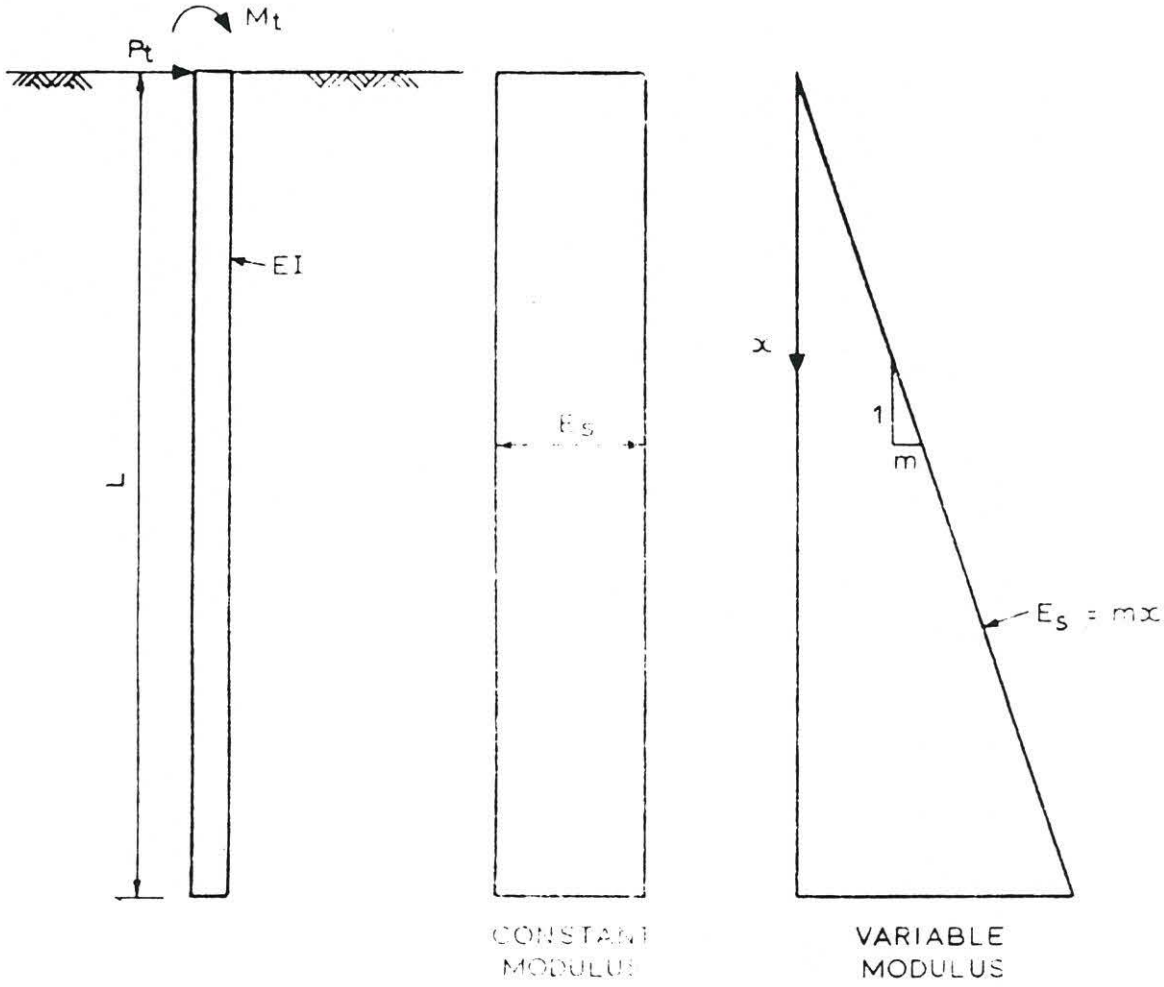

Fig.1 Soil Modulus Variation Adopted in Parametric Study

in which EI is the flexural rigidity of pile and E_s is the Young's modulus of the soil.

For given values of L/T, T/D and ν_s, and for a particular depth x = XT, expressions for deflection y, slope θ, bending moment M, shear force V and soil pressure p can be written as follows :

$$y = (P_t T^3/EI) A_y + (M_t T^2/EI) B_y$$

$$\theta = (P_t T^2/EI) A_s + (M_t T/EI) B_s$$

$$M = (P_t T) A_m + M_t B_m \qquad \ldots (2)$$

$$V = P_t A_v + (M_t/T) B_v$$

$$P = (P_t/T) A_p + (M_t/T^2) B_p$$

From a practical point of view values of A_y, A_s, B_y, B_s at the top of the pile and the variation of A_m and B_m with depth are of importance. Finite element analysis using eight noded elements and harmonic representation of displacements in circumferential direction was employed to evaluate these values (Chandrasekaran and King, 1982). Tables 1 and 2 give the values of A_y, A_s, B_y and B_s for L/T = 5 and T/D = 2, 5, 10 and 20 for values of Poisson's ratio equal to 0.47 and 0.1 respectively. For Poisson's ratio equal to 0.47 the variations of influence factors A_m and B_m with depth factor X are presented in Figs. 2 and 3 respectively.

Table 1

Dimensionless Influence Factors for Piles in a Homogeneous Elastic Continuum

$L/T \geq 5$ $\quad \nu_s = 0.47$ $\quad X = 0.0$

T/D	A_y	A_s	B_y	B_s
2	0.737	- 0.557	0.557	- 0.986
5	1.063	- 0.783	0.783	- 1.230
10	1.262	- 0.897	0.897	- 1.325
20	1.411	- 0.974	0.974	- 1.384

Table 2

Dimensionless Influence Factors for Piles in a Homogeneous Elastic Medium

$L/T \geq 5$ $\quad \nu_s = 0.1$ $\quad X = 0.0$

T/D	A_y	A_s	B_y	B_s
2	0.768	- 0.578	0.578	- 0.976
5	1.067	- 0.780	0.780	- 1.220
10	1.258	- 0.886	0.886	- 1.311
20	1.404	- 0.961	0.961	- 1.370

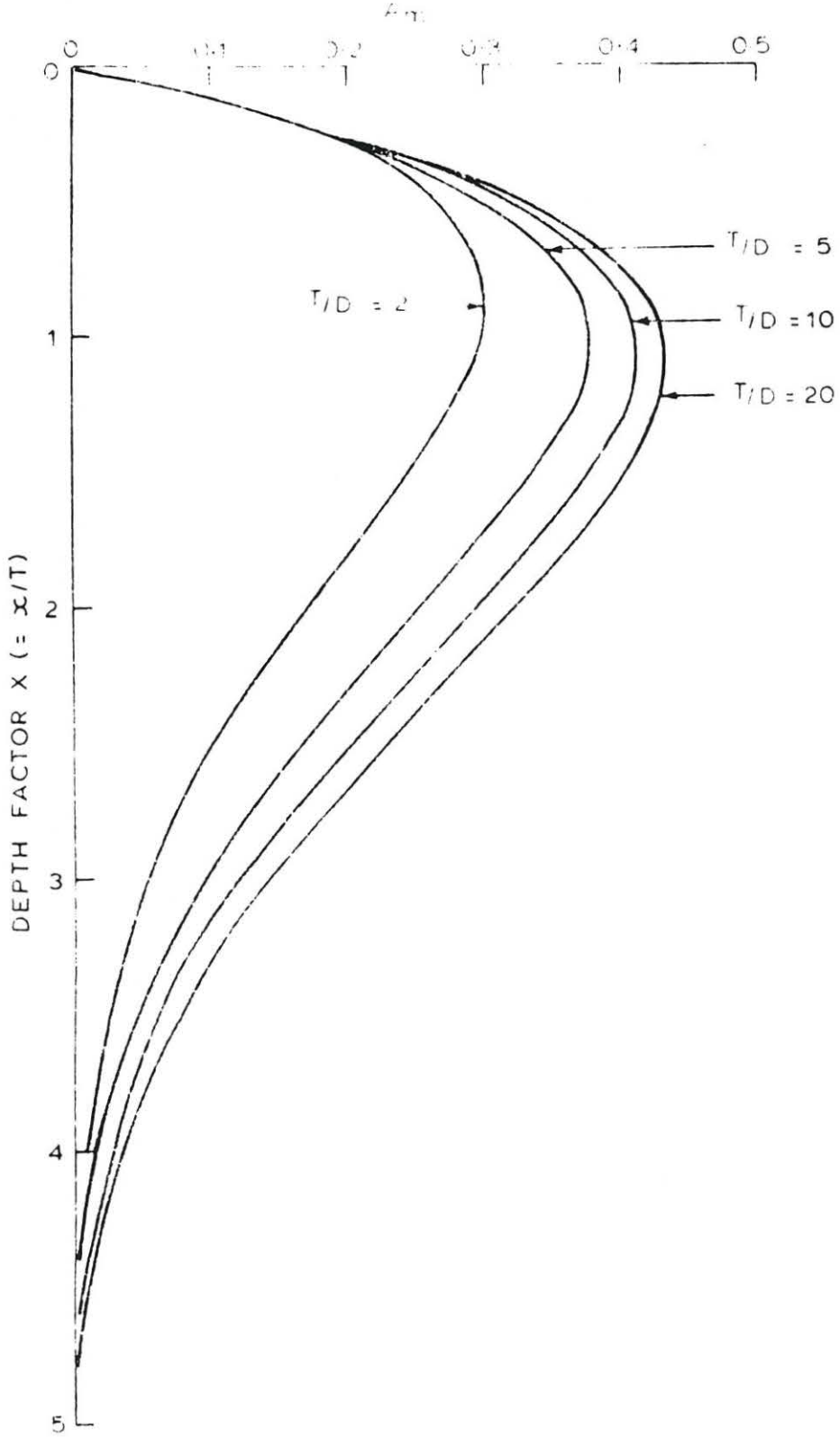

Fig.2 Variation of A_m with Depth Factor for a Homogeneous Medium

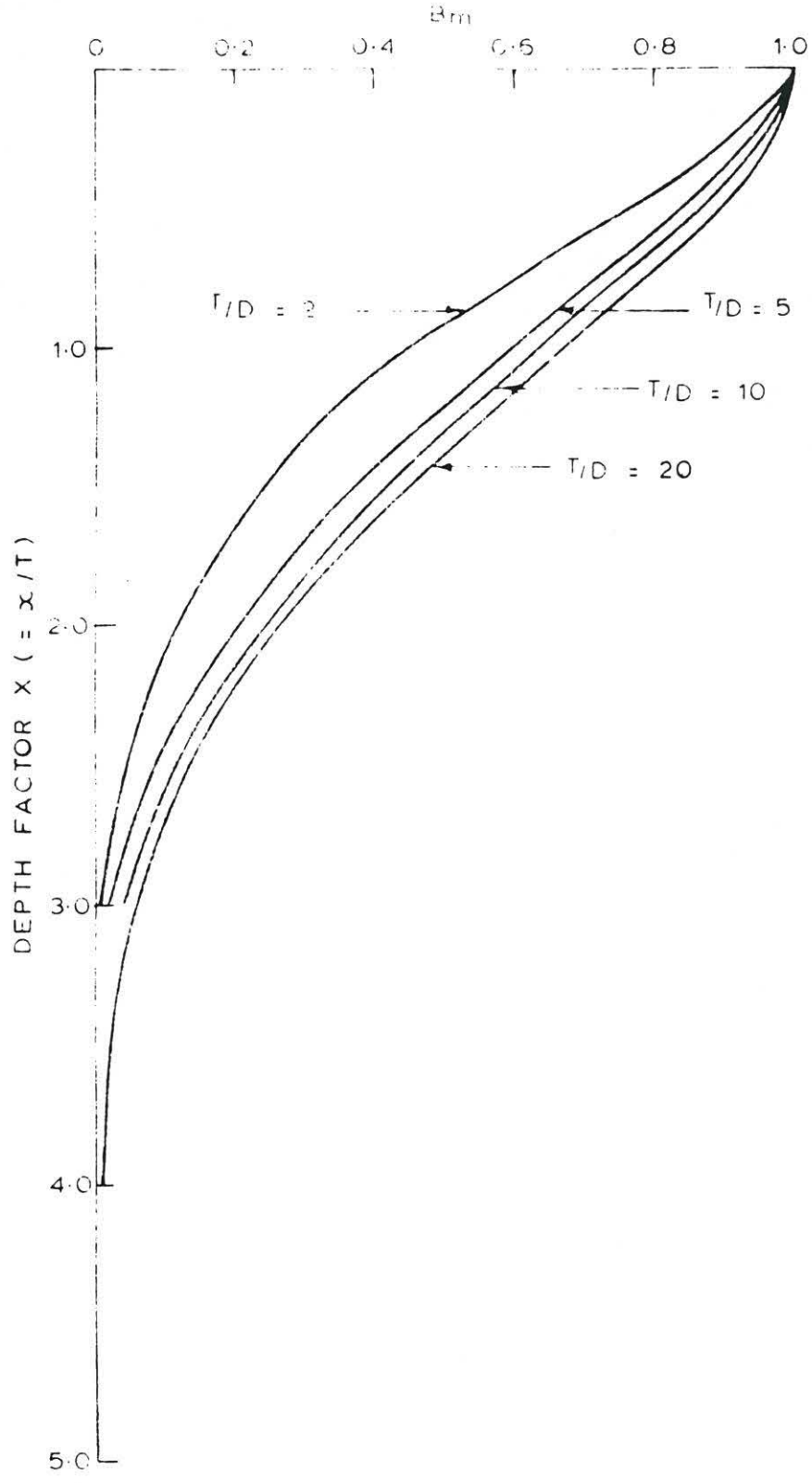

Fig.3 Variation of B_m with Depth Factor for a Homogeneous Medium

Inhomogeneous Medium

Consider a soil medium in which Young's modulus E_s varies according to the equation

$$E_s = mx \qquad \ldots (3)$$

where x is the depth from the soil surface. For a pile having flexural rigidity EI embedded in the medium it is convenient to define a characteristic length T, as

$$T = \sqrt[5]{\frac{EI}{m}} \qquad \ldots (4)$$

For given values of L/T, T/D and ν_s and for a particular depth x = XT, expressions for deflection y, slope θ, bending moment M, shear force V and soil pressure p can again be written by Eqs. (2) but with T given by Eq. (4).

Tables 3 and 4 give the values of A_y, A_s, B_y and B_s at the top of the pile for values of T/D = 2, 5, 10 and 20 for Poisson's ratio equal to 0.47 and 0.1 respectively. For Poisson's ratio equal to 0.47 the variation of A_m and B_m with depth factor X are presented in Figs. 4 and 5 respectively.

This parametric study indicates that the effect of Poisson's ratio on the behaviour of piles subjected to lateral loads is not significant and for the same flexural rigidity and soil modulus, piles of larger diameter give less deflection and bending moment.

Table 3

Dimensionless Influence Factors for Piles in Inhomogeneous Elastic Medium with $E_s = mx$

$L/T \geq 5$ $\quad \nu_s = 0.47$ $\quad X = 0.0$

T/D	A_y	A_s	B_y	B_s
2	1.285	- 0.974	0.974	- 1.254
5	1.804	- 1.289	1.289	- 1.541
10	2.099	- 1.441	1.441	- 1.636
20	2.310	- 1.543	1.543	- 1.695

Table 4

Dimensionless Influence Factors for Piles in Inhomogeneous Elastic Medium with $E_s = mx$

$L/T \geq 5$ $\quad \nu_s = 0.1$ $\quad X = 0.0$

T/D	A_y	A_s	B_y	B_s
2	1.334	- 0.998	0.998	- 1.263
5	1.814	- 1.287	1.287	- 1.535
10	2.099	- 1.433	1.433	- 1.627
20	2.310	- 1.534	1.534	- 1.687

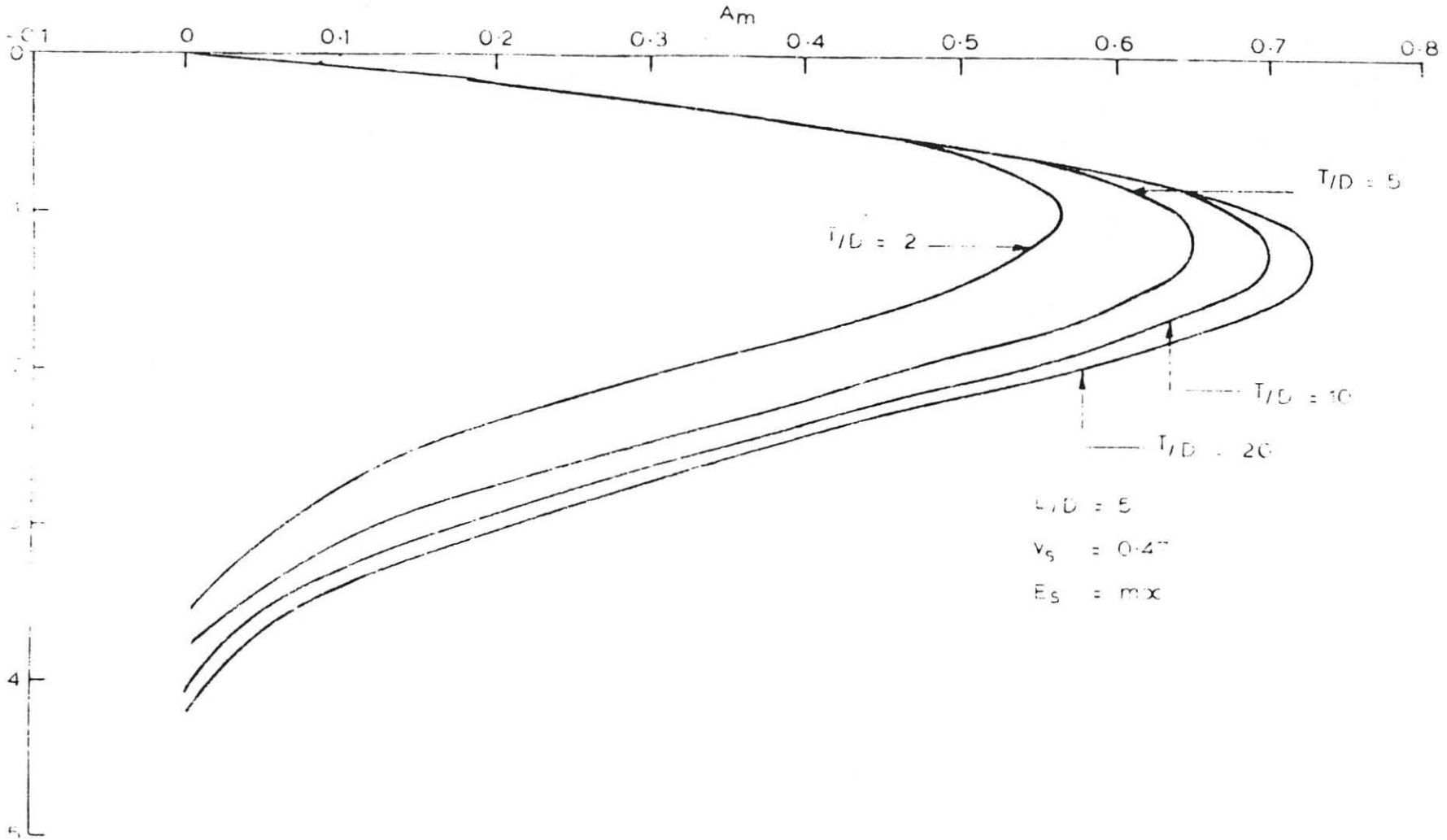

Fig.4 Variation of A_m with Depth Factor for an Inhomogeneous Medium

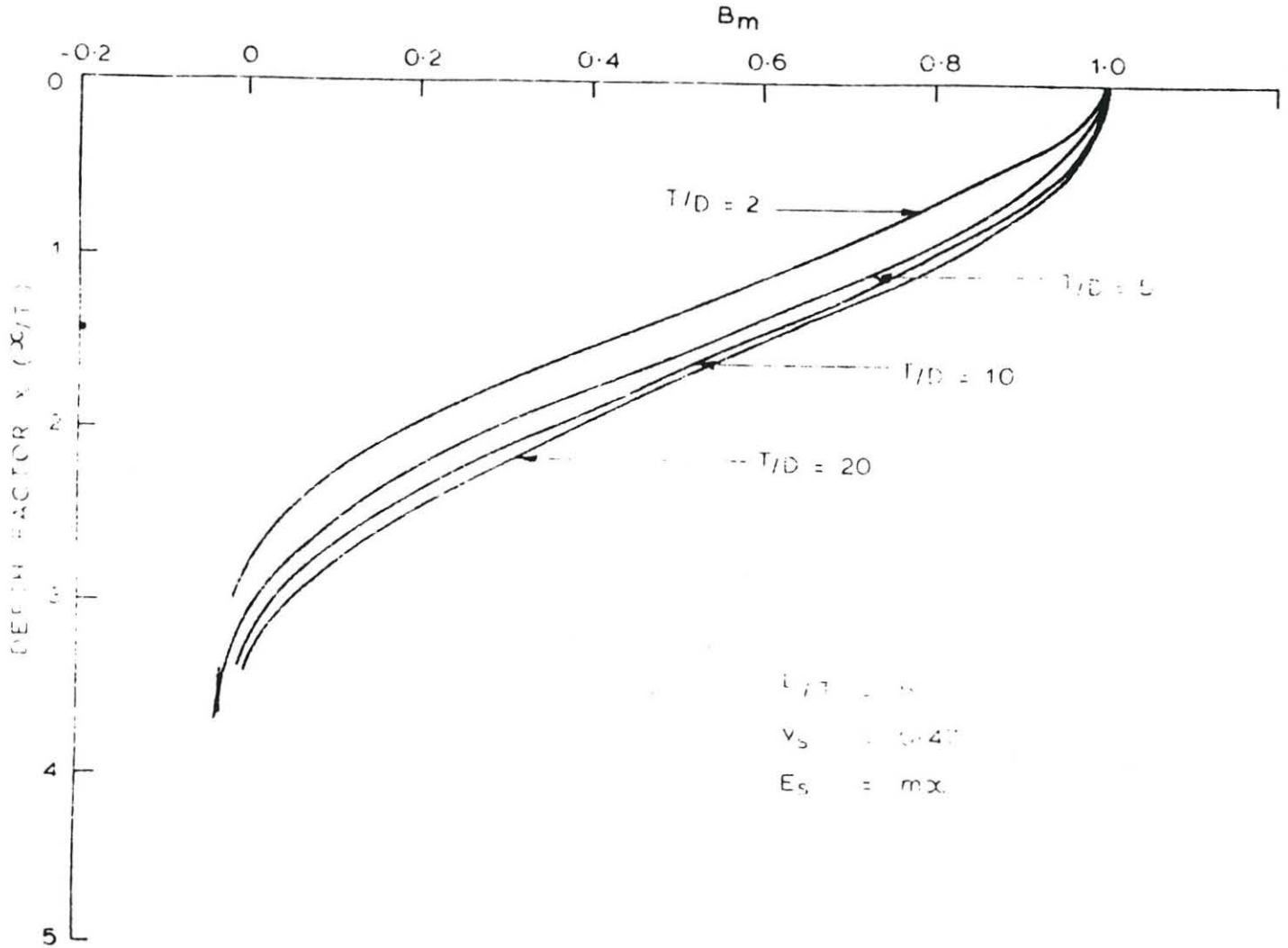

Fig.5 Variation of B_m with Depth Factor for an Inhomogeneous Medium

3. Centrifuge Experiments on Laterally Loaded Piles in Sand

3.1 Centrifuge

The behaviour of piles subjected to lateral loads may be conveniently studied by conducting experiments in centrifuge on scaled models. The modelling principle is dealt with in a number of recent publications (see for example Schofield, 1980).

The experiments were carried out in the centrifuge at Liverpool University, U.K. A detailed description of this centrifuge is given by King, et al (1984). The machine, a model G.380.3A supplied in 1974 by Trio-tech. Inc. of California, USA is shown diagramatically in Fig. 6. The original fixed carriages were replaced with swinging buckets in 1979. The swinging buckets are 0.57 m long, 0.46 m wide and 0.23 m deep. The swinging buckets have an effective radius of 1.15 m and can be operated at an acceleration of 115 g.

Soil used in the Investigation

The soil used in the investigation was dry sand fine grained and uniform. It had an effective size of 150 microns and uniformity coefficient of 1.5. About 80 per cent by weight had particle sizes between 150 and 250 microns. The sand was compacted in layers of 25 to 40 mm thickness using hand vibrator with base dimensions of 100 mm x 150 mm. The unit weight of sand as compacted was 16 kN/m^3. Reasonable reproducibility of the results was ensured.

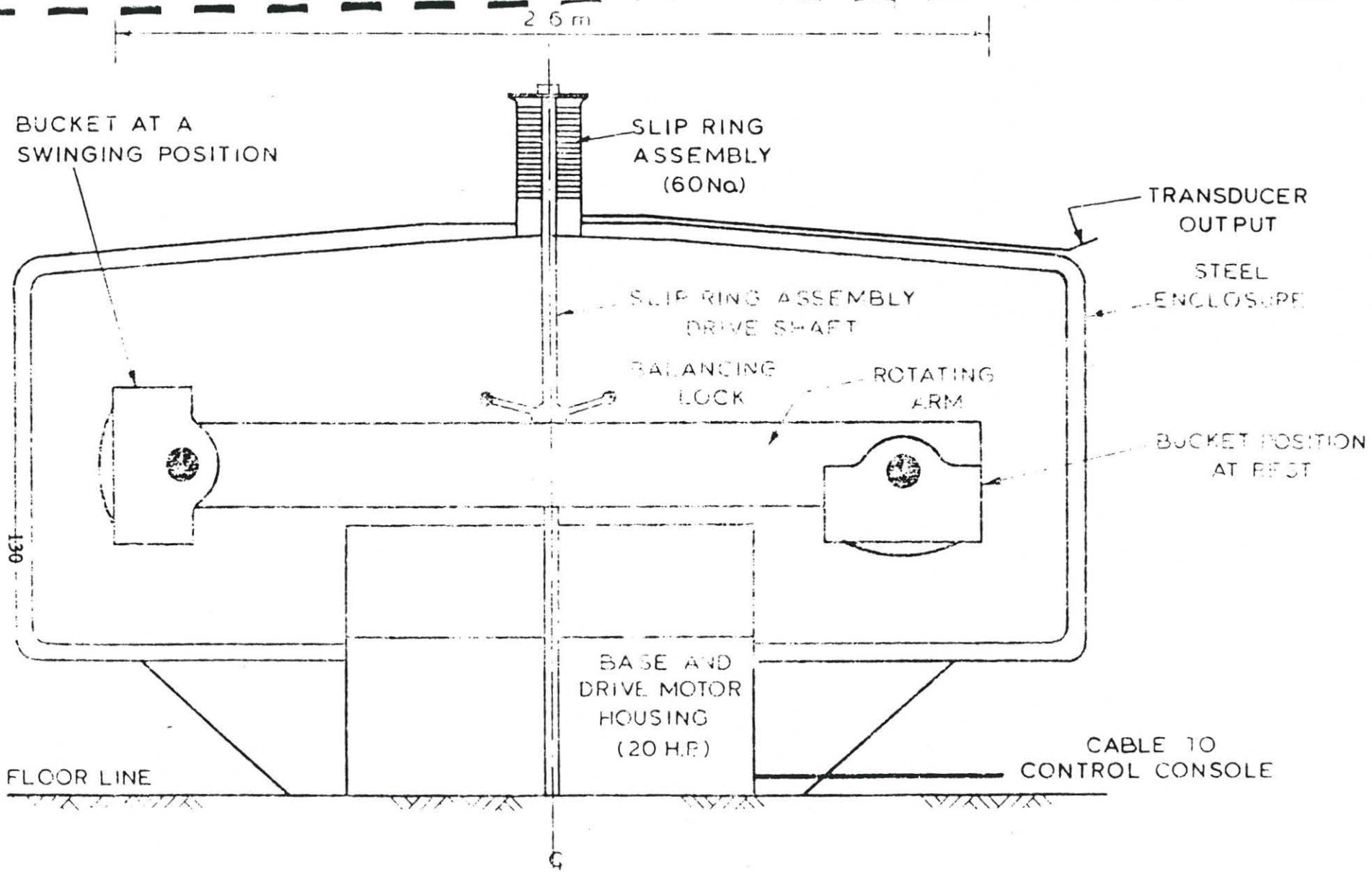

Fig.6 University of Liverpool Centrifugal Test Facility

Pile Properties

The actual dimensions adopted for the model piles were 24.5872 mm OD, 0.3048 mm wall thickness and 330 mm length. The pile had an embedded length of 180 mm. The material of the pile was 304-SS grade stainless steel with an Young's modulus value of 1.9284×10^8 kN/m^2.

The model piles were instrumented with 12 pairs of strain gauges. The strain gauges used were Welwyn make, type EA-125 having a gauge length of 3 mm and a resistance of 120 ohms. They were fixed internally in the tubular section according to the procedure described by King, et, al (1984). Calibration was done in cantilever position by suspending known weights at the free end and recording the half-bridge output of individual gauges. All gauges gave near perfect linear output in several cycles of loading/unloading.

Lateral Load Application

The application of lateral load to the pile cap was through a cable attached to a gear box which is operated by a 18.6 W, single phase A.C. permanent capacitor reversible motor. The gear box gives a speed reduction from 2800 to 8 rpm. The motor is operated externally through slip rings.

The applied lateral load was measured by means of a 500 lb. Novatech load cell introduced between the cap and gear. The horizontal displacement and rotation of the cap

were measured by using two LVDT's fixed as shown in Fig. 7, to a firm support on the bucket frame.

The response of the load cell, displacement transducers and strain gauges were monitored via slip rings by a Vishay-Ellis 220 recording system which is interfaced to a commodare CBM Model 8032 computer. The processed output is obtained directly on a printer.

Results and Discussion

All tests were carried out at a speed of 206.68 rpm of the centrifuge corresponding to an acceleration of 50 g. Thus, the model pile used in this investigation represents a prototype steel pile of 1.23 m diameter, 15.2 mm thickness embedded in sand to a depth of 9 m below ground level.

Lateral load was applied in suitable increments and the corresponding displacements and strain gauge readings were recorded. Loading was continued until the head deflections reached values of about 10 per cent pile diameter i.e. about 2.5 mm. Similar observations were made during unloading. No permanent deformation was noticed in the pile.

The deflection and rotation at the load point are shown in Fig. 8. Similar readings were obtained in the repeat tests. The load deflection curve exhibit three parts : an initial linear variation upto about 8 mm deflection corresponding to about 0.6 per cent a curvilinear portion upto about

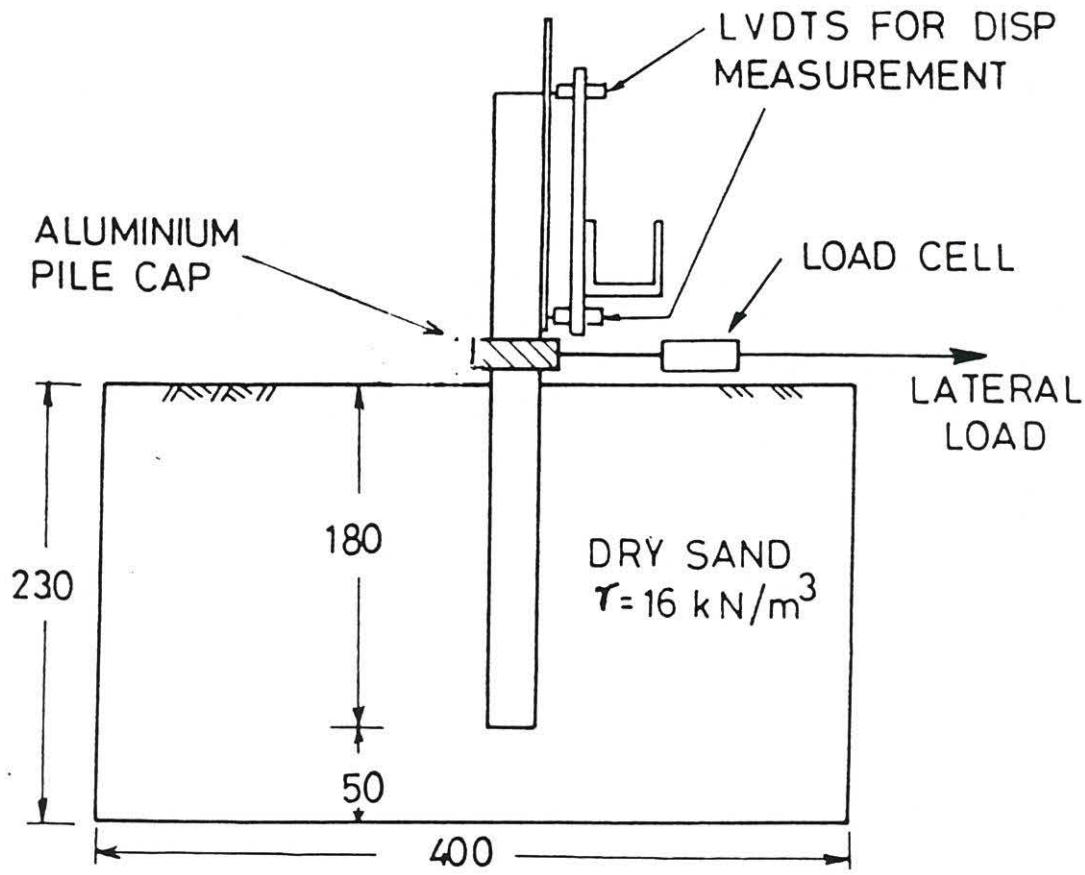

Fig.7 Experimental Set-up

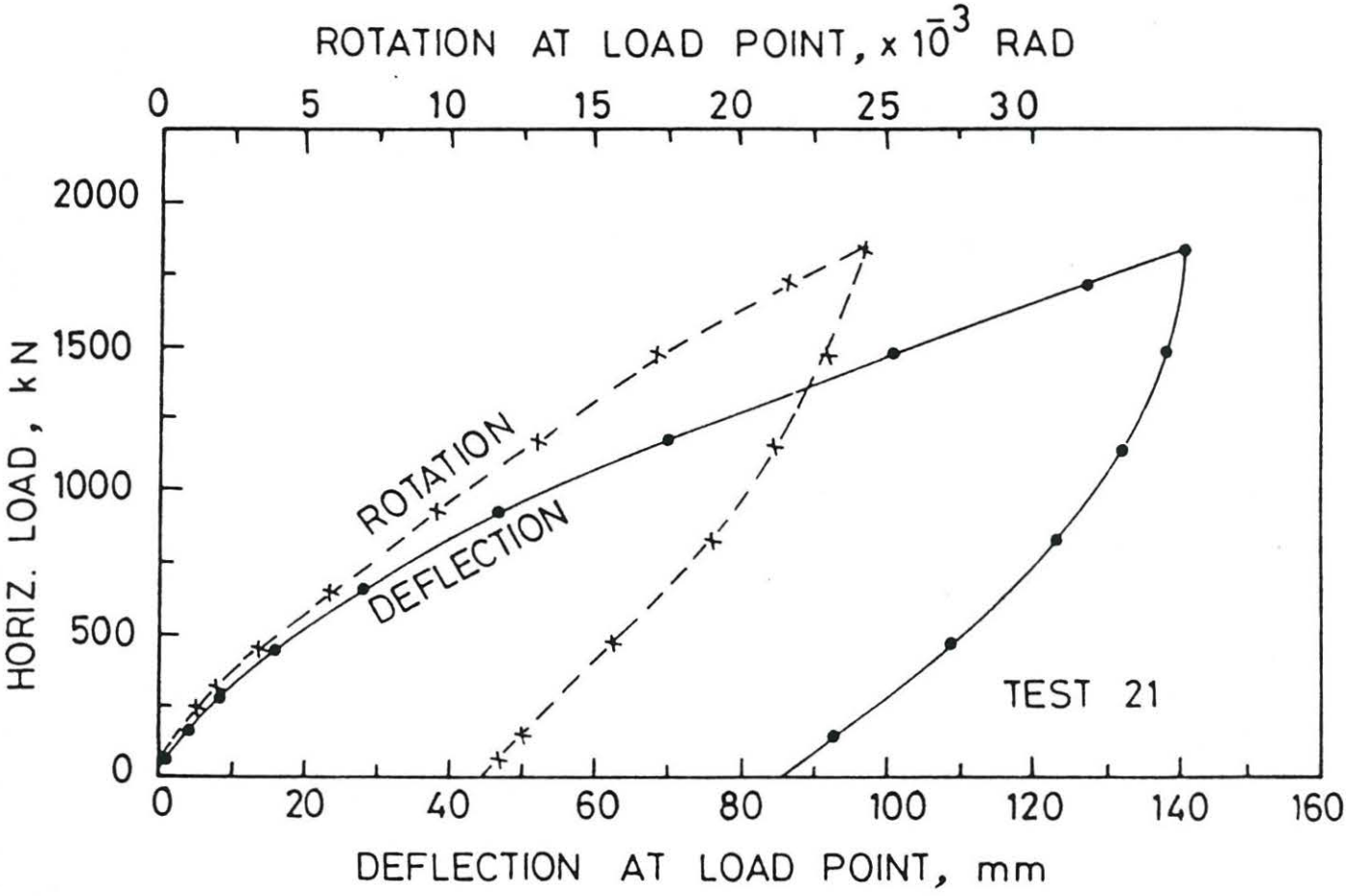

Fig.8 Load-Deflection Diagram

50 mm deflection corresponding to nearly four per cent pile diameter and a third segment which continues to be linear even upto 120 mm deflection corresponding to ten per cent pile diameter. A zone of disturbed soil (persumably failed) soil was visually observed at ground level in the immediate vicinity around the pile. The rotation of the cap also shows similar trend except that the curvilinear part occurs over a smaller range of deflection.

By back-analysis the rate of increase of horizontal subgrade reaction n_h was determined by matching the deflections at levels corresponding to one half and one per cent pile diameter with the help of coefficients developed by Reese and Matlock (1956). The corresponding n_h values worked out to 25676 kN/m^3 and 19929 kN/m^3. The pile length to characteristic length ratios L/T at these deflections were 3.73 and 3.55 respectively. It may be noted that these values are only slightly smaller than the lower limit for long flexible piles.

The results were also back-analysed using the elastic-half space model in which the elastic modulus is proportional to depth and pile is considered to be flexible. The proportionality constant m for elastic modulus was found to have values 9246 kN/m^3 and 6987 kN/m^3 for 0.5 and 1.0 per cent deflections at the ground level. It may be seen that even within the small deflection range of one per cent, there is a large variation in the model parameters n_h and m. This indicates that linear theories have only a limited applicability in the

prediction of pile behaviour.

The bending moment distributions along the pile length computed by both the approaches are shown in Fig. 9 along with the experimental values. Both the distributions agree reasonably well with the observed values in the upper half of the pile while there is some difference in the lower half. The estimates of maximum bending moment and the corresponding depths are also in reasonable agreement with the experiment.

The above analysis shows that the choice of model parameters is of importance for prediction of pile behaviour by the subgrade reaction as well as continuum models. In this respect the subgrade reaction theory is less helpful for design purposes since the n_h parameter is not unambiguously related to basic soil properties.

4. Conclusions

Dimensionless factors are presented in a convenient form for analysing flexible piles embedded in elastic half-space in which the modulus of elasticity is constant or proportional to depth.

The centrifuge experimental results show that with a judicious choice of appropriate parameters the behaviour of single piles can be predicted fairly closely at deflections less than one half per cent pile diameter. At large deflection levels the non-linearity of soils becomes increasingly important.

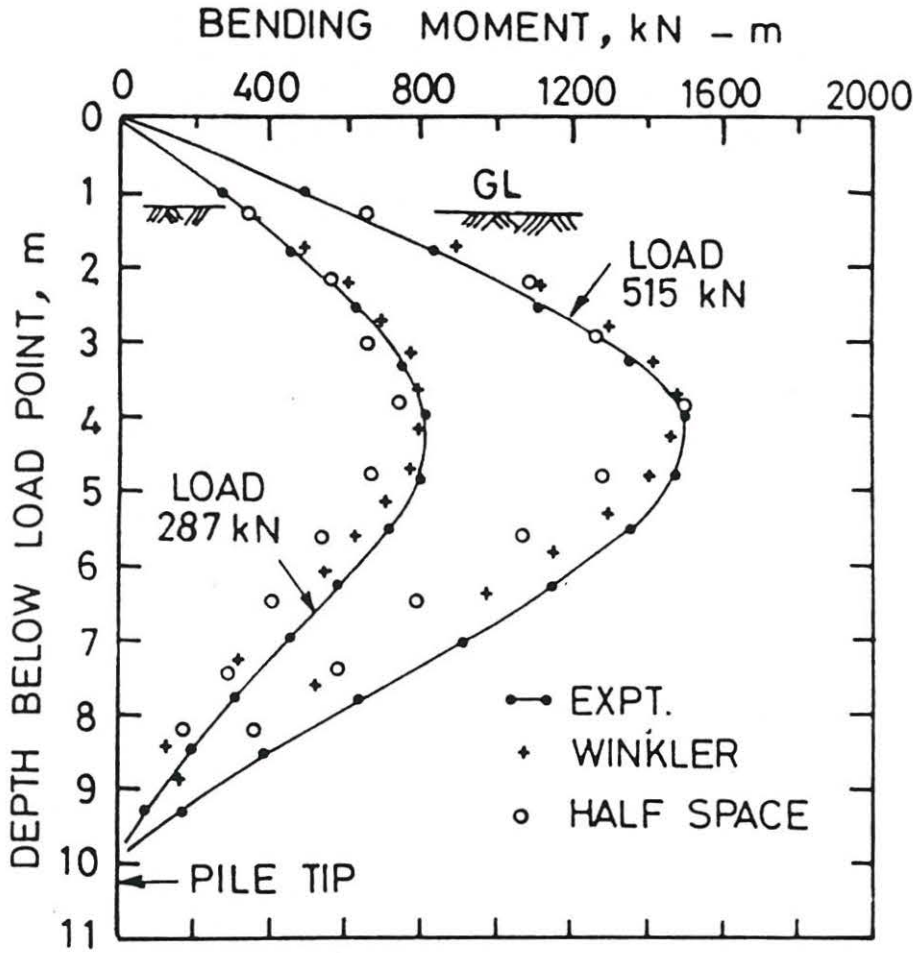

Fig.9 Bending Moment Distribution

References

Banerjee, P.K. and Davies, T.G. (1978). The behaviour of axially and laterally loaded single piles embedded in nonhomogeneous soils. Geotechnique (28), 3, 309-326.

Chandrasekaran, V.S. and King, G.J.W. (1982). Laterally loaded piles : Finite Element analysis and pile centrifugal model studies. Report submitted to the University of Liverpool, U.K.

Davisson, M.T. and Gill, H.L. (1963). Laterally loaded piles in a layered soil system. J. Soil Mech. and Found. Div. ASCE (89), SM3, 66-94.

Davisson, M.T. and Sulley, J.R. (1970). Model Study of laterally loaded piles. J. Soil Mech. and Found. Div. ASCE (96), SM5, 1605-1627.

King, G.J.W., Dickin, E.A. and Lyndon, A. (1984). The development of a medium size centrifugal testing facility. Proc. Symp. on the Application of Centrifuge Modelling to Geotechnical Design. University of Manchester, U.K. 25-46.

Kulkarni, K.R. and King, G.J.W. (1984). Centrifuge tests on laterally loaded pile groups in sand. Report submitted to the University of Liverpool, U.K.

Poulos, H.G. (1971). Behaviour of laterally loaded piles : I-single piles. J. Soil Mech. Fdn. Div., ASCE (97), SM5, 711-731.

Randolph, M.F. (1981). The response of flexible piles to lateral loading. Geotechnique (31), 2, 247-259.

Reese, L.C. and Matlock, H. (1956). Nondimensional solutions for laterally loaded piles with soil modulus proportional to depth. Proc. 8th Texas Conf. SMFE, 1-41.

Reese, L.C., Cox, W.R. and Koop, F.D. (1974). Analysis of laterally loaded piles in sand. Sixth Annual Offshore Technology Conference (II) OTC Paper 2080.

Schofield, A.N. (1980). Cambridge geotechnical centrifuge operations. Geotechnique (30), 3, 227-268.

Terzaghi, K. (1955). Evaluation of coefficient of subgrade reaction. Geotechnique (5), 4, 297-326.

TESTS ON PILES INSTALLED IN FLIGHT ON THE CENTRIFUGE

by M. A. ALLARD*

INTRODUCTION

With the development of much larger piles up to three meters diameter and one hundred and fifty meters in length, simple extension of empirical rules has been difficult and engineers have been forced into studying the mechanics of pile-soil interaction, during driving and under static load.

Prototype scale field experiments on the stress field around driven piles are difficult to carry out because of the variability of soil, and problems of installation of pressure transducers near the pile. In consequence, the few results available are inconclusive or unsatisfactory as a basis for theoretical comparisons. It has therefore been proposed to perform a number of pile experiments in the Caltech centrifuge.

For this investigation, an apparatus capable of driving or pushing a pile in flight on the centrifuge had to be designed and built. Several bearing capacity tests were then made with the pile driven in flight to compare with tests done with the pile driven at 1g.

The pile driving and pile pushing mechanisms designed at Caltech are described, and some results of bearing capacity tests are presented in this report.

THE PILE DRIVING MECHANISM

This mechanism has been specially designed to fit into the pile test container which consists of a long cylindrical vessel, 22 in. high and 6 in. diameter, directly mounted on the centrifuge arm.

Its structure is in two parts.
The first part, **the frame**, consists of two columns held together by two circular plates. One plate of aluminum is fixed at the base of the columns, the other of lucite is near the top (its height is adjustable). The plates' diameter is slightly smaller than 6 in.. Each column has two diametrically opposite rows of notches equally spaced (1/8 in.), over a length of 8 in., which is the driving length. The second part, **the carriage**, consists of a horizontal beam that slides up and down the columns. Ratchets are placed on the carriage such that when in position they fit into the notches of the columns and prevent upward movement of the carriage relative to the frame.

* Graduate Student, Division of Engineering and Applied Science, California Institute of Technology, Pasadena, CA 91125

The mechanism is suspended by its columns to two horizontal rods connected together above the container (see Fig.1). The frame is fixed inside the container. A small air-driven piston ("Tiny Tim") is attached on top of the carriage. The pile is placed underneath the carriage and will be forced down into the soil by the piston, as shown in Fig.2.

1st sketch: the stroke of the piston is near its minimum, the pile is resting in the soil and supports the carriage.

2nd sketch: the stroke is at its maximum, the pile is hit, and by the impact given by the hammer the pile is forced down into the soil. The teflon sleeve slides along the guide, therefore preserving a connection between the pile and the carriage to maintain good alignment.

3rd sketch: due to the effect of gravity the carriage slides down until it rests on the pile again. Because of the ratchets, upward movement is prevented and only downward motion of the pile is permitted.

These sequences are repeated and the pile is driven into the soil. The frequency of the piston strokes is 4Hz.

To prevent tilting of the pile during its driving a teflon guide is placed in the bottom circular plate.

THE PILE PUSHING MECHANISM

This is the same overall mechanism as for the pile driving one. The "Tiny Tim" is removed and the pile is fixed to the carriage. The frame is suspended by its two columns to the two horizontal rods that hinge from a fulcrum bolted to the lip of the container. The outer hydraulic piston alternately pushes and pulls on the two rods. It then transmits an up and down translation to the frame with respect to the container. As before the carriage will undergo only downward movement relative to the frame. See Fig.3.

1st sketch: reference configuration; the piston is in the lower position.

2nd sketch: the piston is going up, pushing the frame up. It can be seen that only the frame undergoes an upward movement. The carriage subjected to the centrifuge acceleration will slide down the frame, and the ratchets will occupy a new position further down the colomns.

3rd sketch: upper position of the piston; the pile is still at the same level.

4th sketch: the piston is going down, pulling the frame down. Because the ratchets prevent upward motion of the carriage relative to the frame, the whole mechanism is forced down. Hence the pile attached beneath the carriage is forced down into the soil.

5th sketch: final configuration after one complete cycle of the piston.

These sequences are repeated and the pile is driven into the soil once every cycle of the piston.

The downward movement of the pile is controlled by regulating the stroke of the piston.

BEARING CAPACITY TESTS

Several bearing capacity tests on piles driven in flight were done using the pile pushing mechanism.

The model pile (a 3/8 in. diameter, 10 in. long, and 0.03 in. thickness aluminum tube with a bottom cap) was driven at 50g in a dry fine Nevada sand with a unit weight of 105 pcf.

Instrumentation

The carriage is instrumented with strain gauges connected to form a Wheatstone bridge. This then constitutes a load cell with which to measure the load applied to the pile during and after driving.

The depth of the pile is calculated from the output of a rotary potentiometer which is fixed to the upper circular plate and connected to the carriage by a string and pulley system . A soft spring is used to maintain continuous tension of the string.

A Linear Variable Differential Transformer (LVDT), connected between the upper circular plate and the top of the container, is used to indicate the movement of the piston, and therefore of the driving mechanism.

Test procedure

The test proceeds in two parts:

1) The centrifuge is spun up to the test acceleration of 50g. The pile is then driven into the soil, to a given depth, where a bearing capacity test is performed. This test is named type (A).

2) The centrifuge is stopped so that relaxation of the soil occurs, but all other conditions are preserved. The centrifuge is then brought up to 50g again, and a second bearing capacity test is done on the pile at essentially the same depth as before. This test is named type (B).

Preliminary results

Bearing capacity tests have been done in the past in the centrifuge with the pile driven into the soil at 1g and the test itself performed at Ng. The present test procedure is such that by stopping the centrifuge and allowing relaxation of the soil, the conditions of the pile driven at 1g are recreated. By preserving the other conditions, namely the soil and position of the pile, the two type of tests can be compared. The only difference between the two tests lies in the stress conditions around the pile.

Figure 4 is a comparison of typical load versus penetration curves for tests A and B. The results obtained show that in the second procedure the bearing load of the pile is smaller. The values are about 75% of the actual values obtained from the first procedure.

Conclusion

From these tests it is apparent that the pile must be driven in flight in the centrifuge to correctly represent the stress distribution around it.

Experiments are in progress at Caltech to investigate the stress field around a pile during driving.

ACKNOWLEDGMENTS

John Lee, research engineer at Caltech, and Mike Becker, former Caltech student, contributed significantly to the design and construction of the mechanisms.

The author is grateful to Chevron Oil Field Research Company and Union Oil Foundation for financial support of this research.

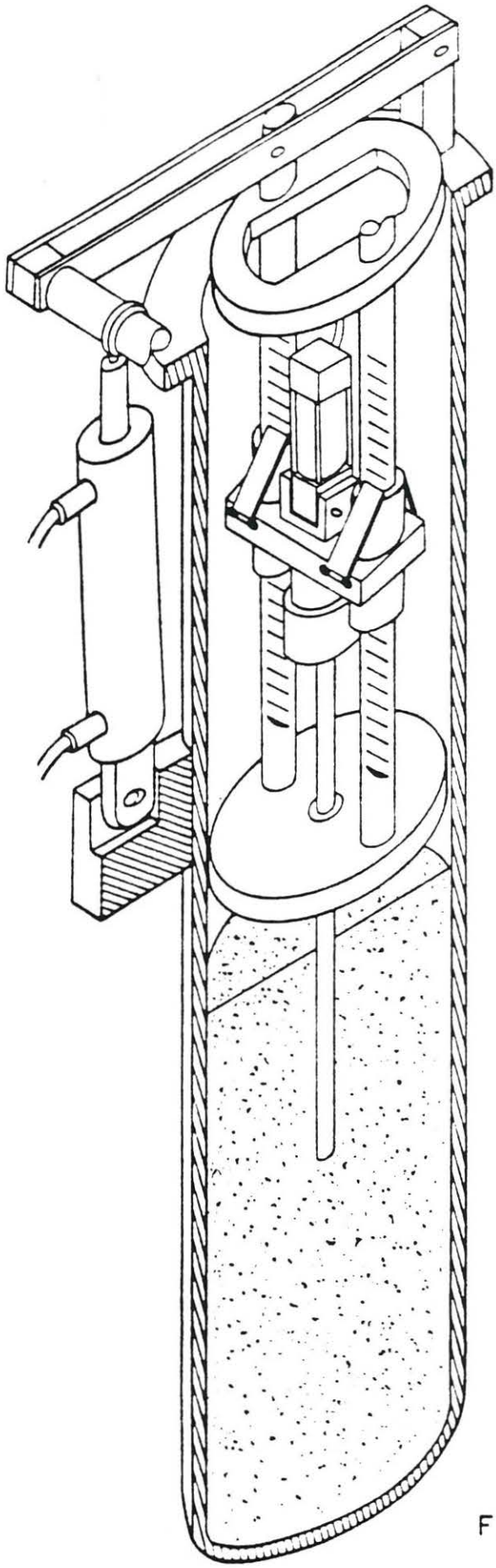

FIGURE I

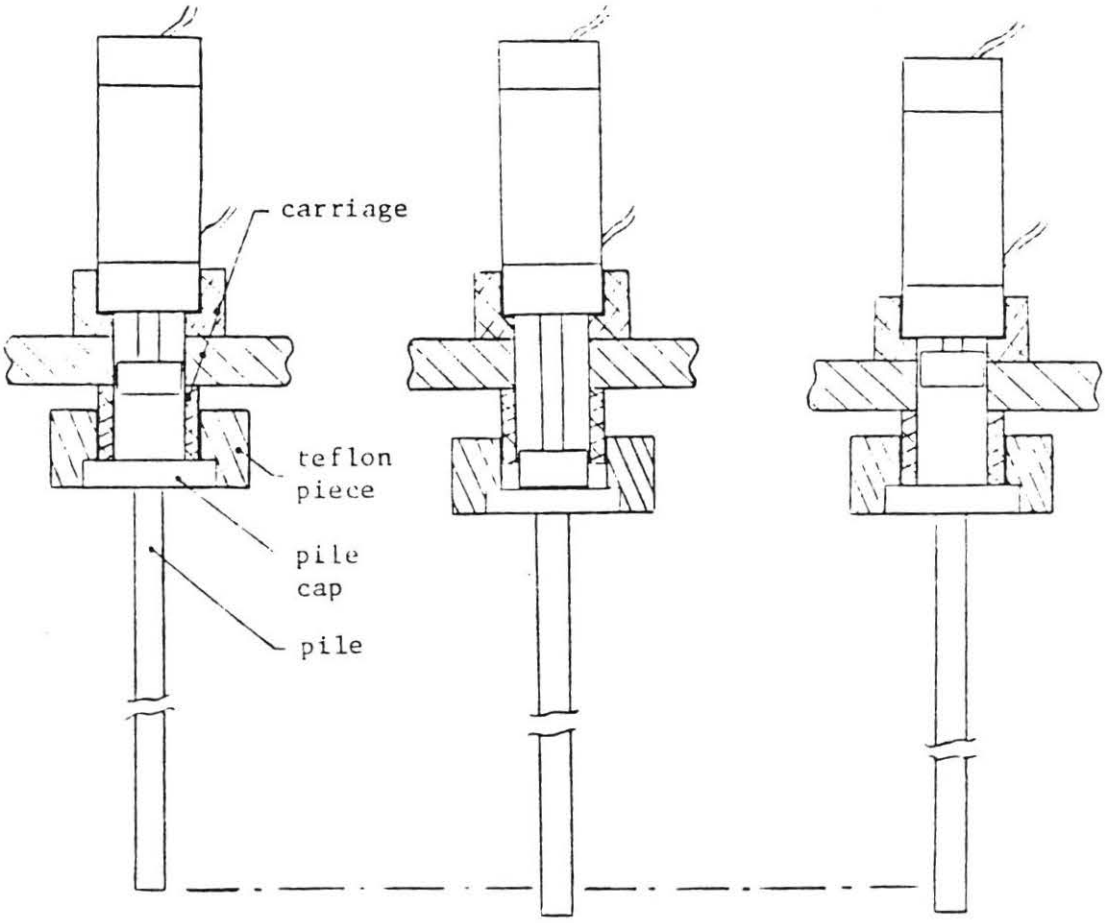

FIGURE 2

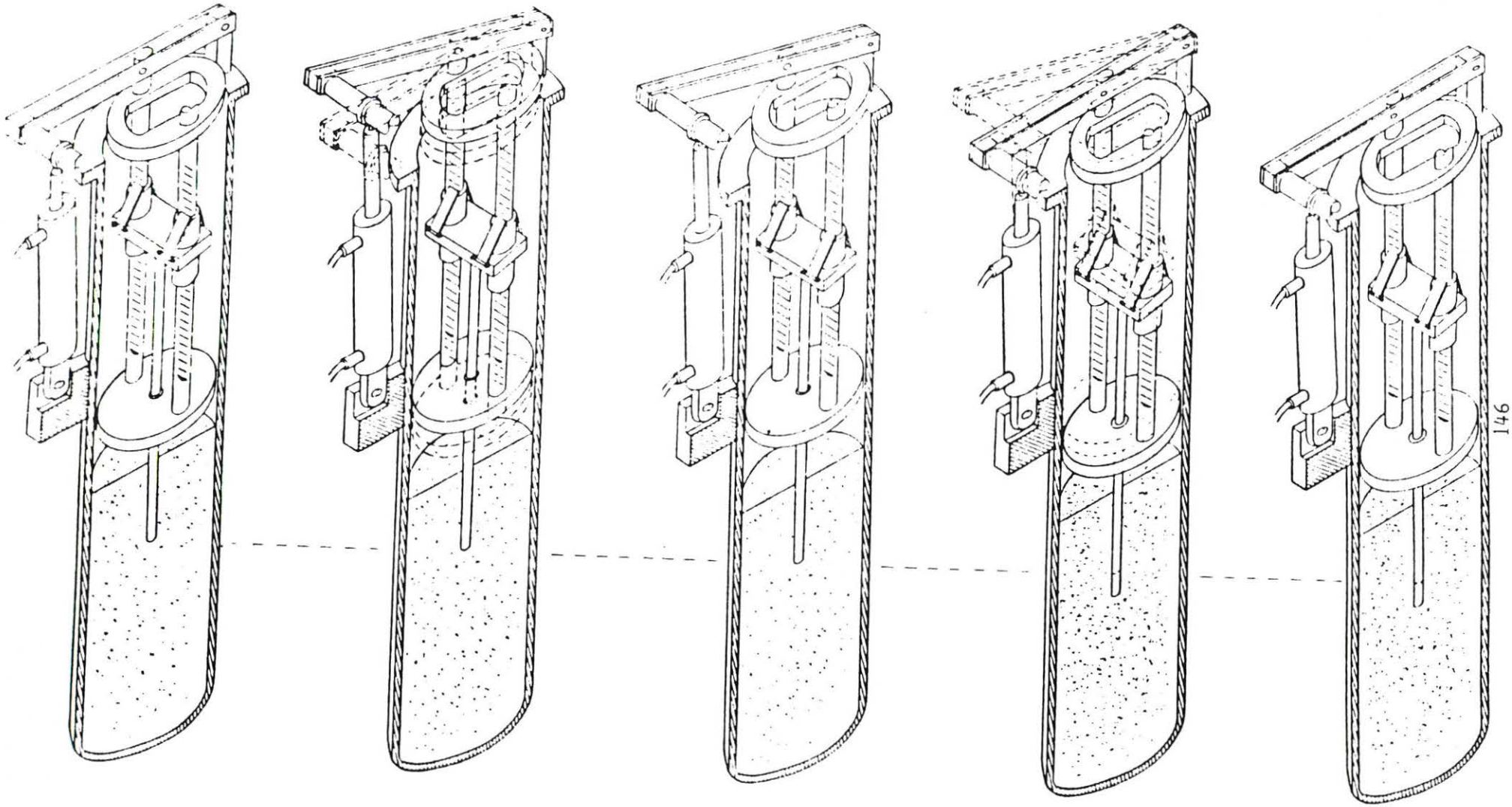

FIGURE 3

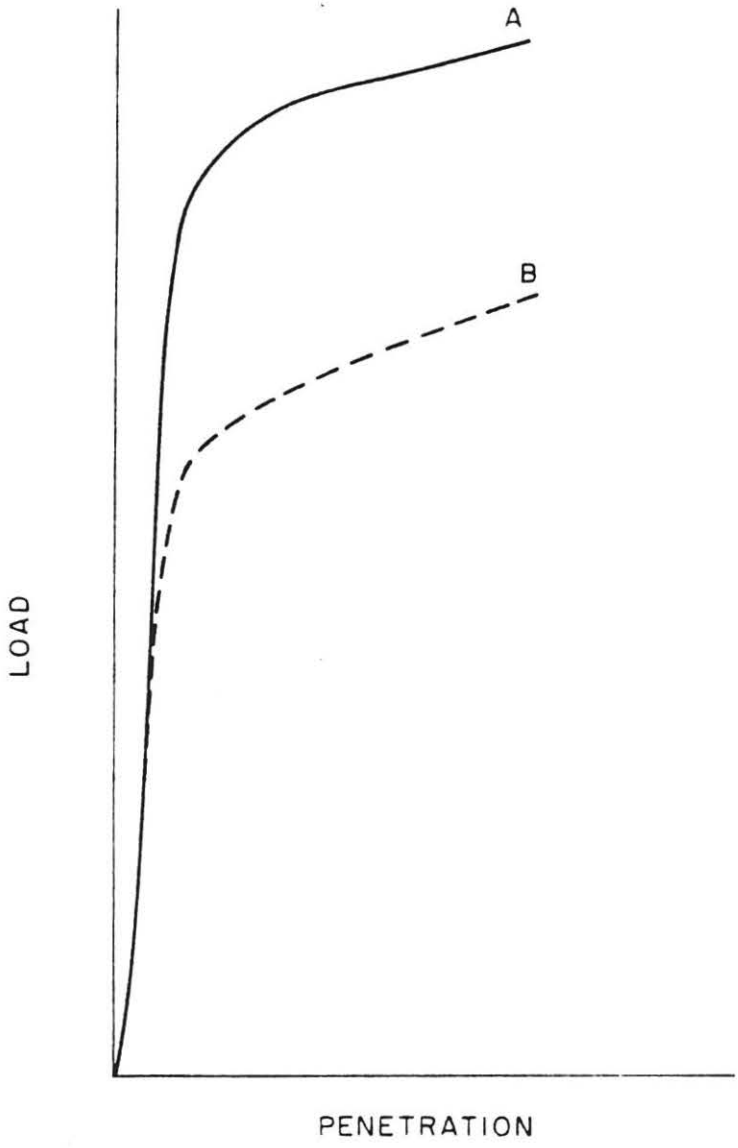

FIGURE 4: Comparison Between Capacity Tests (A) and (B)

ABSTRACTS II

CENTRIFUGAL MODEL TESTS FOR ULTIMATE BEARING CAPACITY OF FOOTINGS ON STEEP SLOPES IN COHESIONLESS SOIL 1/

By

Mark C. Gemperline
Bureau of Reclamation

Analytical methods that are frequently used to predict the ultimate bearing capacities for shallow spread foundations on slopes yield widely varying solutions. As a result, the allowable foundation bearing pressures used for design are selected conservatively. This leads to the construction of shallow spread foundations that may be larger and more costly than necessary.

To address this situation, the Department of the Interior, Bureau of Reclamation, initiated a research program to evaluate the state of the art as it pertains to predicting the ultimate bearing capacity of shallow spread foundations located on or near slopes; to experimentally determine the maximum bearing pressure of four prototype shallow spread footings using scaled models; and to compare test results with state-of-the-art analytical solutions.

Test equipment was fabricated to permit model footings to be loaded and their response to be measured at accelerations 100 times that of gravity. The model test results were compared with the results of theoretical solutions obtained using limit analysis and limit equilibrium, as well as methods suggested by G. G. Meyerhof, J. E. Bowles, J. B. Hansen, and J. P. Giroud.

1/ Gemperline, Mark C., Centrifugal Model Tests for Ultimate Bearing Capacity of Footings on Steep Slopes in Cohesionless Soil, Report No. REC-ERC-84-16, Bureau of Reclamation, Denver, Colorado, 1984.

RELATIONSHIPS FOR MODELLING WATER FLOW IN GEOTECHNICAL CENTRIFUGE MODELS

by

Deborah J. Goodings
University of Maryland

ABSTRACT

Appreciation of the importance of water pressures in the behavior of soil was a major turning point of modern soil mechanics, and correct prediction of the pressures and assessment of the effects on soil has remained fundamental to geotechnical design and research. Replication of the pore fluid behavior in saturated and partially saturated soil is therefore critical to effective modelling, although this ideal cannot always be achieved. Furthermore, different pore fluid events will take place at different rates in a reduced scale centrifuge model, influenced by the reduction in scale and by the increase in self-weight, depending on the nature of the flow. For example, seepage will be governed by different laws depending on whether the soil is saturated or partially saturated. Once seepage water emerges and drains away as surface runoff, other laws will govern its runoff behavior, and erosion, governed by still other relationships, may change the soil profile causing slope instability.

This paper will investigate the relationships between centrifuge model and prototype water effects under steady state and transient seepage conditions, in saturated and unsaturated soil, as well as those relationships which dictate erosion and other effects of surface water on soils. In most cases the paper will be based on relationships already existing in the literature, although in areas where this is found tc be incomplete, new analysis will be developed.

Abstract:

Unexpected Scaling Effects in Flow Through
Centrifugal Models of Permeable Soils

by: Deborah J. Goodings
University of Maryland

Submitted to: ASCE Geotechnical Journal

Presented at: Symposium on Recent Advances in
Geotechnical Centrifuge Modelling,
UC Davis July 1984

Experimental verification of modelling laws governing flow of water through centrifuge models of permeable soils is not common in research literature. This article examines three studies of flow through centrifuge models of embankment dams in which the shapes of the observed phreatic surfaces were not as expected, and may be indicating scaling effects. In one instance, a change in phreatic surface was associated with a change in flow regime from laminar to transitional at high accelerations. In the other two cases, migration of fines and their accumulation downstream in the embankment appeared to have been responsible for distortion in the laminar flow phreatic surfaces; there is speculation that this also may be a result of a scaling effect.

For both behaviours, the scaling effects will be functions of particle size distribution, hydraulic gradient and centrifugal acceleration. These may offer the reduced scale modeller opportunities to observe flow behaviour which normally is very difficult to model at 1g. Alternatively, they may be important scaling effects to avoid, and may cause restrictions on the smallest model scale that may be selected while still ensuring hydraulic similitude in model and prototype. Verification of the absence or presence of these effects is an important preliminary step in models with high rates of through flow.

PHYSICAL AND NUMERICAL SIMULATIONS OF SUBSIDENCE IN FRACTURED SHALE STRATA

BY

Herbert J. Sutherland
Lee M. Taylor

Sandia National Laboratories
Albuquerque, New Mexico 87185

and

Steven E. Benzley

Brigham Young University
Provo, Utah 84602

The motions of fracture shale strata that overlie a void of increasing size are studied using physical and numerical simulations. The physical simulation is conducted on the Sandia 25-Foot Centrifuge, the largest operating centrifuge in the United States. The physical model described here is composed, primarily, of fractured Devonian shale (to simulate a jointed overburden). For the model scale of 150, the experiment simulates an overburden of 86.3 m. The void beneath this strata is 7.62 m high and its width is increased in four steps from 0 m to 106.7 m. The experiment shows the progressive failure of the overburden, the formation of a failure arch, and, eventually, the formation of a surface subsidence trough. To gain insights into the phenomenology of failure mechanisms and the influence of joints (fractures) on the displacement of the shale strata, the physical simulation is analyzed using three numerical techniques. The first is the "BLOCKS" model that treats the rock strata as an assemblage of blocks. The equations of motion for each block are solved using an explicit integration operator. The displacements, rotations and collisions of each block are calculated in the model. The other two techniques are based on finite element techniques and the previously described "rubble" element. The first finite element model uses an explicit formulation for each joint in the overburden and the second incorporates the joints directly into the element. In the former, the joints are treated as "slip surfaces" and in the latter the joints are formulated in a continuum theory as a "ubiquitous joint" element. The predictions of these analyses agree with the response of the physical model.

PHYSICAL AND NUMERICAL SIMULATIONS OF SUBSIDENCE ABOVE HIGH EXTRACTION COAL MINES

by

Herbert J. Sutherland
Albert A. Heckes
Lee M. Taylor

Sandia National Laboratories
Albuquerque, New Mexico 87185

Modeling the failure and settlement of strata above mine openings requires a knowledge of several different geomechanical processes such as the failure of the rock mass above the opening, the fall of this mass into the opening, the associated bulking of the rock rubble, and the recompaction of the rubble under subsequent loading. These processes are studied in this paper using physical models and analytical models. The former are based on centrifuge simulation techniques, and the latter on numerical techniques. The centrifuge experiment described here simulated the response of a shale overburden after being undermined by a long wall panel. This simulation shows progressive failure of the overburden, the formation of a failure arch, and the formation of a subsidence trough. The data from these experiments are analyzed with a numerical analysis scheme called "BLOCKS." This model treats the overburden as an assemblage of blocks. The equations of motion for each block are solved using an explicit integration operator. The displacements, rotations and collisions of each block are calculated in the model.

PART III

SOIL DYNAMIC AND EARTHQUAKE APPLICATIONS

DYNAMIC BEHAVIOR OF FOUNDATIONS: AN EXPERIMENTAL STUDY IN A CENTRIFUGE

B. Hushmand[1]

SUMMARY

Correctly-scaled rigid model structures with foundations of different shapes and sizes resting on the surface or embedded in a cohesionless soil were subjected to forced vibrations in their coupled rocking-sliding mode in a centrifuge. A medium-dense fine sand was used in the experiments and the centrifugal acceleration was equal to 50 g. For the dynamic loading of the model structures, a miniature shaker was designed to produce steady-state shaking of the models in a low to high amplitude vibration range. The response of the model structures to the input dynamic motion was measured by accelerometers and pressure and displacement transducers. Results of the experiments indicate that almost in every test, the foundation lifts off the soil surface and the soil at the edge of the foundation-soil contact area yields. The yielded zone gradually moves inward as the number of vibration cycles or amplitude of vibration increases. Therefore, the foundation-soil system behaves non-linearly under the effects of both lift-off and plastic deformation of the contact soil.

1. INTRODUCTION

Recently, the response of dynamically loaded foundations has received a good deal of attention. This arises from the growing need to design dynamic load-resistant foundations and to include the effect of the ground behavior on the overall response of the structures.

Analysis and design of foundations under low-amplitude dynamic loads such as those generated by machine vibrations and vehicular traffic were the original reasons for consideration of this problem. However, research in earthquake engineering and dynamic behavior of structures under other sources of high-amplitude loads such as those generated by bomb blasts, or loading due to sea wave action has demonstrated a need to improve the dynamic models of buildings and other structures by including the soil-structure interaction effect.

Many investigations of both an analytical and experimental nature on the dynamic response of footings have been conducted. For analysis, different approximate methods have been used in studying foundation vibration problems, such as "In-Phase Mass" method (Crockett and Hammond 1949, Rao 1961), or

---

[1]Earth Technology Corporation, Long Beach, CA 90807; formerly graduate student, Calif. Inst. Tech., Pasadena, CA 91125

"Dynamic Subgrade Reaction" (Hayashi 1921, Terzaghi 1943, 1955, Hetenyi 1946, Barkan 1962). However, elastic-half-space theory has received the greatest attention. Because of its idealized nature, certain mathematical simplifications which are not quite realistic had to be introduced. Over many years, the gap between the results of this theory and real-life behavior of foundations has been narrowed. These half-space studies are mainly concerned with dynamic response of rigid foundations which can be divided into two basic groups: (1) resting on the soil surface, and (2) embedded in the soil. In the majority of these investigations circular foundations are considered and the soil medium is simulated by a homogeneous isotropic elastic half-space. The early analytical solutions were based on the classic work by Lamb who formulated and solved the problem of a harmonically varying point force acting on the surface of an elastic half-space. Using his solution many investigators solved the foundation vibration problem by considering a prescribed stress distribution over contact areas of regular geometry such as circular, strip, or rectangular shapes (e.g. Reissner 1936, Sung 1953, Bycroft 1956, Thomson and Kobori 1963). These solutions were followed by mixed boundary-value treatment of the problem in which an oscillating displacement is prescribed in the loaded region and stresses are defined over the rest of the boundary surface (e.g. Veletsos and Wei 1971, Luco and Westmann 1971). To improve the mathematical model of the problem, other continuum models such as viscoelastic, layered, poroelastic subgrade, etc. have been considered (e.g., Hoskin and Lee 1959, Veletsos and Verbic 1973, Kausel 1974, Luco 1974, Halpern and Christiano 1982).

Foundations of most structures such as buildings, machines, nuclear power plants, etc., are usually placed partially below the soil surface. This has a great effect on the vibration characteristics of these footings and has been much investigated in recent years. Several analytical methods, including the finite element method, have been used (e.g., Baranov 1967, Novak and Beredugo 1971, 1972, Bielak 1975, Kuhlemeyer 1969, Kausel 1974).

All these theoretical methods for analyzing the dynamic response of foundation-soil systems are based on a number of simplifying assumptions regarding soil properties and system geometry. In particular, real non-linear hysteretic soil properties are generally not included, or are approximated only. As a result, the application of theoretical results is questionable in many cases, such as, in particular, high amplitude vibration of the foundation soil system during strong earthquake ground motion. Therefore there has

existed a great need for experimental studies to calibrate theoretical techniques and to clarify the ambiguities produced by using simplified mathematical models.

Experimental studies on the dynamic behavior of surface and embedded foundations have been reported by many investigators. Barkan 1962, Novak 1960, 1970, Fry 1963, Drnevich and Hall 1966, Beredugo 1971, Stokoe 1972, Tiedemann 1972, Erden 1974 and many others studied the vertical, torsional, rocking and sliding modes of vibration of surface and embedded footings.

All the experimental work cited above has been performed on model or small prototype footings in the field or in the laboratory. Since the stress conditions on a soil element have a considerable effect on its behavior under both static and dynamic loadings it is expected that a soil mass behaves differently under full-scale and model conditions. Running full scale tests on foundations comparable in size and weight with foundations of real structures is very expensive and in some cases even impossible. Because of the limitations in the one-g testing of model or full-scale foundations the best approach appears to be to conduct properly-scaled shaking tests on model foundations in a centrifuge. This technique is described more in the next sections.

2. CENTRIFUGE MODEL TESTING

Most soil properties depend on continuum stresses which are generally gravity-induced. Thus, in order to have the same stress conditions on soil elements at two homologous points in model and prototype unit weight of model material should be scaled properly to produce same confining stresses. For a geometrically similar model N times smaller than its prototype we should have

$$\gamma_M = N\gamma_p$$

where

γ_M = unit weight of model material

γ_p = unit weight of soil in prototype

This can be achieved either by choosing a model material with a density N times the density of the prototype soil or by increasing the gravitational acceleration on the soil at the model scale. It is more convenient to use prototype material, but to increase the gravitational acceleration by the lineal scale factor N. Thus, if a 1/50th scale model, made of the same material as the prototype is subjected to a gravitational acceleration 50 times that of the prototype, the confining stresses, and thus the properties

and behavior of the model, are the same as in the prototype. A centrifuge is a machine that can provide model gravity as desired (Bucky 1931, Pokrovsky and Fyodorov 1975, Scott et al 1977).

Since in this research rigid prototype footings of different shapes and sizes were simulated using model footings with high rigidity compared with soil stiffness, only the geometrical and inertial characteristics of the models were scaled to the required ratios. Table I lists the relations between prototype and model (centrifuge) parameters when a centrifuge is employed (Rowe 1975, Scott 1977).

In the experiments described here, N was chosen to be 50, so that model dimensions were 1/50 of the prototype linear dimensions, and the model (centrifugal) acceleration was 50 times normal terrestrial gravity.

3. EQUIPMENT

The centrifuge used is shown in Figure 1 and has been described elsewhere (Scott et al 1982). The capacity (payload) of the centrifuge is about 10,000 g-lbs. This means that at 50g's, the maximum load of model structure, soil and container that it can sustain is about 200 lbs. A miniature air-driven counterrotating mass shaker was designed for steady-state forced excitation of the model structures in their coupled rocking-sliding mode of vibration. Because of its small size, reasonable force amplitude output, and high value of frequency response, it forms ideal loading equipment for any dynamic test in centrifuge. The main part of the shaker is a three gear arrangement (Figure 2), two of them in parallel in the horizontal plane and the third one a vertical gear that transfers motion of the lower horizontal gear to the upper one in the opposite direction. Two flywheels made from phenolic, a light and strong composite material, are assembled on the parallel gears and have counterrotating motion. Compressed air was used as the source of energy to run the shaker. Air flows with very high velocity from two nozzles on the sides of the shaker pushing forward circular cups machined on the circumference of the lower flywheel. Different eccentric masses can be used to adjust the force of vibration independently of the shaker speed. The maximum frequency output of the shaker at 50g centrifugal acceleration was about 750 Hz which is equivalent to 15 Hz prototype frequency and its output force amplitude varied from very small values up to few pounds depending on the amount of eccentric mass and speed of the shaker. Other properties of the

TABLE I. Scaling Relations

Parameter	Full Scale (Prototype)	Centrifugal Model at Ng's
Acceleration	1	N
Linear dimension	1	1/N
Area	1	$1/N^2$
Volume	1	$1/N^3$
Stress	1	1
Strain	1	1
Force	1	$1/N^2$
Mass	1	$1/N^3$
Mass density	1	1
Weight density	1	N
Time (dynamic)	1	1/N
Time (consolidation)	1	$1/N^2$
Frequency	1	N

TABLE II. Properties of the Air-Driven Shaker

Diameter (in)	Height (in)	Eccentricity (in)	Height of Center of Gravity (in)	Weight (lbf)	Mass Moment of Inertia (lb - in^2)
1.73	1.38	0.74	0.67	0.23	0.08

TABLE III. Properties of the Models Used in Different Parametric Studies

Soil-Foundation Parameters	Model Properties			
	Weight (lbf)	Mass Moment of Inertia (lb-in^2)	Height of Center of Gravity (in)	Footing Semi-Dimension (in)
Footing Shape & Size:				
Circular Model I	0.97	8.71	3.66	1.0, 1.25, 1.50
Model II	1.85	11.08	3.75	1.0, 1.25, 1.50
Square	1.85	11.08	3.75	1.0, 1.25, 1.50
Rectangular	1.85	11.08	3.75	See Fig. 12
Ecentric Mass of Shaker Model I	1.75	9.08	2.75	3.00
Model II	1.85	11.08	3.75	2.50
Depth Of Embedment	1.47	7.85	3.10	3.00

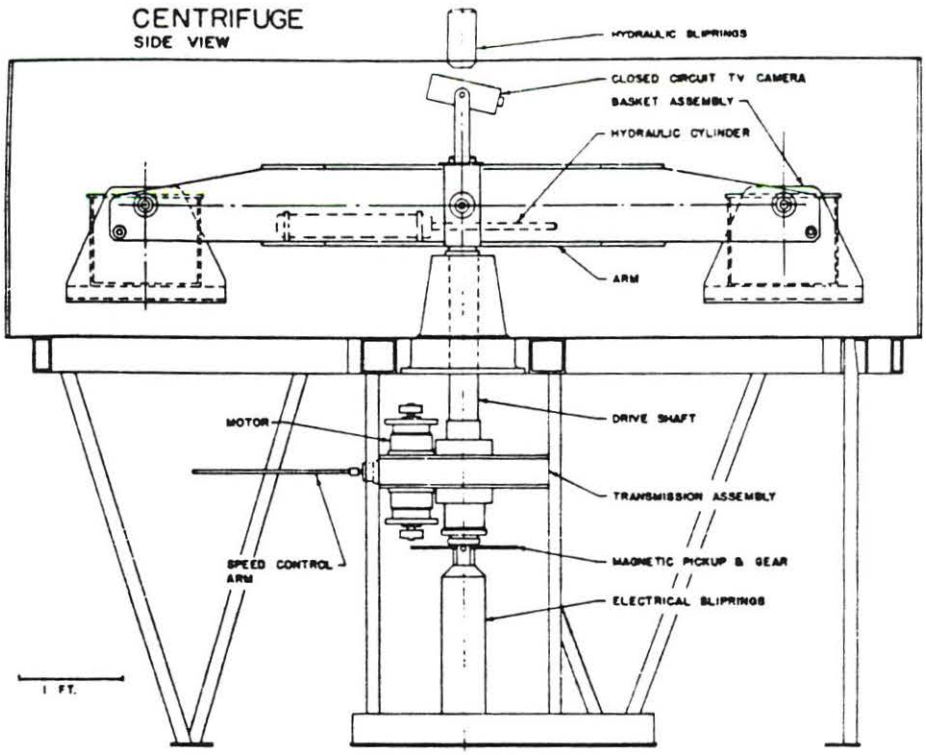

SIDE VIEW OF CALTECH CENTRIFUGE
FIGURE 1

COMPONENTS OF THE AIR-DRIVEN SHAKER
FIGURE 2

shaker are summarized in Table II. Frequency of the shaker was measured by a frequency counter, an LED, a photocell, and a number of reflecting silver strips bonded to the upper surface of the shaker.

The model structures used were all rigid hollow or solid aluminum cylindrical and rectangular tubes attached to rigid footings of different shapes and sizes. At 50g the models simulated prototype structures with footings of 8 ft to 15 ft diameter, masses of 121 kips to 266 kips, and mass moment of inertias (with respect to an axis passing through the base) ranging from 47,000 kips-ft to 92,000 kips-ft. Figure 3 shows the model structures and the model footings used in the experiments. The characteristics of the models are summarized in Table III.

The model towers were instrumented with three Entran model EGA-125F-500D miniature accelerometers to record the tower motion at different elevations in order to measure the acceleration components of the coupled rocking-sliding mode of vibration. Horizontal displacement components of the models in the direction of applied force and the transverse direction were measured at the top of the tower using a double axis optical transducer, Model PIN-SC/10D obtained from United Detector Technology, Inc. In addition four Entran Model EPF-200-50 pressure transducers were mounted on the bottom surface of the footings to measure the contact pressure distribution along the diameter (Figure 4). The accelerometers were calibrated by placing them in the centrifuge at known rotation speeds and recording their outputs at corresponding centrifugal acceleration. Calibration of pressure transducers in order to measure the absolute pressure amplitudes introduces some difficulties because of soil-structure interaction effect between transducer and soil (Weiler and Kulhawy, 1982). Pressure transducers were calibrated by placing them on the floor of a bucket full of water or a uniformly dense sand while spinning the centrifuge at different centrifugal accelerations. This calibration technique provides an approximate measure of absolute pressures and a precise measure of relative pressure amplitudes. Thus, pressure distribution configuration can be reliably evaluated.

All the signals were suitably amplified and filtered to eliminate high frequency noise, passed through slip rings, and then recorded digitally by an analog-to-digital convertor (ADC) and a microcomputer system.

The soil used in the tests was Nevada 120 silica sand in a dense (104 ± 1 pcf) dry state. The soil container was a 12 inch diameter 10 inch deep aluminum cylindrical bucket.

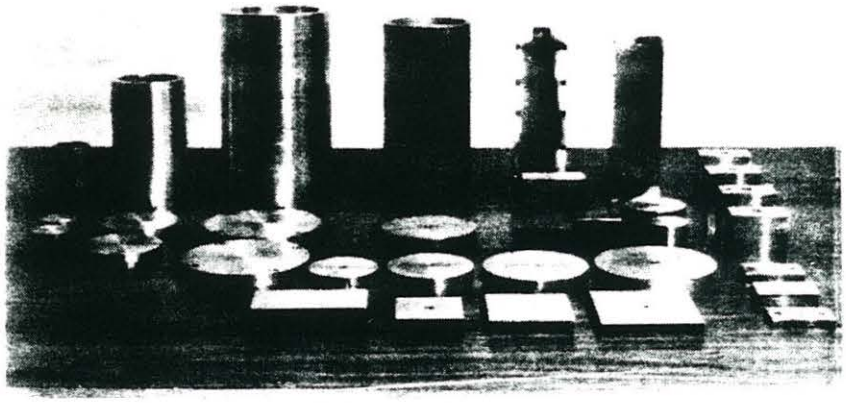

COLLECTION OF TOWERS, FOOTINGS AND MASSES USED IN TESTS

FIGURE 3

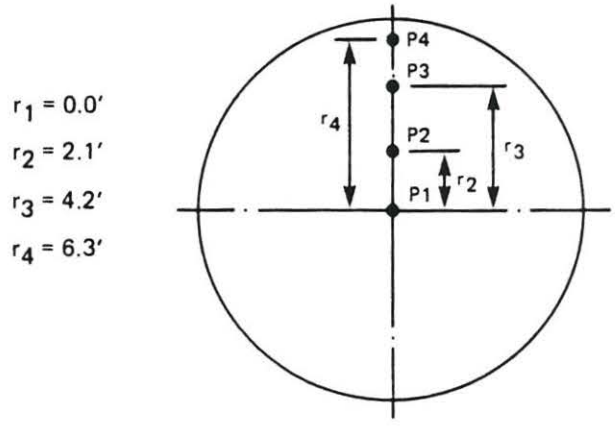

PATTERN OF PRESSURE TRANSDUCER HOUSINGS ON FOOTINGS

FIGURE 4

4. EXPERIMENTAL PROCEDURE

Dry Nevada Fine Sand (NFS) was placed in the centrifuge bucket to a predetermined depth and density. The soil surface was leveled and smoothed particularly where the footing was to be located. Next, the model structure with appropriate transducers and the air-driven shaker was securely placed on the sand. In the embedded foundation tests, after locating the tower on the soil surface, more sand was placed around the tower and compacted carefully to the required density and depth of embedment. After the centrifuge was brought up to required speed the shaking machine was run through a range of frequencies while the tower motions were recorded at different frequencies of the oscillation. The signals were recorded by the data acquisition system (ADC) and then accessed by the micro-computer and stored on disks. Data reduction included plotting the raw data, calculation of Fourier transforms, filtering of noise, sine fitting to calculate amplitude and phase, plotting amplitude versus frequency curves for each test, and fitting the curves by the response of a single degree of freedom damped oscillator to determine resonant frequency and equivalent damping of the system.

5. RESULTS

The effect of different soil-footing parameters on the dynamic characteristics of the model structures and contact pressure distribution measurements are presented in the following sections. Results are presented by response amplitude curves and plots showing variation of resonant frequency with the change of different parameters of the soil-foundation system. The y-axis of the response amplitude curves is expressed in terms of displacement and pressure amplitude per frequency squared which is equal to amplitude per unit force ratio for an imaginary shaker of unit mass-times-eccentricity product. The unit for the y-axis labeled as "Amplitude/Force" is in "in-sec^2" for displacement data and "psi-sec^2" for pressure signals. In the following sections all parameters are given in prototype scale.

The static pressure distributions along the diameter of a rigid circular footing, 12.5 feet diameter, resting on the surface of sand were measured for different soil depths (Figure 5). The static pressure distribution for the footing on maximum soil depth of 33.3 feet has an approximately parabolic shape which is comparable with the theoretical triangular distribution shape

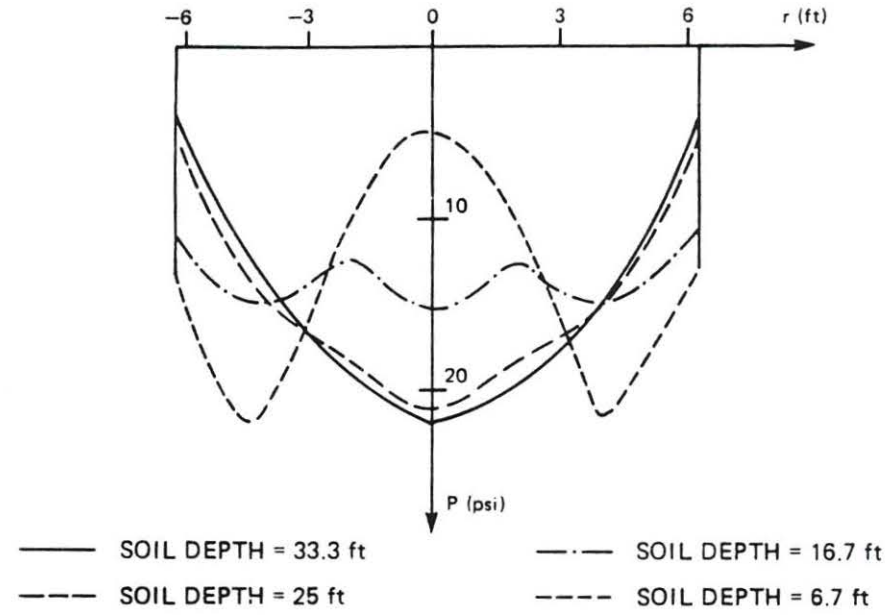

STATIC PRESSURE DISTRIBUTIONS ALONG FOOTING DIAMETER AT DIFFERENT SOIL DEPTHS

FIGURE 5

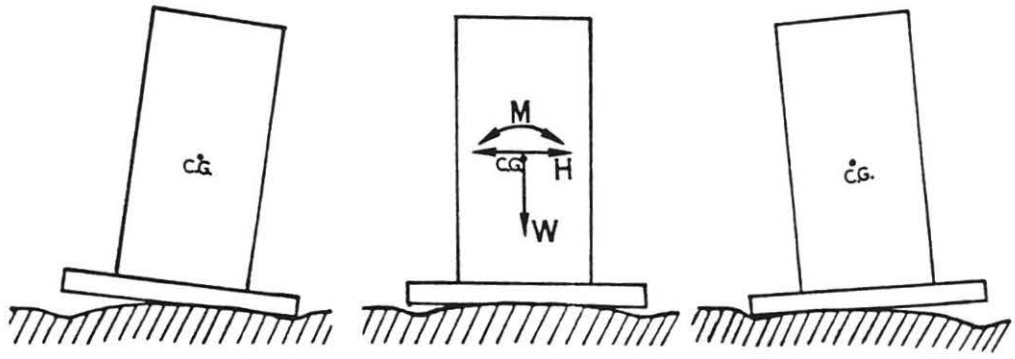

MECHANISM OF FOUNDATION LIFT-OFF AND ROUNDING OF THE CONTACT SOIL SURFACE

FIGURE 6

suggested by Meyerhof (1951). Both theoretical and observed distributions indicate that because of low confining pressure in the sand under the edges of the footing, it can sustain very little stress, and strength and stiffness increase towards the center where the sand is more confined. The addition of the rocking moment during dynamic test will cause further yielding, densification and settlement of the soil along the leading edge in addition to the initial statically yielded zone and results in more separation of the footing and soil along the trailing edge due to foundation lift-off and deformed outer zone (Figure 6). Since the vertical load on the footing remains constant during the test, for equilibrium the volume under the contact stress diagram should vary continuously until the contact soil surface assumes a stable configuration. Figure 7 shows the static pressure distribution before and after applying the dynamically varying moment and going through resonance during a test. It is observed that because of reduction in contact width the stress diagram has reverted to a much narrower wedge shape configuration. Two distinct dynamic pressure distribution patterns were observed depending on the amplitude of vibration. In the case of low amplitude vibration the dynamic pressure amplitude increases from a minimum value at the footing center to a large amount at the footing edge (Figure 8). This configuration of pressure distribution remains unchanged until there is some yielding and lift-off around the foundation edge, where, a progressive change of dynamic pressure distribution along the footing diameter occurs as the amplitude increases (Figure 9).

In two series of tests on model structures with different masses the size of the circular foundation was varied keeping all other model parameters constant. The resonant frequency of the model increases approximately linearly as the footing radius increases (Figure 10). Figure 11 presents similar results derived for square footings. Natural frequency of the square footings with equivalent semi-dimensions (equal to radius of a circular footing having area equal to that of the square footing) are very close to the values for equivalent circular footings. However, the resonant frequencies of square footings are slightly bigger than the ones for equivalent circular foundations over the entire range of frequencies of interest. The effect of foundation shape on resonant frequency of vibration is shown in Figure 12. The length-to-width ratio for rectangular footings was varied while other parameters were kept constant. As expected, narrow footings rocking around an axis parallel to their longer side have low values of rocking frequencies and

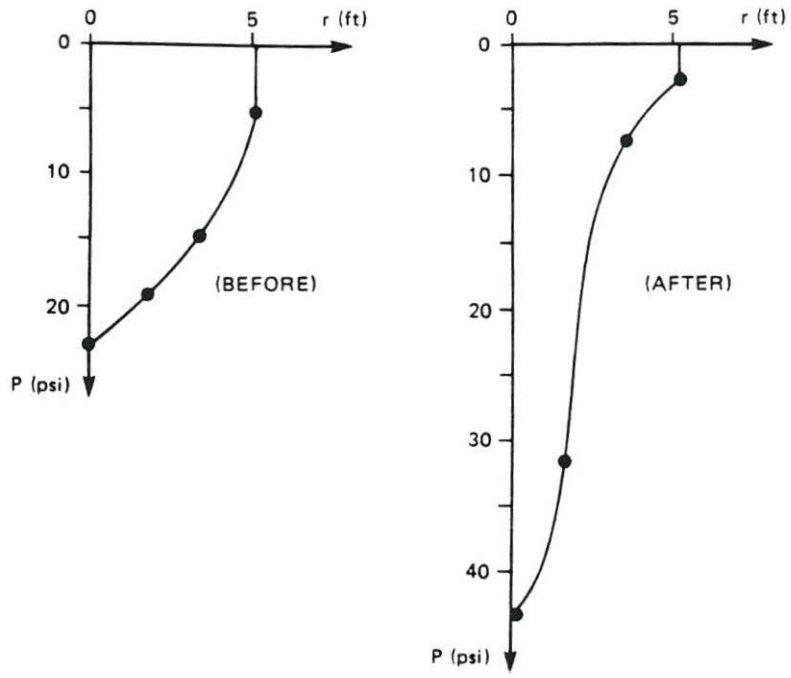

STATIC PRESSURE DISTRIBUTION BEFORE AND AFTER TEST

FIGURE 7

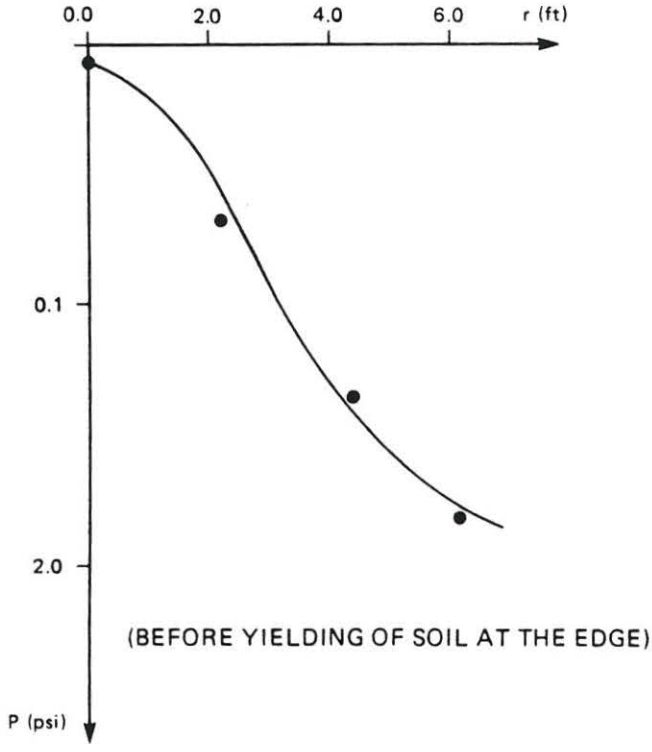

DYNAMIC PRESSURE DISTRIBUTION UNDER ROCKING FOUNDATION DIAMETER

FIGURE 8

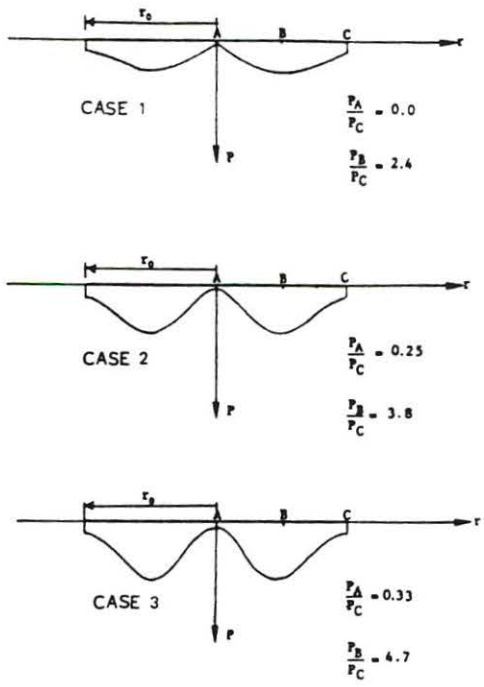

DYNAMIC PRESSURE DISTRIBUTION UNDER ROCKING FOUNDATION ALONG DIAMETER AND AT INCREASING ROCKING AMPLITUDES FROM CASE (1) TO (3) IN FIGURE (AFTER YIELDING OF SOIL AT THE EDGE)

FIGURE 9

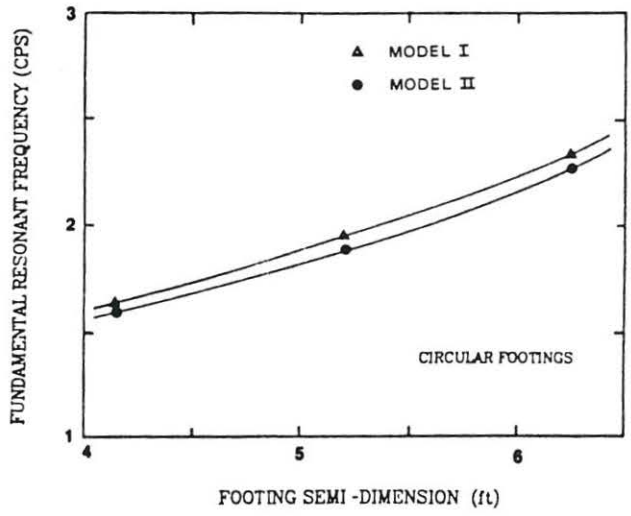

EFFECT OF FOUNDATION SIZE ON ROCKING-SLIDING RESONANT FREQUENCY

FIGURE 10

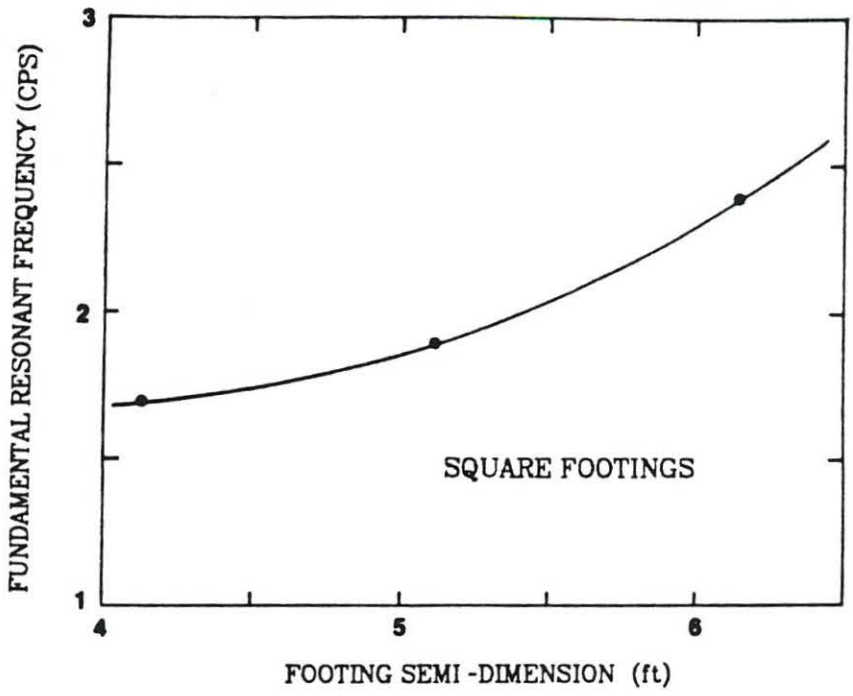

EFFECT OF FOUNDATION SIZE ON ROCKING-SLIDING RESONANT FREQUENCY

FIGURE 11

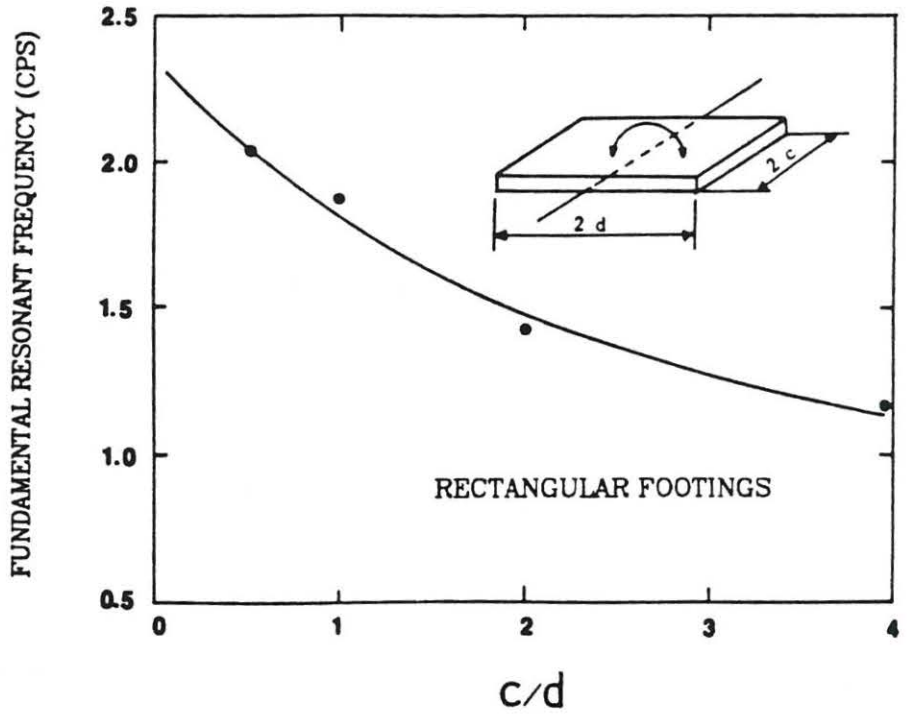

EFFECT OF FOUNDATION SHAPE ON ROCKING-SLIDING RESONANT FREQUENCY

FIGURE 12

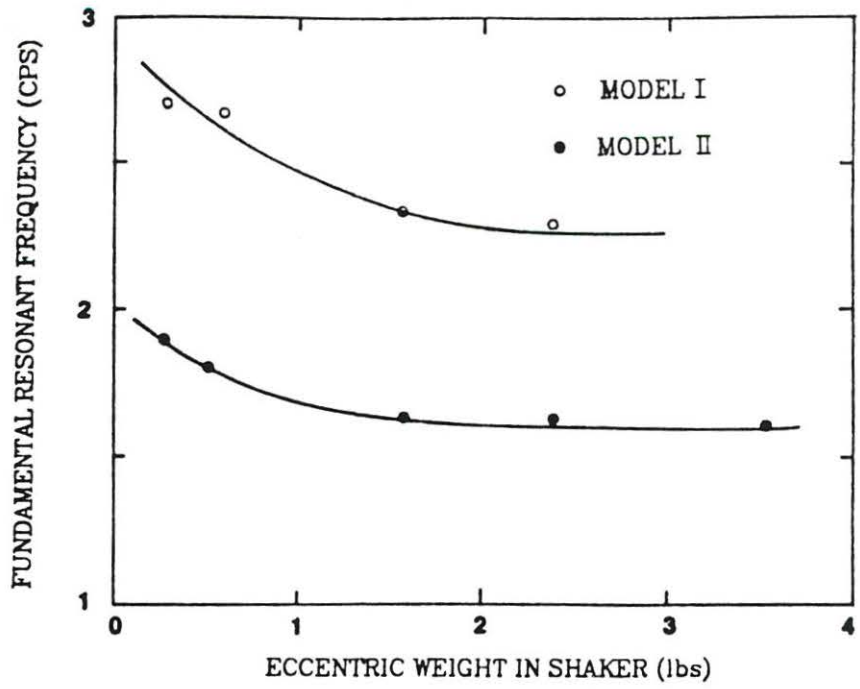

EFFECT OF ECCENTRIC WEIGHT OF SHAKER ON ROCKING-SLIDING RESONANT FREQUENCY

FIGURE 13a

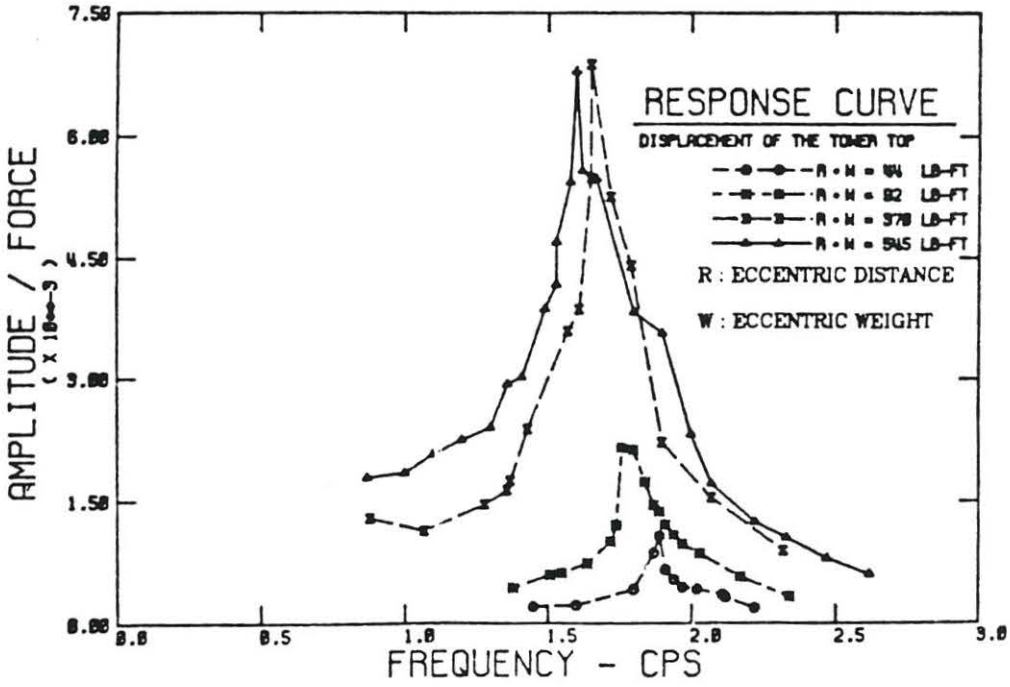

RESPONSE CURVES OF TOWER DISPLACEMENT UNDER DIFFERENT FORCE LEVELS

FIGURE 13b

can be excited very easily in their rocking mode of vibration with larger amplitudes of motion compared with footings rocking around an axis parallel to the shorter side of footing.

Increasing the eccentric weight in the shaker increases the force amplitude at a particular frequency of shaker rotation. This causes higher shear strain amplitudes in the soil under the foundation which results in more softening and nonlinear behavior of the soil. As a result the resonant frequency of the system decreases while damping and amplitude of vibration increase. These phenomena were observed in the experiments showing a clear trend of decrease in resonant frequency with increase in the eccentric mass of the shaker (Figure 13a). A better physical picture of this phenomenon is presented by depicting the response curves for four tests with different shaker masses (Figure 13b).

Increasing the embedment depth of the foundation increases the stiffness of the soil-structure system and therefore results in an increase in natural frequency of the structure. This phenomenon was observed in a series of tests changing the depth of embedment from 0 to 1.5 times the radius of the tower base for both low and high amplitude vibration (Figure 14). As was expected,

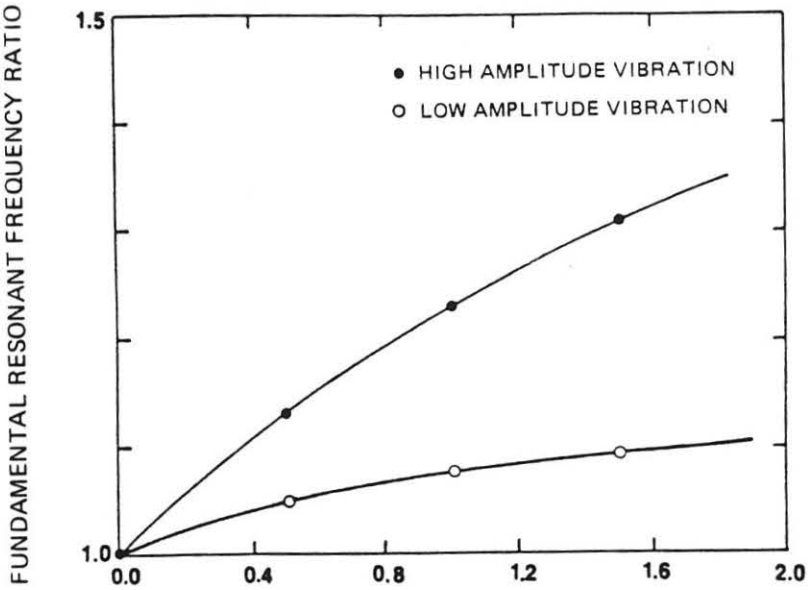

EFFECT OF DEPTH OF EMBEDMENT ON FUNDAMENTAL ROCKING-SLIDING FREQUENCY OF TOWER

FIGURE 14

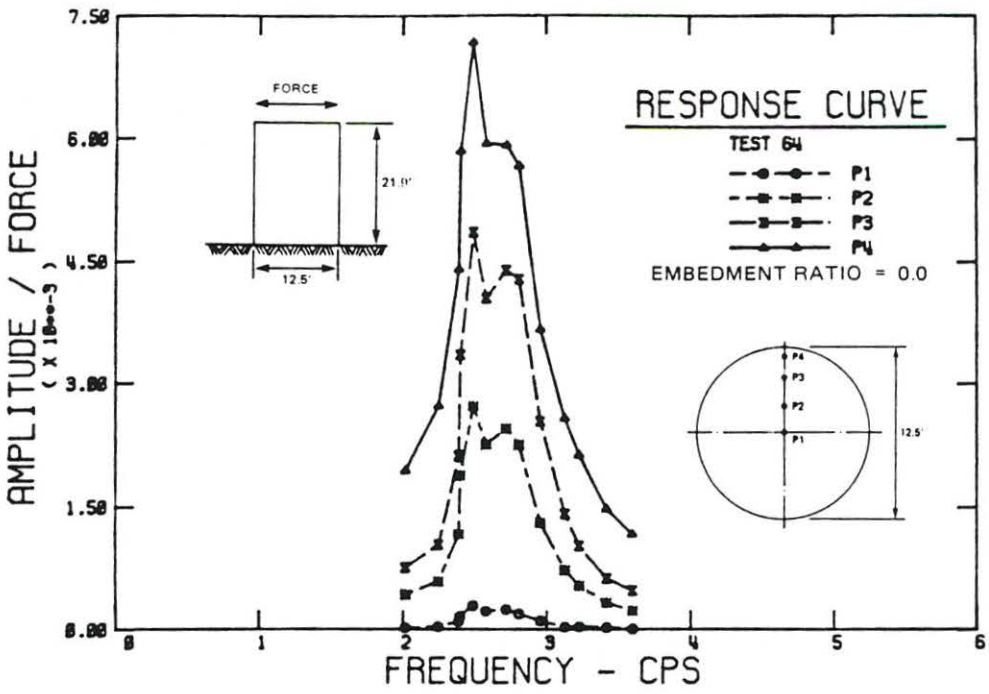

FIGURE 15a

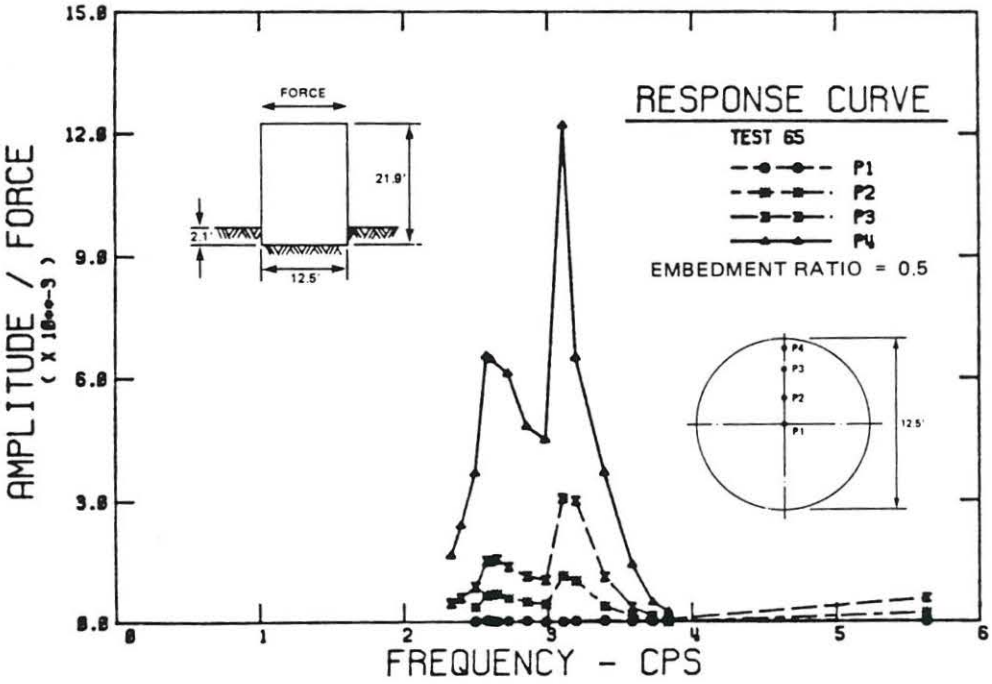

RESPONSE CURVES FOR PRESSURE SIGNALS ALONG DIAMETER AT DIFFERENT EMBEDMENT RATIOS

FIGURE 15b

increase of resonant frequency with embedment is not very large for high amplitude vibration. This is because of ineffective contact between the circular tower side walls and the soil mass. Stokoe and Richart (1974) in an experimental study on model circular footings (8 inch diameter) embedded in a dense, dry sand subjected to rocking excitation showed that embedment without adequate lateral support was essentially ineffective. The contact pressure distribution changes considerably because of embedment. The confining pressure in the soil at the footing edge changes from zero to a finite value over the range from no embedment to an initial depth of embedment. Figures 15a and 15b show variation of pressure distribution with increase of embedment depth by comparing the response amplitudes of pressure signals.

Further parametric studies including tests of foundations on the centrifuge and comparison with theory have been performed (Hushmand, 1983).

CONCLUSIONS

1. Static pressure distribution for a rigid footing on a dense, dry sand has a parabolic shape.

2. Dynamic pressure at low amplitude vibration increases from center to edge, while in case of high amplitude vibration it reduces to zero at the edge because of yielding of the soil.

3. Resonant frequency of footings increases approximately linearly as the size of foundation increases.

4. Resonant frequency of rectangular footings decreases with an increase in length of foundation side parallel to rocking axis.

5. Increasing eccentric mass of the shaker increases nonlinearity of the system, results in decrease of resonant frequency, while damping ratio and amplitude of vibration increase.

6. Effect of embedment under high amplitude vibration reduces considerably because of loss of effective contact between foundation side walls and soil mass.

7. Results of centrifuge model tests are in reasonable agreement with prototype results in high amplitude vibration tests.

8. Incorporation of permanent deformation of the contact soil and foundation-soil separation in the dynamic analysis and design of shallow foundations is recommended.

ACKNOWLEDGEMENT

This work was performed during graduate study of author in California Institute of Technology, Pasadena under the supervision of Professor Ronald F. Scott. The investigation was partially sponsored by Grant No. CEE82-19068 from the National Science Foundation.

REFERENCES

(1) Baranov, V. A., "On the Calculation of Excited Vibrations of an Embedded Foundation," (in Russian), Voprosy Dinamiki, Prochnocti, Polytechnical Institute of Riga, No. 14, 1967, pp. 195-206.

(2) Barkan, D. D., "Dynamics of Bases and Foundations," McGraw-Hill Book Co., Inc., New York, N.Y., 1962, 434 pp.

(3) Beredugo, Y. O., "Vibration of Embedded Symmetric Footings," Ph.D. Thesis, Faculty of Engineering Science, The University of Western Ontario, London, Canada, 1971.

(4) Bielak, J., "Dynamic Behavior of Structures with Embedded Foundations," Int. Journal of Earthq. Engrg. and Struct. Dyn., Vol. 3, No. 3, Jan.-March 1975, pp. 259-274.

(5) Bucky, P. B., "Use of Models for the Study of Mining Problems," Am. Inst. Mining and Metallurgical Engineers Tech. Pub. No. 425, 1931.

(6) Bycroft, G. N., "Forced Vibrations of a Rigid Circular Plate on a Semi-Infinite Elastic Space and on an Elastic Stratum," Philosophical Trans., Royal Society, London, Ser. A, Vol. 248, 1956, pp. 327-368.

(7) Crockett, J. N. A., and Hammond, R. E. R., "The Dynamic Principles of Machine Foundations and Ground," Proc. Institution of Mechanical Engineers, London, Vol. 160, No. 4, 1949, pp. 512-523.

(8) Drnevich, V. P., and Hall, J. R. Jr., "Transiet Loading Tests on a Circular Footing," Journal of Soil Mech. and Found. Div., Proc. ASCE, Vol. 92, No. SM 6, Nov. 1966, pp. 153-167.

(9) Erden, S. M., "Influence of Shape and Embedment on Dynamic Foundation Response," Ph.D. Thesis, University of Massachusetts, Massachusetts, March, 1974.

(10) Fry, Z. B., "Development and Evaluation of Soil Bearing Capacity, Foundations of Structures," WES, Tech. Rep. No. 3-632, Report No. 1, Jul. 1963.

(11) Halpern, M., and Christiano, P., "Dynamic Impedance of a Poroelastic Subgrade," Proceedings-Third-Engineering Mechanics Division Specialty Conference, ASCE, The University of Texas at Austin, Austin, Texas, pp. 805-808, Feb. 1982.

(12) Hayashi, K., "Theorie des Tragers auf Elastischer Unterlage," Julius Springer (Berlin), 1921, 301 pp.

(13) Hetenyi, M., "Beams on Elastic Foundation," The University of Michigan Press (Ann Arbor), 1946, 255 pp.

(14) Hoskin, B. C., and Lee, E. H., "Flexible Surfaces on Viscoelastic Subgrades," Journal of the Engineering Mechanics Division, ASCE, Vol. 85, No. EM4, Proc. Paper 2195, pp. 11-30, Oct. 1959.

(15) Hushmand, B., "Experimental Studies of Dynamic Response of Foundations," Ph.D. Thesis, California Institute of Technology, 1983.

(16) Kausel, E., "Forced Vibrations of Circular Foundations on Layered Media," Ph.D. Thesis, Massachusetts Institute of Technology, 1974.

(17) Kuhlemeyer, R., "Vertical Vibrations of Footings Embedded in Layered Media," Ph.D. Thesis, University of California, Berkeley, 1969.

(18) Luco, J. E., "Impedance Functions for a Rigid Foundation on a Layered Medium," Nuclear Engineering and Design, Vol. 31, No. 2, 1974.

(19) Luco, J. E., and Westmann, R. A., "Dynamic Response of Circular Footings," Journal of Engng. Mech. Div., ASCE, 1971, Vol. 97, No. EM5.

(20) Meyerhof, G. G., "The Ultimate Bearing Capacity of Foundations," Geotechnique, Vol. 2, 1951, pp. 301.

(21) Novak, M., "The Vibrations of Massive Foundations on Soil," Int. Assoc. Bridge Struct. Eng., Publ. No. 20, 1960, pp. 263-281.

(22) Novak, M., "Prediction of Footing Vibrations," Journal of Soil Mech. Found. Div., Proc. ASCE, Vol. 96, No. SM3, May 1970, pp. 337-361.

(23) Novak, M., and Beredugo, Y. O., "The Effect of Embedment on Footing Vibrations," Proc. 1st Can. Conf. Earthq. Engng. Research, Vancouver, B.C., May 1971, pp. 1-14.

(24) Novak, M., and Beredugo, Y. O., "Vertical Vibration of Embedded Footings," Journal of Soil Mech. Found. Div., Proc. ASCE, Vol. 98, No. SM12, Dec. 1972, pp. 1291-1310.

(25) Pokrovsky, G. I., and Fyodorov, I. S., "Centrifugal Model Testing in the Construction Industry," draft translation prepared by Building Research Establishment Library Translation Service, Great Britain, 1975.

(26) Rao, H. A. Balakrishna, "The Design of Machine Foundations Related to the Bulb of Pressure," Proc. 5th ICSMFE, Vol. 1, 1961, pp. 563-568.

(27) Reissner, E., "Stationare, exialsymmetrische durch eine Schuttelnde Masse erregte Schwingungen eines homogenen elastischen Halbraumes," Ingenieur-Archiv, Vol. 7, Part 6, Dec. 1936, pp. 381-396.

(28) Rowe, P. W., "Application of Centrifugal Models to Geotechnical Structures," Proc. symp. geotech. struct., University of New South Wales, Australia, 1975.

(29) Scott, R. F., "Centrifuge Studies of Cyclic Lateral Load-Displacement Behavior of Single Piles," Soil Mechanics Laboratory, California Institute of Technology, Pasadena, California, 1977.

(30) Scott, R. F., Liu, H-P., and Ting, J., "Dynamic Pile Tests by Centrifuge Modeling," Proc. 6th World Conf. Earthquake Eng., Paper 4-50, New Delhi, 1977.

(31) Scott, R. F., Ting, J. M., and Lee, J., "Comparison of Centrifuge and Full Scale Dynamic Pile Tests," International Conf. on Soil Dynamics and Earthq. Engrg., Southampton, UK, July 1982.

(32) Stokoe, K. H., II, "Dynamic Response of Embedded Foundations," Ph.D. Dissertation, Univ. of Michigan, Jan. 1972, 251 pp.

(33) Stokoe, K. H., II, Richart, F. E., Jr., "Dynamic Response of Embedded Machine Foundations," Journal of the Geotechnical Engineering Division, ASCE, Vol. 100, No. GT4, April 1974.

(34) Sung, T. Y., "Vibrations in Semi-Infinite Solids Due to Periodic Surface Loadings," Symposium on Dynamic Testing of Soils, ASTM-STP No. 156, 1953, pp. 35-64.

(35) Terzaghi, K., "Theoretical Soil Mechanics," John Wiley and Sons, Inc. (New York), 1943.

(36) Terzaghi, K., "Evaluation of Coefficients of Subgrade Reaction," Geotechnique, Vol. 5, 1955, pp. 297-326.

(37) Thomson, W. T., and Kobori, T., "Dynamical Compliance of Rectangular Foundations on an Elastic Half-Space," J. Appl. Mech., Trans. ASME, Vol. 30, Dec. 1963, pp. 579-584.

(38) Tiedemann, D. A., "Vertical Dynamic Response of Embedded Footings," Bureau of Recl. Report, REC-ERC-72-34, Eng. Research Center, Sept. 1972.

(39) Veletsos, A. S., and Verbic, B., "Vibration of Viscoelastic Foundations," Int. Journal of Earthq. Engrg. and Struct. Dyn., 1973,2,87.

(40) Veletsos, A. S., and Wei, Y. T., "Lateral and Rocking Vibrations of Footings," Journal of Soil Mech. Found. Div., ASCE, 1971, 97, SM9.

(41) Weiler, W. A., Jr., Kulhawy, F. H., "Factors Affecting Stress Cell Measurements in Soil," Journal of Geotech. Engrg. Div., ASCE, Vol. 108, No. GT12, Dec. 1982, pp. 1529-1548.

BEHAVIOR OF A TUNNEL DURING A RAPID EARTHQUAKE FAULTING EPISODE

by P. B. Burridge*

INTRODUCTION

The Southern California Rapid Transit District plans to construct a subway system known as Metro Rail for the Los Angeles area. A portion of the proposed tunnel passes through the 45° dipping Hollywood fault at approximately right angles and, as shown in Figure 1, lies on sandstone bedrock 60 feet below the alluvium surface. Probable fault displacement is estimated at 3.7 feet of vertical offset. Since there have been no documented occurrences of the behavior of a modern tunnel subjected to fault displacements, information is lacking as to the interaction of tunnel and soil, the stress levels to be expected in the tunnel and the length of tunnel that will be affected. To help answer these questions, a limited series of rapid fault displacement tests was conducted on a scaled model tunnel imbedded in soil in the geotechnical centrifuge at the California Institute of Technology. This paper presents: a) the faulting mechanism used for the fault displacement tests, b) the results of two tests, and c) the results of a one-dimensional finite element analysis of the tunnel.

FAULTING MECHANISM

A device had previously been constructed to simulate the action of a 45° reverse fault on the centrifuge (1). As shown in Plates 1 and 2, the device consists of a test container with a false floor, the right-

* Graduate Student, Division of Engineering and Applied Science, California Institute of Technology, Pasadena, CA 91125

hand side of which, together with the end wall, is capable of moving down at 45° to the left side which is stationary. The moving portion is kept in place until activated by a toggle control supported in a position beyond top dead center (TDC). In its initial position the floor is level, as seen in Plate 1, and the model tunnel is placed on it and covered with soil. When the centrifuge is running with the test container at the appropriate g-level, and the data acquisition system is turned on, the toggle is released by a push from a hydraulic cylinder controlled by the operator. Once it passes over TDC, the weight of the moving portion of the box plus soil (with the in-flight acceleration level of approximately one hundred g's, this amounts to more than one ton) propels it downward to the stops, to the position shown in Plate 2. The fault is thereby activated and propagates through the soil to the surface. The tunnel and superincumbent soil are displaced as they would be in a fault rupture event.

The vertical offset of the false floor shown in Plate 2 is 1/4 inch and represents a 2 foot fault displacement at 100 g. Although the geologically expected vertical displacement of the Hollywood fault is 3.7 feet, an offset of only 2 feet was modeled for the centrifuge tests since calculations indicated that the full geological offset would permanently damage the instrumented model tube.

MODELING OF THE PROTOTYPE TUNNEL

The proposed tunnel construction consists of a number of precast reinforced concrete slabs bolted together to make one 3-1/2 foot long "ring" section, as shown in Figure 2. These "rings" in turn bolt together along the tunnel axis to form the complete tunnel. Since the

bending properties of the slab units vary along the tunnel axis and circumferentially around the cross-section, an equivalent uniform prototype section was chosen and a uniform aluminum tube used for the centrifuge model. The most important property of the prototype tunnel to be modeled was the in-plane "ring" stiffness, that is, the stiffness associated with deformation of the circular tunnel cross-section. Consequently, the inside diameter and the EI per unit length of the tunnel were the quantities used to correctly scale the centrifuge model tube. The aluminum model tube is shown in Plate 3, instrumented with strain gauges for longitudinal flexure (i.e., bending of the tunnel as a beam) and transverse flexure (i.e., deformation of the circular cross-section).

FAULT TEST PREPARATION OF THE MODEL TUBE

The ends of the model tube were covered to prevent the entrance of sand and the tube was placed at right angles to the fault in the test container, with the false floor in the raised position. A hard plastic sleeve extending to the wall which moves with the fault was placed over the rigid end of the tube to accommodate shortening of the box with fault displacement and prevent axial compression of the tube. At the left end of the tube was a 3/4 inch gap between the tube and end wall, which became filled with sand once the model overburden was placed over the tube for the fault displacement tests. Plate 4 shows the model tube placed in the test container prior to filling with sand and Plate 5 shows the test container after completion of a test with the right end displaced downward 1/4 inch and the container appropriately shortened. Two fault displacement tests were conducted, the first representing a

loose soil condition of 93 pcf unit weight, and the second representing a dense soil condition of 102 pcf unit weight. These conditions were intended to bracket the range of probable soil conditions at the Hollywood site.

CENTRIFUGE TEST RESULTS

The prototype longitudinal bending moments and flexural stresses for the fault tests at γ = 93 pcf and 102 pcf are presented in Figures 3 and 4. The prototype transverse bending moments and flexural stresses are shown in Figure 5 for the 93 pcf fault test. These figures are oriented to match Plates 1 and 2 so that points to the right of the fault are displaced downward relative to those on the left side of the fault which remain fixed. The static pretest values represent the tunnel condition immediately prior to fault rupture, the dynamic values represent the maximum moments and stresses during fault rupture (unless indicated minimum) and the static post-test residual values represent the tunnel condition after all transients of fault rupture have died away.

In the longitudinal direction, the maximum bending moment of 8.6×10^5 kip-ft and maximum flexural stress of 27.1 ksi occur directly over the fault for γ = 102 pcf. It should be noted that throughout the tests the model aluminum tube remained linear in its response and hence one would not expect a stress of 27.1 ksi to actually develop in a reinforced concrete tunnel. Instead, one would expect such a tunnel to yield and fail at a stress of approximately 6 ksi over a distance of at least 30 feet either side of the fault as indicated by Figure 3.

In the transverse direction, the maximum bending moment of 59 kip-ft/ft and maximum flexural stress of 10.5 ksi occur 10 feet from the fault on the downthrown side for the 93 pcf fault test. The maximum transverse flexural stress is noted to be less than half the maximum longitudinal flexural stress.

Figures 6 and 7 show the dynamic characteristics of longitudinal bending moment directly over the fault for the 93 pcf test during fault rupture. Figure 7 is an enlarged version of a section of Figure 6 showing, in more detail, the dynamic response of the tunnel immediately after initiation of fault rupture. It is observed that fault displacement takes place in less than 0.1 seconds and the time between data points is approximately 6 milliseconds (2).

ONE-DIMENSIONAL STATIC FINITE ELEMENT ANALYSIS

A one-dimensional static finite element model of the tunnel was constructed using planar beam elements. As shown in Figure 8, the beam elements were supported by springs at the nodes and the nodal forces were computed from the overburden plus a nonlinear correction for soil-tunnel interaction. This correction was additive or subtractive depending on the relative movement between tunnel and soil and its magnitude accounted for the softening of soil with increasing strain (2). The finite element model was calibrated by adjusting its parameters to obtain the closest possible agreement with the static residual longitudinal bending moment curves of the centrifuge tests (Figure 3). Figure 9 shows how close a match could be achieved. This calibration quantified the amount of soil-tunnel interaction experienced during the centrifuge tests.

In spite of the plastic sleeve placed over the right end of the centrifuge tube, shortening of the faulting container developed an axial force in the tube directed to the right and a shear force directed downward at the capped left end of the aluminum model tube. Inclusion of the shear force at the left end was found necessary in the analysis to match the numerical to the experimental results as shown in Figure 9.

With the nodal springs and soil-tunnel interaction of the finite element model calibrated by the centrifuge test results, the boundary conditions were removed from the finite length numerical model to allow it to predict the longitudinal bending moments of the infinite length prototype tunnel. The predicted longitudinal bending moment profile is shown in Figure 10. The maximum moment for the infinite length model occurs directly over the fault for the dense (102 pcf) soil test and has a value of approximately 6.4×10^5 kip-ft. This compares very favorably with the maximum moment for the finite length model and centrifuge test results of Figure 9.

CONCLUSION

Despite the finite length of the centrifuge model and the boundary effects associated with the centrifuge fault displacement tests, the centrifuge does appear to capture the essential behavior of an infinite length prototype tunnel during a rapid earthquake faulting episode.

ACKNOWLEDGMENTS

The centrifuge and finite element model studies were carried out under a subcontract between the California Institute of Technology and

Lindvall, Richter and Associates (who were directly contracted by the Southern California Rapid Transit District to study the earthquake response of the proposed Metro Rail system).

The centrifuge tests were performed with the invaluable assistance of J. R. Lee while the finite element studies were carried out by Professor J. F. Hall. The entire Caltech effort was supervised and guided by Professor R. F. Scott.

REFERENCES

1. Roth, W. H., Scott, R. F. and Austin, I., "Centrifuge Modeling of Fault Propagation Through Alluvial Soils," Geophysical Research Letters, Vol. 8, No. 6, pp. 561-564, May 1981.
2. Lindvall, Richter and Associates, "Centrifuge and Numerical Studies to Evaluate Effect of Fault Displacement on Metro Rail Tunnel for Southern California Rapid Transit District," July 1984.

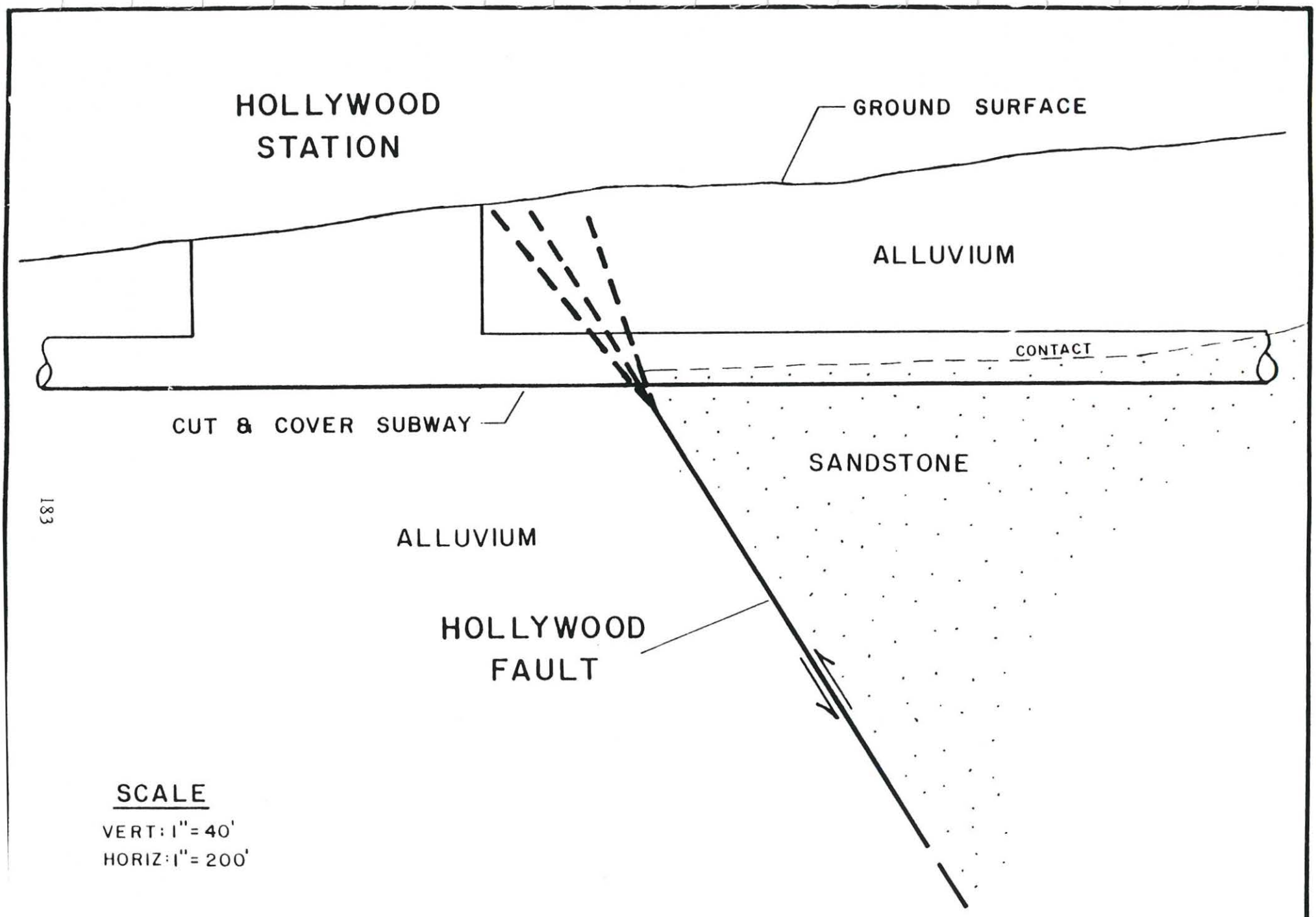

LINDVALL RICHTER & ASSOCIATES
EARTHQUAKE SCIENCES AND ENGINEERING GEOLOGY

SUBWAY PROFILE AT HOLLYWOOD FAULT CROSSING

FIGURE 1

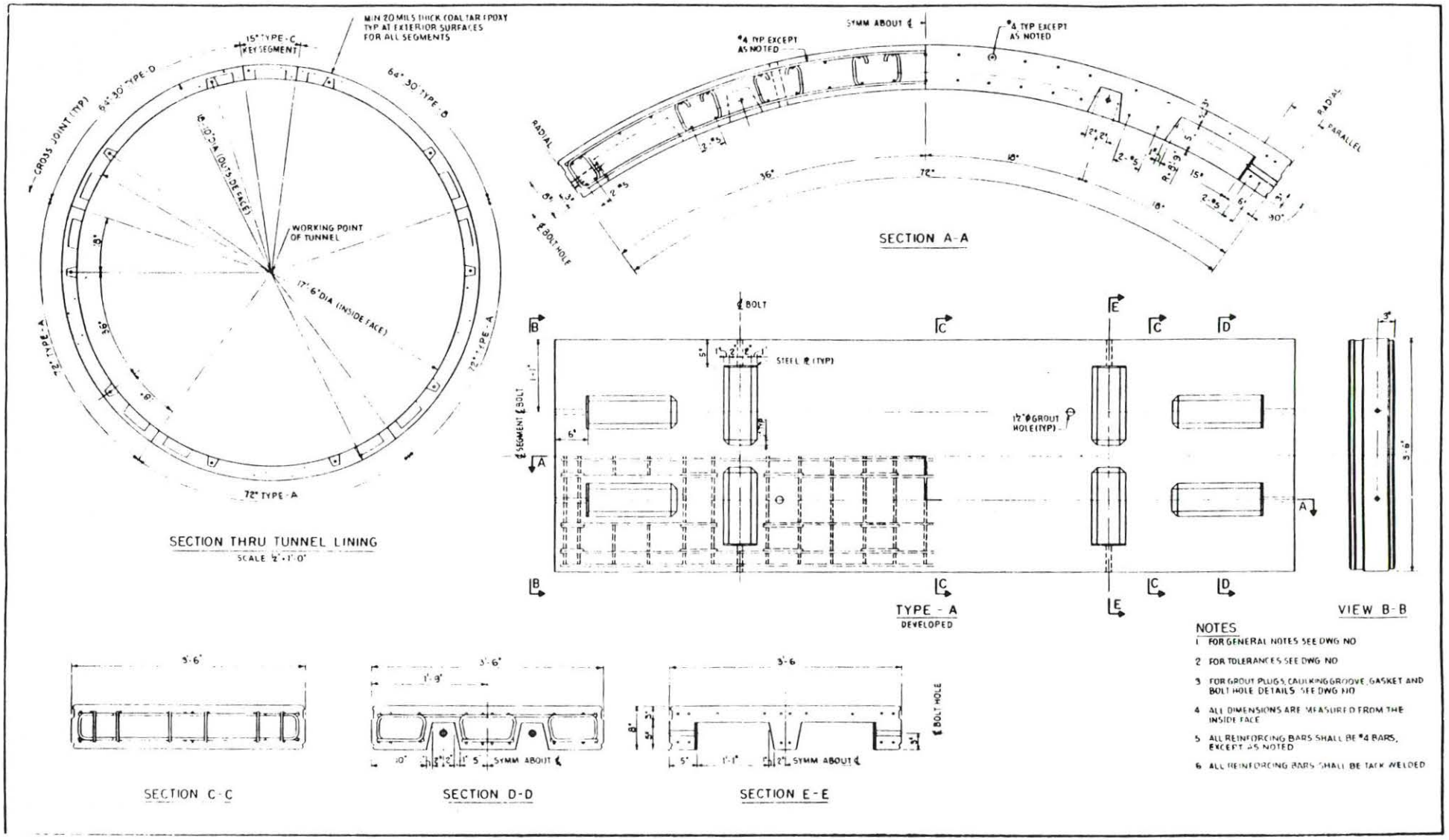

Figure 2 Structural drawings of prototype tunnel

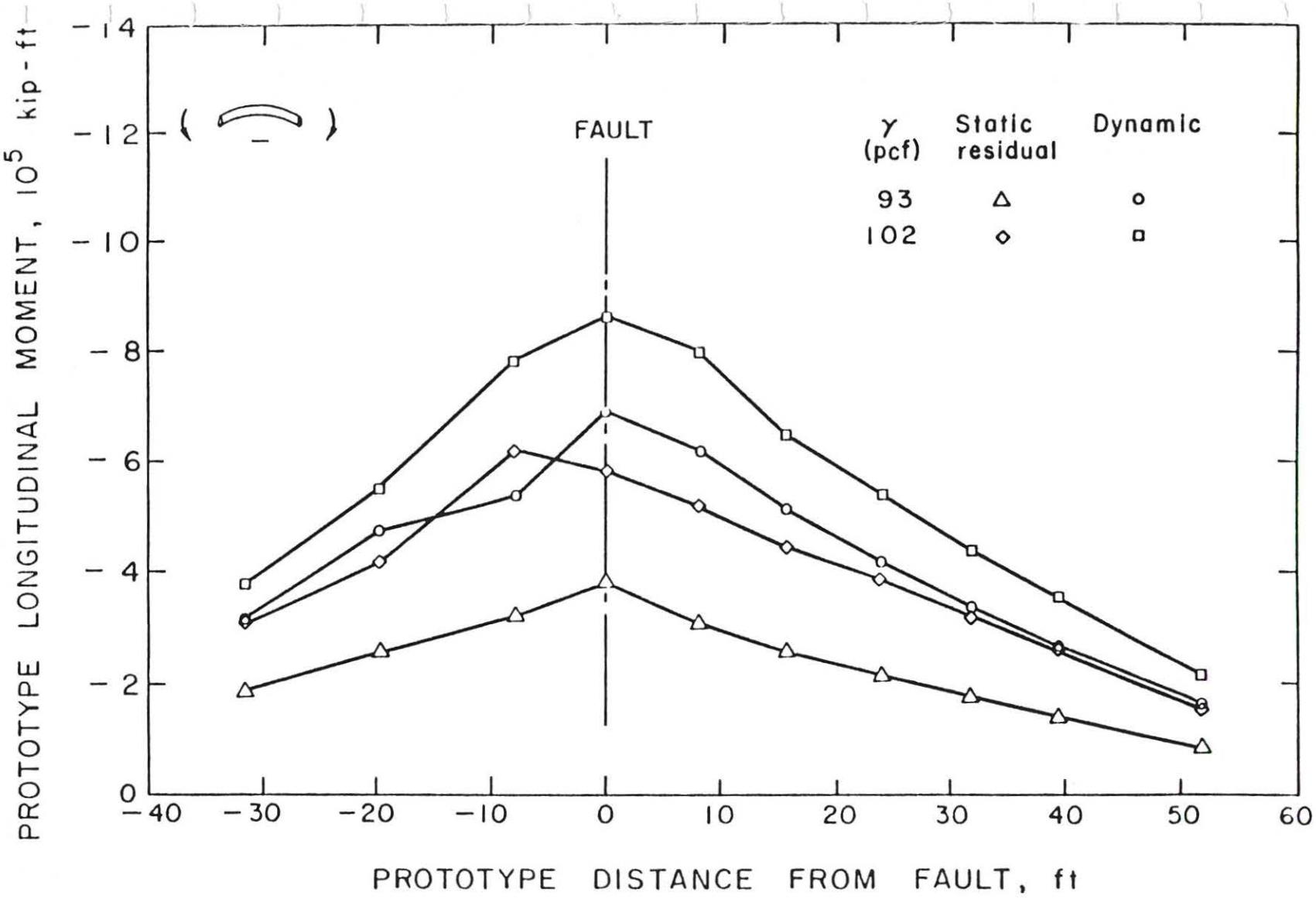

Figure 3 Prototype longitudinal moments due to faulting in loose soil (93 pcf) and dense soil (102 pcf).

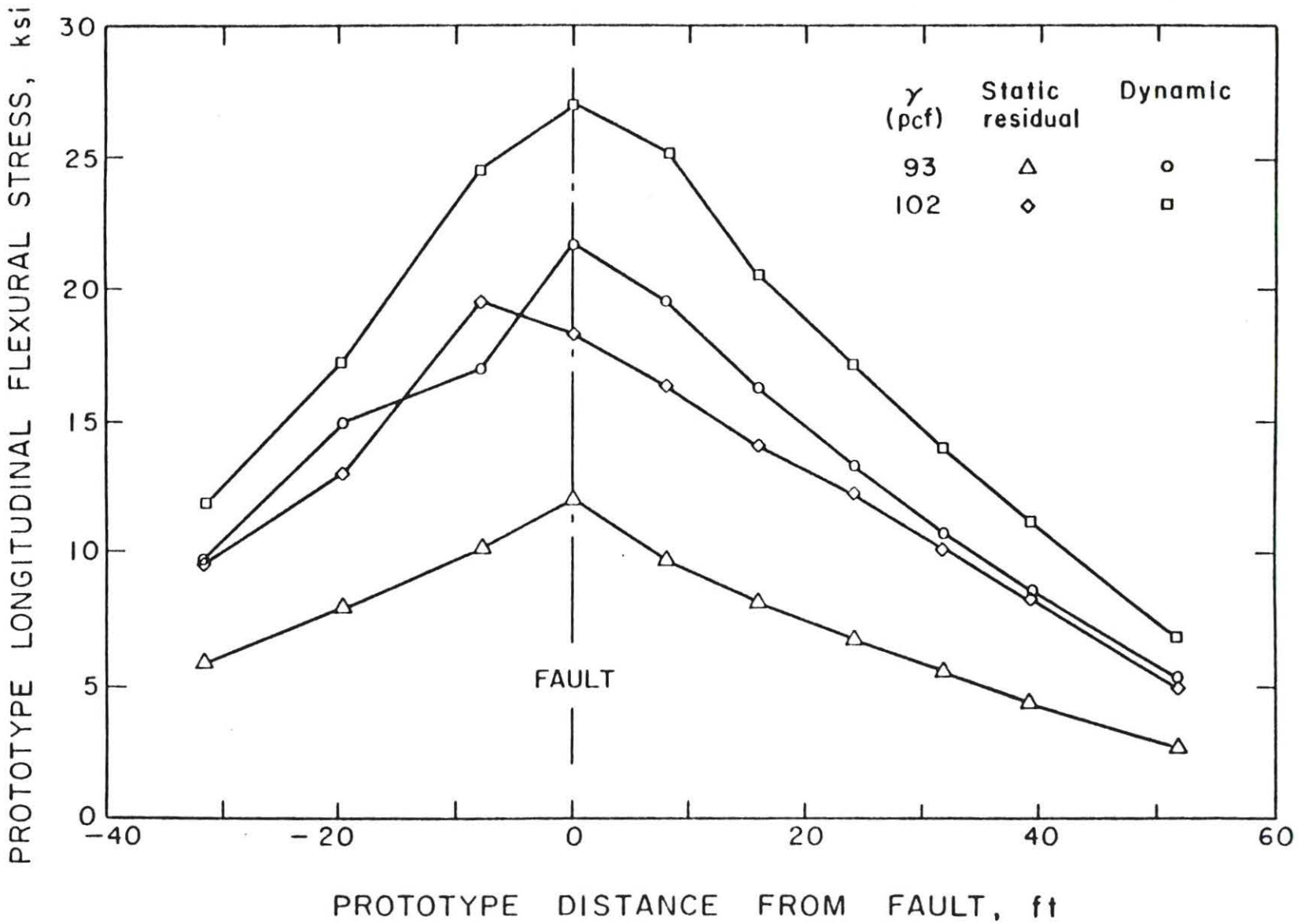

Figure 4 Prototype longitudinal stresses due to faulting in loose soil (93 pcf) and dense soil (102 pcf).

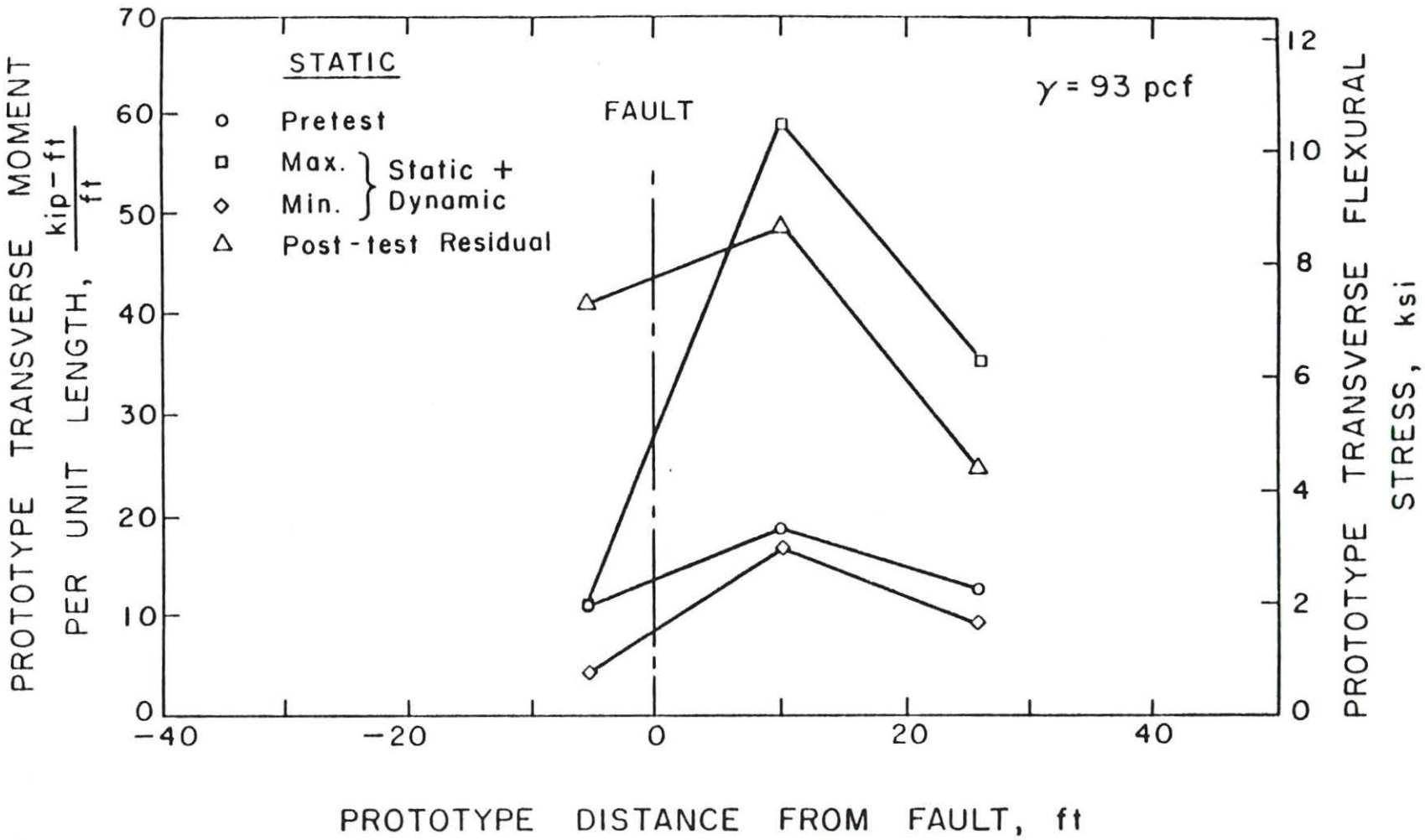

Figure 5 Prototype transverse moments and stresses due to faulting in loose soil (93 pcf).

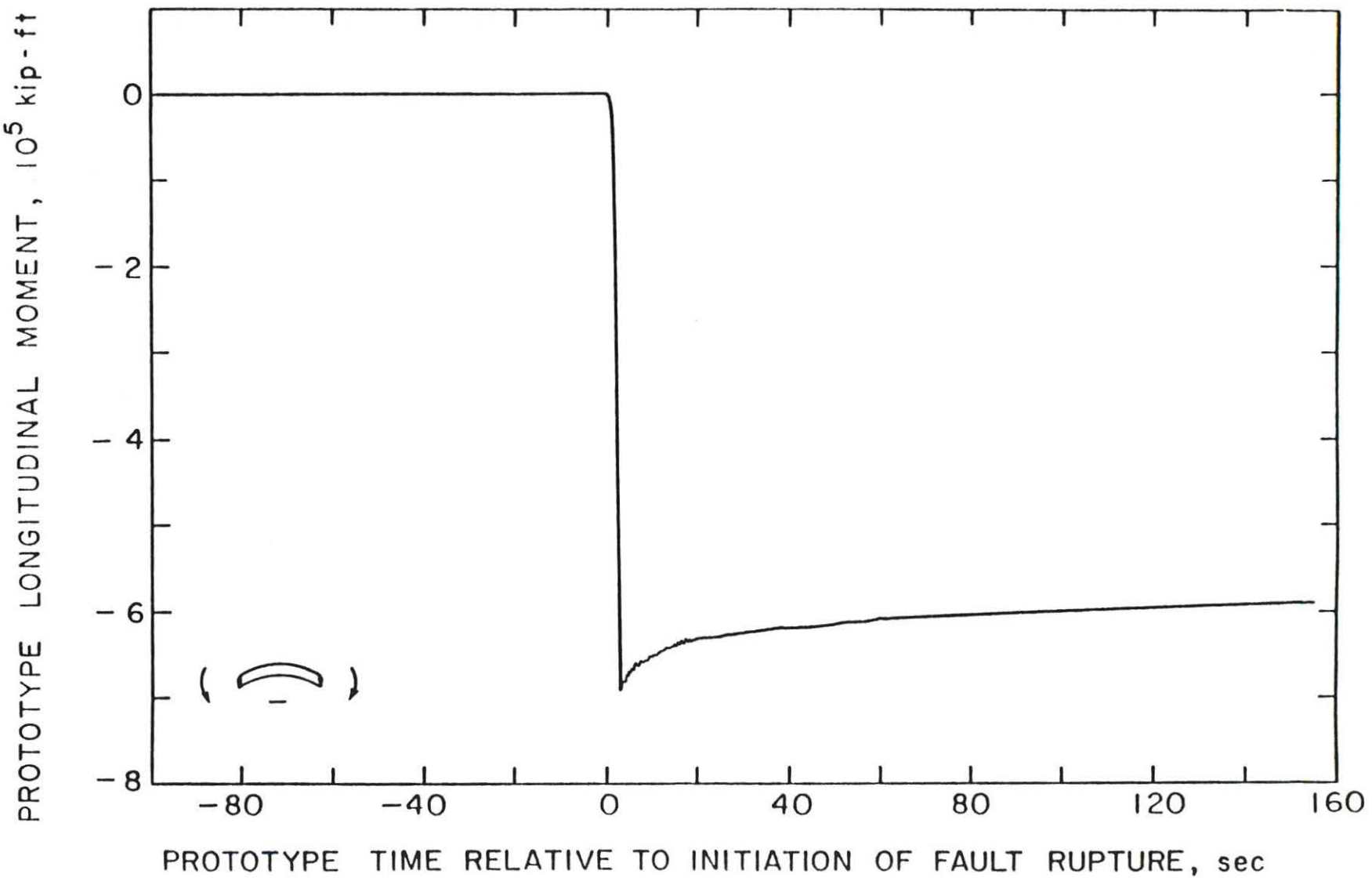

Figure 6 Prototype longitudinal moment directly over fault as a function of prototype time during faulting; loose soil (93 pcf) test.

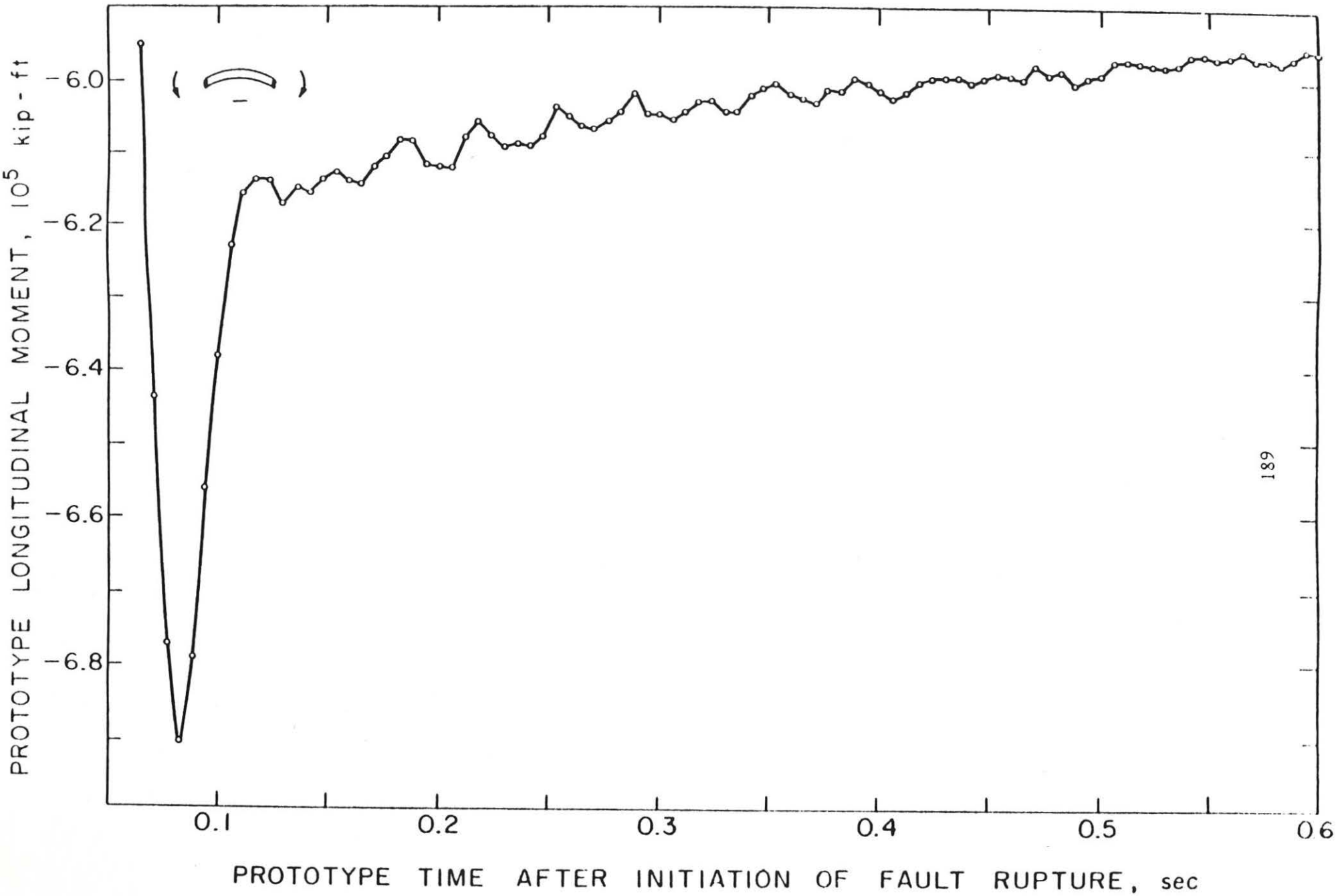

Figure 7 Prototype longitudinal moment directly over fault as a function of magnified prototype time during faulting; loose soil (93 pcf) test.

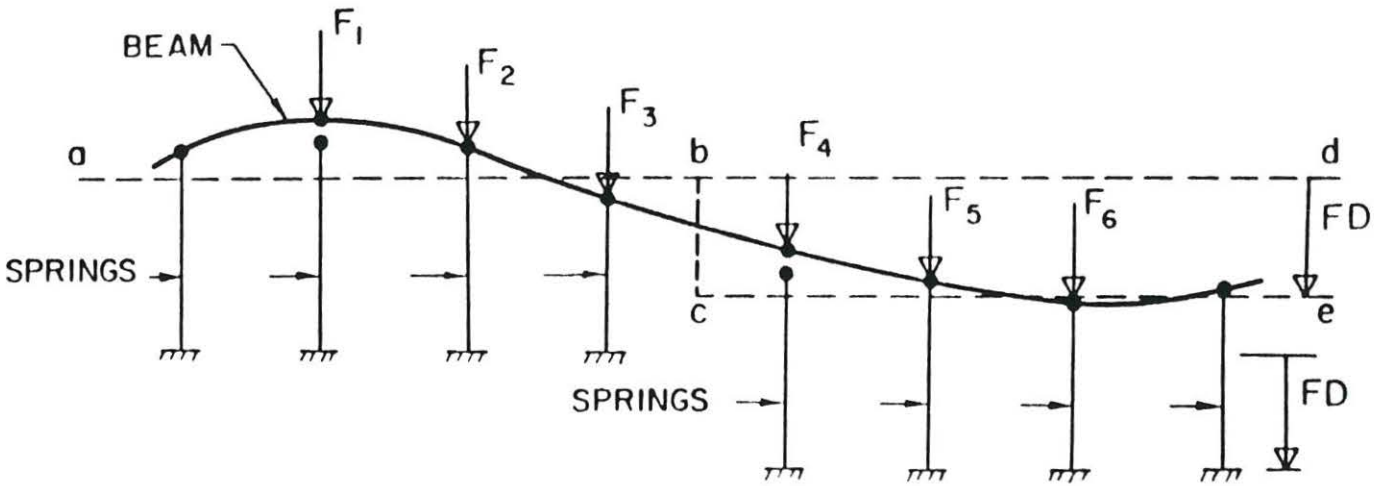

Figure 8 Finite element model. Line a-b-d is the initial location of the beam elements (horizontal) and line b-c is the fault line. During faulting, the soil and spring bases to the right of b-c move down a vertical distance FD (2 ft), representing the vertical component of fault displacement. In particular, the soil at level b-d moves down to c-e.

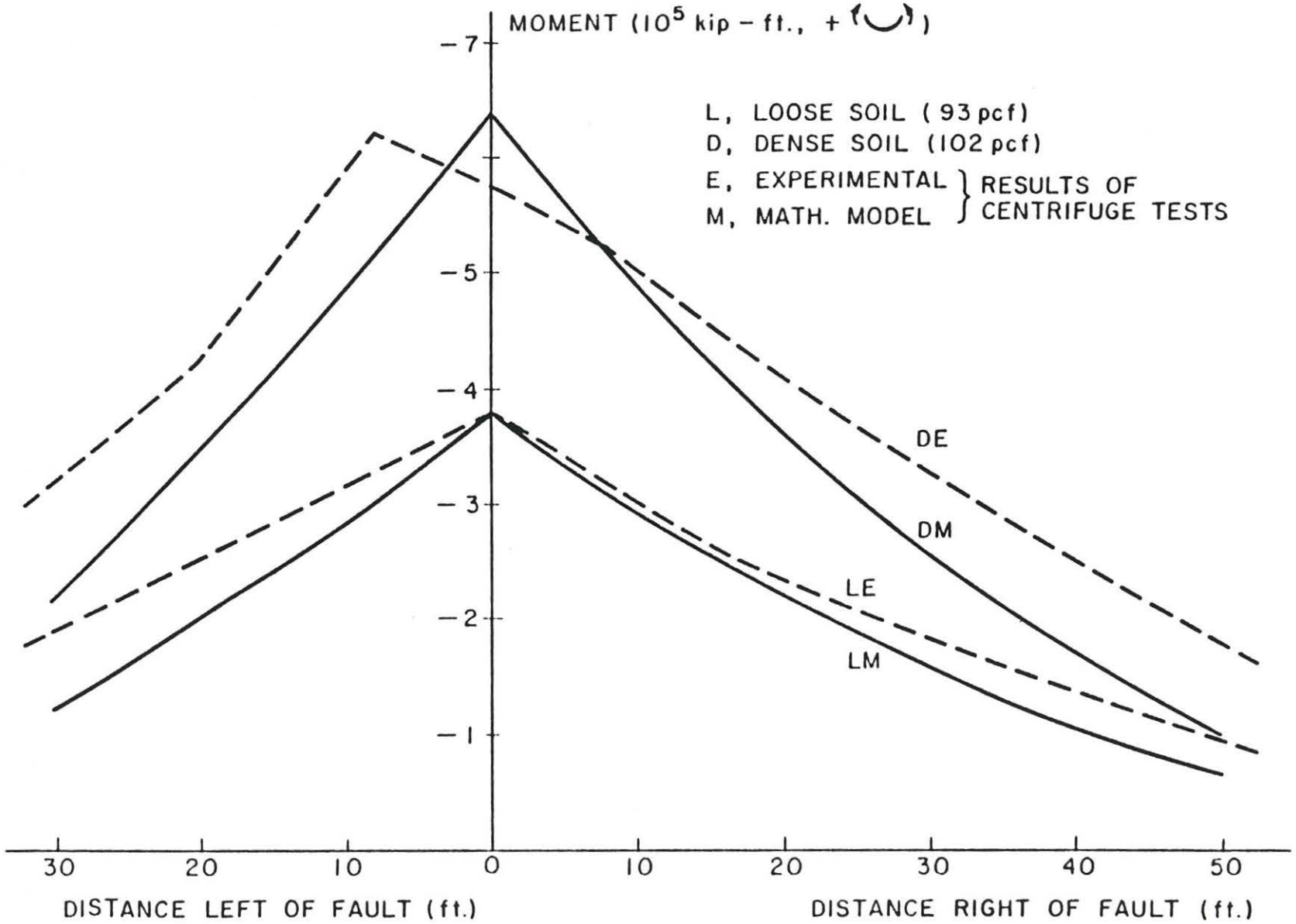

Figure 9 Comparison of prototype longitudinal moments from finite length numerical model and centrifuge fault displacement tests.

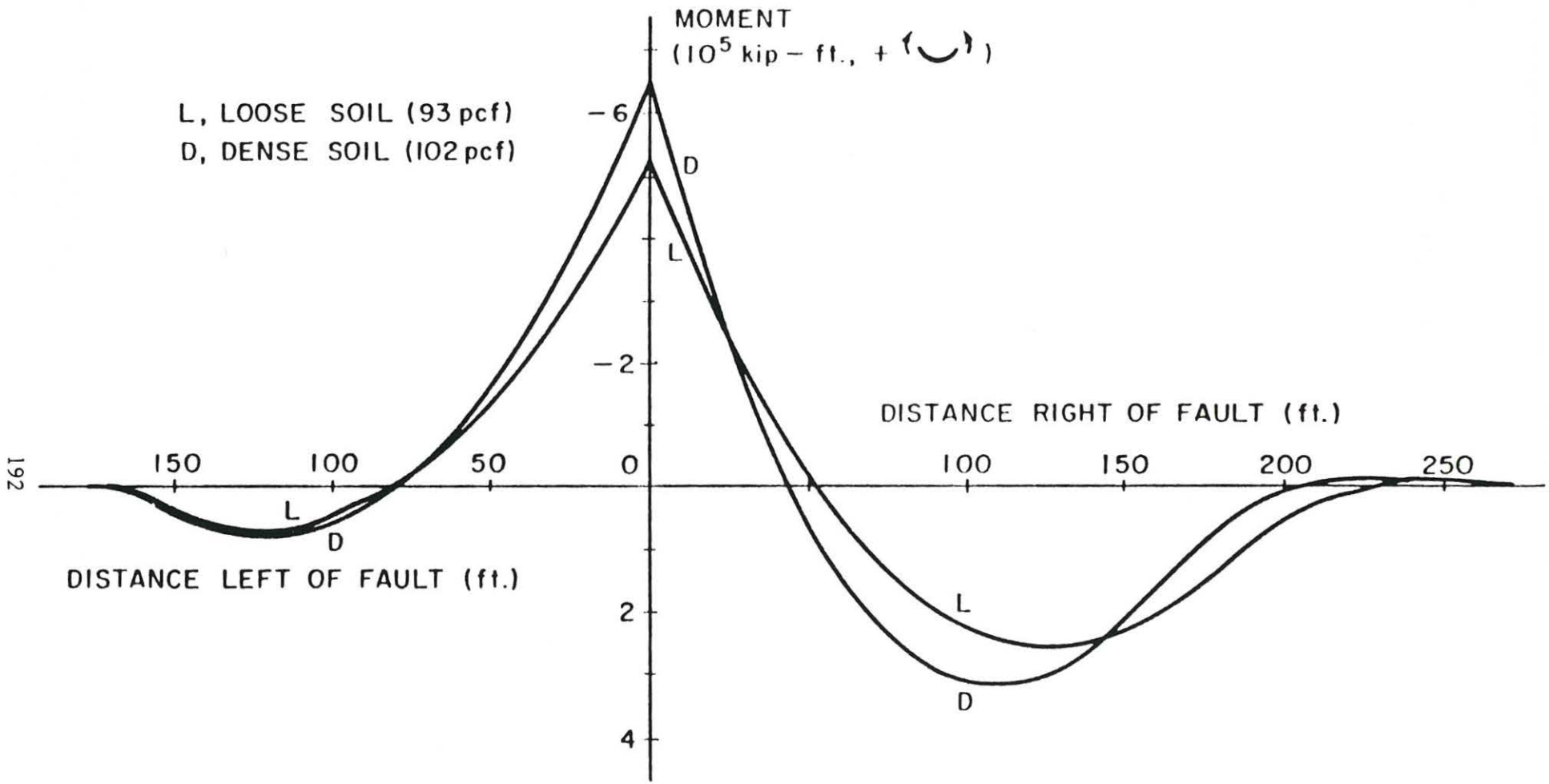

Figure 10 Prototype longitudinal moment profile predicted by infinite length numerical model.

Plate 1 Side view of fault actuation mechanism, front panel removed. False floor in level position.

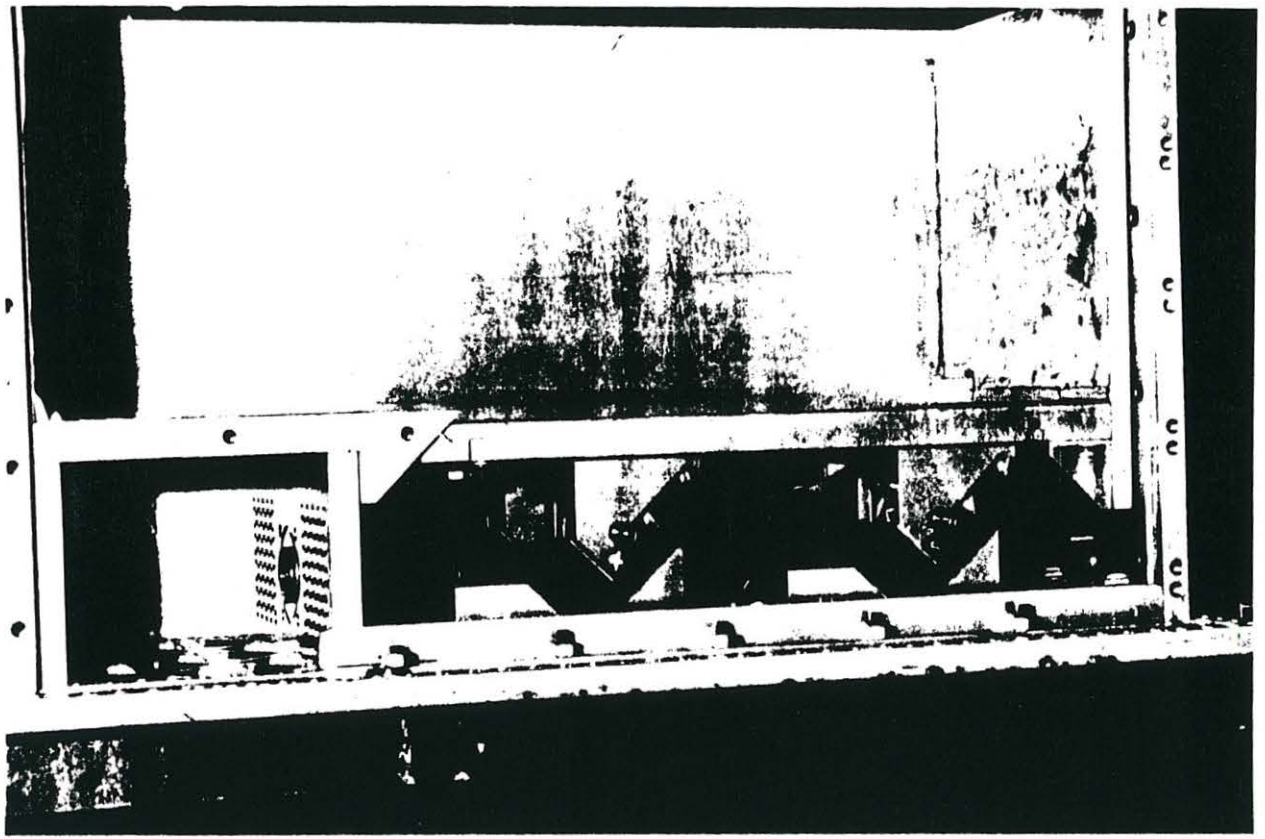

Plate 2 Side view of fault actuation mechanism, front panel removed. Fault displaced 0.25 inches.

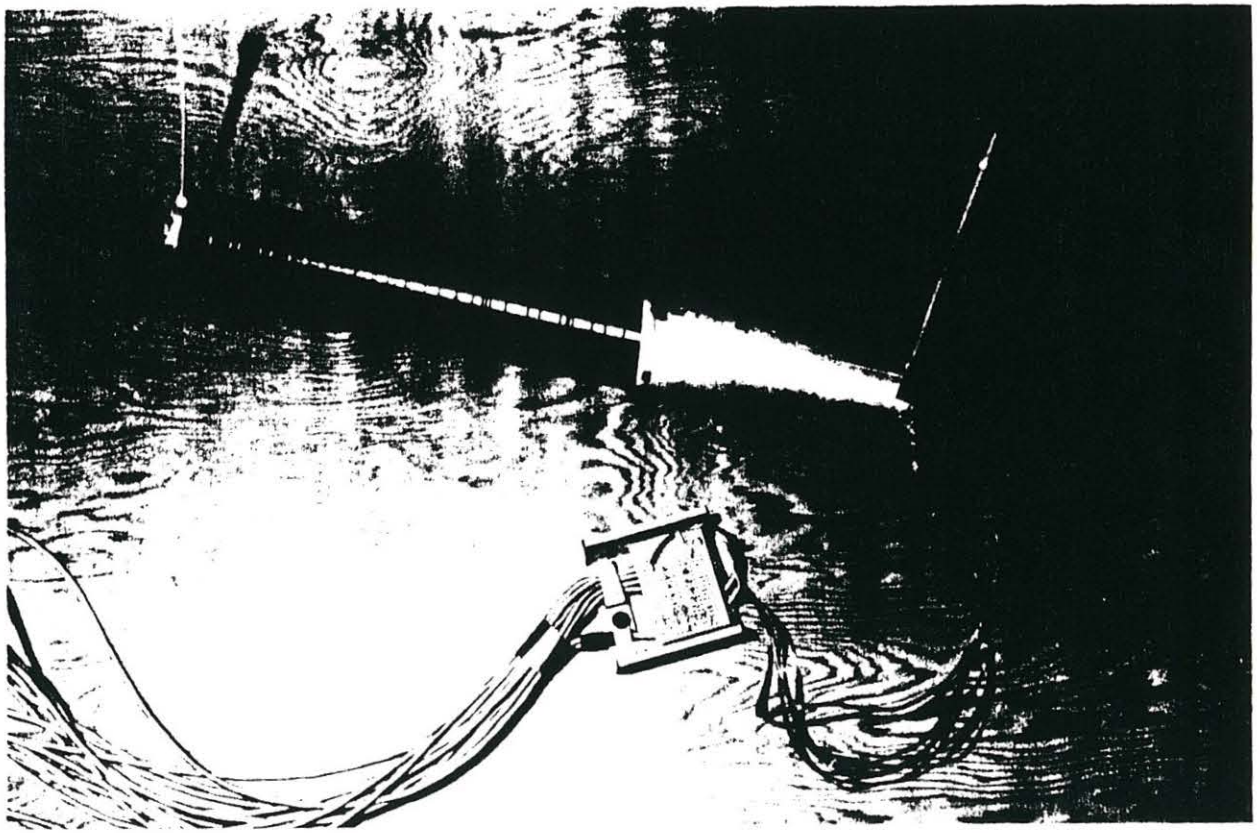

Plate 3 Aluminum model tunnel and strain gauge instrumentation.

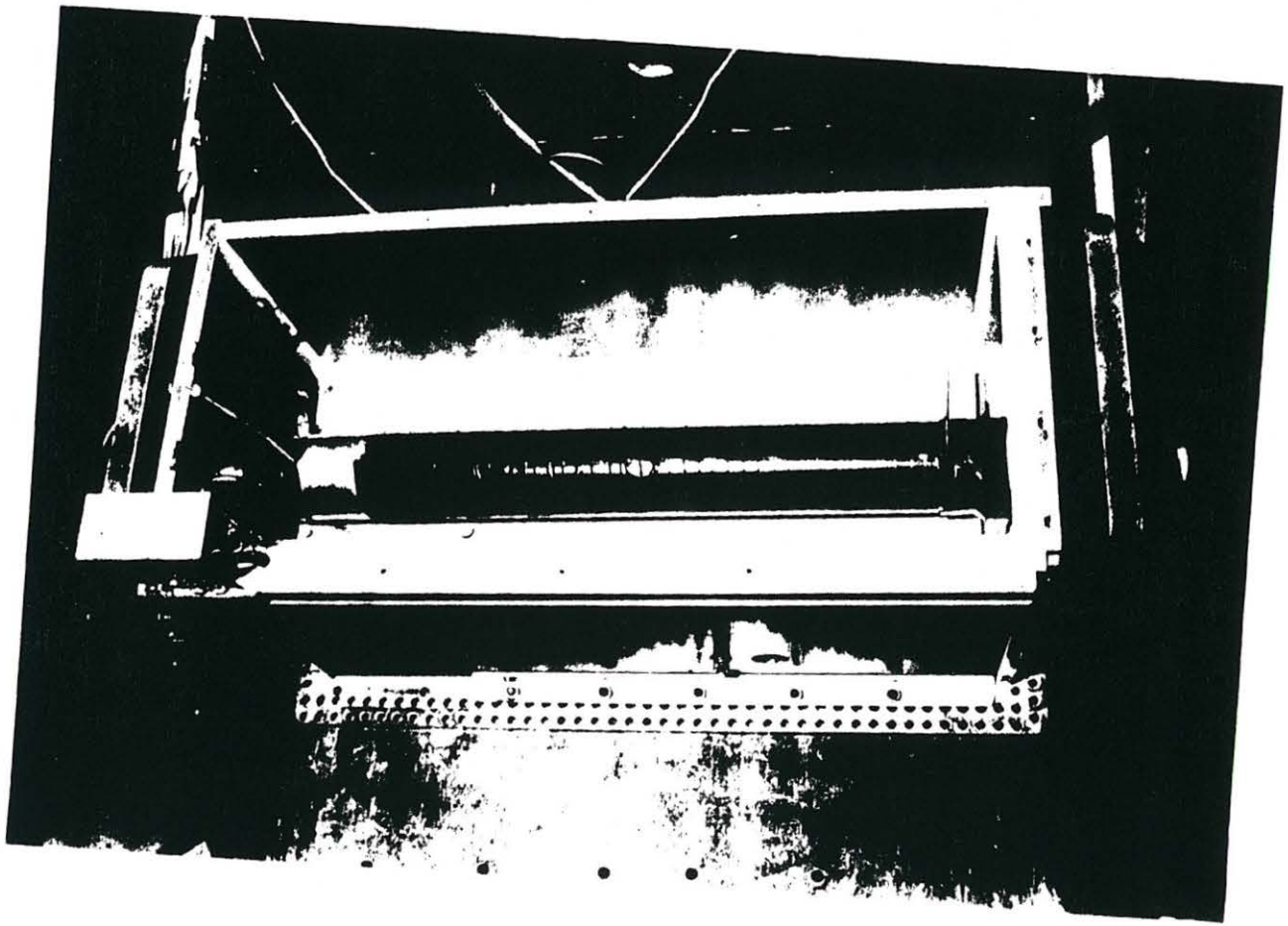

Plate 4 View from above of model tunnel installed in test container. Vertical displacement rods mounted at each end.

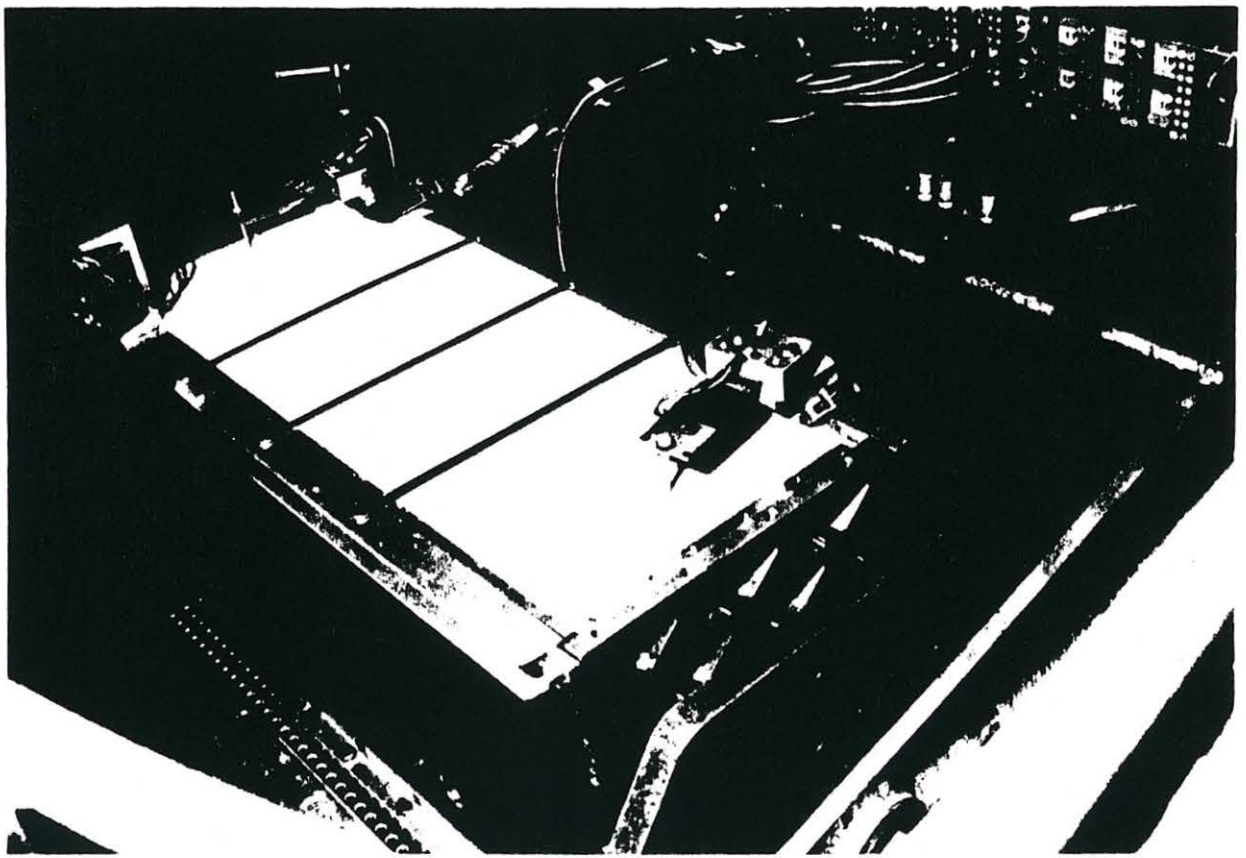

Plate 5 Test container after rapid faulting test. Vertical soil displacement visible with respect to side of container at right-hand end.

CENTRIFUGE MODELLING OF ARTIFICIAL SAND ISLANDS IN EARTHQUAKES

Lee, F.H.
Senior Tutor,
National University of Singapore.
(On study leave at Cambridge University).

Schofield, A.N.
Professor of Engineering,
University of Cambridge.

1. Introduction

Increasingly over the past decade, artificial islands have been constructed for various purposes, most having been constructed in less than 13 m of water with relatively unprotected slopes and with short design lives. However, as oil and gas exploration and production and as port expansion move to deeper waters and the need for more secure and economical designs for such islands develops, more complex forms of island construction have evolved, such as the use of sand-filled caissons on submarine berms, Fig. 1. Where artificial sand islands are constructed in seismically active regions, the behaviour of these soil structures in earthquakes has to be considered. Little quantitative data is currently available on the response of artificial islands to earthquakes, one of the better known sets of data being the pore pressure and acceleration records collected from Owi Island No. 1 in Tokyo Bay during the Chiba earthquake (Ishihara et al, 1981). This paper describes the results of two centrifuge model tests carried out using the Bumpy Road Facility at the Cambridge Geotechnical Centrifuge (Schofield, 1981). In these test, the artificial islands were modelled by two-dimensional embankments in fine sands submerged in silicone oil: further development is now taking place with earthquake tests on three-dimensional circular island models. Rigid steel plates placed on the crest of the embankments represent surcharge on prototype islands, Figs. 2. Both models were tested at a centrifuge acceleration of 40g.

2. Modelling Requirements and Prototype Representation

2.1 Model Scale

A summary of the scaling relationship for geotechnical centrifuge model tests with earthquake shaking is as follows:

Quantity	Ratio of Model to Prototype
Length	1/N
Velocity	1
Acceleration	N
Force	$1/N^2$
Stress	1
Energy	$1/N^3$
Frequency	N
Time	1/N

At prototype scale, there are regions of the island in which excess pore pressure gradients lead to significant pore water diffusion in periods of time equal to the duration of the event, in this case an earthquake. In the absence of inertial effects, it would have been usual to scale times by a model scale factor of $1/N^2$ in order that time factors for consolidation or swelling processes in compressible ground should correspond in model and prototype. If water had been used as the model pore fluid in these two models, it would have been appropriate for the duration of the model event to be only $1/N^2$ times that of the prototype event. This is incompatible with the requirement that the model event should have a duration of 1/N times that of the prototype event in order to scale inertial effects correctly. So the time factors for the model were altered by replacement of water by a more viscous pore fluid: in this case the model pore fluid was 42 centistokes silicone oil to correspond with a model scale factor of approximately 40.

It has been shown that in flow regimes for which Darcy's Law is applicable, diffusion time is directly proportional to pore fluid viscosity (Terzaghi and Peck, 1967), so that the time distortion factor mentioned above can be eliminated by choosing a pore fluid which is N times as viscous as water. Muskat (1946) noted that Darcy's Law is applicable to laminar flow regime with sufficiently low Reynolds number, a requirement which has been found to be satisfied by prototype flow in silt through to medium sand (Lambe and Whitman, 1969). For Darcy's Law to be valid for centrifugal models, the same criterion have to be satisfied. Let

$$Re_p = (\rho_p\, v_p\, d_p)/\mu_p \quad \ldots\ldots\ldots\ldots\ldots\ldots (1)$$

and

$$Re_m = (\rho_m\, v_m\, d_m)/\mu_m \quad \ldots\ldots\ldots\ldots\ldots\ldots (2)$$

in which Re_p, ρ_p, v_p, d_p and μ_p are the prototype Reynold number, pore fluid density, apparent velocity, effective pore size and prototype pore fluid viscosity, respectively; and Re_m, ρ_m, v_m, d_m and μ_m the corresponding model quantities. Then

$$(Re_m/Re_p) = (\rho_m/\rho_p)(v_m/v_p)(d_m/d_p)(\mu_p/\mu_m) \quad \ldots\ldots\ldots\ldots (3)$$

If the same soil is used in model and prototype, $d_m/d_p=1$. Moreover, density of silicone oil is approximately equal to that of water so that $\rho_m = \rho_p$. If the viscosity of the silicone oil is adjusted so that $\mu_m = N\mu_p$, then Eqn. (3) becomes

$$(Re_m/Re_p) = (v_m/v_p)(1/N) \quad \ldots\ldots\ldots\ldots\ldots\ldots (4)$$

In the flow regime in which Darcy's Law is valid, the apparent velocity

$$v = (k/\mu)(dh/ds) \quad \ldots\ldots\ldots\ldots\ldots\ldots (5)$$

where k is a constant of the porous medium, μ the pore fluid viscosity and dh/ds the hydraulic gradient. hence

$$(v_m/v_p) = (\mu_p/\mu_m)(dh/ds)_m/(dh/ds)_p$$

$$= (1/N)(dh/ds)_m/(dh/ds)_p \quad \ldots\ldots\ldots\ldots (6)$$

In scaled centrifuge models, $(dh/ds)_m = N(dh/ds)_p$ so that $v_m/v_p = 1$. Hence $(Re_m/Re_p) = 1/N$ $\ldots\ldots\ldots\ldots\ldots\ldots (7)$

Since N is invariably greater than 1, Re_m is always less than Re_p. Thus, provided the prototype flow system is laminar and therefore obeys Darcy's Law, scaling of diffusion time by increasing pore fluid viscosity may be validly applied as it results in a lower Reynolds number and therefore preserves the laminar flow regime.

2.2 Model Materials and Form

The main purpose of the test reported here, as also of the succession of other studies on the Cambridge Geotechnical Centrifuge was to study the mechanics of problems in general and not only of a succession of different sites with different soils (Kutter, 1982, Dean and Schofield, 1983, Schofield and Venter, 1984). In the majority of previous tests, standard sand and clay have been used allowing comparisons of results in different studies. However, some tests have been undertaken using soils from specific sites (Schofield and Venter, 1984).

The models were constructed of Leighton-Buzzard B.S. 52/100 fine sand and had a height of 90 mm, crest width of 200 mm and slopes of about 1 in 3. Forty two centistokes silicone oil was used as the model pore fluid. The prototype problem is a flat crested submerged embankment of the same sand, with a height of 3.6 m, crest width of 8 m and slopes of about 1 in 3. Mild steel plates of 5 mm, 10 mm, and 20 mm thicknesses were used for model surcharges at different stages of the tests. These correspond to average prototype surcharge loadings of about 15 kPa, 31 kPa and 61 kPa, respectively.

3. Model Preparation Method

The model was constructed at 1 g and model preparation procedure follows largely that developed and used by Dean (1983), with minor modifications. As shown in Fig. 2, the model was constructed on a sloping concrete base which was bolted to the base of the container, the 1 in 40 slope of the concrete base being designed to account for the loading imposed by the Earth's gravity field on the model when the latter is in centrifugal flight at 40g. The model preparation method consists of the following stages:

(a) Forty two centistokes silicone oil was de-aired so as to prevent air bubble formation in the model embankment. This was achieved by drawing it into a vacuum chamber and leaving it under vacuum for at least 24 hours.

(b) Formworks were used to shape the embankment during model preparation and to minimise risk of damage to the model when the package was being moved around. As shown in Fig. 3, the formworks consisted of two major sets of components, as follows,

(i) Two trapezoidal arches which acted as the main load bearing elements of the formworks.

accelerometer) and is taken to be that actually applied to the model. K_{out} is calculated by the formula

$$K_{out} = 50(|a_{max}|+|a_{min}|)/(Ng) \quad \% \quad \ldots\ldots\ldots(8)$$

where a_{max} and a_{min} are the maximum and minimum values of acceleration measured by the reference accelerometer. K_{out} is generally quoted as less in long-term records than in short-term records. This is because less sampling points are used over the time of the earthquake, so the actual maximum and minimum values are usually missed. In the discussion below, the short-term value is taken to be the relevant one.

The time records are plotted as a sequence of horizontal traces, the horizontal axis being labelled in model time, equivalent prototype time can be computed by multiplying model time values by the g-level, that is 40. On the right hand side is the name and number of the device (ACC for accelerometer, PPT for pore pressure transducer) as well as the scale in engineering units per cm. Acceleration is presented in percent strength and pore pressures in kPa. Since both these quantities are preserved in prototype and model, the figures may also be taken to be prototype values . On the left hand side are the maximum and minimum values of the quantity being plotted. Further details on the format of these time history plots can be found in Dean and Schofield (1983).

After these time history plots in Figs. 9 to 15, there are some Lissajous Figures 16 and 17 which are obtained by plotting the record of one transducer against that of another. Phase difference can be estimated from the shape of the figure and some typical plots are shown in Appendix I.

6. Discussion of Results

6.1 Test FHL01, Earthquake 5

Figs. 9 a and b show the short-term and long-term records of a 12% earthquake. The surcharge was a 10 mm steel plate which is estimated to exert an average bearing pressure of 31 kPa in both model and prototype. As the surcharge is rigid, the actual distribution of bearing pressure is unlikely to be uniform. In Fig. 9 a, ACCs 1258, 988, 728 and 1244 show fairly well-coupled motion up to the mid-height of the model. Lissajous Diagrams in Figs. 16 indicate that there is virtually no phase difference between the fundamental frequency components of these four accelerometer records.

All pore pressure transducers show positive response, the maximum being attained by PPT 68 located just beneath the surcharge near the centreline of the model. PPT 2331 located near the slope experienced the minimum pore pressure generation, as would be expected from its proximity to a free-draining boundary.

(ii) Forteen U-section beams spanning between the two arches were used to maintain the shape of model. These beams were placed as the model was being constructed.

(c) Leighton-Buzzard B.S. 52/100 fine sand was used to form the entire model except the toes which were constructed with B.S. 14/25 and B.S. 25/52 sands to prevent erosion. Along various levels of the embankment, layers of blue-dyed 52/100 sand were poured near the side windows. Upon completion of model construction, these horizontal blue sand layers were pierced by a thin rod to create a set of roughly vertical blue sand traces, which, in conjunction with the horizontal blue sand layers, forms a blue sand grid, Fig. 4. Large scale permanent deformations of the embankment section may be detected by the distortion of this blue sand grid. To ensure full saturation of the model, the sand-silicone oil mixture was de-aired under vacuum before pouring. The de-aired sand-silicone oil mixture was then scooped out in small portions using a plastic beaker which was then immersed in the oil already present in the container and tipped over, thus allowing the sand to pluviate through silicone oil without air bubble formation. In spite of the apparent crudeness of this method, the results for both models were remarkably consistent, as will be seen later. More recently, an improved method of model preparation has been developed, which will be described briefly in Section 7. The average relative density of both models described in this paper was estimated to be between 60% to 70%.

(d) Transducers were placed at appropriate heights in the embankment as sand pouring progressed. Dynamic signals were measured by DJB A23 piezoelectric accelerometers and Druck PDCR 81 pore pressure transducers. Sangamo LVDTs were also used to record surcharge settlement after each earthquake.

Mild steel plates 156 mm long and 200 mm wide were used as model surcharge. As shown in Fig. 2b, three steel plates were arranged lengthwise in series to span the whole length of the embankment. It was felt that this arrangement would reduce interaction between the central segment of the embankment length, where most of the transducers were placed, and the end segments near the windows. To minimise seepage of silicone oil through the gaps between steel plates, thin polyethylene strips each about 2 cm wide were placed beneath the steel plates across the joints, Fig. 2b. Fine sand was glued onto the undersurfaces of the steel plates using araldite to increase friction at the embankment-surcharge interface.

4. Bumpy Road Earthquakes

The workings of the Bumpy Road Facility have been described by Schofield (1981). The model earthquake consists of ten roughly sinusoidal pulses of lateral acceleration on the model container which is transmitted to the model as a base-shaking motion. Typical time records of the base shaking acceleration (see Fig. 5) show that the amplitude of these sinusoidal pulses varies slowly with time. The allowable maximum magnitude of base shaking acceleration that may be applied to the container depends

on the g-level of the test. At 40g, the magnitude of the base shaking acceleration may be varied between 0 and about 16g, the latter being 40% of the centrifuge acceleration and may be considered adequate for strong earthquakes. The frequency and duration of these roughly sinusoidal pulses are about 80 Hz and 125 msecs, respectively, these being equivalent to prototype values of about 2 Hz and 5 secs.

Fig. 6 shows the response spectra of some typical Bumpy Road earthquakes. As will be expected from the roughly sinusoidal variation of the earthquake time records, the response spectra are much narrower than those of natural earthquakes (Newmark and Rosenblueth, 1971). This prevents direct modelling of specific natural or design earthquakes but allows the possibility of modelling of models (Dean and Schofield, 1983) and creates an ideal system to provide dynamic response data for mechanistic studies as well as for verification of analytical and numerical computations.

Analog signals from accelerometers and pore pressure transducers were recorded on a forteen-channel Racal tape recorder. Tape segments containing the relevant earthquake records were then played back and the analog signals digitised using the FLY14 program developed by Dean (1983).

5. Earthquake Time Records

A total of forty two earthquakes were fired in the two model tests which were designated FHL01 and FHL02; each with three different surcharges, viz 5 mm, 10 mm and 20 mm mild steel plates. Figs. 7 and 8 show transducer positions for each model with accelerometer and pore pressure transducer abbreviated to ACC and PPT, respectively. Owing to the finite size of these devices and their movements within the models during the tests, their exact locations could not be determined. Hence, the positions marked in Figs. 7 and 8 should only be regarded as approximate ones. The results from seven earthquakes are presented and discussed here; a complete collection of the results can be found in Lee (1983). For each of these seven earthquakes, short-term and long-term time records are plotted from Figs. 9 to 15 after one 3-point smoothing pass (see Dean and Schofield, 1983). The data point spacings for short-term and long-term records are 200 microsecs and 1600 microsecs, respectively. The much smaller data point spacing of short-term records allows details of the earthquake event to be captured whilst the larger data point spacing of long-term records means that post-earthquake pore pressure changes can be plotted. Referring to Figs. 9 to 15 again, at the bottom right of each set of time records appears the following information.

(a) G, the g-level.

(b) K_{in}, which is a control number associated with the testing apparatus. As it does not affect the interpretation of results, it will be ignored hereinafter.

(c) K_{out} is the earthquake strength measured by an accelerometer mounted on the container (hereafter designated as the reference

6.2 Test FHL01, Earthquake 8

Fig. 10 a shows the short-term time records of a 21% earthquake on the same model with the same surcharge. Again, the record of ACC 728 is very similar to that of ACC 1258 indicating that there is no slip between the base of the model and the concrete base. In fact, over the first $1^1/_2$ cycles of the earthquake, all acceleration records are very well-coupled to that of the base excitation. From the third to the fifth cycle, the phase difference between ACC 734 and ACC 1225 increases rapidly as illustrated in the Lissajous Diagrams in Figs. 17. It indicates a progressive softening of the soil beneath the surcharge. After the fifth cycle, the acceleration of ACC 734 dropped to a relatively low value as the surcharge is almost completely isolated from the base shaking motion.

This indicates that a drastic development has occurred. If the surcharge were, for example a barge resting on top of a prototype island with wells drilled down into the island for production of gas or oil, at this stage the risers could be sheared off because the barge would begin to slip to and fro relative to the top of the island.

Simultaneously, PPT 68 registered a steady excess pore pressure of 45 kPa, almost 1.5 times the average surcharge pressure on the crest. The soil at the crest is probably liquefied at this stage. PPT 2338 located off-centre at the crest show much lower pore pressure generation than PPT 68, indicating that pore pressure is not uniform across the crest and that only the region around the centreline may have liquefied. Even after liquefaction, ACC 1225 at the crest beneath the surcharge still registered fairly high accelerations. This may be due to the confining effects of the surrounding soil in the off-centre zones which has not liquefied. All this time, PPT 2331 located near the slope registered fairly low excess pore pressure.

In the long-term records of the same earthquake (Fig. 10b), all pore pressure transducers, with the exception of PPTs 2342 and 2332, measured monotonically decreasing pore pressures after the earthquakes. These two pore pressure transducers both were located at mid-height of the model and they highlight the significance of dissipation effects in causing pore pressure increase in regions around the liquefied zone. The delayed failure of the Lower San Fernando Dam in 1971 has been attributed to such dissipation effects (Seed, 1979).

6.3 Test FHL01, Earthquake 13

Figs. 11 shows the time records for earthquake 13 of strength 33% on the same model with the same surcharge viz. 10 mm steel plates. Instead of the liquefaction phenomenon described in the previous sub-section, ACC 734 measured fairly high acceleration indicating that there is little loss of shear strength in the soil beneath it. Furthermore, ACC 1244 experienced much higher acceleration peaks than that of the base input. PPTs 68, 2342 and 2331 now measured fairly large negative pore pressures for at least parts of the cycles. Only PPT 2332 showed a positive pore pressure response. As will be explained in Section 6.6, this drastic change from the liquefaction behaviour observed in earthquake 8 (see previous sub-

section) may be associated with intense shearing in parts of the model and the dilatancy induced by it.

6.4 Test FHL01, Earthquakes 17 and 24

Figs. 12 show the time records for earthquake 17 of strength 28% on the same model, but with thicker steel plates, viz. 20 mm. The average surcharge pressure on the crest is now estimated to be approximately 61 kPa. The increase in surcharge leads to positive pore pressure once again, although complete liquefaction of the kind observed during earthquake 8 did not occur. The trend indicated by this as well as earlier earthquakes is that successive earthquakes have caused progressive densification of the soil medium and generation of positive pore pressures, resulting in a material which dilates at large earthquakes. Increasing the overburden pressure once again resulted in the model exhibiting positive pore pressure response. The consistency of this trend is seen again for earthquake 24, a 36% earthquake on the same model and same surcharge, in Figs. 13. PPTs 68, 2342 and 2331 show large negative pore pressure response indicative of dilatancy. Furthermore ACC 1244 experienced high acceleration amplification relative to the base with strong high frequency component. The effect of seismic history on the behaviour of models in successive earthquakes is a striking feature of these centrifuge test results.

6.5 Test FHL02, Earthquake 14

Test FHL02 was performed with a model with approximately the same cross- section as test FHL01 but with transducers sited at different locations. Figs. 14 show the time record of earthquake 14, a 28% earthquake, on this model with 20 mm steel plates as surcharge. ACC 1244 on the surcharge again exhibited rapid attenuation of acceleration after the fourth cycle of the earthquake, whilst PPT 2338 located centrally beneath the surcharge registered a high steady excess pore pressure of 78 kPa during the earthquake. PPTs 68, 2335, 2252 and 2331 are all located off-centre along the crest and mid-height of the model. The long-term records of these four pore pressure transducers in Fig. 14 b shows increasing pore pressures after the earthquake as pore fluid drained outwards from the liquefied zone near the centreline towards the free-draining boundaries, that is, the slopes. The similarities between the observations in this earthquake and the liquefaction behaviour for earthquake 8 in Test FHL01 discussed in Section 6.2 is further strong evidence that liquefaction can be modelled on a centrifuge.

6.6 Test FHL02, Earthquake 18

Earthquake 18, a 37% strong earthquake was applied to the same model and surcharge as that discussed in the previous section. In the short-term time records in Fig. 15, significant amplification in acceleration was observed in ACC 734 located centrally beneath the surcharge. In addition, sharp 'spiky' acceleration pulses with absolute values about 3 to 4 times that of the base excitation were observed in ACCs 728 and 988 located at the shoulders of the model. These spikes occurred in alternating half-cycles and their appearance in the two accelerometer records are out-of-phase, suggesting very strongly an asymmetric

phenomenon. In later tests not reported here, the phenomenon was again consistently observed near the shoulders of the model. Such spikes would be consistent with a jerky motion, with gradual acceleration phases alternating with rapid deceleration phases, leading to large permanent deformation if the acceleration phases occupied a larger part of each cycle than the deceleration phase. There is evidence for such movements having taken place. Fig. 18 shows photographs taken of one slope before and after the test. Substantial bending of the blue sand grid was seen, indicating that intense shearing had taken place in the upper slopes and the shoulders during the experiments.

7. Conclusions

(a) Dynamic modelling using the Bumpy Road Facility has provided novel data for studying mechanisms which are active in a submerged embankment or sand island in an earthquake.

(b) Two such mechanisms can be readily identified.

(i) Positive pore pressure generation in a central zone at the crest, resulting in the extreme case, liquefaction and loss of shearing resistance in the soil beneath the surcharge. Pore pressure dissipation takes place outwards and towards the slopes.

(ii) High acceleration peaks attributed to intense shearing at the upper slopes and shoulders during strong earthquakes.

(c) Data of successive earthquakes on models show a striking influence of seismic history in the response of the models.

(d) Developments of techniques of modelling and of data processing are now progressing rapidly. An improved method of model construction has recently been developed. Briefly, this consists of constructing the model in a dry state, evacuating the air in the model under a vacuum and then using this vacuum to draw in the silicone oil. So far, the results indicate that it has been quite successful and these will be reported in a later paper. Work is now underway to investigate the three-dimensional response of circular islands under similar base shaking excitation.

8. References

Cottril, A. (1981). North American Arctic Review, Offshore Engineer, August, pp 8 - 17.

Dean, E.T.R. (1981). Aspects of Earthquake Effects on Model Embankment Dams, M. Phil. Thesis, Cambridge University.

Dean, E.T.R. (1983). Private communication.

Dean, E.T.R. and Schofield, A.N. (1983). Two Centrifuge Model Tests: Earthquakes on Submerged Embankments, Proc. Atti Del XV Convegno Nazionale

Di Geotechnica, Spoleto, pp 115 - 129.

Haag, J. (1962). Oscillatory Motions, Belmont, Wadsworth.

Ishihara, K., Shimizu, K. and Yamada, Y. (1981). Pore Water Pressures Measured in Sand Deposits During an Earthquake, Soils and Foundations, Vol. 21, No. 4, pp 85 - 100.

Kutter, B.L. (1982). Centrifugal Modelling of the Response of Clay Embankments to Earthquakes, Ph.D. Thesis, Cambridge University.

Lambe, T.W. and Whitman, R.V. (1969). Soil Mechanics, New York, John Wiley & Sons.

Lee, F.H. (1983). Partial Liquefaction in a Centrifuge Model Embankment in an Earthquake, M.Phil. Thesis, Cambridge University.

Muskat, M. (1946). The Flow of Homogeneous Fluids Through Porous Media, J.W. Edwards, Ann Arbor, Michigan.

Newmark, N.M. and Rosenblueth, E. (1971). Fundamentals of Earthquake Engineering, Prentice-Hall, N.J.

Schofield, A.N. (1981). Dynamic and Earthquake Geotechnical Centrifuge Modelling, Proc. Int. Conf. Recent Advances Geotech. Earthquake Engng. Soil Dyn., Vol. 3, St. Louis, pp 1081 - 1100.

Schofield, A.N. and Venter, K. (1984). Earthquake Induced Pore Pressures in the Foundation of a Sea Dyke, Presented at the International Symposium on, Geotechnical Centrifuge Model Testing in Tokyo, April 3 - 5.

Seed, H.B. (1979). Earthquake Resistant Design of Earth and Rockfill Dams, Nineteenth Rankine Lecture, Geotechnique, Vol. 29, No. 3, pp 213 - 263.

Terzaghi, K. and Peck, R.B. (1967). Soil Mechanics in Engineering Practice, 2nd Edition, New York, John Wiley & Sons.

Figure 1 Diagram of an artificial island (Cottril, 1981).

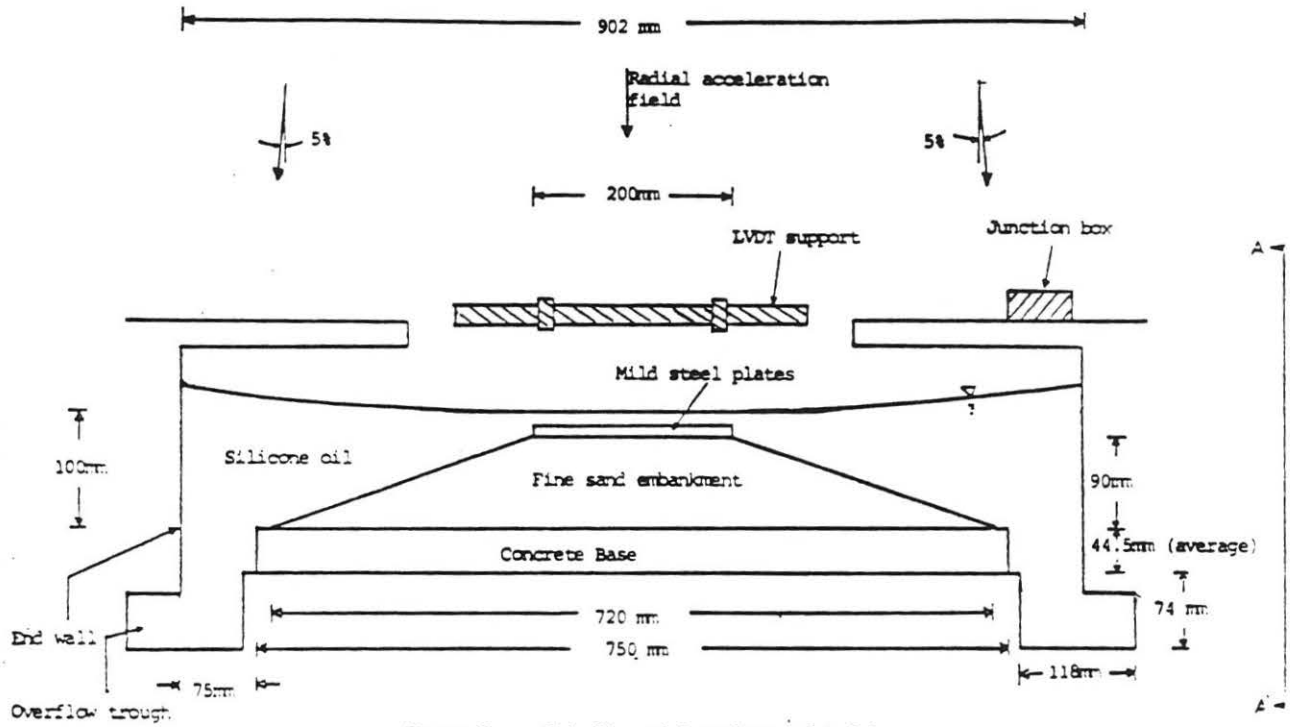

Figure 2 a Side View of Container and Model

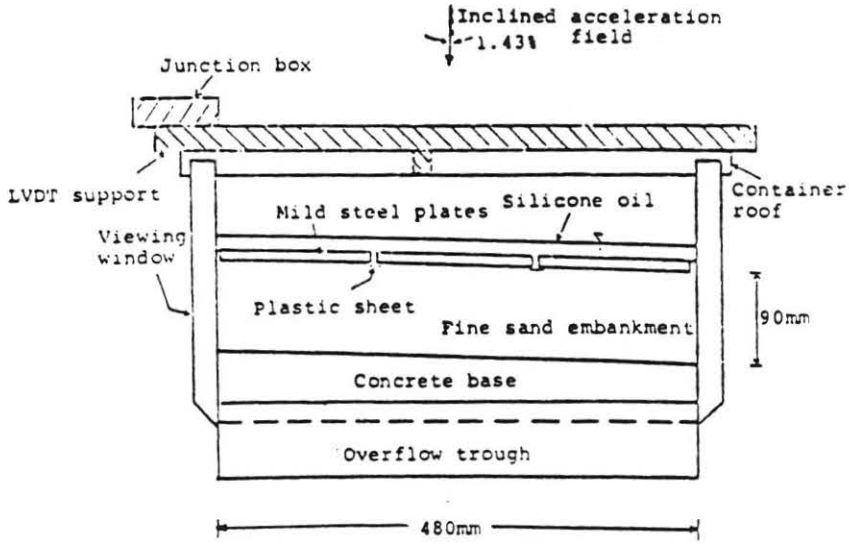

Figure 2 b End View of package(AA')

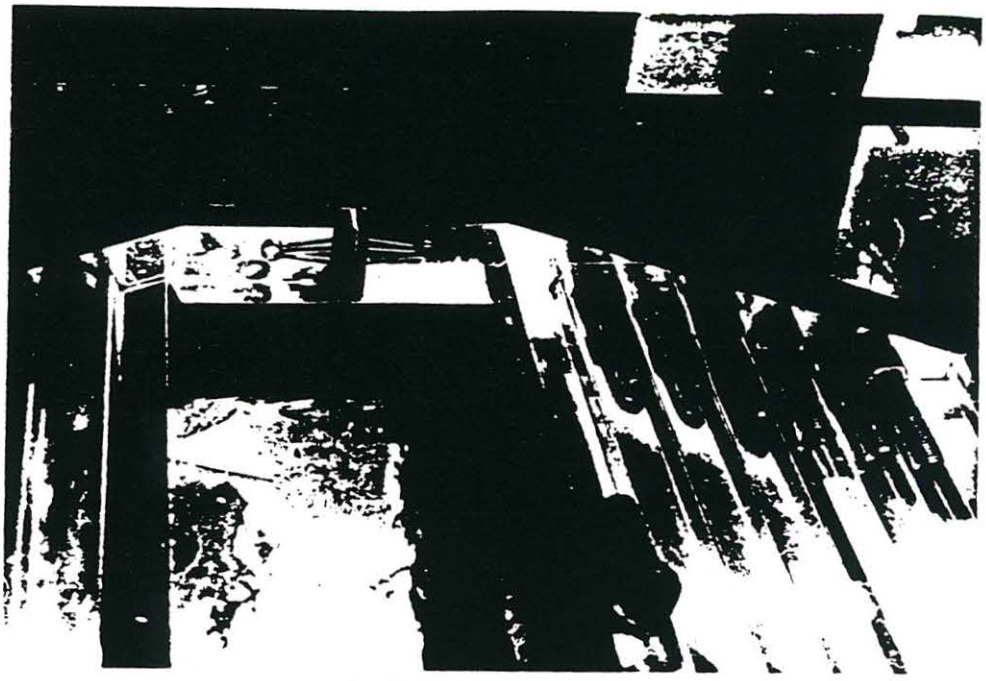

Figure 3 Embankment formworks showing trapezoidal arch and U-section beams.

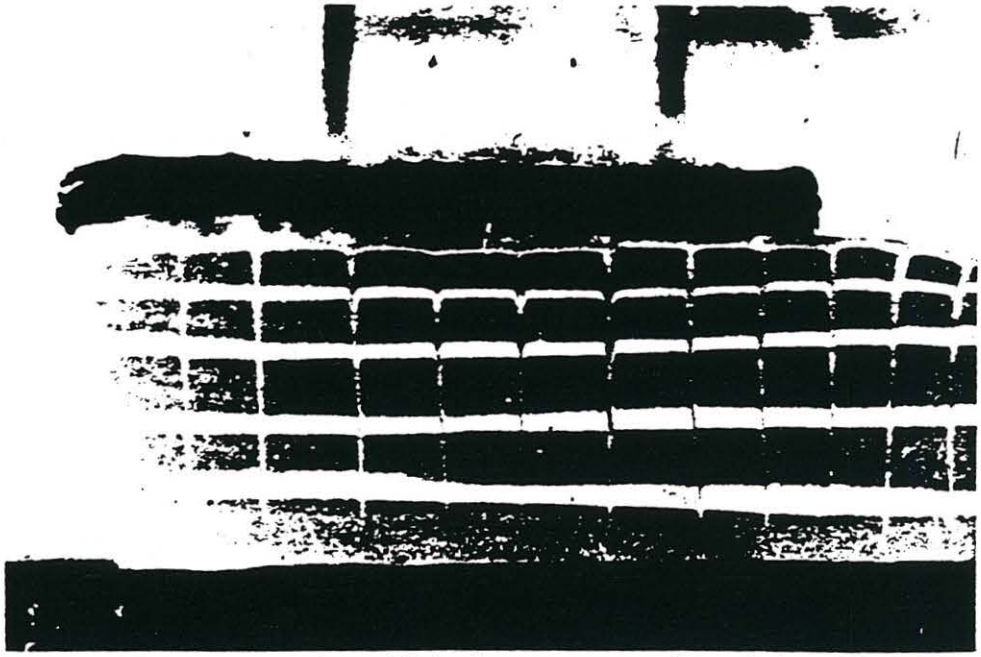

Figure 4 Blue sand grid below crest of model. The surcharge can also be seen (This is a negative).

All acceleration records are plotted from raw data.

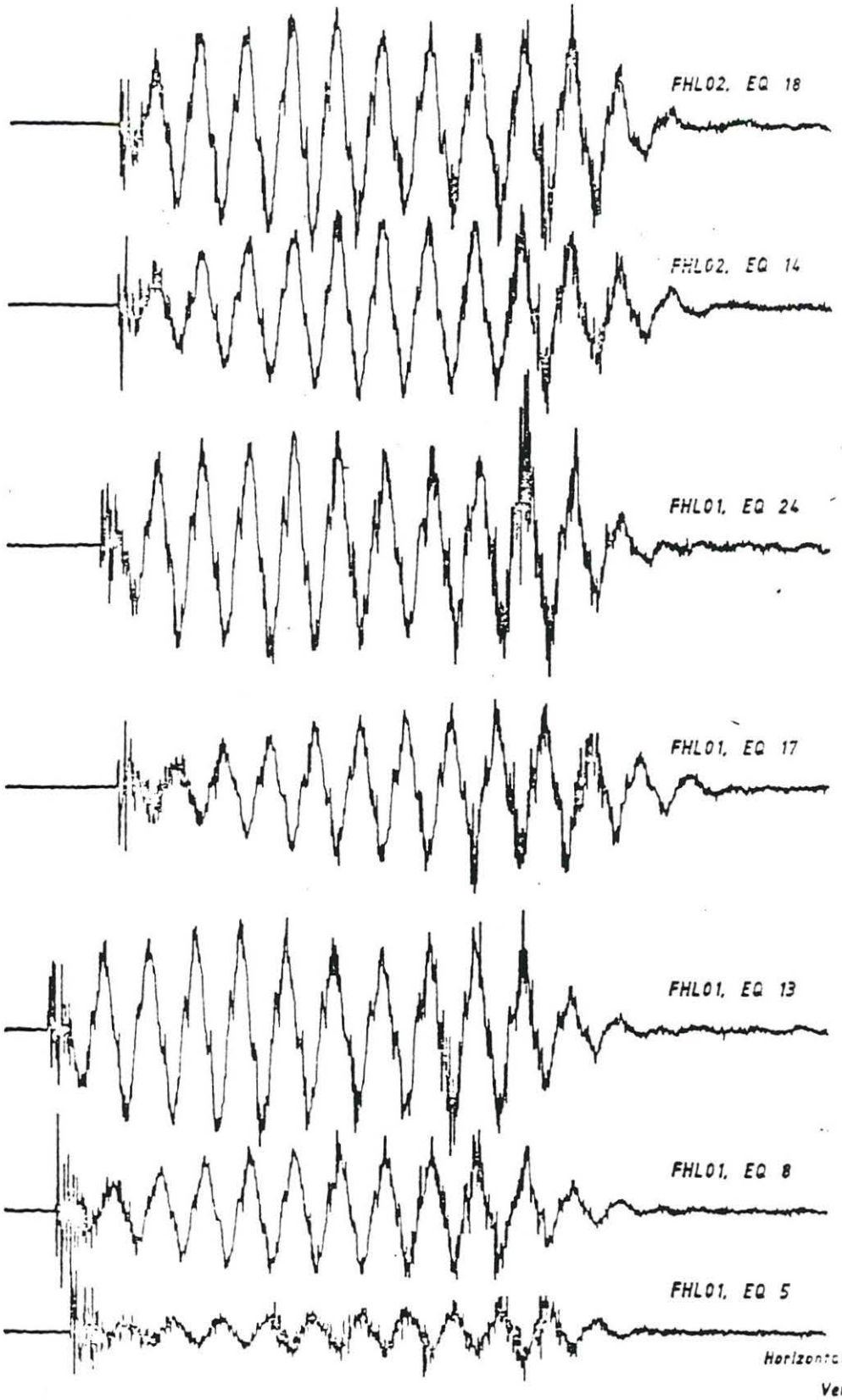

FHL01/02	TYPICAL EARTHQUAKES RECORDS	FIG. NO. 5

Velocity spectra plotted from raw digitised data.

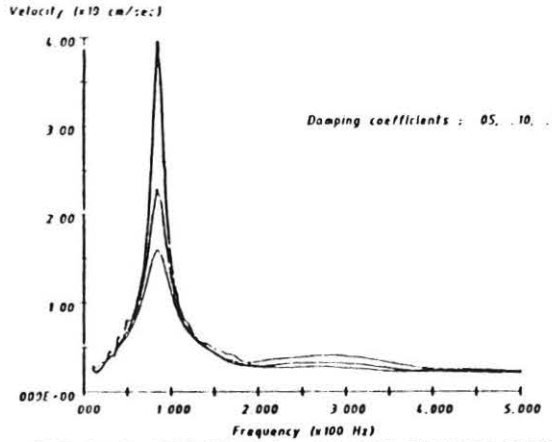

TEST FHL01, EARTHQUAKE 5 - VELOCITY RESPONSE SPECTRA

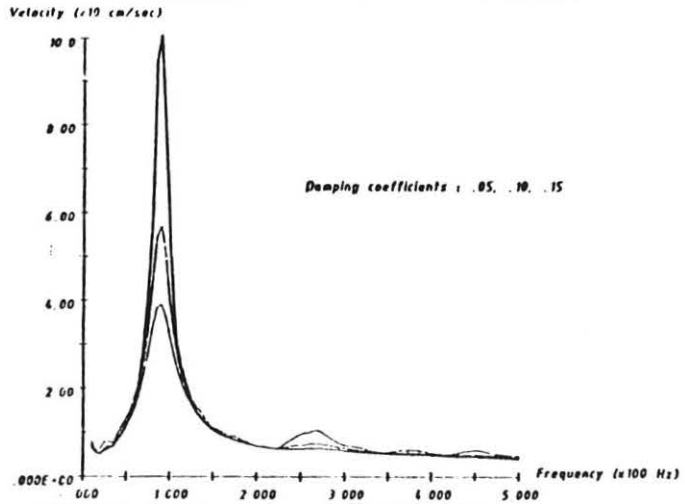

TEST FHL01, EARTHQUAKE 8 - VELOCITY RESPONSE SPECTRA

FHL01	EARTHQUAKE RESPONSE SPECTRA	FIG NO 6a

Velocity spectra plotted from raw digitised data.

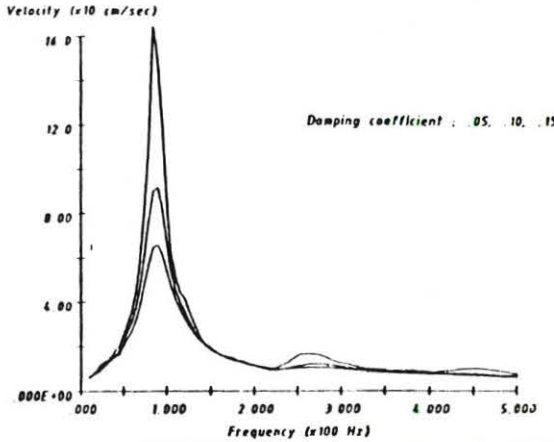

TEST FHL01, EARTHQUAKE 13 - VELOCITY RESPONSE SPECTRA

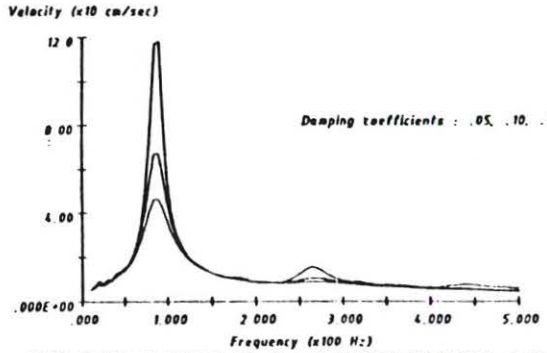

TEST FHL01, EARTHQUAKE 17 - VELOCITY RESPONSE SPECTRA

FHL01	EARTHQUAKE RESPONSE SPECTRA	FIG NO 6b

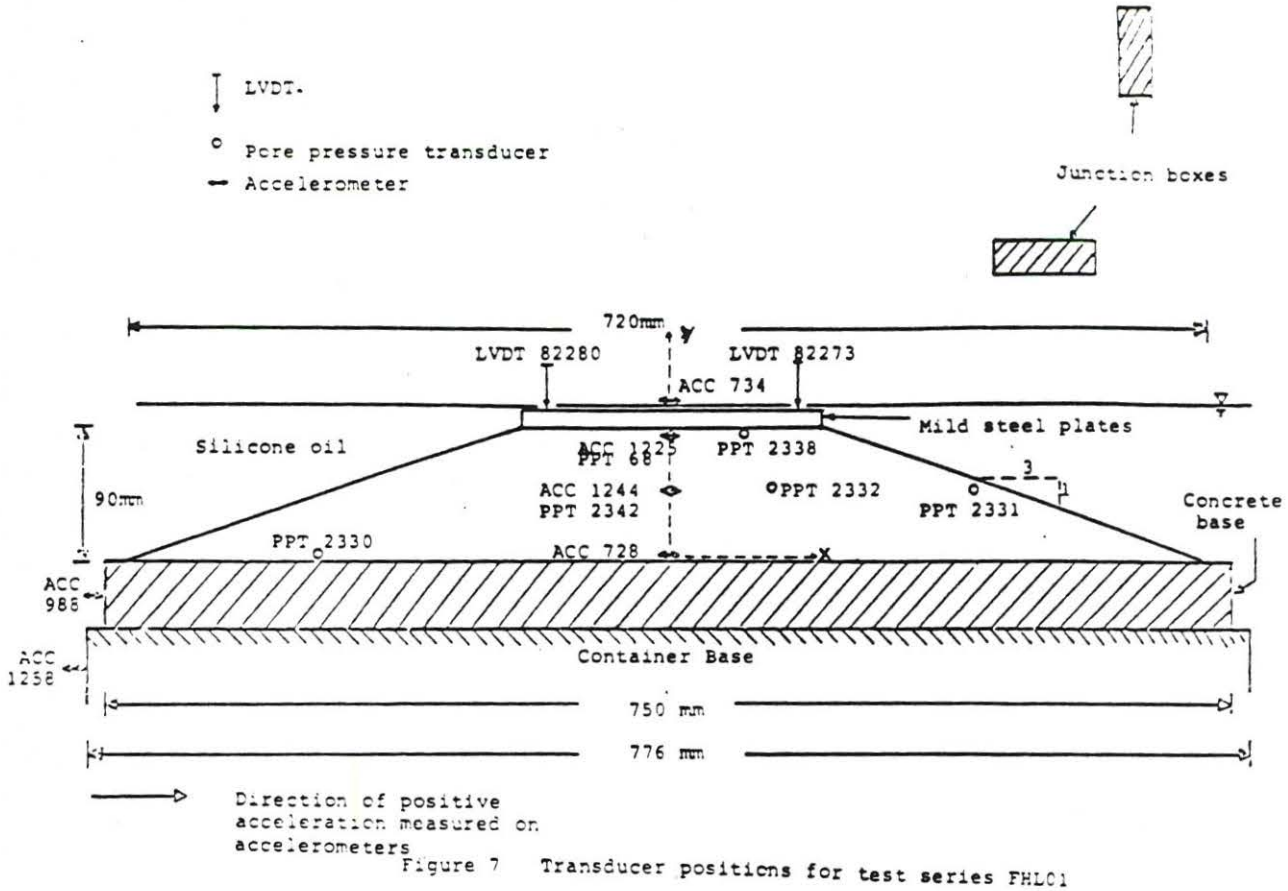

Figure 7 Transducer positions for test series FHL01

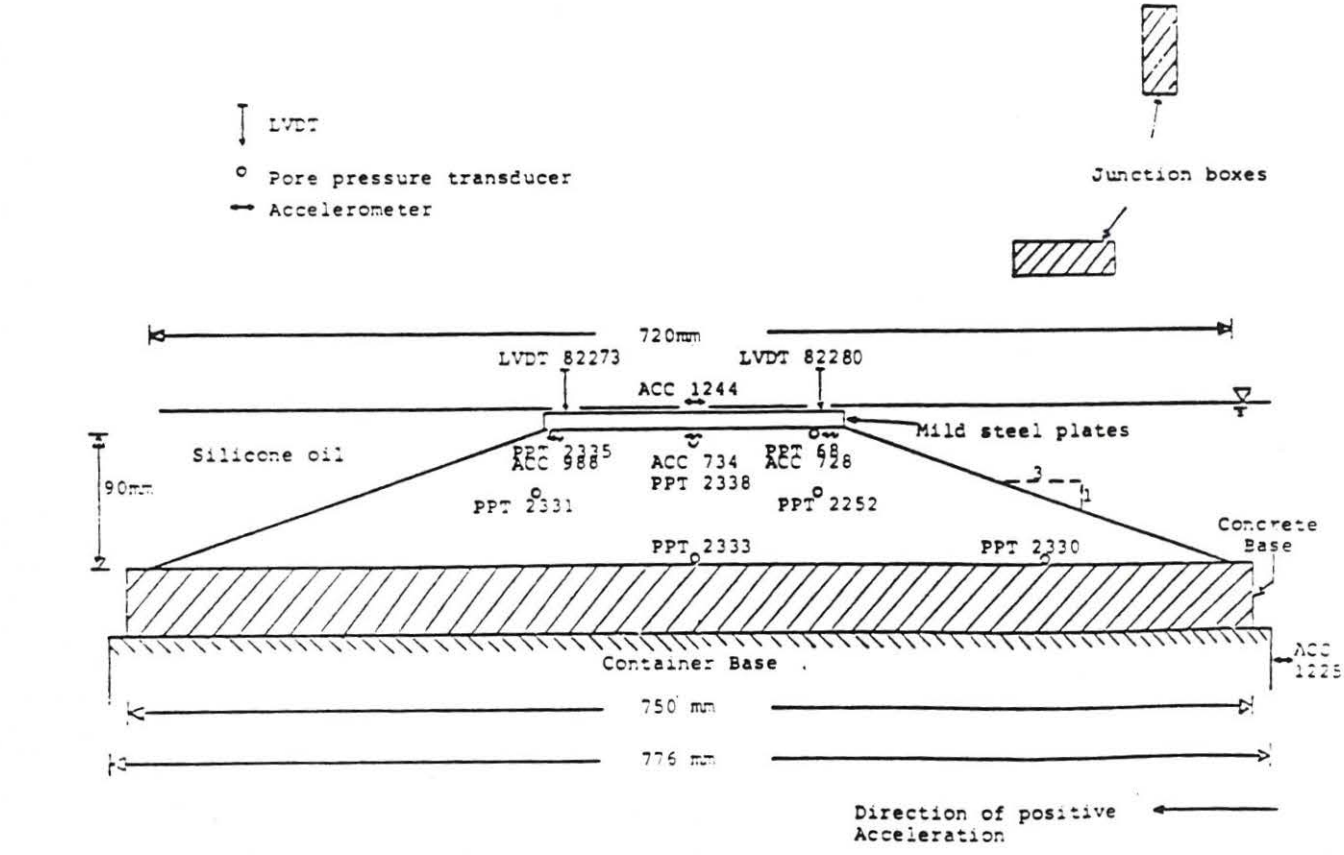

Figure 8 Transducer positions for test series FHL02

1024 data points per transducer, plotted after 1 smoothing pass

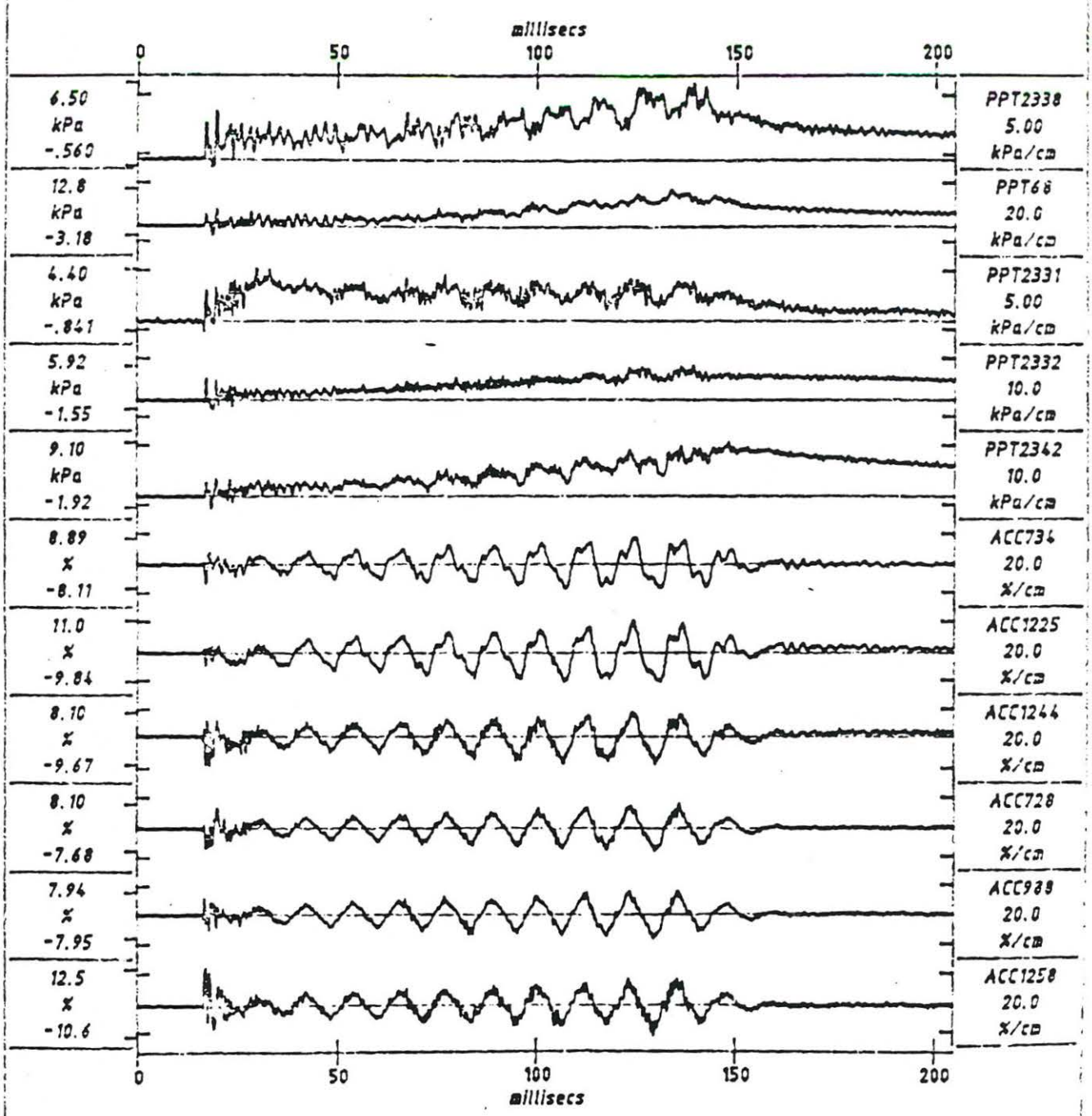

Scales : model

TEST FHL01B MODEL SE01S2 FLIGHT 2	EQ5	SHORT-TERM TIME RECORDS	G = 40.2g Kin = 2.01% Kout = 11.6%	FIG. NO. 9a

1024 data points per transducer, plotted after 1 smoothing pass

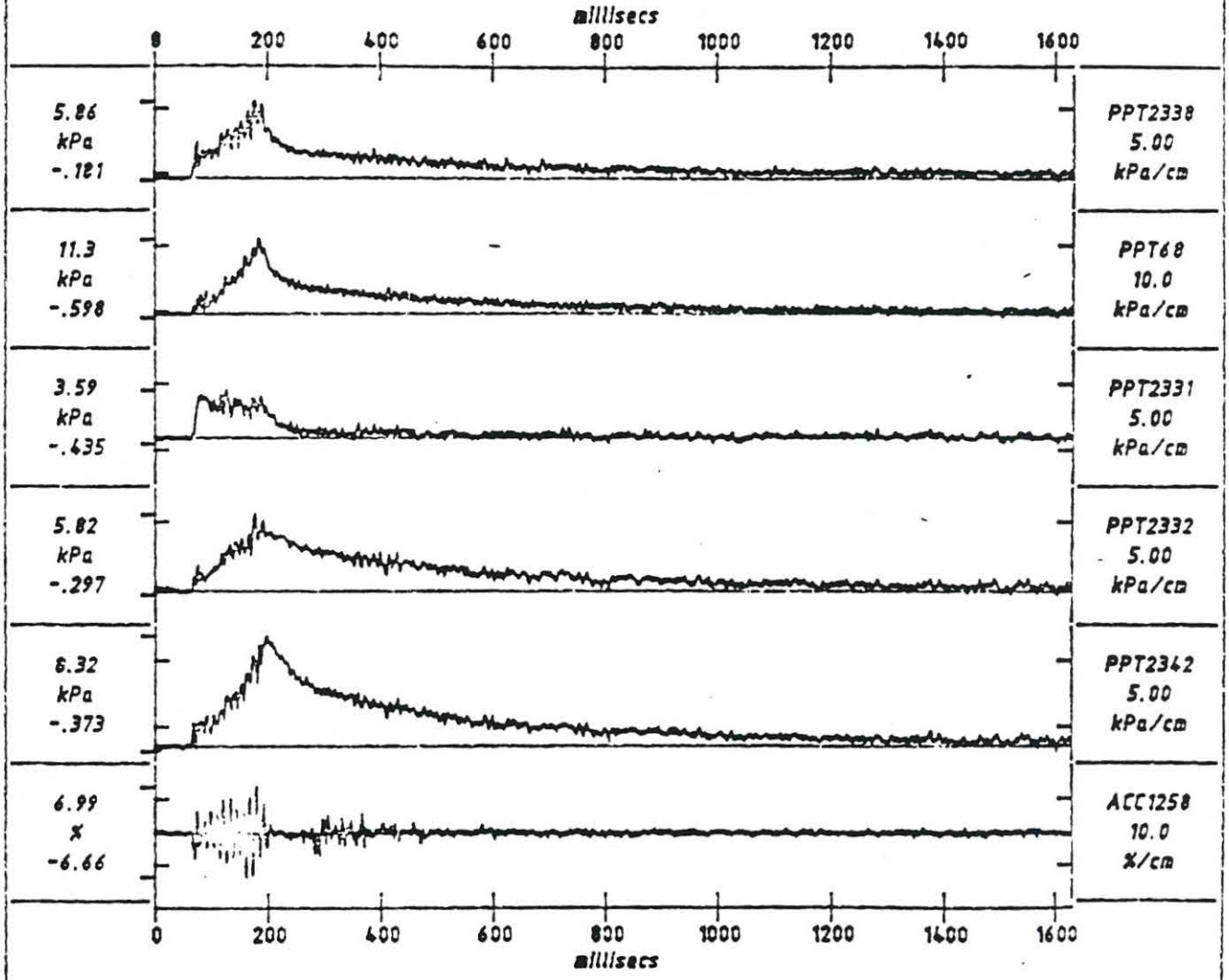

Scales : model

TEST FHL01B MODEL SE01S2 FLIGHT 2	EQ5	LONG-TERM TIME RECORDS	G = 39.4g Kin = 2.01% Kout = 6.83%	FIG. NO. 9b

1024 data points per transducer, plotted after 1 smoothing pass

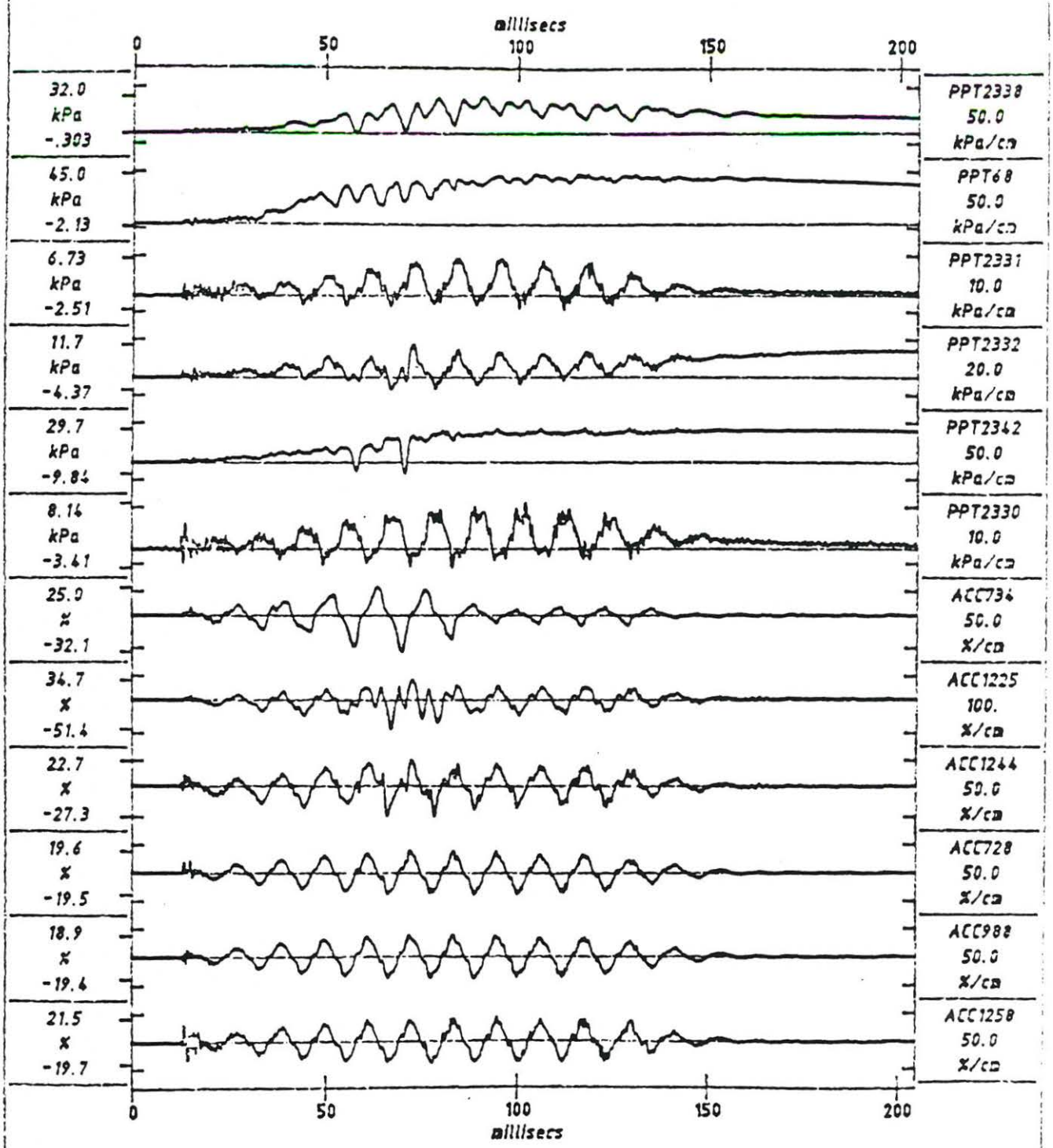

Scales : model

TEST FHL018 MODEL SE01S2 FLIGHT 2	EQ8	SHORT-TERM TIME RECORDS	G = 40.2g Kin = 3.54% Kout = 20.6%	FIG. NO. 10a

1024 data points per transducer, plotted after 1 smoothing pass

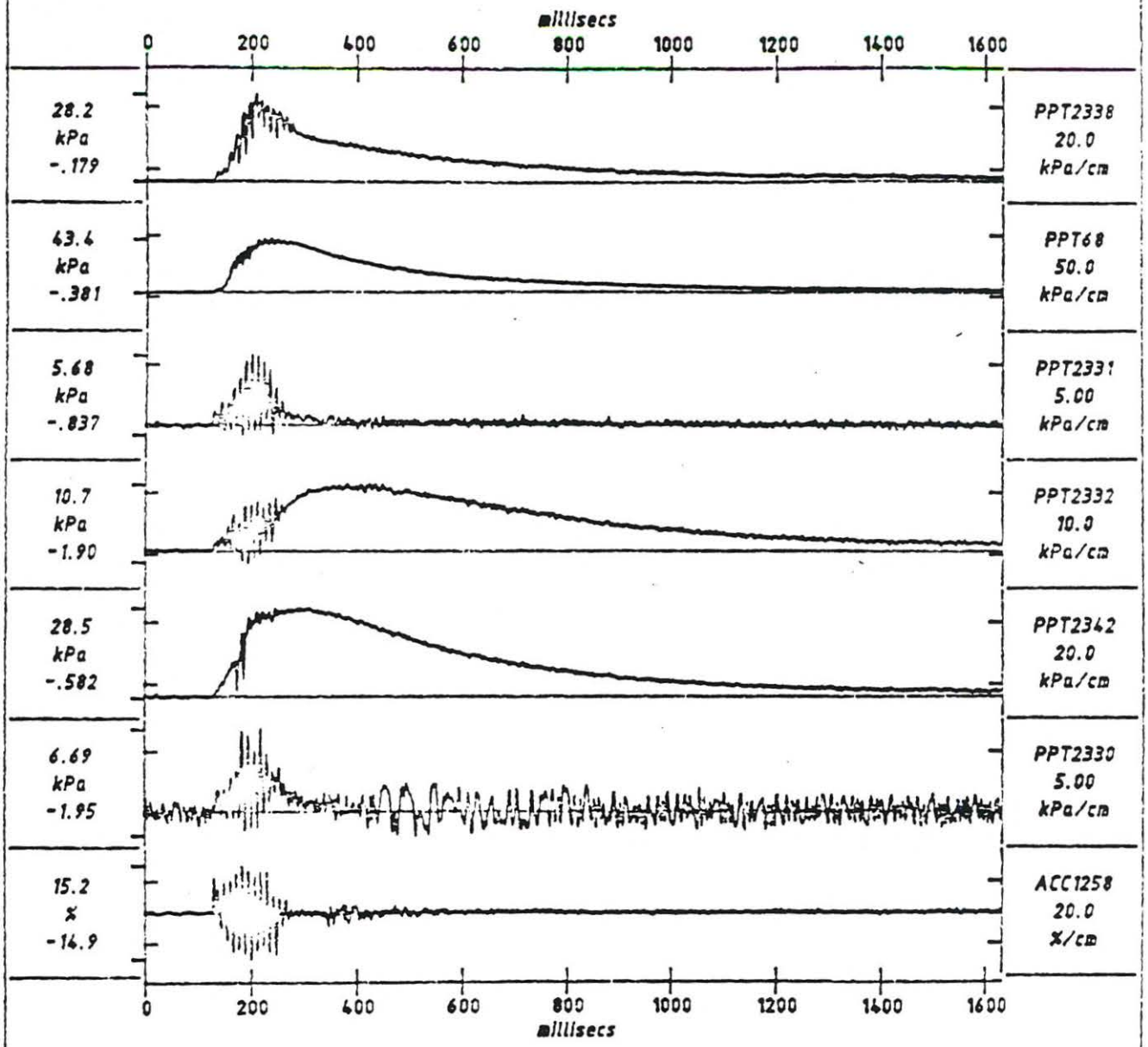

Scales : model

TEST FHL01B MODEL SE01S2 FLIGHT 2	EQ8	LONG-TERM TIME RECORDS	G = 39.4g Kin = 3.54% Kout = 15.1%	FIG. NO. 10b

1024 data points per transducer, plotted after 1 smoothing pass

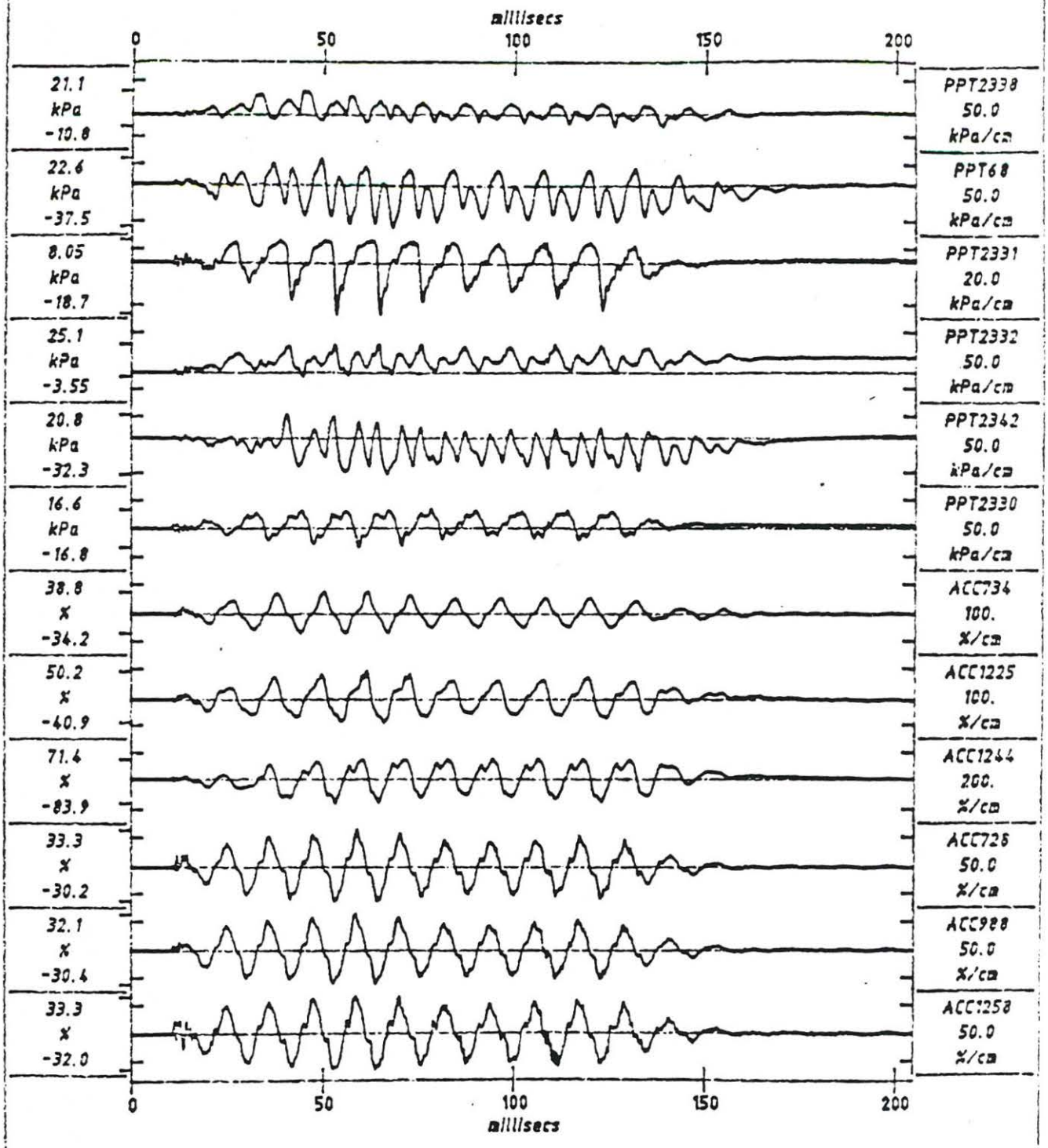

Scales : model

TEST FHL01B MODEL SE01S2 FLIGHT 3	EQ 13	SHORT-TERM TIME RECORDS	G = 40.2g Kin = 6.95% Kout = 32.7%	FIG. NO. 11a

1024 data points per transducer, plotted after 1 smoothing pass

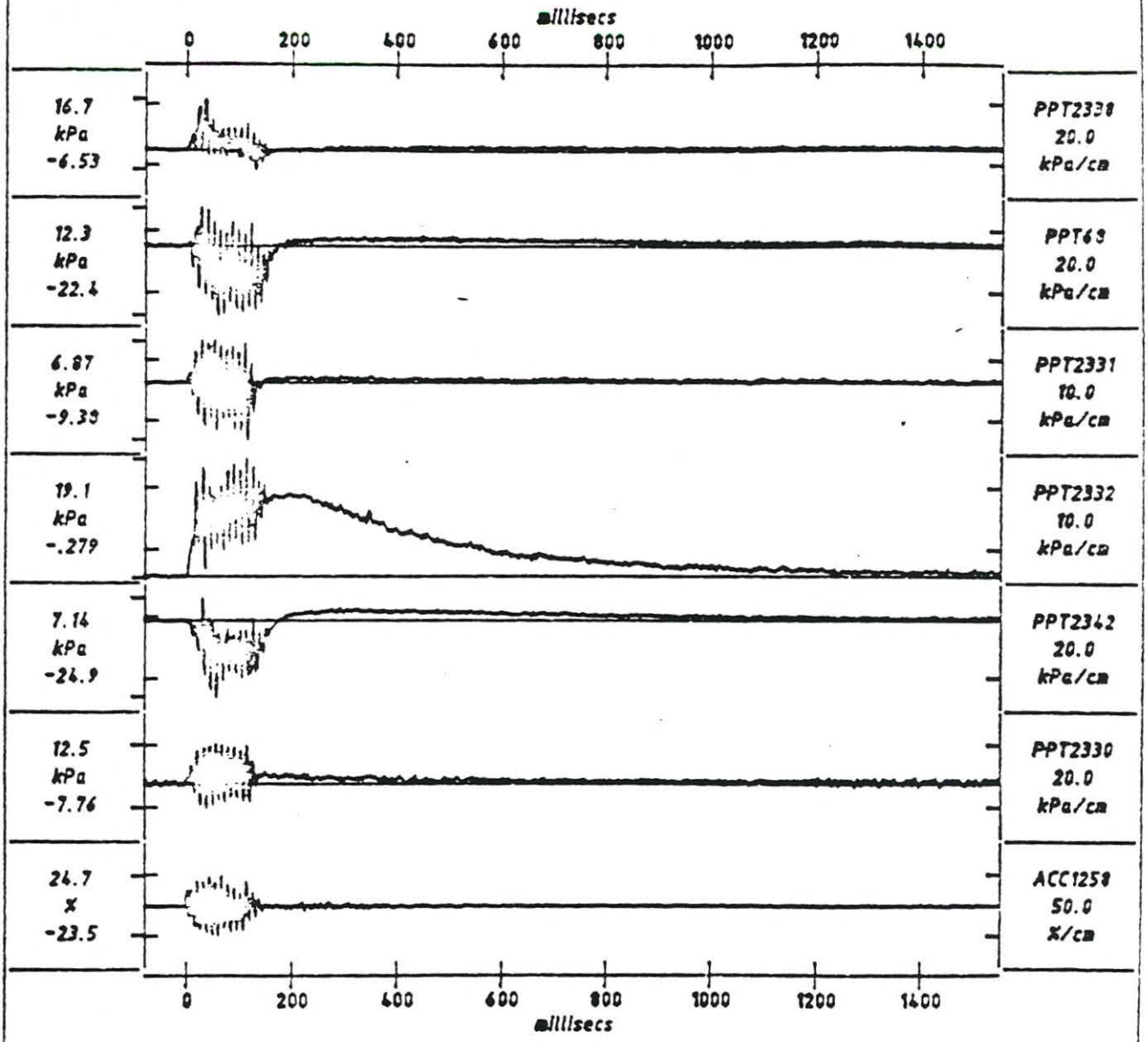

Scales : model

TEST FHL01B MODEL SE01S2 FLIGHT 3	EQ 13	LONG-TERM TIME RECORDS	G = 39.4g Kin = 6.95% Kout = 24.1%	FIG. NO. 11b

1024 data points per transducer, plotted after 1 smoothing pass

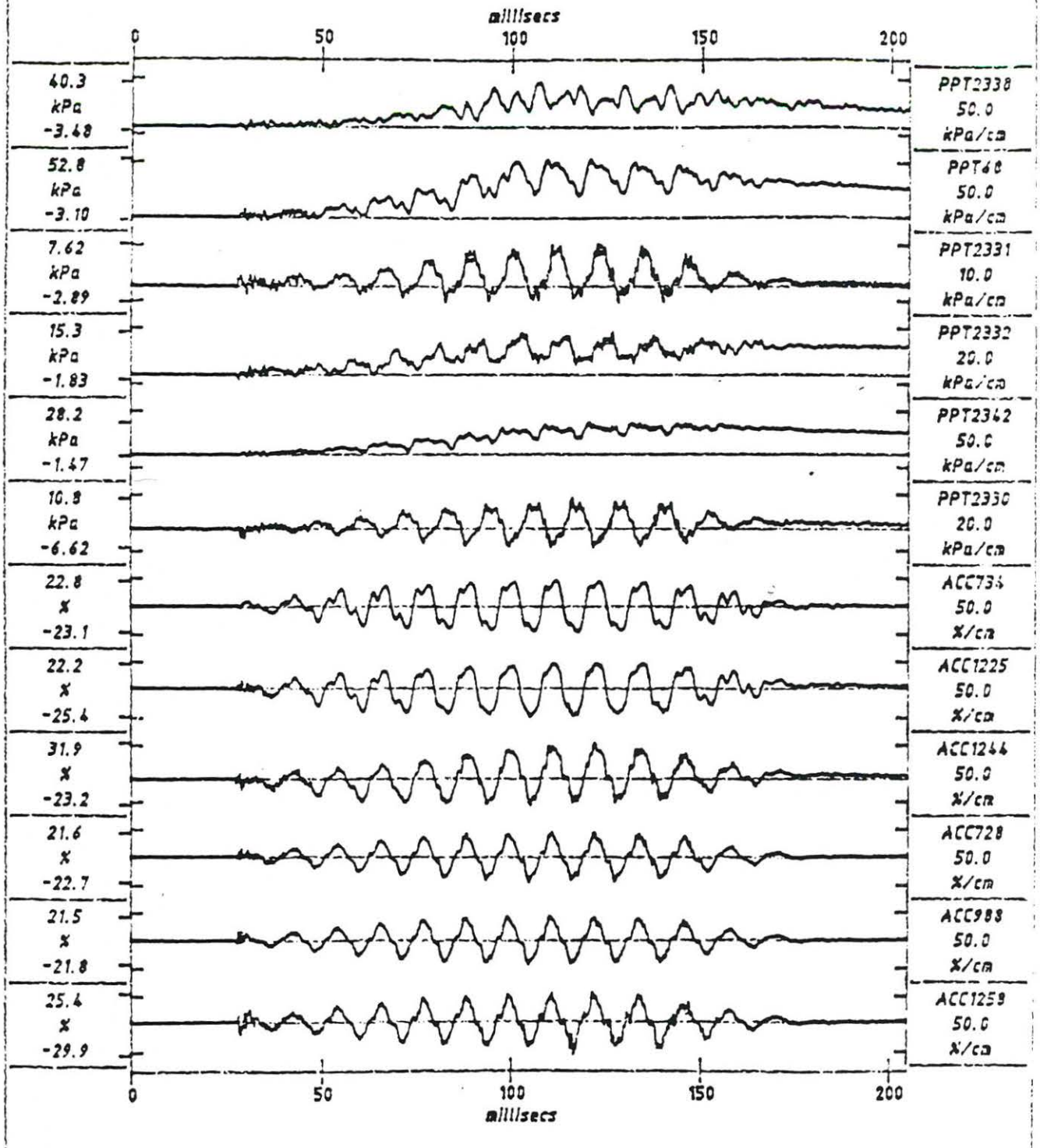

Scales : model

TEST FHL01C MODEL SE01S3 FLIGHT 4	EQ 17	SHORT-TERM TIME RECORDS	G = 40.2g Kin = 3.53% Kout = 27.6%	FIG. NO. 12a

1024 data points per transducer, plotted after 1 smoothing pass

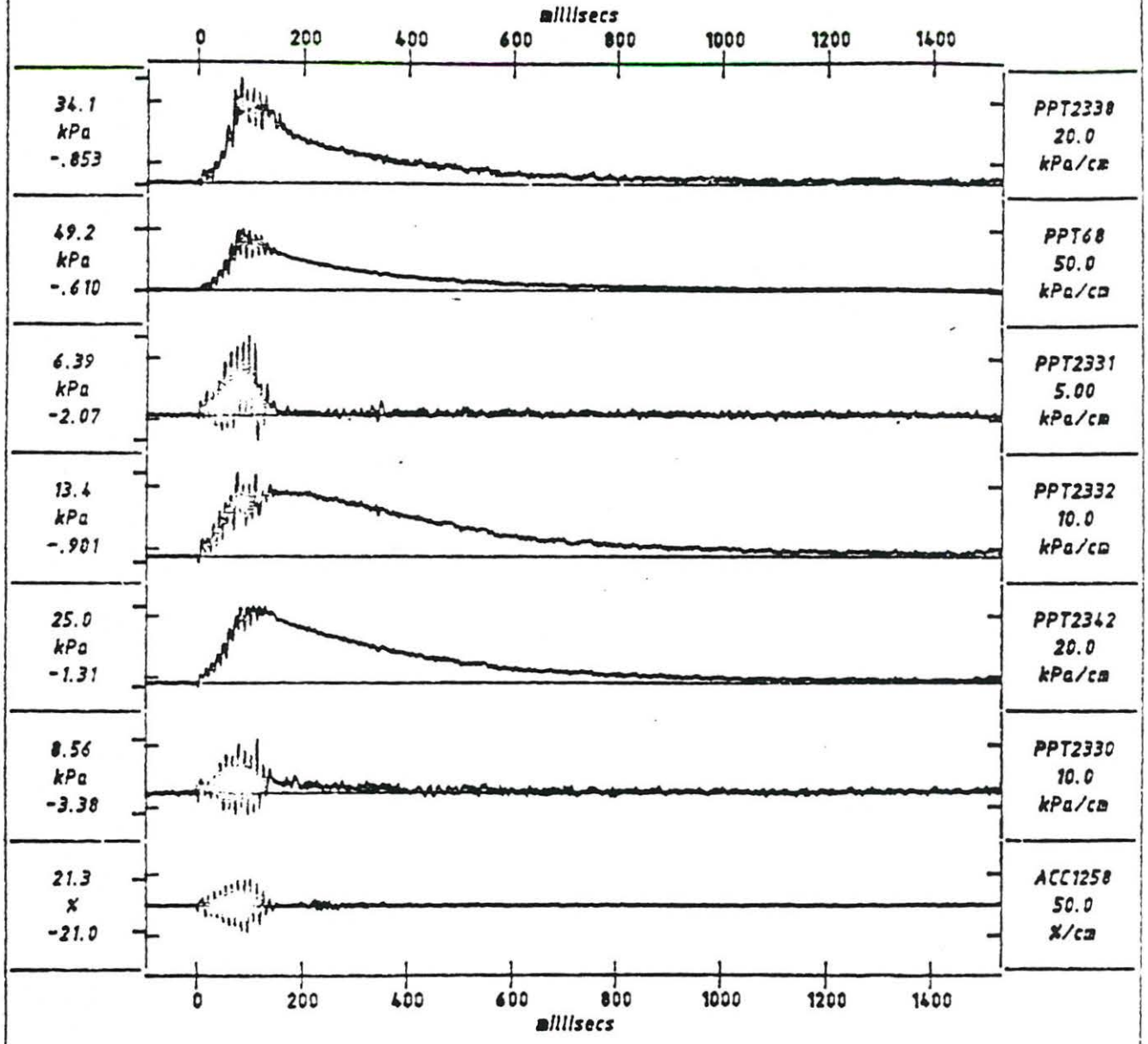

Scales : model

TEST FHL01C MODEL SE01S3 FLIGHT 4	EQ 17	LONG-TERM TIME RECORDS	G = 39.4g Kin = 3.53% Kout = 21.1%	FIG. NO. 12b

1024 data points per transducer, plotted after 1 smoothing pass

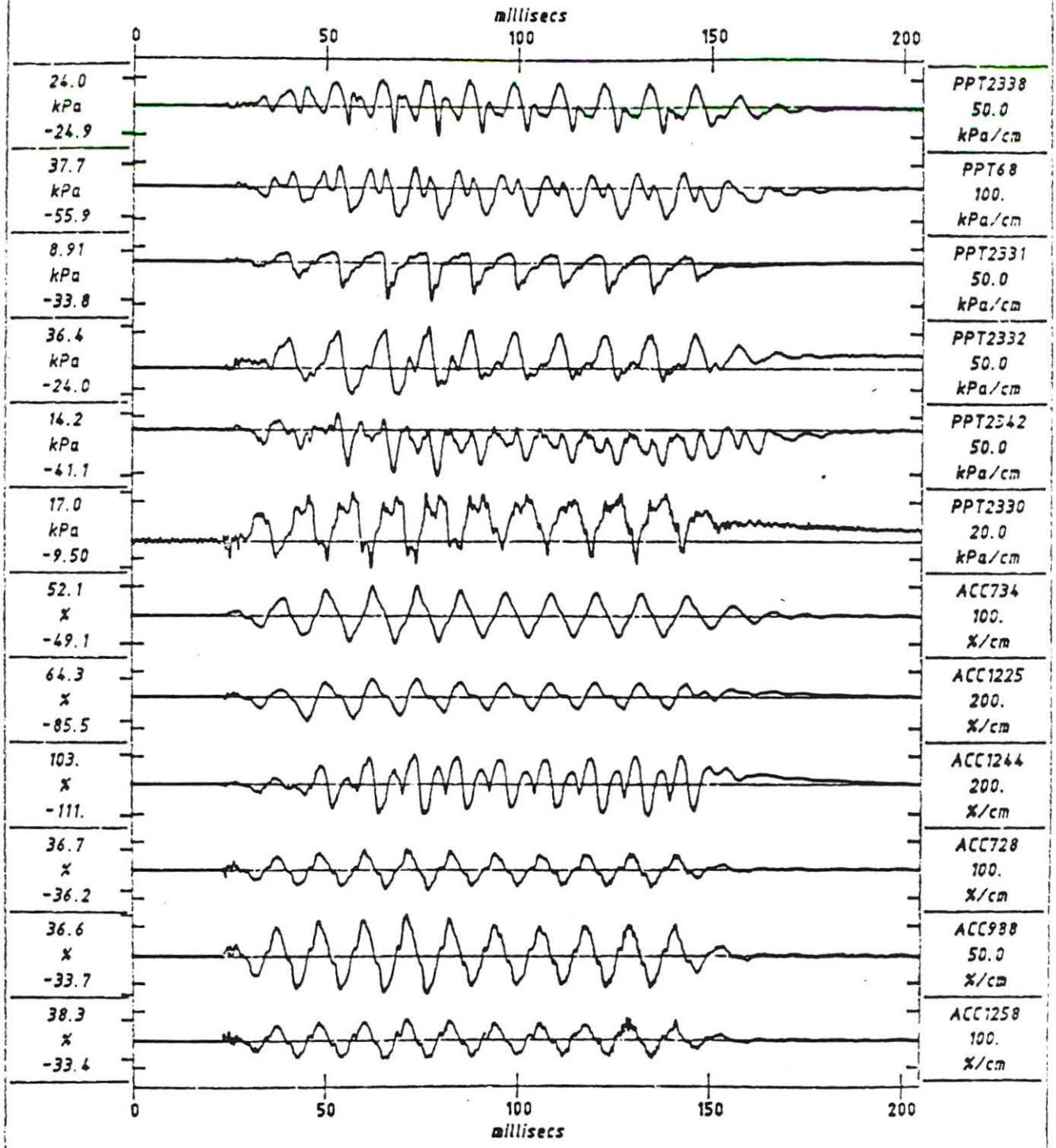

Scales : model

TEST FHL01C MODEL SE01S3 FLIGHT 5	EQ24	SHORT-TERM TIME RECORDS	G = 40.2g Kin = 7.98% Kout = 35.8%	FIG. NO. 13a

1024 data points per transducer, plotted after 1 smoothing pass

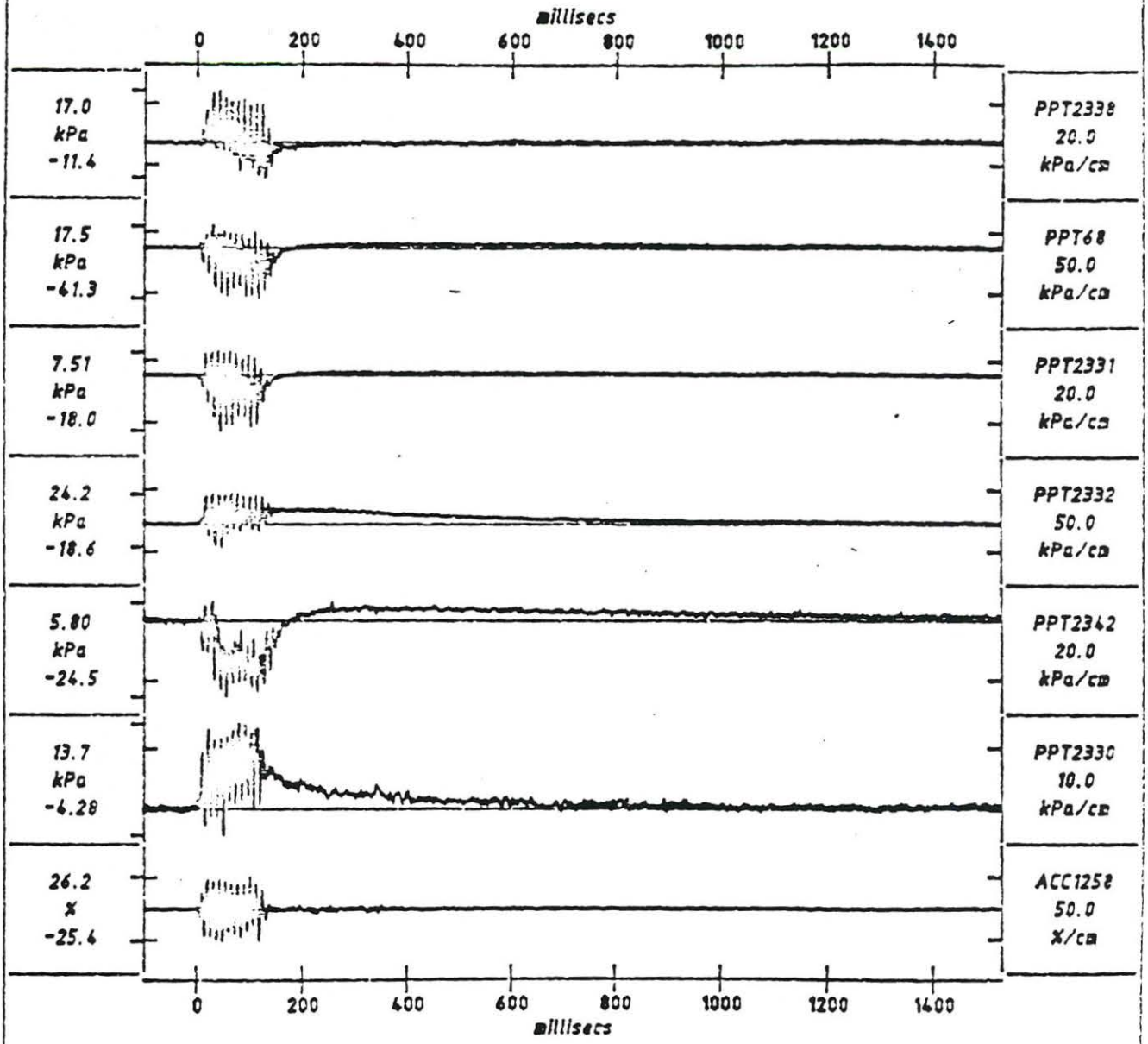

Scales : model

TEST FHL01C MODEL SE01S3 FLIGHT 5	EQ24	LONG-TERM TIME RECORDS	G = 39.4g Kin = 7.98% Kout = 25.8%	FIG. NO. 13b

1024 data points per transducer, plotted after 1 smoothing pass

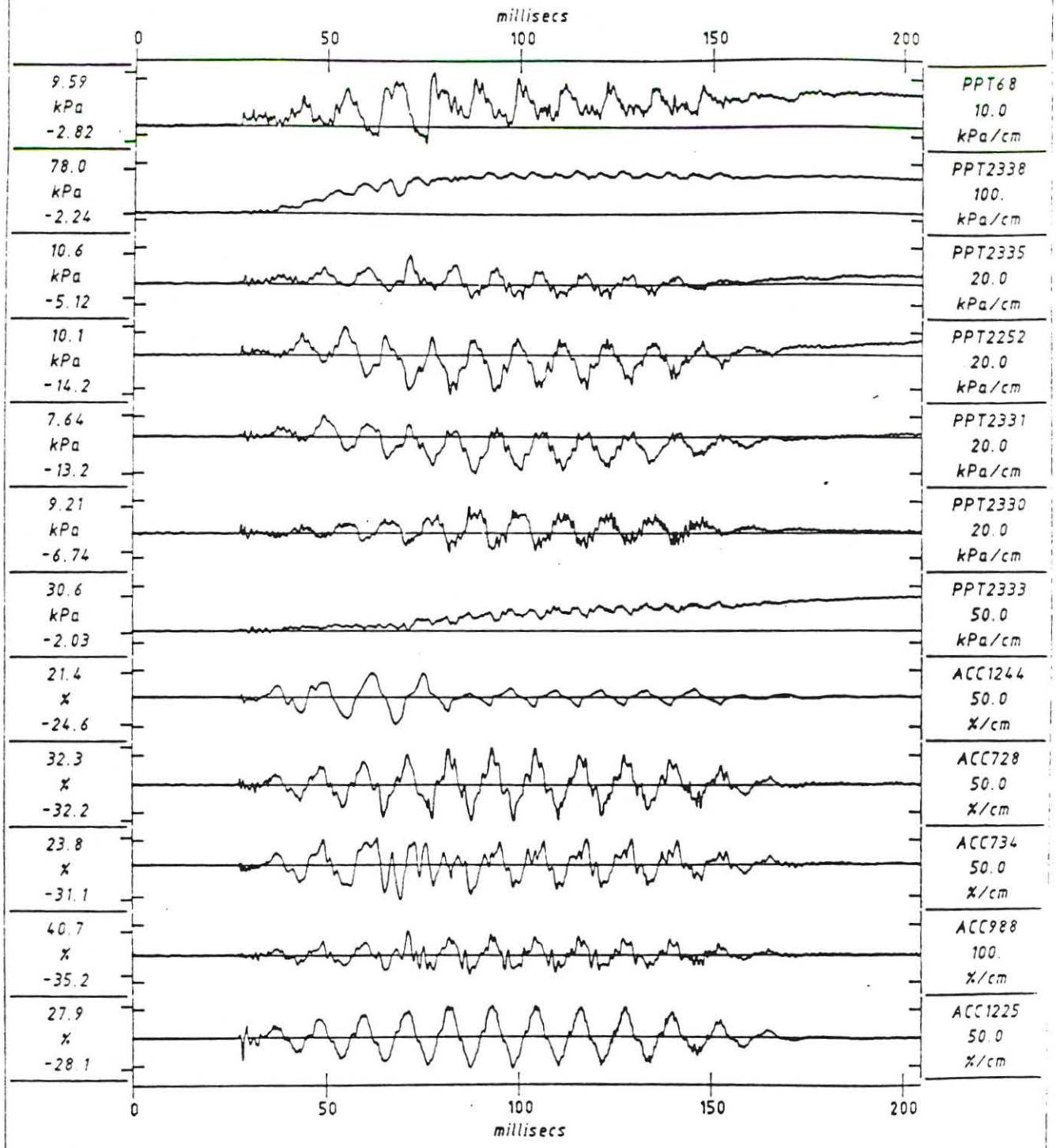

Scales : model

TEST FHL02C MODEL SE02S3 FLIGHT 3	EQ 14	SHORT-TERM TIME RECORDS	G = 39.4g Kin = 4.56% Kout = 28.0%	FIG NO. 14a

1024 data points per transducer, plotted after 1 smoothing pass

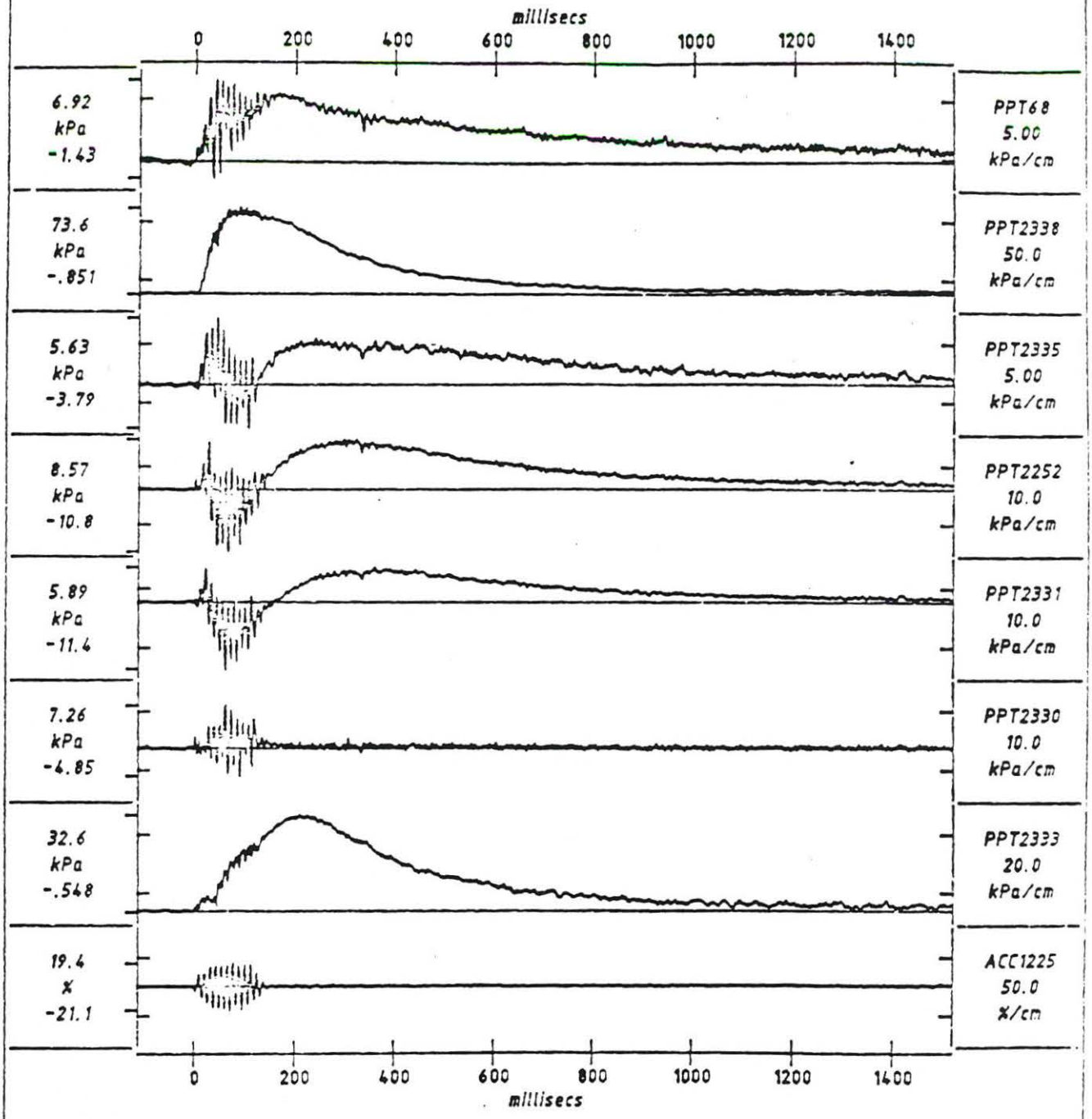

Scales : model

TEST FHL02C MODEL SE02S3 FLIGHT 3	EQ 14	LONG-TERM TIME RECORDS	G = 39.4g Kin = 4.56% Kout = 20.3%	FIG. NO. 14b

1024 data points per transducer, plotted after 1 smoothing pass

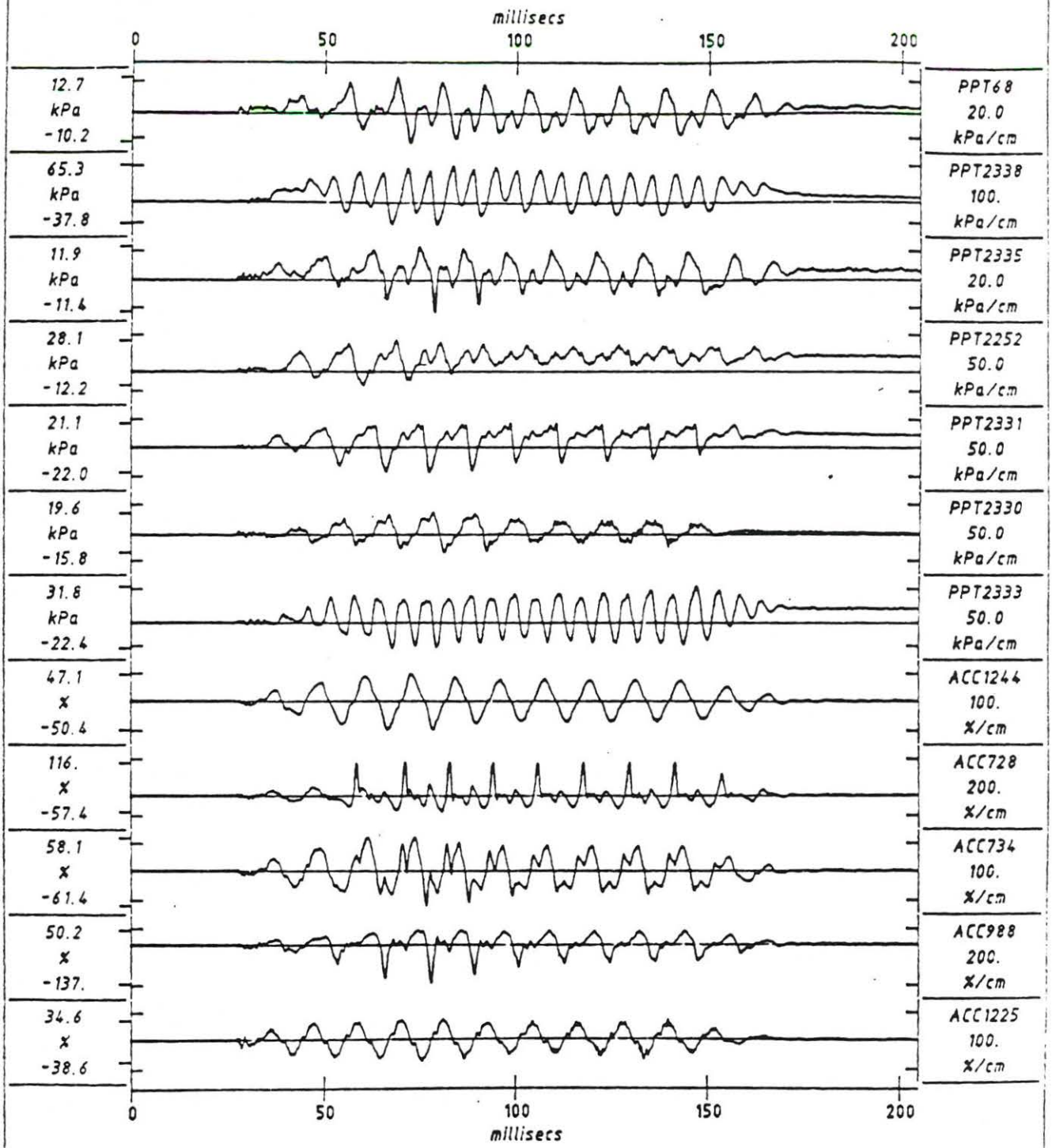

Scales : model

TEST FHL02C MODEL SE02S3 FLIGHT 3	EQ 18	SHORT-TERM TIME RECORDS	G = 39.4g Kin = 7.07% Kout = 36.6%	FIG. NO. 15a

1024 data points per transducer, plotted after 1 smoothing pass

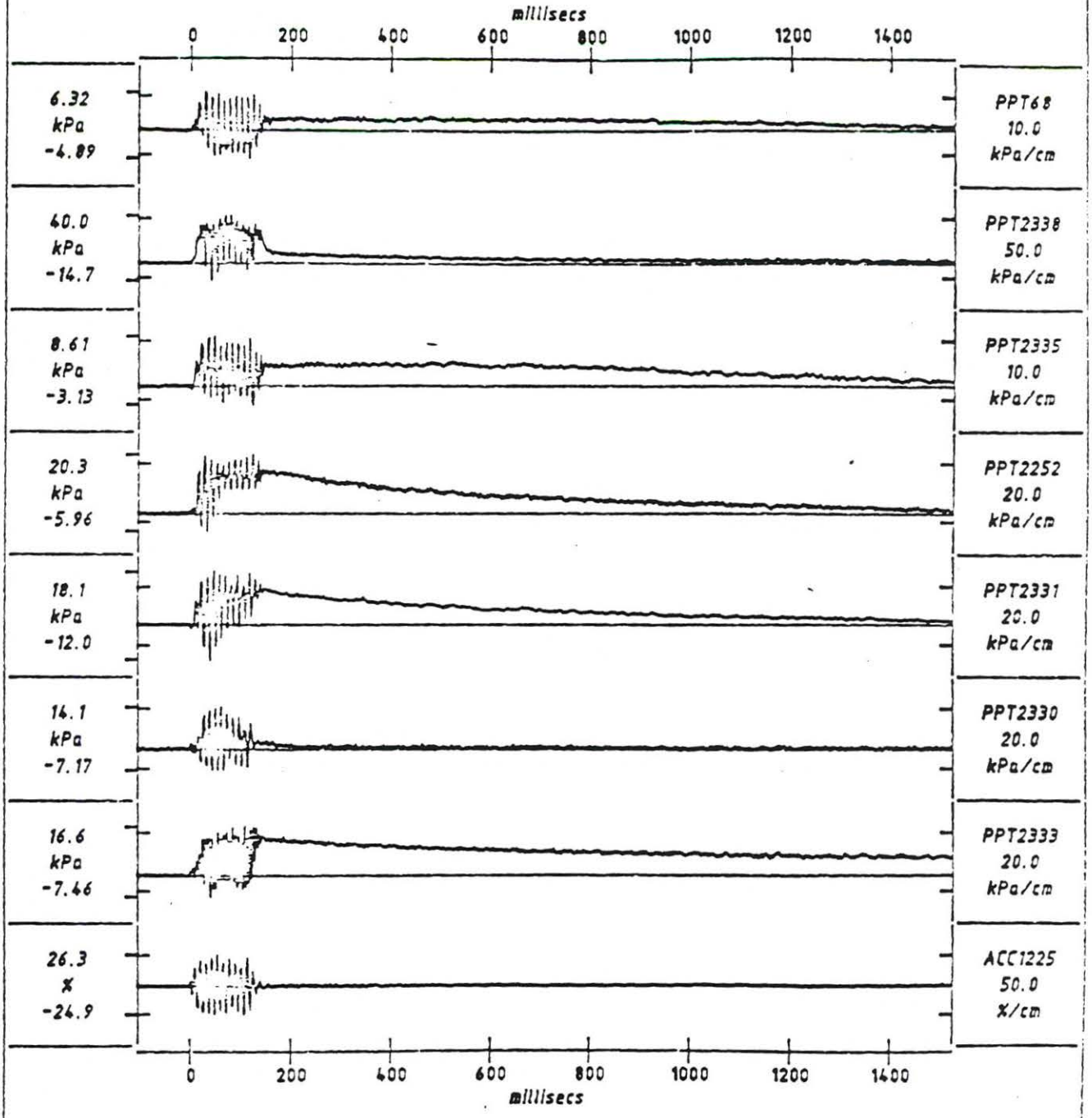

Scales : model

TEST FHL02C MODEL SE02S3 FLIGHT 3	EQ 18	LONG-TERM TIME RECORDS	G = 39.4g Kin = 7.07% Kout = 25.6%	FIG. NO. 15b

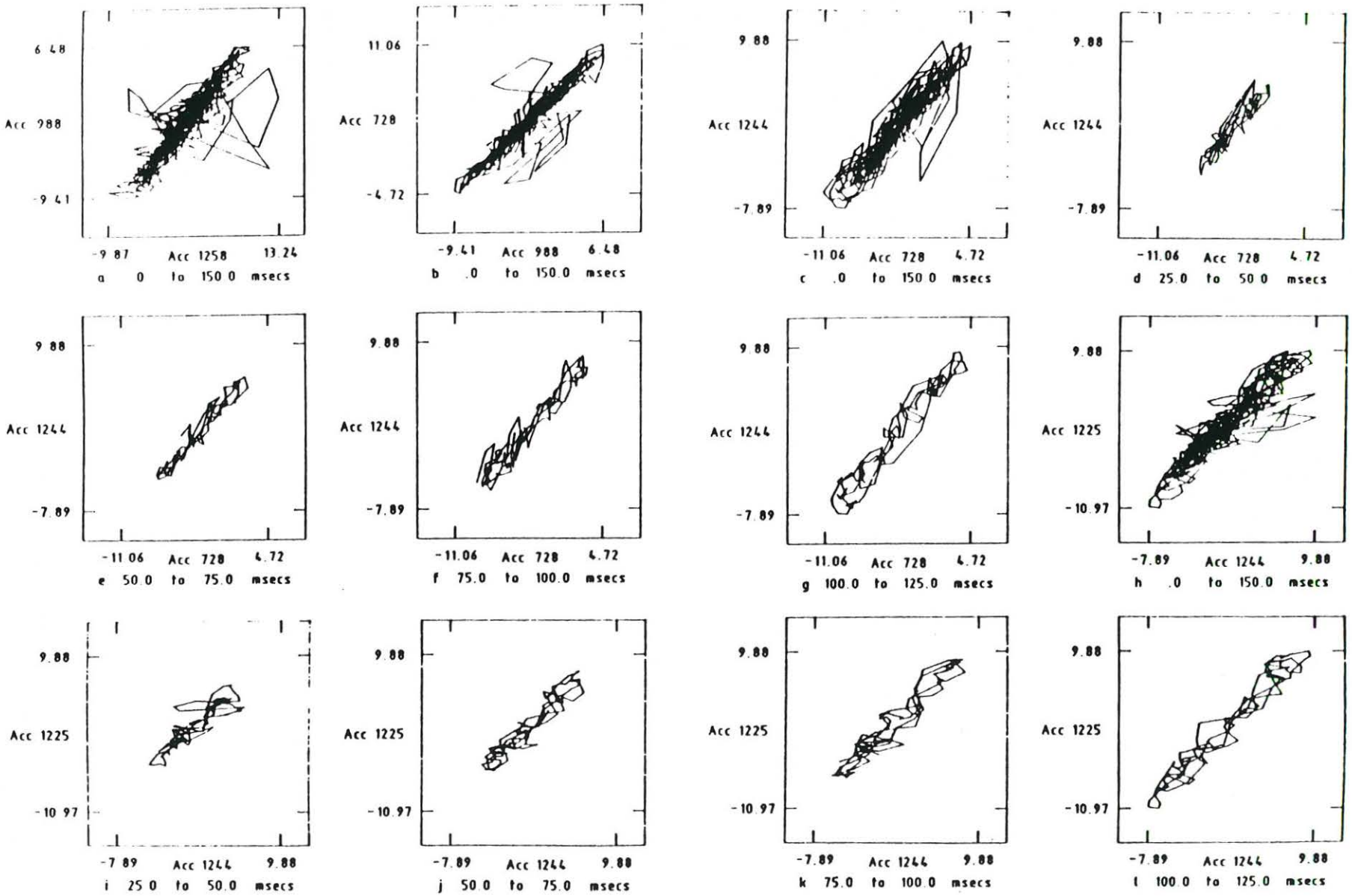

Figure 16 a - l Lissajous Figures for earthquake 5, test FHL01.

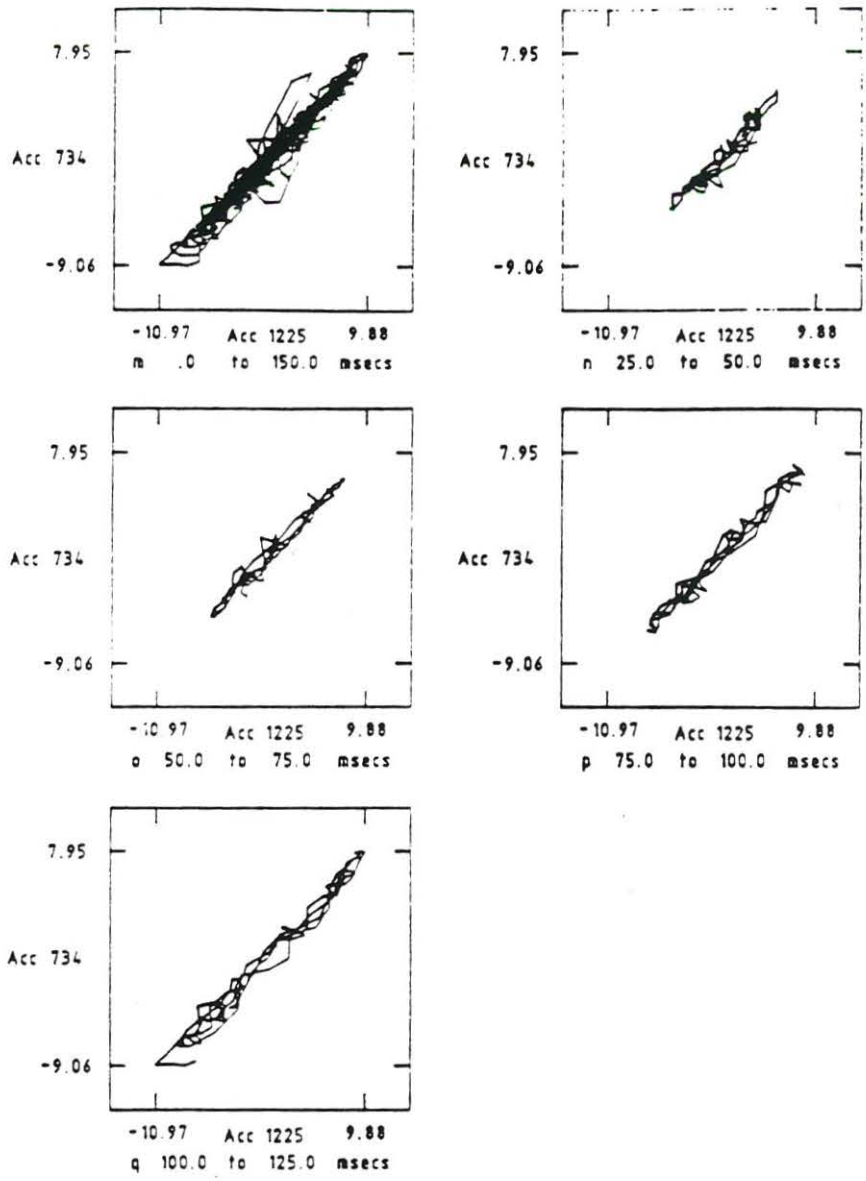
7.95
Acc 734
-9.06
-10.97 Acc 1225 9.88
m .0 to 150.0 msecs
7.95
Acc 734
-9.06
-10.97 Acc 1225 9.88
n 25.0 to 50.0 msecs
7.95
Acc 734
-9.06
-10.97 Acc 1225 9.88
o 50.0 to 75.0 msecs
7.95
Acc 734
-9.06
-10.97 Acc 1225 9.88
p 75.0 to 100.0 msecs
7.95
Acc 734
-9.06
-10.97 Acc 1225 9.88
q 100.0 to 125.0 msecs

Figure 16 m - q

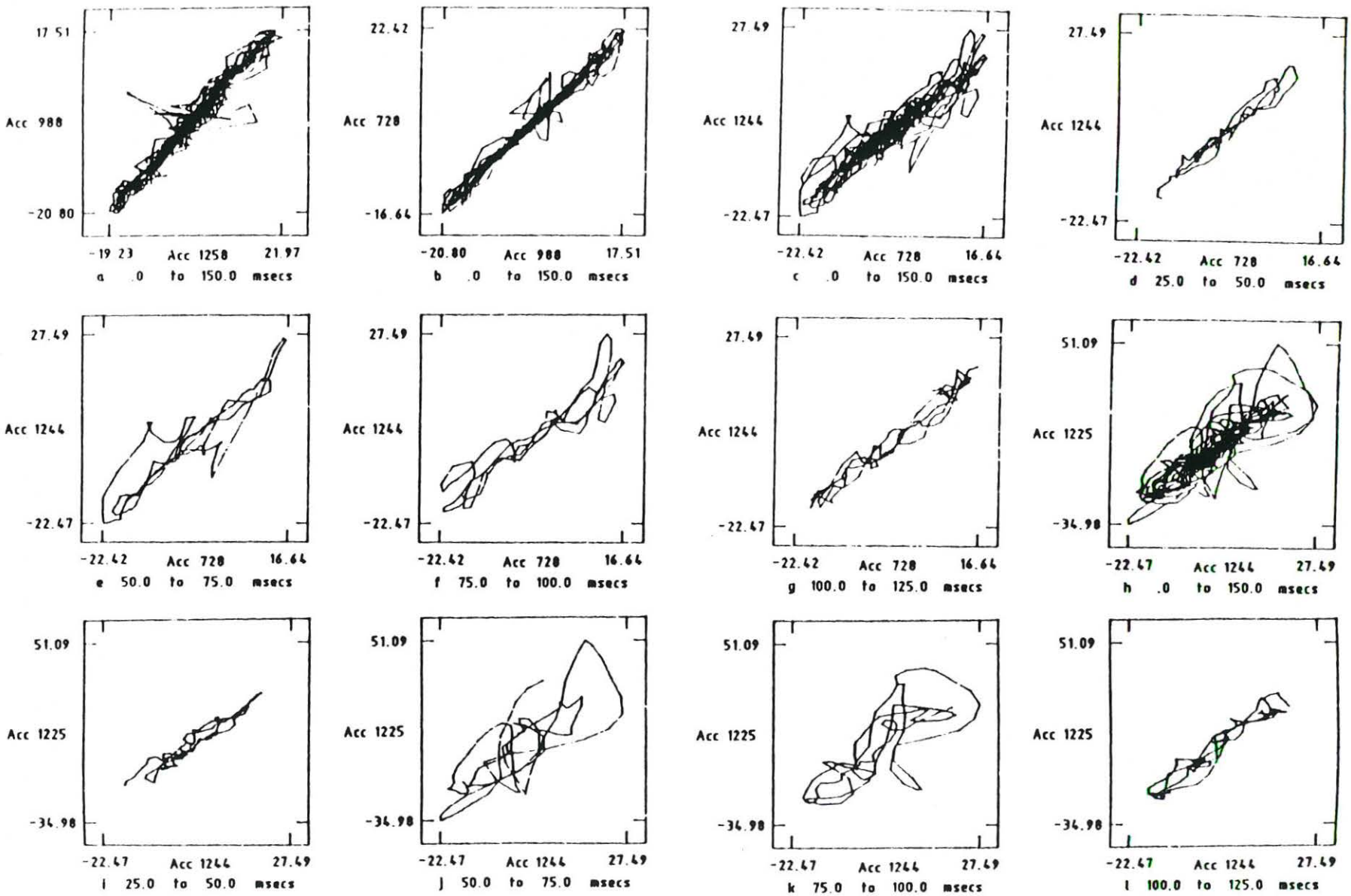

Figure 17 a - l Lissajous Figures for earthquake 8, test FHL01.

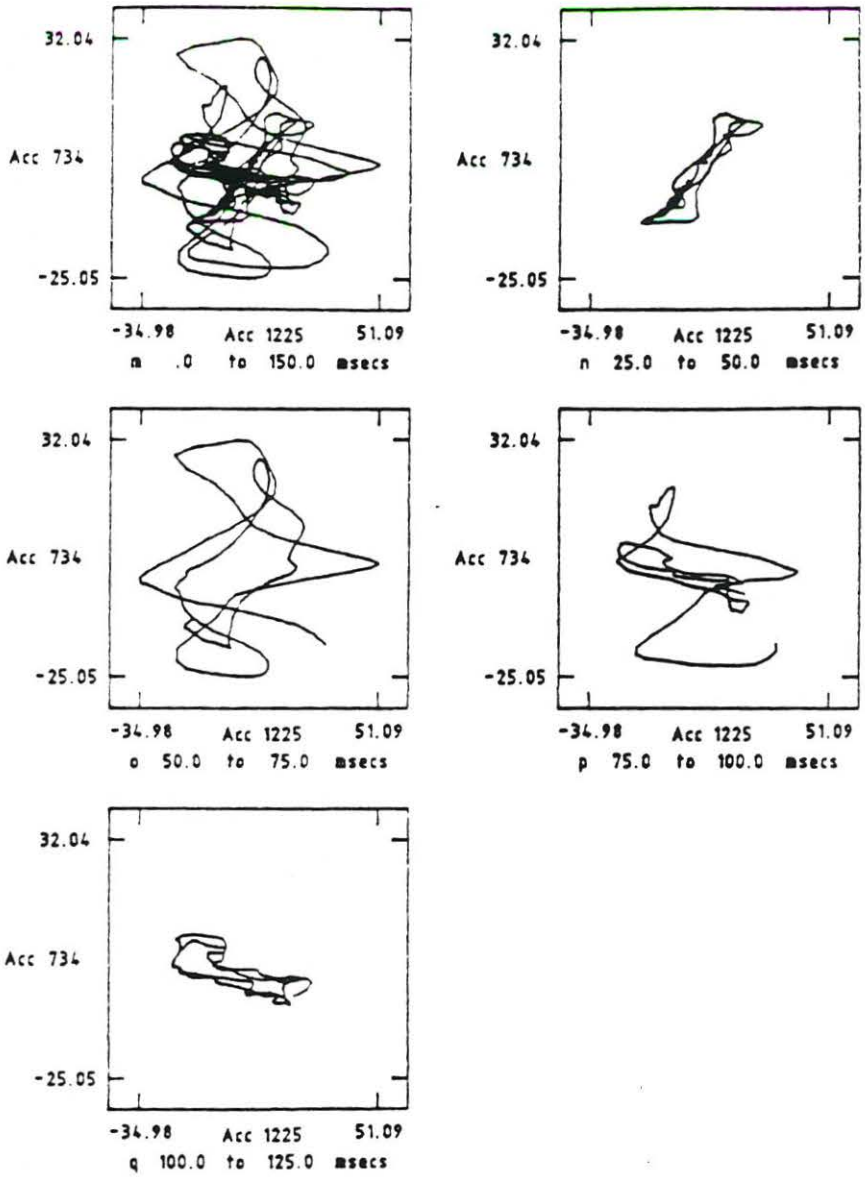
32.04
Acc 734
-25.05
-34.98
Acc 1225
51.09
m .0 to 150.0 msecs
n 25.0 to 50.0 msecs
o 50.0 to 75.0 msecs
p 75.0 to 100.0 msecs
q 100.0 to 125.0 msecs

Figure 17 m - q

Figure 18a Negative of blue sand grid before test FHL02.

Figure 18b Negative of blue sand grid after test FHL02.

APPENDIX I

LISSAJOUS FIGURES

3.1 Sinusoidal Waves (after Haag, 1962)

a. Wave on y-axis has a frequency twice that of wave on x-axis and lags the latter by a phase angle of β. For various values of β, the Lissajous figures are as shown in Fig. I.1 below.

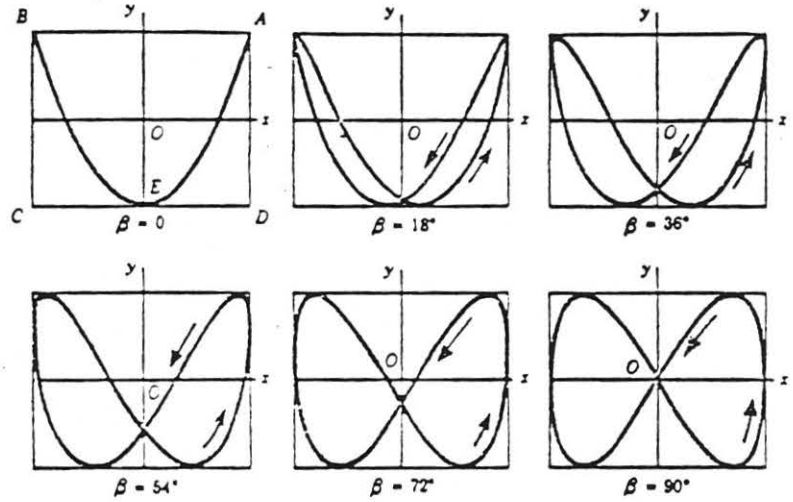

Figure I.1 (after Haag, 1962)

b. Wave on y-axis has a frequency 1.5 times that of wave on x-axis and lags the latter by a phase angle of β. For various values of β, the Lissajous figures are as shown in Fig. I.2.

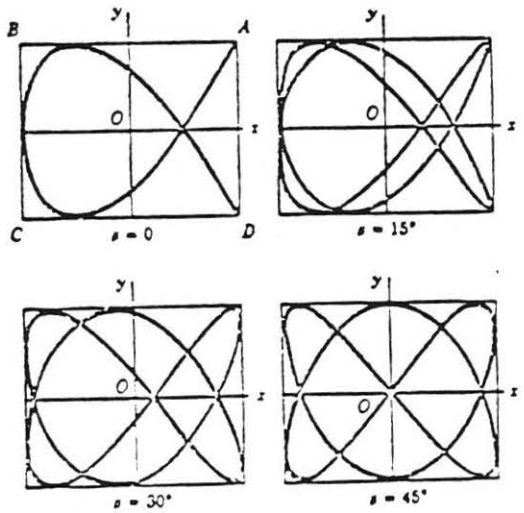

Fig. I.2 (after Haag, 1962)

3.2 Triangular Waves (after Dean, 1981)

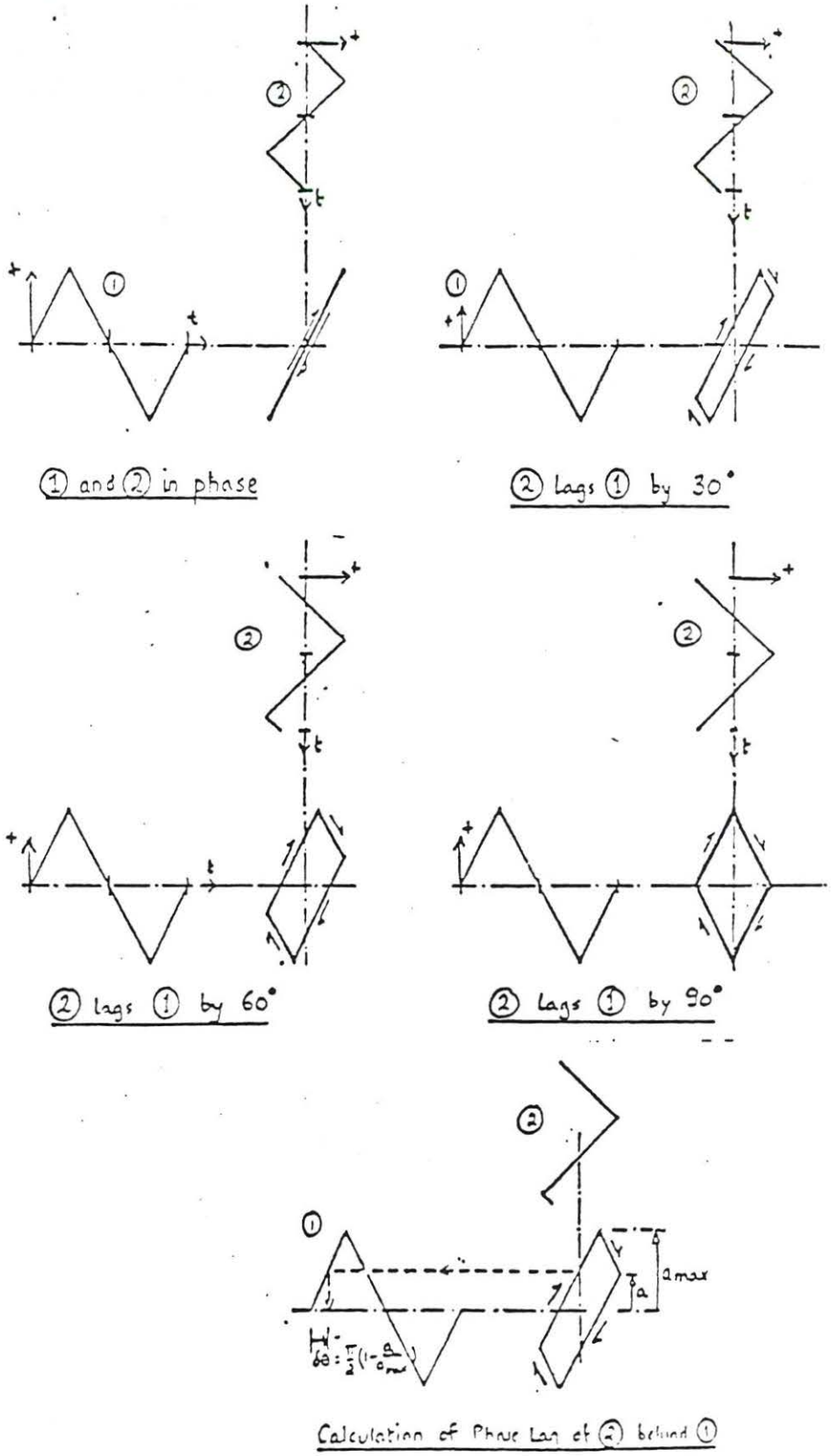

① and ② in phase

② lags ① by 30°

② lags ① by 60°

② lags ① by 90°

Calculation of Phase Lag of ② behind ①

Figure L3 Lissajous Figures for Triangular Waves (after Dean, 1981)

3.3 Square Waves and Triangular Waves (after Dean, 1981)

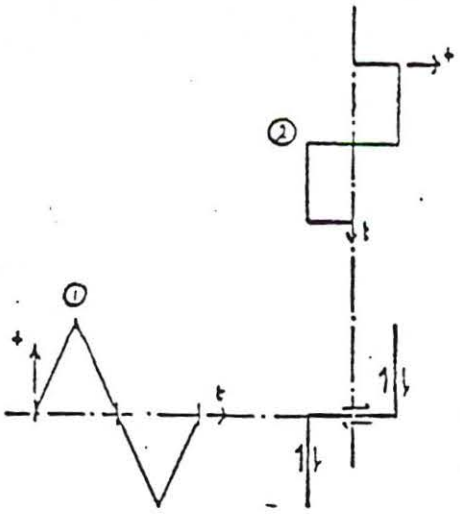

Square and Triangular 'in phase'

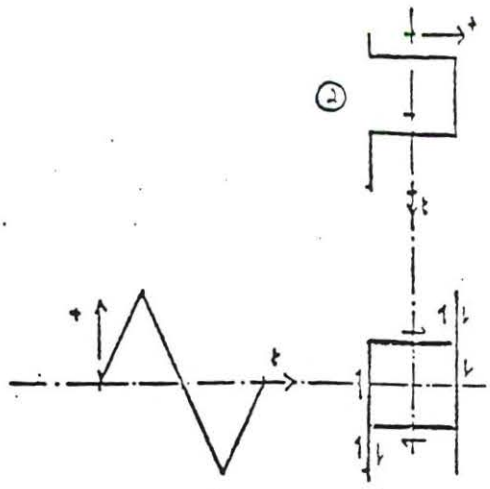

Square lags Triangular by 45°

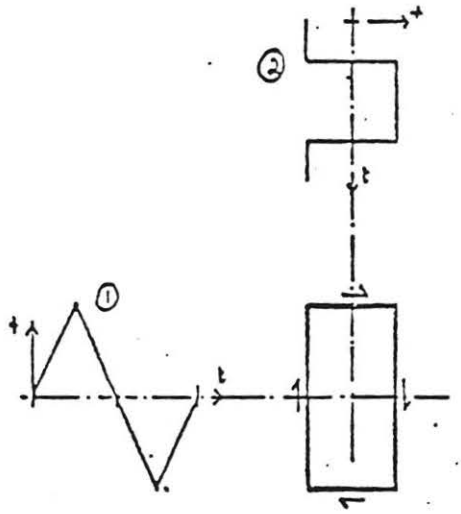

Square lags Triangular by 90°

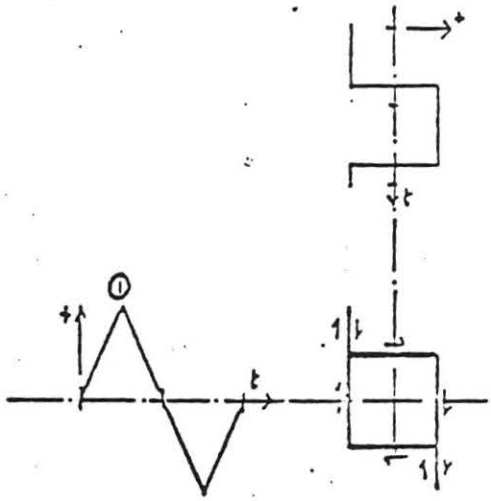

Square lags Triangular by 135°

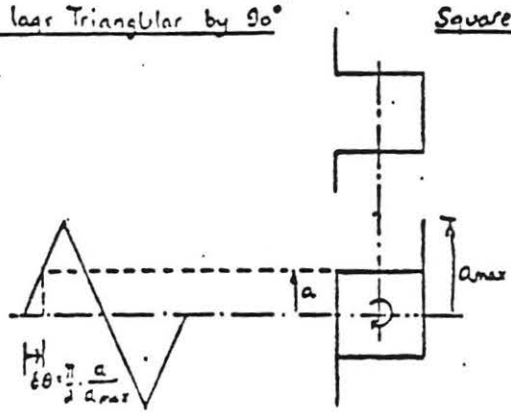

Calculation of Phase Lag

Figure I.4 Square Wave Lagging Triangular Wave (after Dean, 1981).

FULFILMENT OF BOUNDARY CONDITIONS FOR SEISMIC SIMULATION

by

Amos Zelikson

Laboratoire de Mécanique des Solides

Ecole Polytechnique

Palaiseau, France.

1. INTRODUCTION

Experimental simulators where gravity is correctly scaled appear as both necessary and sufficient for a systematic study of structure - foundation - soil interaction during earthquakes. The primary aim is to solve as completely as possible the engineering problems. Only thus can the large sums involved with the models by justified. Solution of academic problems will come out in parallel.

While setting out experiments according to ad hoc codes, it is recognized that one of the main products of a systematic study would be a new code for seismic resistance. The present paper deals with bringing out the questions involved and giving some examples of partial solutions.

2. THE SYSTEM

In situ the structural system has three components : superstructure, foundations, infinite soil. In the model the soil is confined within a cell, which forms a forth component. The soil in the model represents a domain D in situ, the boundary of which is ∂D. During an earthquake velocities and tractions appear on ∂D, the compounded effect of the seismic energy coming from outside and the superstructure - foundation - soil energy comming from inside. A correct simulation requires the scaled velocities and tractions on the soil adjacent to the cell's walls.
The degrees of liberty (e.g. displacements) of the superstructure are grouped into internal (d) and foundation connection ones (Δ). The only excitation of the superstructure in the case of earthquakes are the reactions of the foundations R in terms of generalized forces for Δ.
Taking for simplicity the foundations as part of the soil component, the boundary values are Δ, R at the superstructure - soil junction. The soil's degrees of freedom on the rest of the boundary are called b and the related forces F_b.

3. INTERNAL BOUNDARY CONDITIONS

As far as the soil is concerned, the presence of the superstructure is equivalent to a boundary condition : the Δ, R relation. For example, if the superstructure is viscoelastic a relation between the Fourier transforms $\hat{\Delta}$, $\hat{R}$ is as follows :

$$-\omega^2 \begin{vmatrix} M_d & 0 \\ 0 & M_\Delta \end{vmatrix} \begin{matrix} \hat{d} \\ \hat{\Delta} \end{matrix} + i\omega \begin{matrix} C_d & \underline{c} \\ \underline{c}' & C_\Delta \end{matrix} \begin{matrix} \hat{d} \\ \hat{\Delta} \end{matrix} + \begin{matrix} K_d & \underline{K} \\ \underline{K}' & K_\Delta \end{matrix} \begin{matrix} \hat{d} \\ \hat{\Delta} \end{matrix} = \begin{matrix} 0 \\ \hat{R} \end{matrix}$$

putting $\underline{c} \cong 0$:

$$\begin{matrix} -\omega^2 M_d + i\omega C_d + K_d & \underline{K} \\ \underline{K}' & -\omega^2 M_\Delta + i\omega C_\Delta + K_\Delta \end{matrix} \begin{matrix} \hat{d} \\ \hat{\Delta} \end{matrix} = \begin{matrix} 0 \\ \hat{R} \end{matrix}$$

Solving by Gauss elimination :

$$\left(-\underline{K}' \left[-\omega^2 M_d + i\omega C_d + K_d\right]^{-1} \underline{K} - \omega^2 M_\Delta + i\omega C_\Delta\right) \hat{\Delta} = \hat{R}$$

In the frequency domain of interest, any other superstructure for which the above relation $(\hat{\Delta}, \hat{R})$ holds with good approximation can replace the original one, as far as the soil is concerned. Nor does it have to be an actual structure, because using a computer and an array of actuators, than at least in principle this $(\hat{\Delta}, \hat{R})$ relation can be implemented. In fact $f = m\ddot{x}$ is an arrangement for creating a force proportional to the second derivative of the displacement. This arrangement is "mass". Mechanical models can use a Guyan type approximation or a modal one. In the Guyan case $c_d \cong 0$ and $[-\omega^2 M_d + K_d]^{-1}$ is developped in series. The first order gives $K_d + \omega^2 M_d$

so $\hat{R} = (-\underline{K}' K_d \underline{K} - \omega^2 \underline{K}' M_d \underline{K} - \omega^2 M_\Delta + i\omega C_\Delta + K_\Delta)\hat{\Delta}$

which is the transform of $M_\Delta^* \ddot{\Delta} + C_\Delta \dot{\Delta} + K_\Delta \Delta = R(t)$

where $M_\Delta^* = M_\Delta + \underline{K}' M_d \underline{K}$

and $K_\Delta^* = K_\Delta - \underline{K}' K_d \underline{K}$

In the modal approximation only some of modes are retained and corrections added, resulting in a new superstructure. (The static loads must be correct.

4. EXTERNAL BOUNDARY CONDITIONS

The conditions for the rest of soil, i.e. for b and F_b are called external. Their role in the model is to insure the correct values of Δ and R. External conditions are devided into passive and active. The passive ones do not vary with time, e.g. free surface, rigid wall. The active ones are imposed by the experimenter.

In situ, an excitation of R_i causes signals at i and the other points j as the wave travels out. Some echoes come back later on from reflexions below. In the model there exist also reflexions form the walls. These perturbations distort radiation of energy from the structure to infinity, which is the main contribution to damping. So models of structures must be small relative to the cell. Howaver, very large structures are to be considered and on the centrifuge cell dimensions and length scale reduction are limited. The performance of the seismic simulator might be greatly improved by processing the signals digitally, either in real time or later on. The necessary codes should be designed together with the actuators and the cell to give the optimal result of the processed signals.

4.1. Some numerical tools

The soil is certainly not a linear system. However, corrections can be applied in a linear way, following a time honoured procedure going back to Froud.

A system of linear differential equations has a Green's function $G(t,\tau)$ which transforms the forcing term $x(t)$ to the solution $y(t)$:

$$y(t) = \int^t G(t,\tau)\, x(\tau)\, d\tau$$

If the equation has constant coefficients $G(t,\tau) = G(t-\tau)$ and $y = G * x$ (convolution product).

A property of the integral transformation by Green's function is that the transform acquires the smoothness of G. For example even if $x(t)$ is only piece-wise continuous and $G(t,\tau)$ has second continuous derivatives, then $y(t)$ has second continuous derivatives. Thus a convolution can be used to smooth function and a good example is the shock spectrum.

Several integral transformations exist which transform a function of time to a function of frequency (and inversely) ; a function of time to a function of an integer (and inversely) ; an analytic function to a function of an integer (and inversely) ; and finally a function of an integer on another one of its kind and inversely. In all those cases the following exists : if the integral transformation is $y = F[X]$, then :

$$F[X_1 * X_2] = (F[X_1]) \cdot (F[X_2])$$

It follows that $\log F[X_1 * X_2] = \log y_1 + \log y_2$. convolution is associative, so the graph of the logarithm of the transform, or Bode's diagram, is in fact a superposition of the graphs of the different factors of the convolution. This graph is accordingly amenable to procession by linear numerical algorithms which are normally called filters. One aim is to come out with F[G] if G is not known. As $F[G^{-1}] = 1/F[G]$ an inverse convolution (called deconvolution) is possible giving $x = G^{-1} * y$. A second aim might be to first separate between the superimposed log graphs in order to recombine them premultiplied by weights, i.e. to make corrections. The corrected graph is the logarithm of the corrected signal's transform, so by exponentiation and inverse integral transformation the corrected signal is obtained.

The key to the efficiency of procedures is the fast discrete Fourier transform. If signals are sampled at T intervals ($t = nT$ when $n \in 0, 1, .. N-1$) they form vectors of N components. The components can be drawn on a drum, so that $X_0 = X_N$, $X_1 = X_{N+1}$, etc... to give periodic functions. In exactly the same way to discrete Fourier transform is a vector of N components, drawn on the same drum. The fast transform algorithms executes the passage from one vector to the other rapidly. Convolutions are calculated by first putting the factors on a drum and then Fourier transforming.

4.2. Echoes

According to the principle of Huygens, the echoes can be looked upon as coming from secondary sources on the boundaries. The secondary emission $y_s(t)$ is given :

$$y_s = G_s * X(t - T_s)$$

where X(t) is the source and T_s is the time of travel from the source to the boundary. The signal received is given by $y_r = G_r * y_s(t - T_r)$ when T_r is the time of travel from the secondary source to the receiver. In the present case, the sources and receivers are the points of connection between the foundations and the superstructure. The relation between the digital signals $(y_r)_n$ and X_n can be written as :

$$(y_r)_n = \sum_{k=1}^{M} \alpha_k X_{n-n_k}$$

α_k are distorsion factors, n_k is the delay of the echo n° k .

Let : $\delta_n^{n_k} = \{ 0 , n \neq n_k \; ; \; 1 , n = n_k \}$

then : $G_n = \sum_{k=1}^{M} \alpha_k \delta_n^{n_k}$

and : $(y_r)_m = \sum_n G_{m-n} X_n \equiv (G * X)_m$

An example taken from [1] : (one echo)

$$G_n = \delta_n^0 + \alpha \delta_n^{\ell} \quad , |\alpha| < 1.$$

$$F[y_r] = F[x] F[G] \; ; \quad F[G] \equiv \sum_{n \in -\infty}^{\infty} G_n e^{-i\omega n} = 1 + \alpha e^{-i\omega \ell}$$

and has a period of $2\pi/\ell$.

Log F[G] has the same period. Taking log F[G] as the Fourier transform of a function g, the result is $g = \sum_{k=1}^{\infty} (-1)^{k+1} \alpha^k / k \; \delta_n^{k\ell}$ which is a sequence of pulses decaying as $|\alpha|^k/K$ at intervals equal to ℓ on the time index axis ($t = \ell T$). In parallel log F[X] is taken as the Fourier transform of ξ_n (i.e. $F[\xi] = \log F[x]$). If $\xi_n \neq 0$ in a different region on the index line, than the two can be separated (for example by dilating every $n = k$ component). Ref. [1] gives examples of successful application of this procedure in acoustics and seismology.

The experimental procedure should be to apply pulses at point i and measure respons at all the points of connection. According to the last example separation of G will be manageable if the duration of the pulse is different from any time of travel from the different walls. In relation to the model this means that echo filtering will succeed better if non of the natural frequencies of the soil and wall system is predominant in either the model or the earthquake, as could have been expected.

The qualification of the cell for echoes during centrifugation might be quite expensive. For clays, once consolidated, tests could be carried out in the laboratory. For sands, the necessary rigidification pressure can be applied by a rubber membrane on the free surface. Such tests were carried out at CESTA on a large rigid steel cell, later used for Hydraulic Gradient seismic simulation. As the echoes intensity at the middle of the cell was founded to be relatively small, no filtering procedure was undertaken. It seems however interesting to see the form of the signals which are either horizontal (A_H) or vertical (A_V) accelerations at a depth of 10 cm. The dry sand was rigidified by vacuum. The source was a dropped metallic mass, of a very short duration (fig. 1, 2, 3, taken from [2]).

4.3. Non reflecting boundaries

At a shear wave velocity of 300 ms^{-1} and frequency of 300 Hz the wave length is 1 m. In order to be effective any "break-water" system must be at least one quarter wave thick. As this layer is on the outer perimeter, it consumes much volume and weight. Tests on the cell of fig.1 showed that a 2 cm layer of elastomer did not change anything.

By supporting the walls of the soil with mud pressure accross a rubber wall, the longidutinal wave motion energy is transmitted to the mud and can be arranged to be carried away hydraulically. This dissipates the pressure waves, which due to their larger phase velocity have larger wave length at equal frequencies. The rubber wall is a free surface for the transversal motion. This boundary thus separates between the transversal and longitudinal wave motions, a situation that might be convenient for echo corrections.

Wave energy at the boundary can be absorbed by boundary motion, in the same way that a ball bounced from a receding car becomes limp. For example a plane wave travelling from the origin according to $u = f(t - \frac{x}{c})$ would not be reflected at point $X = \ell$ if u is forced to be $f(t - \frac{\ell}{c})$ at that point. The same result can be obtained by changing the impedence at $X = \ell$ in a closed loop arrangement where u is measured at, say, $X = 0$. This installation exists in the 12 m diameter 105 m long shock tunnel of Gramat which simulates nuclear air blasts with very good results [3].

Writing once again the reflected signal y_r as $y_r = \int^t G(t,\tau) X(\tau) d\tau$ The form of G must be chosen to that the directionality and coherence of the echoes is destroyed. This can be achieved by introducing a random process into G both in time and location. In this case, the ordered wave energy is transformed to noise. The relatively small level of echoes in the described cell might be attributed to such a mechanism acting in the non linear non homogeneous sand.

4.4. Seismic generators

4.4.1. The desirable motion

The amount of information about real ground motion is scant. The bed-rock signal is filtered through the upper layers and once more through buildings at and near the accelerometer. Fig. 4 from centrifuge tests shows the difference between shock spectra at the same soil point with and without the structure. One result of the filtering is the absence of correlation between the 3 motion's components.

Wherus the basic motion variable is the velocity, (which times stress gives power) for technical reason it is the acceleration which is recorded. By the process of differentiation high frequency noise is greatly enhanced, and accelerograms are very difficult to compare.

At the moment a numerical filter is used to transform the acceleration A into a velocity V by the procedure of shock spectrum analysis. This filter corresponds to the physical system of one degree of freedom viscoelastic resonator. The viscosity adds to the smoothing effect of the convolution. The logarithmic scale further subdues variations, and many earthquakes look alike. Codes give very simple curves for spectra's envelops.

The filter used for the shock spectrum had the merit in the past that it could be calculated by analog methods. This merit no longer exists. A more satisfying procedure would be to take the Fourier transform, which is also a velocity, and smooth it up. A much better procedure would be to use the velocity, and compare it numerically to some master curves, by a computer procedure fixed by the codes. In the models 2 - 3 component motion can and should be produced. The codes give no indication how to combine them. One way to do it, is to use the free field motion to excite 3 - 4 degree of motion systems corresponding to either symetric or non symetric rigid bodies on the soil, representing the soil by spring - dashpot units. In the symetric case (no twist) the vertical motion is not coupled to the horizontal and rocking one so 2 x 2 matrices describe the system, in a way that can be hand calculated. Such an integration was carried out for free field motions on centrifuge. The results are seen in figure 5.

Actual velocity curve's comparison also takes in account the number of cycles. This is a very important parameter, both for liquefaction and for transfer of energy between different modes, a process which takes time. In situ the earthquake is a wave that has a given profil in the soil near the surface and which propagates at a certain velocity. This information is not available.

In problems related to liquefaction the stresses of the free field wave are important. They are not available. At least in principle an earthquake signal can be characterized by the stress field. This possibility exists for model tests.

Once a desired free field motion is given, the problem is to sustain it by boudary excitation.

4.4.2. Seismic generators

When the same momentum p is imparted to masses m_1 and m_2 in a collision, the energies imparted are $0.5p^2/m_1$; $0.5p^2/m_2$;

the smaller is the mass the greater is its share of energy. Efficiency of power requires models to be shaken against larger masses. For a shaking table the reactive mass is in the heavy foundation. Putting the experimental cell on such a table is feasible for models using the Hydraulic Gradient simulation. For models on a centrifuge shaking of the whole cell can be carried out when it is a small one fixed on a heavier support, with a substential loss in pay-load, or as it has been done to shake the cell against the centrifuge building or the centrifuge itself.

If part of the cell's boundary is shaken, than the accompanying mass has the volume of about L^3 when L is a typical dimension of the shaken part. This seems to be the correct way. The situation most similar to real earthquake is a running wave along the bottom of the cell, and containing both horizontal and vertical components. Such an installation would have to support the weight of the model during centrifugation and would have to be watertight. Thus it is estimated to consume quite a lot of pay-load, which however seems justified. The solution adopted at CESTA was to shake one side of a longish cell.

A tailored signal is a shaking system tuned by several tests so to give required free field as measured at different points in the soil. Once all is set up signals must be repetitive.

A servomechanism is a feed back controlled system which corrects itself automatically relative to a given signal. As a wave profil is the required quantity, a situation must exist where one variable controls the whole field. This variable can be the velocity on a rigid plate (e.g. the shaking table) or the pressure on a rubber membrane. It could be a field transducer reading. In that case the cell must be sufficiently large in order to eliminate the structure's filtering effect. Also the weighed sum of signals of several transducers can be the controlling variable. All this operation can be performed either by an analog computer or a digital one. Not all fields are controllable, especially in a non linear material. A servomechanism may loose control and become destructive, a disagreable situation on the centrifuge.

A tailored signal is dependent on the presetting of several physical fixtures, and its variability is somewhat limited, and setting takes time and labour.

A servomechanism is as variable as the library of curves it follows, of which there are actually not many. Thus in many cases a closed loop system acts in fact as part of a tailored signal generator, its main function being to assure repettivity. According to the last chapter the best control variable is the free field velocity. Apart from being the correct wave parameter, the scale of which is conserved, velocity has smooth signals which reduces the tolerance requirements on the servovalves.

4.5. Tailored pneumatic generators

A pneumatic seismic generator was tested at CESTA on the cell of fig. 1. This is a rigid cell made of steel. The soil sample is 1.8 m by 0.8 m by 0.5 m depth. This cell is currently in use at the Ecole Polytechnique for Hydraulice Gradient seismic simulation. A lighter cell of aluminium (1.3 m by 0.8 m by 0.4 m) is used on the CESTA centrifuge. In the tests to be described on the steel cell the soil was dry sand, rigidified by a pressure of 0.2 MPa on a thin rubber membrane spread over the soil's free surface.

The operation principle of a pneumatic generator is very much the same at that of a car engine. Energy in large quantities is stored either in compressed gas containers or as the chemical energy of combustibles. It is released according to a program either by valves or by electronic ignition. In the case of shock tubes the valves are metal membranes covering the tube's end. Membranes are either pierced mechanically or burst by small explosive charges, a system applied with great success in the Gramat shock tunnel.

The word tuning comes from musical instruments, and shows that an arrangement of cavities and openings will give repeatedly the same signal. This is because the boundaries are quite rigid relative to the air, and the opening large and not likely to be obstructed by debris. Added to this is the precise energy release rate of detonators and explosive pellets.

According to Helmholtz's model, cavities act as capacitances (or springs) the air volumes in the openings as inductances (or masses) and the resistances to flow in tubes as electric resistanced. Up to the shock range of pressures Mach's similitude is valied, (which is the same as for the soil model) : if stresses are conserved than velocity is conserved and the time scale equals the length scale. That means that doubling all the geometrical dimensions will double all the vibration periods. When the space is limited, as was the case for the Aluminium cell for the centrifuge, additional solid masses are included in the filter in order to reduce frequencies. Thus tuning of the filter is a quite simple operation. Once tuned, the signals are very repetitive.

Apart from general precautions in dealing with volumes of highly compressed gas, there are the special regulations for explosive handling. However, many combustibles are suitable which are not defined as explosives, being unsensitive. Sensitivity particularly means the amount of electric energy needed for ignition. There is no problem in providing suitable electric "sparks".

In the cells of CESTA explosive pellets and detonators are used, pre-packed inside cavities in a steel block, the function of which is to protect one charge from the others. The cost of the system is low and it has been used for years with no maintenance at all. Using shock tubes at the Ecole Polytechnique gave similar soil signals. The preparation of the test is more complicated than with explosives.

The quality of the signal was tested by 10 accelerometers placed in the sand at depths of 5 cm, 10 cm and 20 cm. The results showed that the wave filtered through the tapered part of the cell near the source to becomes regular. The lateral and longitudinal uniformity is shown in fig. 6 (spectra are given in fig. 7-10). The vertical uniformity was confirmed by comparison of signals at different depths. The wave traverses the cell attenuated first like a pressure wave, later on like a surface wave. Fig. 6 shows horizontal and vertical accelerations of similar amplitudes. Placing the generator at lowest level possible did not give very different results.

Some softening of the sand near the source was observed, and that zone was later strengthened by gravel.

5. CONCLUSIONS

An example was given of an apparently satisfactory boundary conditions settup for seismic simulation based on a tailored signal generated by explosions.

A rethinking of the whole problem has been discussed in order to make Centrifuge and Hydraulic Gradient models the major tools the should become in solving the engineering seismic problem. Such a procedure seems the more relevant because most of the large geotechnical centrifuges have quite similar features, so the same boundary condition arrangement could be used for them all.

Remark :

The centrifugal models described were built and tested by the Centre d'Etudes Scientifiques et Techniques d'Acquitaine (CESTA) of the Commissariat à L'Energie Atomique at Le Barp near Bordeaux.

The Hydraulic Gradient and shock tube models were constructed and tested in the Ecole Polytechnique.

REFERENCES :

1. A.V. Oppenheim, R.W. Schafer. Digital Signal Processing, Prentice Hall, New Jersey (1975).
2. B. Devaure, M. Mathivet. Essais de Simulation de Seisme. (compte rendu pour 1978-1979, CESTA).
3. A. Cadet, J.B.C. Monzac. Le Simulateur de souffle à Grand Gabarit du Centre d'Etudes de Gramat. Proc. 7th. Int. Symp. on Military Application of Blast Simulation (MABS). Medicin Hat, Canada (1981).
4. A. Zelikson, J. Bergues. Running Waves in Large Sand Models for the Study of Liquefaction Utilizing The Hydraulic Gradient Similarity Method. MABS 7, Canada (1981).

- - -

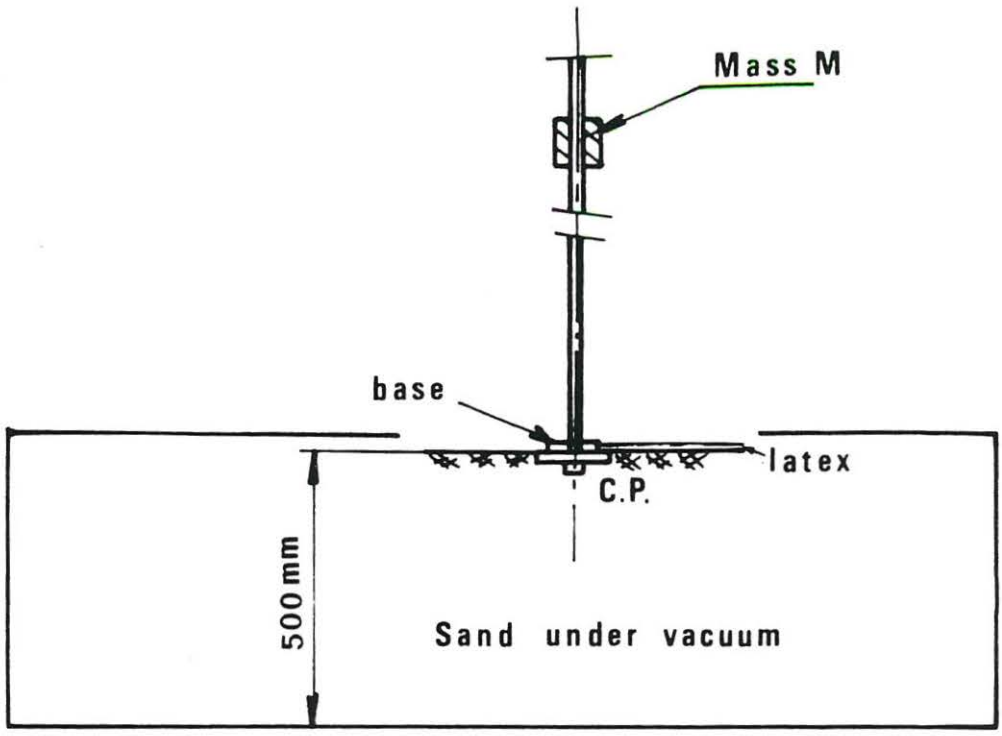

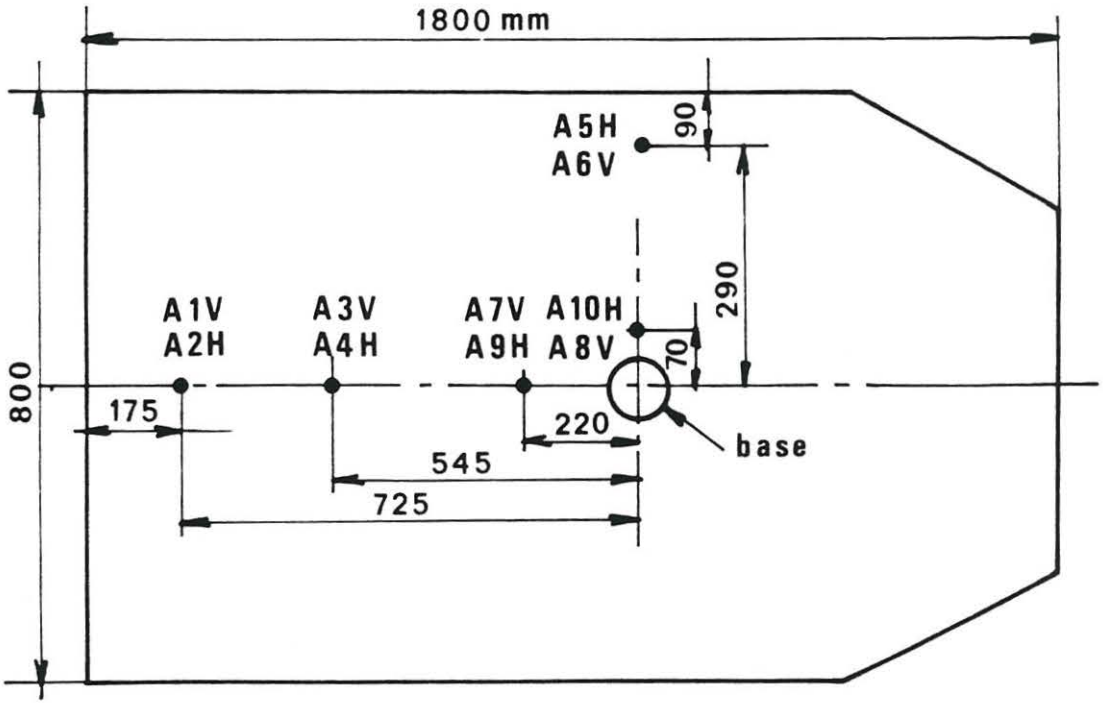

AH : acceleration - horizontal

AV : " - vertical

Fig. 1 Study of echoes by a falling mass

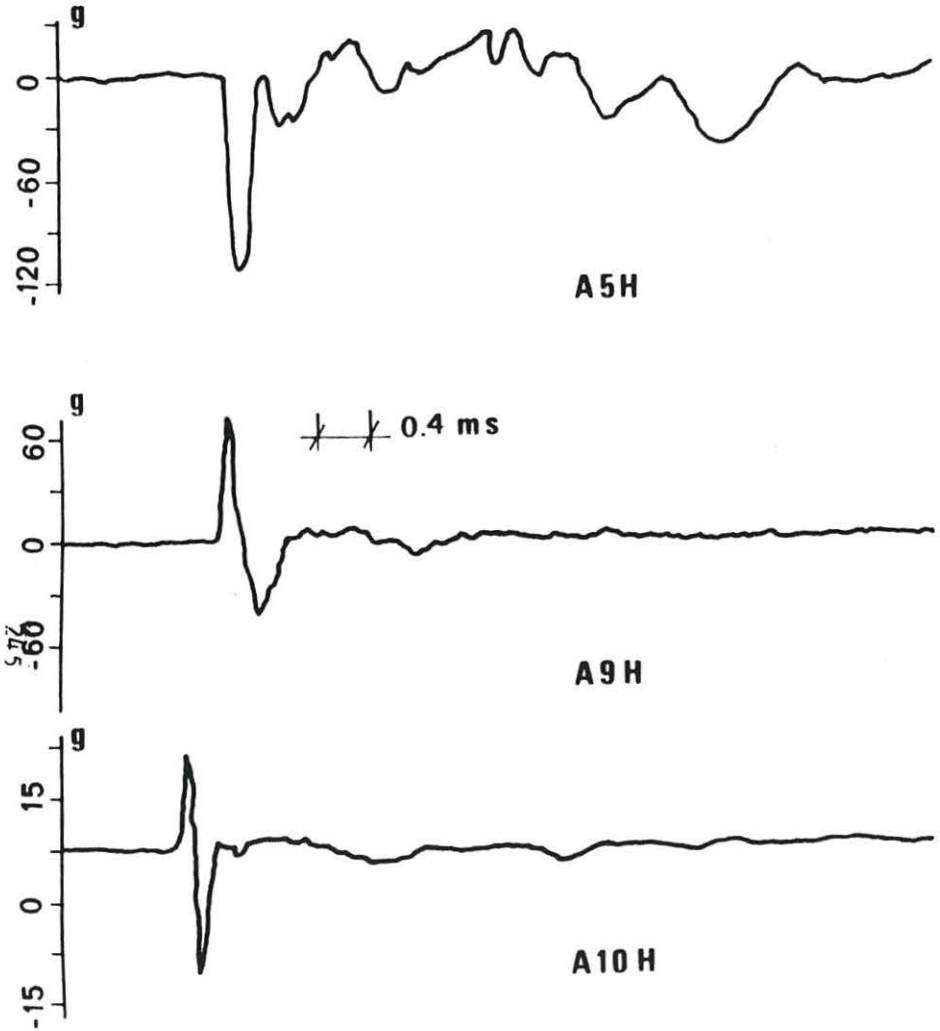

Fig. 2 Accelerations Depth 10 cm

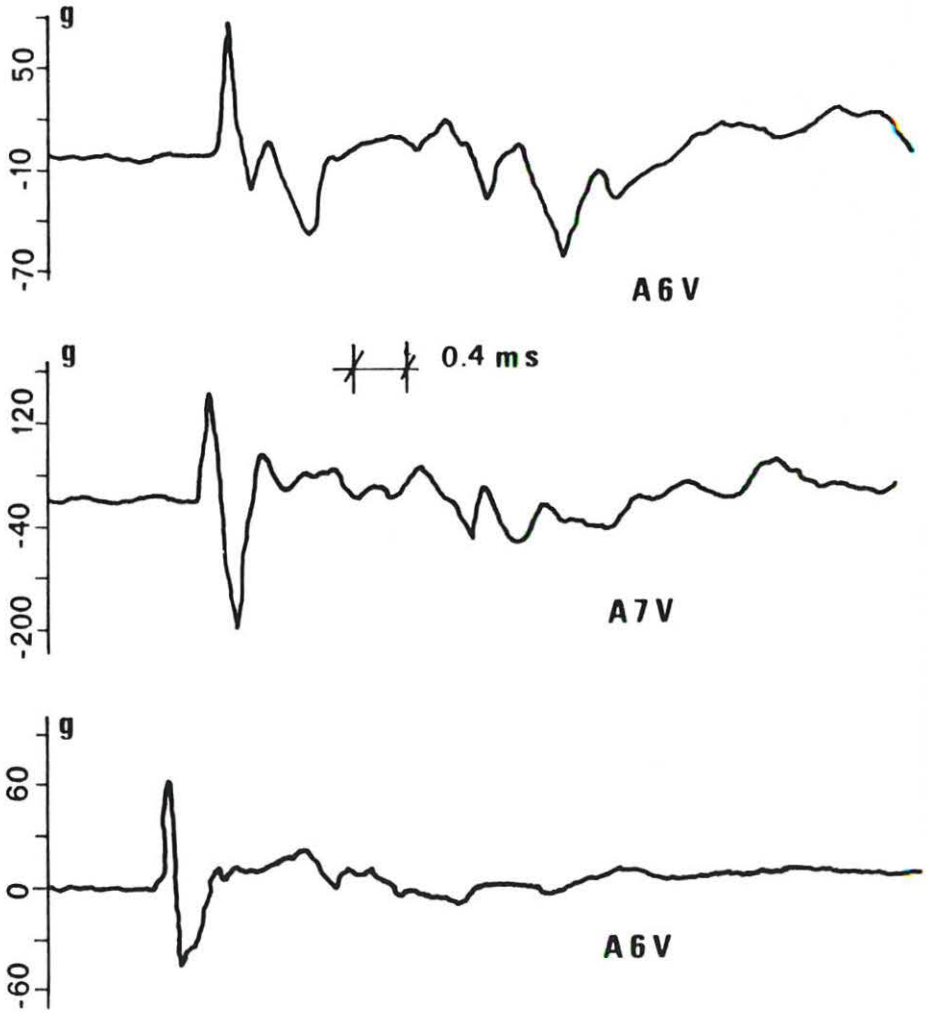

Fig. 3 Accelerations Depth 10 cm

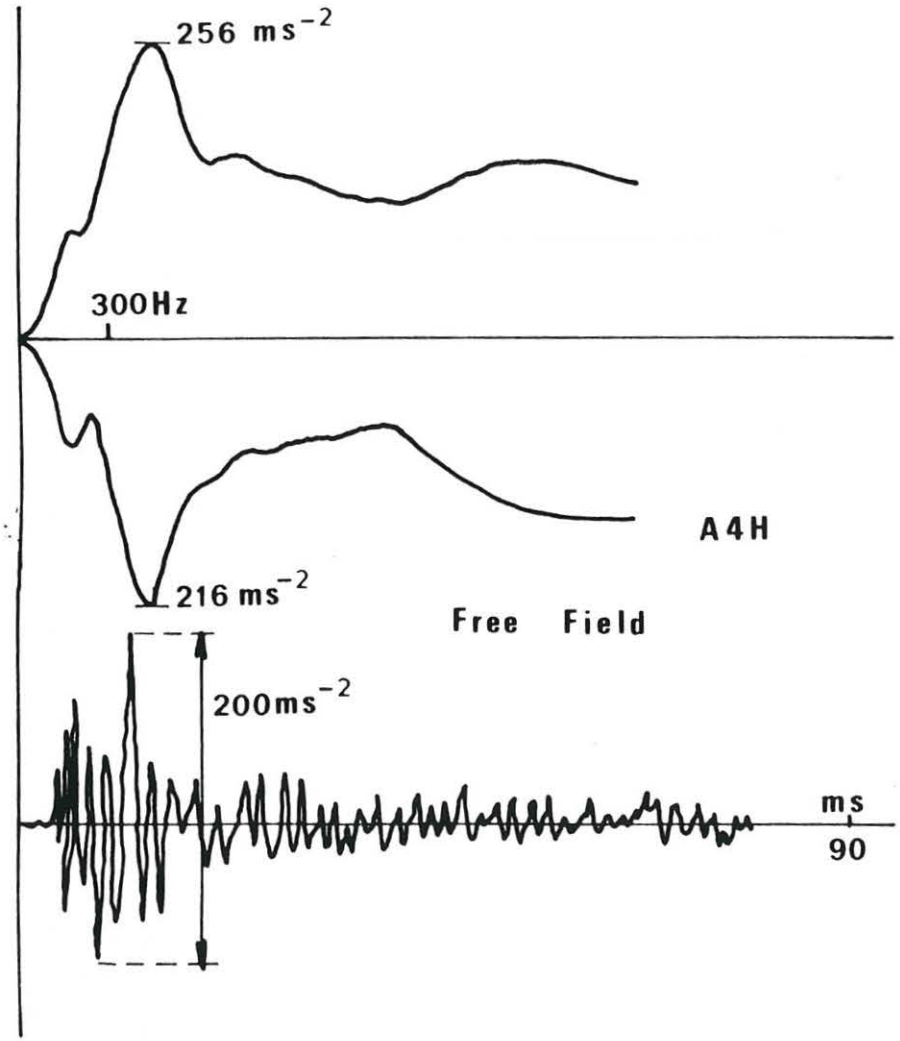

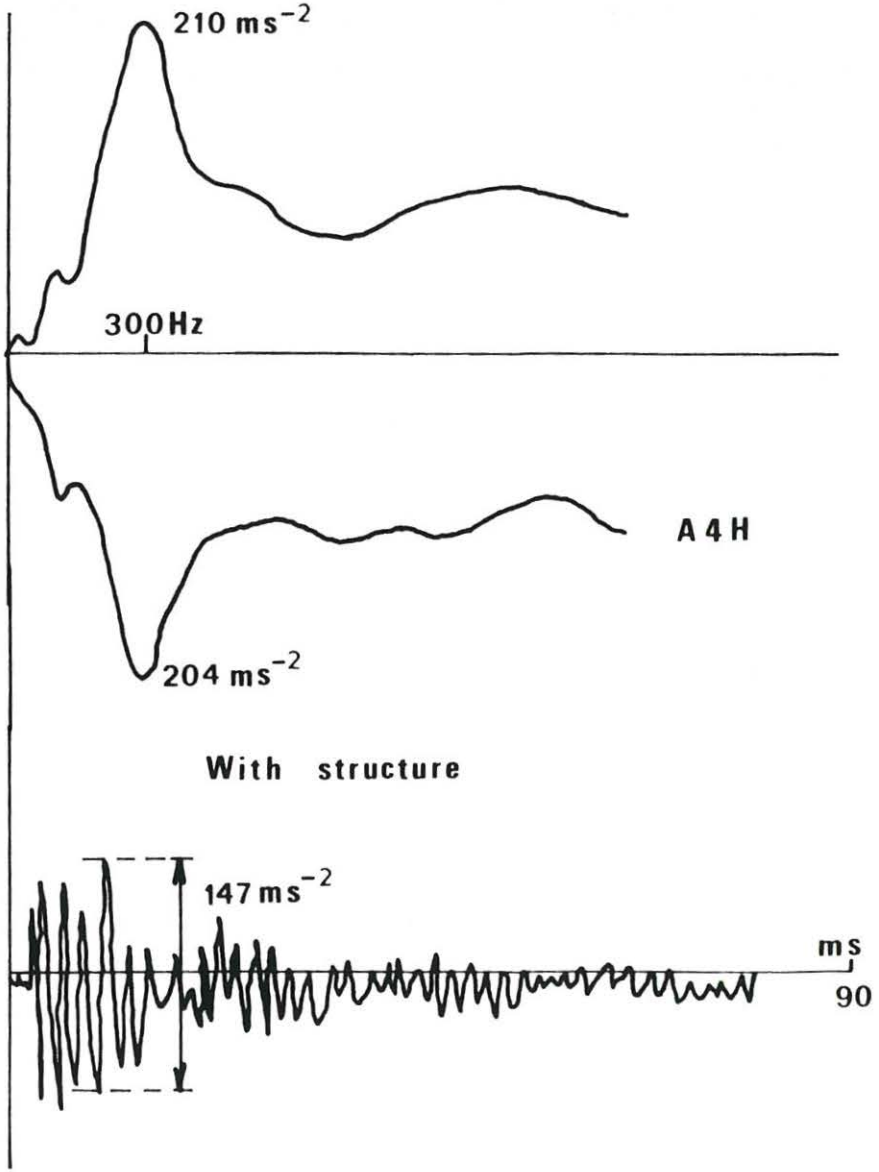

Fig.4 Influence of the structure

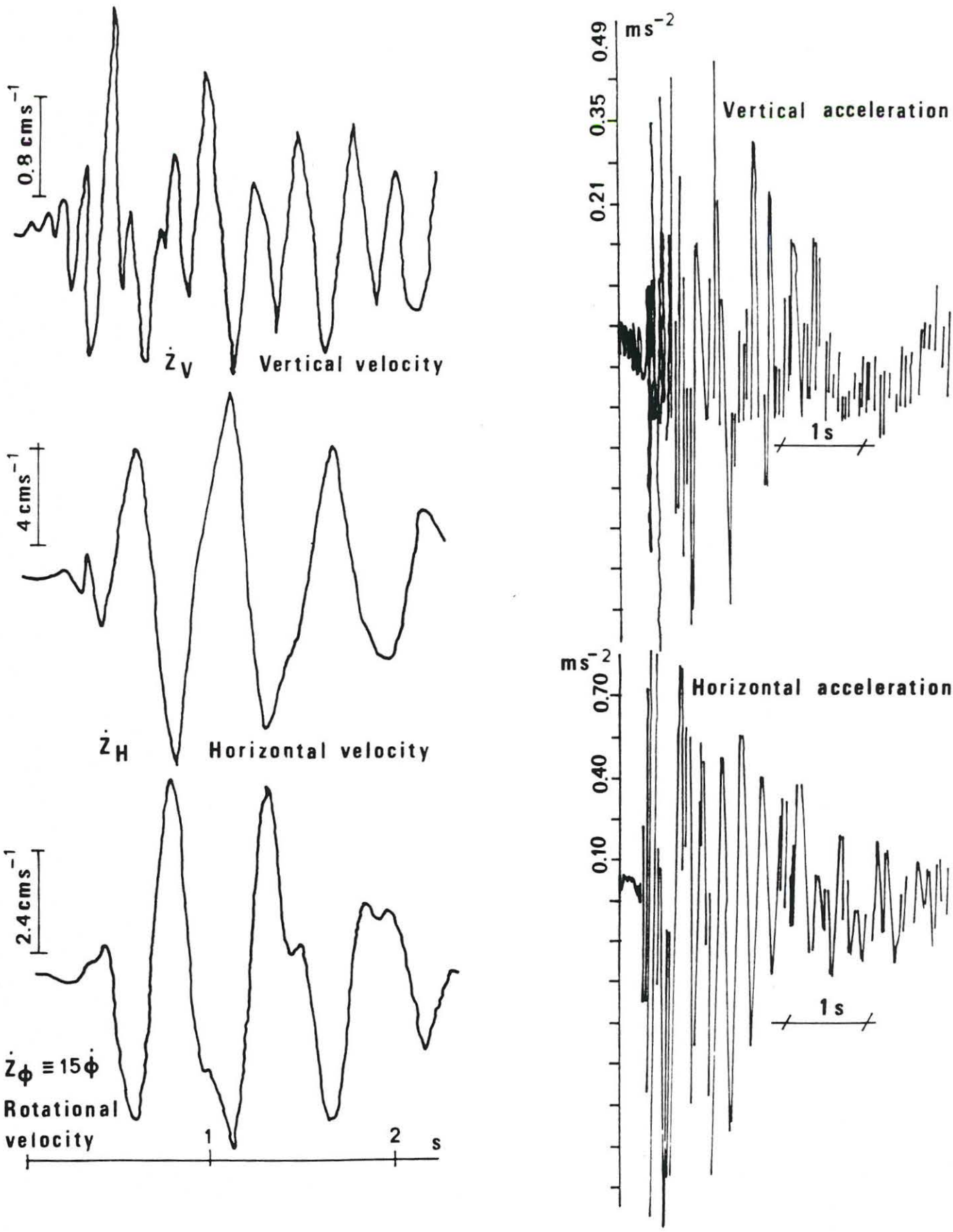

Fig.5 Calculations of 3deg. rigid structure

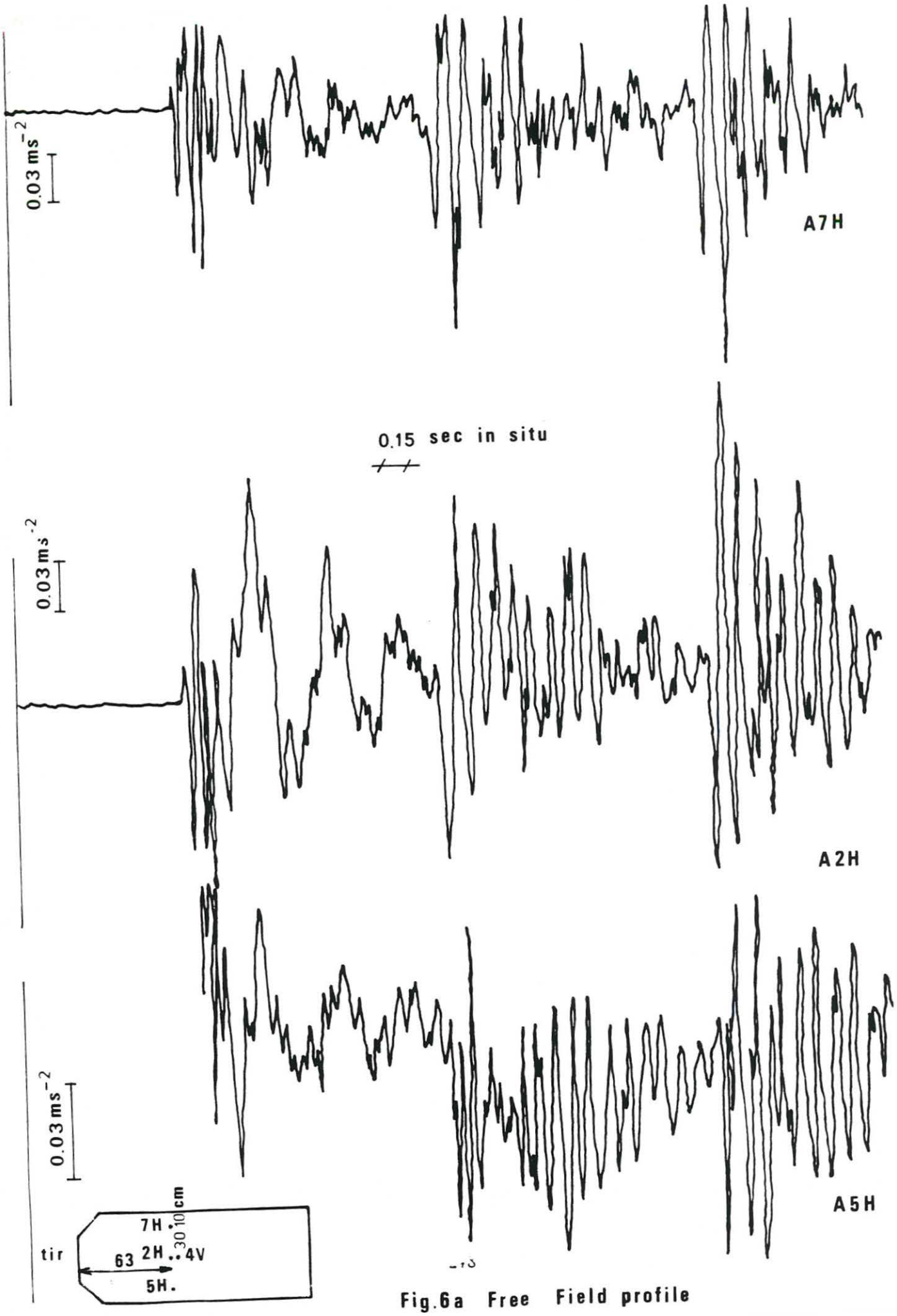

Fig.6a Free Field profile

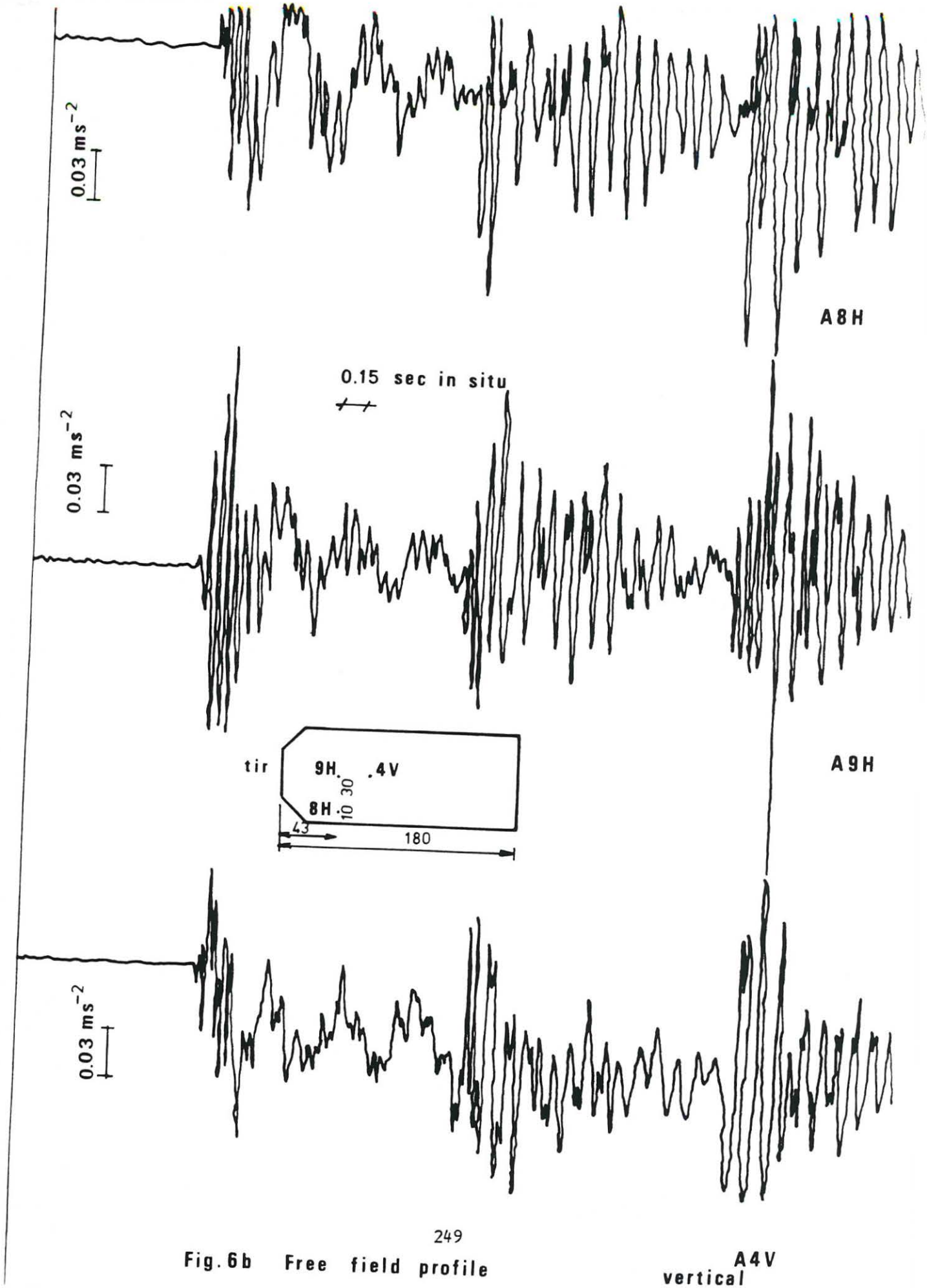

Fig. 6b Free field profile

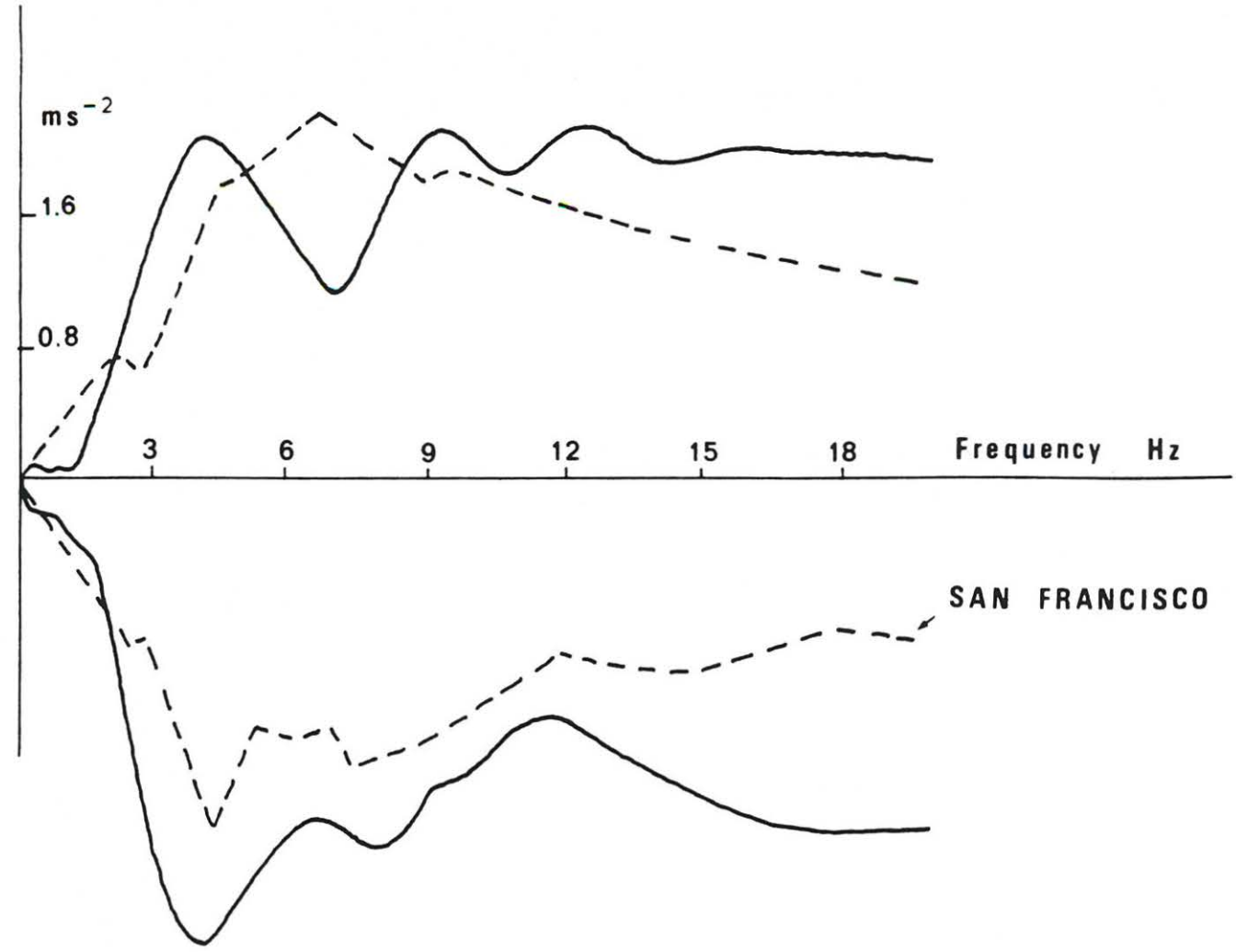

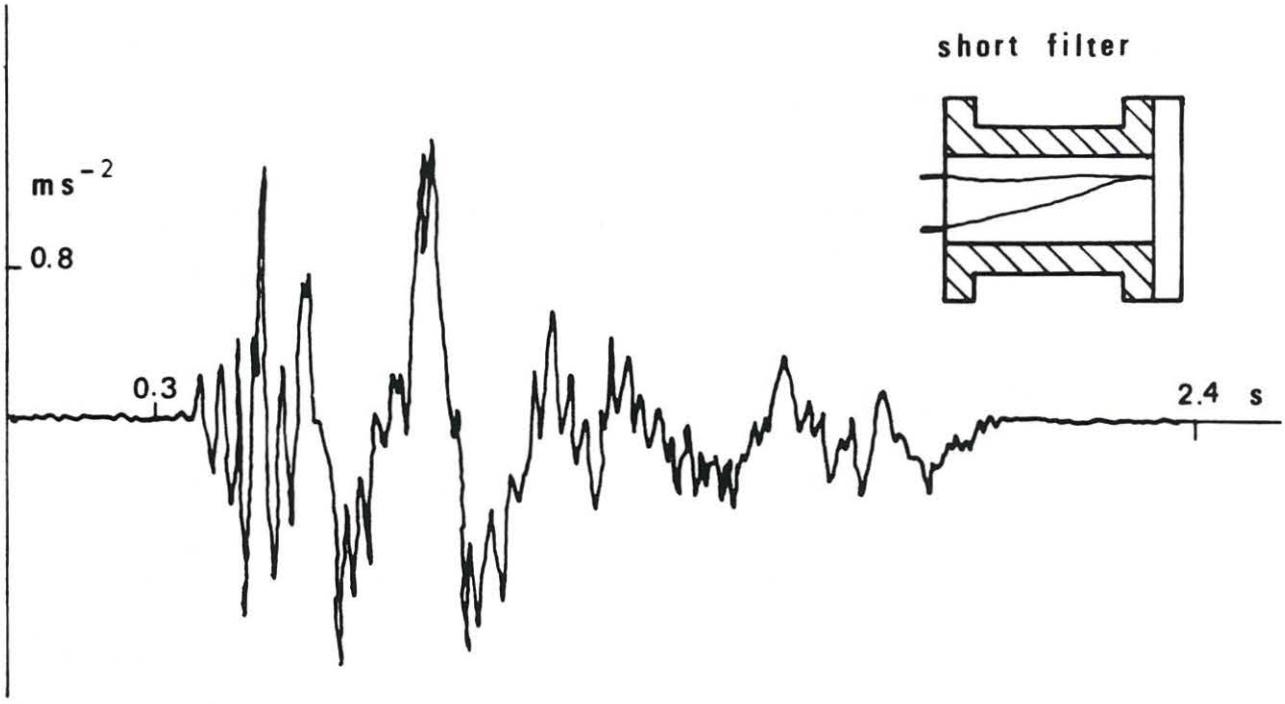

Fig.7 Spectrum of Fig.6

A1H

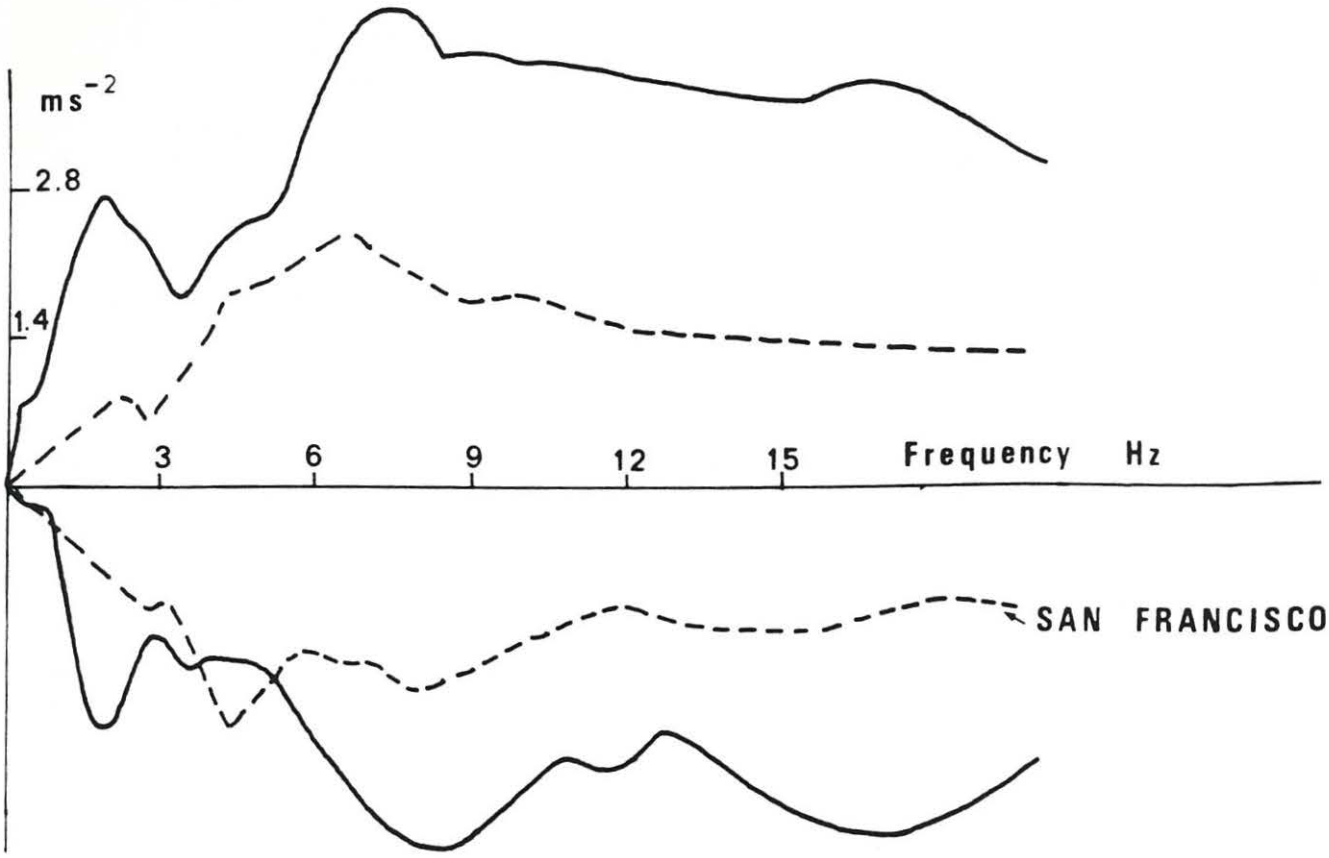

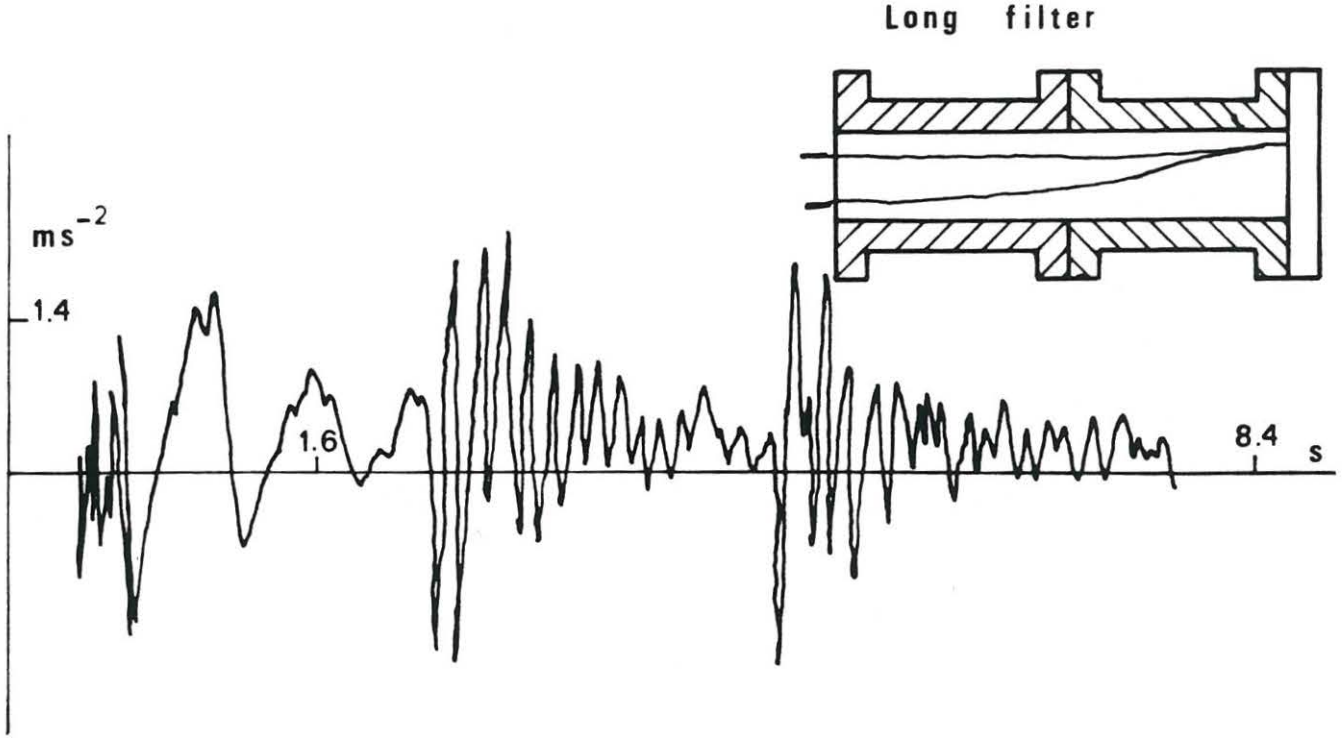

Fig. 8 Spectrum A2H

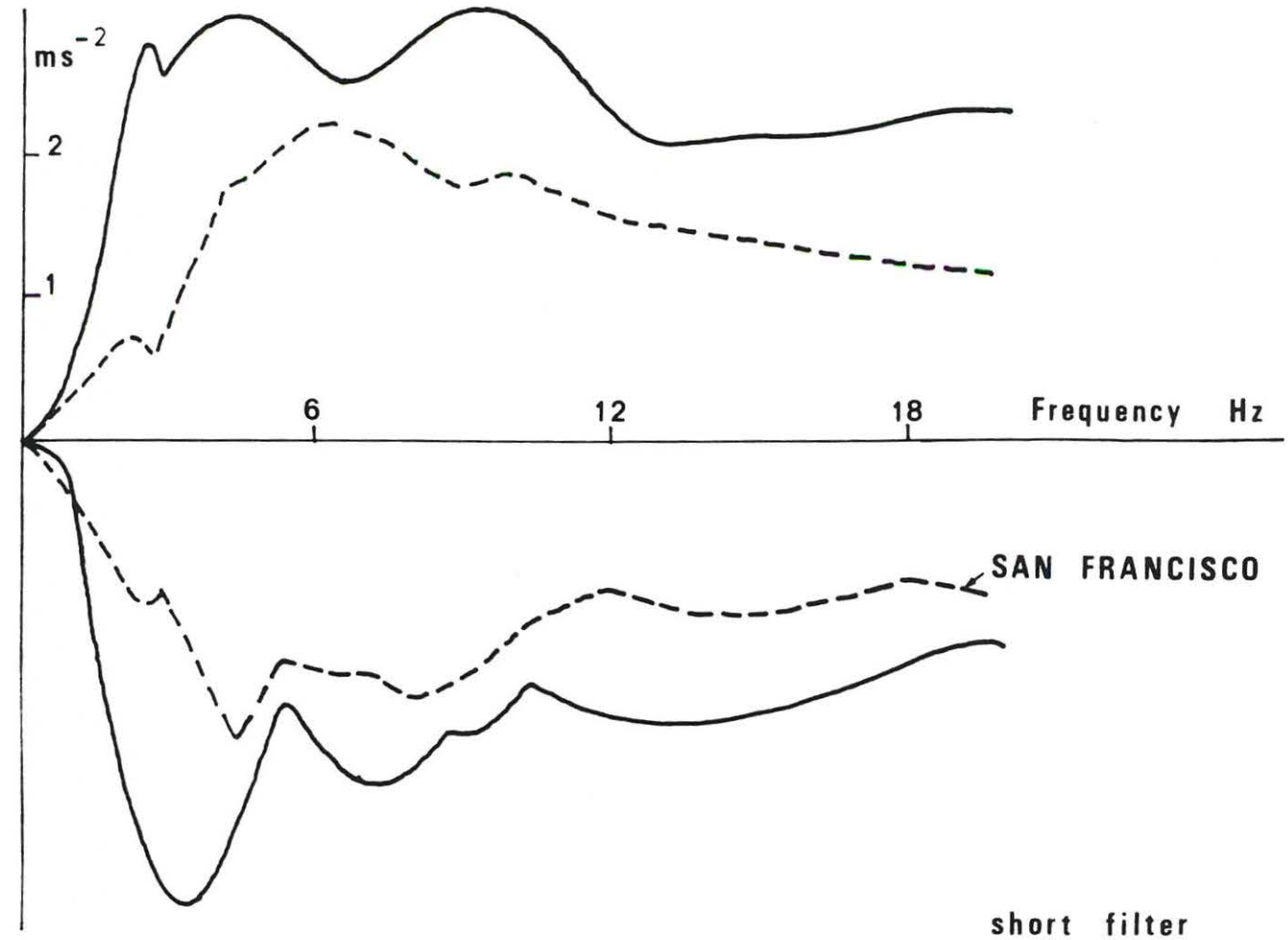

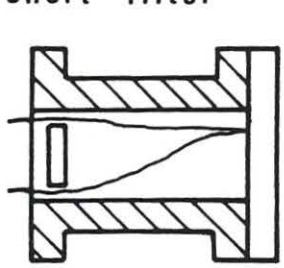

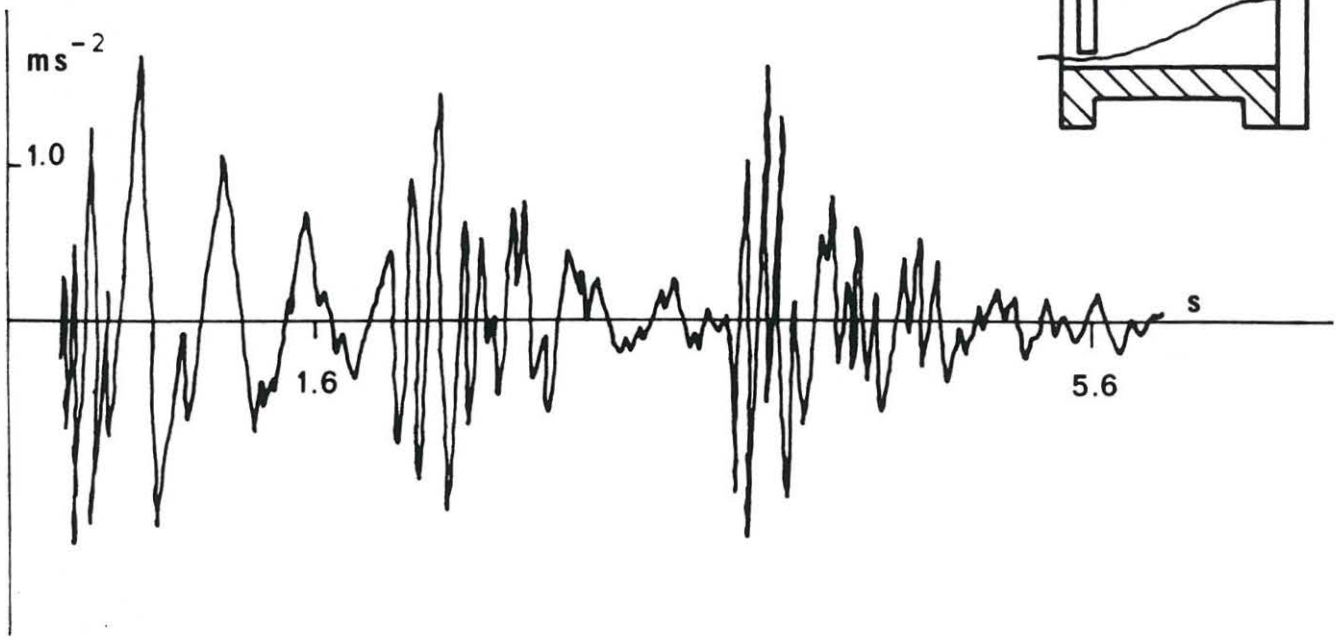

Fig. 9 Spectrum A2H

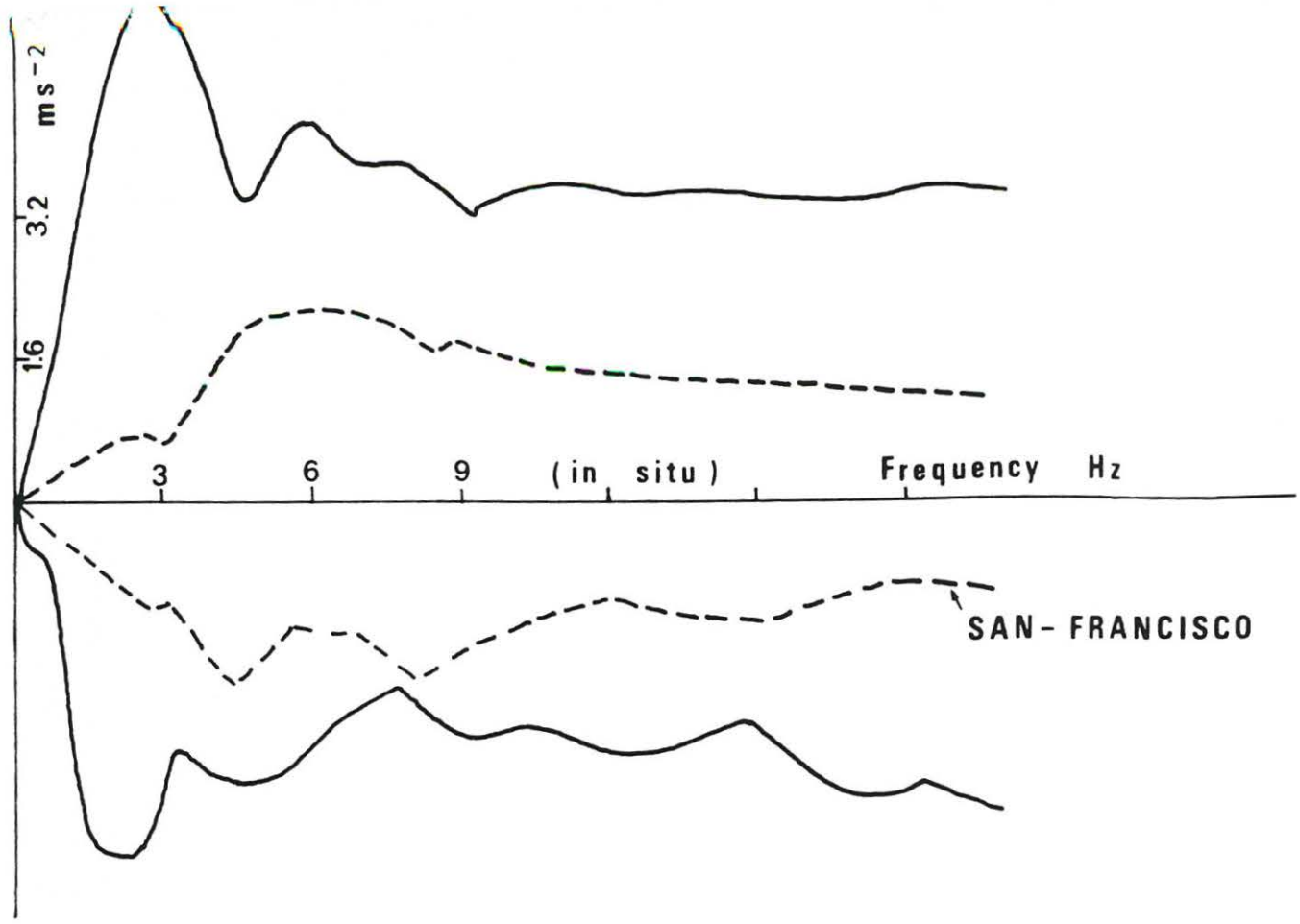

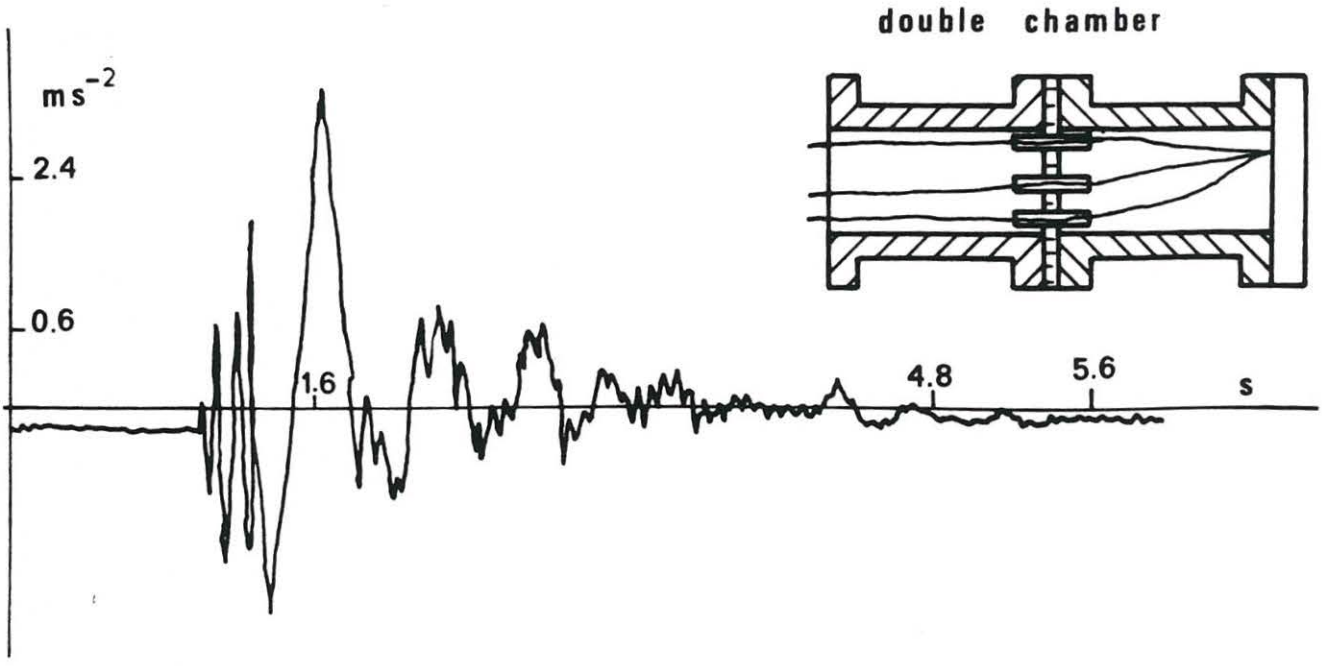

Fig. 10 Spectrum A 2H

(Damping 0.125 in all spectra)

ABSTRACTS III

EXPERIMENTS INVOLVING LIQUIFAILURE AND THE INFLUENCE OF BOUNDARIES

by

Robert V. Whitman
Massachusetts Institute of Technology
Cambridge, Massachusetts USA

Abstract

The first part of the presentation summarizes results from tests in which saturated fine sand was tested on the centrifuge at the University of Cambridge, using primarily bumpy road excitation. Tests with sand alone studied the generation and dissipation of excess pore pressures; the rate of generation and the time required for dissipation agreed with theoretical predictions, but improvements to theory were necessary in order to predict the details of the dissipation process. Tests with a simulated structure on the surface gave several interesting results which are still under investigation: reduced average pore pressures beneath structure during shaking; fluctuation of pore pressure at the forcing frequency, owing to fluctuation of total stress; horizontal migration of pore pressure following shaking and large settlements during shaking but more afterwards.

The second part examined evidence concerning the influences of the boundaries of the container for the sand. Several questions arise concerning the use of stacked ring containment. Static arching effects were observed, but may have resulted more from local arching over stress gages than from global arching within the container. The column of sand bent rather than deforming only in pure shear, but shear deformations predominated. The rings and the soil moved more-or-less together, although differences precluded using measured motions of ring to give accurate values for strains within the soil. It is concluded that use of stacked rings was quite satisfactory for preliminary experiments and for study of the generation and dissipation of excess pore pressure, but that a height/diameter ratio less than 1/2 should be used. Experiments using a rigid box for confinement revealed strong influences of the end wall, especially by restraining the large strains that tend to develop once a $\bar{\sigma}_i = 0$ condition is reached.

SYMPOSIUM ON RECENT ADVANCES IN GEOTECHNICAL MODELING
University of California at Davis, 19-20 July 1984

CRATERING MODEL VERIFICATION: A CENTRIFUGE PREDICTION VERSUS FIELD RESULT FOR A 40-TON EXPLOSIVE EVENT.

K. A. Holsapple - University of Washington FS-10, Seattle, WA 98195
R. M. Schmidt - Boeing Aerospace Co., MS 13-20, Seattle, WA 98124

The centrifuge has proved to be a powerful tool in the study of the mechanics of explosive and impact cratering. Over the past several years, centrifuge parametric studies in a variety of materials have resulted in a new understanding of the proper scaling for the phenomena,[1,2,3,4] and have resulted in new interpretations of the relatively few existing full-scale events. In addition, a few "after-the-fact" simulations of previous full-scale field events provided validation of the sub-scale technique.[5,6,7,8]

Recently, an important verification of the technique was accomplished. A centrifuge experiment at 1/200 linear scale of a complex 40-ton explosive field event was performed "before-the-fact" as a prediction of the result of that full-scale event. This example furnished a rare opportunity for a comparison of a full-scale event with a centrifuge result.

A description of that experiment and the results will be presented. The design of the experiment at this small scale required a number of compromises be made in the model. The rationale for these compromises will be presented.

The results were very gratifying. In contrast to the "state-of-the-art" numerical prediction, which proved to be in error by over 100% in volume of the crater, the single-shot centrifuge prediction was accurate to within 12%. Subsequent refinement of the model gave even better accuracy.

1. Schmidt, R. M., and Holsapple, K. A., Theory and experiments on centrifuge cratering. **J. Geophys. Res. 85(B1),** 235-252, 1980.

2. Holsapple, K. A., and Schmidt, R. M., On the scaling of crater dimensions-1: Explosive processes. **J. Geophys. Res. 85(B12),** 7247-7256, 1980.

3. Holsapple, K. A., and Schmidt, R. M., On the scaling of crater dimensions-2: Impact processes, **J. Geophys. Res. 87(B3),** 1849-1870, 1982.

4. Holsapple, K. A., A comparison of scaling laws for planetary impact cratering: Experiments, calculations, and theory (abstract). **Lunar and Planetary Science XIII,** 331-332, Lunar and Planetary Institute, Houston, 1982.

5. Holsapple, K. A., and Schmidt, R. M., A subscale simulation of two 20-ton cratering events (abstract). **EOS (Trans. Amer. Geophys. U.) 61,** 1021, 1980.

6. Schmidt, R. M., Centrifuge simulation of the JOHNIE BOY 500 ton cratering event. **Proc. Lunar and Planet. Sci. Conf. 9th,** 3877-3889, 1978.

7. Schmidt, R. M., Meteor Crater: Energy of formation – implications of centrifuge scaling. **Proc. Lunar Planet. Sci. Conf. 11th,** 2099-2128, Lunar and Planetary Institute, Houston, 1980.

8. Schmidt, R. M., Holsapple, K. A., and Piekutowski, A. J., Centrifuge simulation study of the PRAIRIE FLAT multi-ring crater (abstract). **Conference on Multi-ring Basins: Formation and Evolution,** 71-73, Lunar and Planetary Institute, Houston, 1980.

ADDENDUM

ROCK MECHANICS PROBLEMS

FACTORS IN THE DESIGN OF A ROCK MECHANICS CENTRIFUGE FOR STRONG ROCK

By

George B. Clark*

Background

Most existing geotechnical centrifuge facilities have been designed for soil mechanics research. The large dead load capacity centrifuge at Ames Labs, when completed, will provide for the testing of large soil models and may have a maximum level of g operation of 300 g's. The machine under construction at Colorado University will have a rated capacity of about 2 tons at 200 g's. The construction of these facilities show that centrifugal research has established a fundamental place in the geotechnical community in progressive national teaching and research program in soil mechanics.

Very small scale rock mechanics centrifugal testing was begun in 1930 at Columbia University, but machines for larger model weight capacity are needed for effective research with rock models (Figure 1). High costs, availability of high strength materials for rotor construction, lack of design experience, difficulties in modeling complex geologic structures, design and use of sensors, and related problems have impeded the progress of the development of rock mechanics centrifuges and this science has not advanced as rapidly as has soil mechanics. The successful development of soil mechanics centrifugal research, however, indicates that rock mechanics centrifugal research can be developed in a parallel manner.

Rock mechanics investigations to date have dealt largely with model artificial and natural rock simulating sections of stratified mine roofs, photoelastic studies with three photoelastic techniques; and with lined and unlined circular tunnels, studies of irregular underground openings, faulted structures, massive strata, and rock slopes. The principles applied to simulated cratering studies for sand can be extended to rock, taking into account its blasting resistance including the modeling of the explosive pulses induced in earth materials.

Advanced designs will be required for large high-g centrifuges for rock mechanics because larger models will be needed for more accurate simulation of geologic structures. These also must be loaded at higher body forces than provided by soil mechanics machines because of the high strengths and moduli of most natural rock materials of engineering interest. Both the dead load and g-forces also determine the stresses, loads, couples, and forces on the critical parts of the rotor, bearings,

---

*Research Professor of Mining Engineering, Colorado School of Mines, Golden, Colorado.

and supporting structures of the centrifuge. The turbulence of air in the standard centrifuge enclosure absorbs a critical amount of horsepower and generates excessive heat in the air.

The loads, stresses, rpm, and consequent kinetic and potential energies inherent in a large rock mechanics centrifuge will exceed those of machines now in operation. These factors present new design problems, and existing concepts must, thus, be extended to meet the new requirements. Their solution should be proceeded by feasibility studies planned to evaluate the projected factors involved. This will necessitate among other factors an investigation of the properties of the construction metals required, their adaptability to machine and design stress loads, their availability, and cost.

With greater loads the wear and temperature effects on bearings must be considered. The turbulence and heating of air in the enclosure by the rotor has been a continuing problem with most large centrifuges. This may be solved by operation in a partial vacuum or in a light gas atmosphere such as helium.

An underground chamber with about 100 to 150 ft of rock cover appears to be the only feasible means of obtaining the desired environment for a large high rpm rotor. This will also provide the necessary containment for flying objects in the event of an accident. Surface laboratory building structures to house such a centrifuge do not appear to be either structurally feasible or affordable cost-wise. Also, underground space is usually less costly than conventional surface building space. Other factors in a rock mechanics centrifuge construction program which must be addressed are the design of sensors and instrumentation, planning of adequate modeling facilities, site selection, and related problems. Methods of rock modeling, the uses of photoelasticity, novel methods of transmission of sensor reading, all require innovative study and planning.

Another critical aspect of the program is the proper planning of effective analysis of experimental results, such as the formulation of constitutive equations for geologic materials, synthesis of behavior patterns for rock masses, and the integration of usable concepts to this type of integrated analysis is essential to the overall success of the rock mechanics centrifugal testing program.

Some of the general types of research subjects which may be planned for the centrifuge, most of which cannot be investigated effectively by other methods of loading, are:

1. The advancement of the state-of-the-art of the modeling of medium strength rock simulant materials.

2. Use of photoelastic materials for model construction, loading, and analysis of geologic structure, their stress and failure under

continuous loading by body forces, either by stress freezing or by means of transmitted stroboscopic or polarized light through models in flight.

3. Use of stress-coat for study of continuously changing complex stress patterns in rock models by means of reflected stroboscopic light.

4. Extended study of stratified roofs of strong rocks. Only weak rocks (shales) and rock simulants have been studied to date.

5. Investigation of pre-failure stress and post-failure behavior of competent, faulted, and jointed rock masses.

6. Stress associated with underground openings, and their initial and continued failure due to static body force generated loads.

7. Effect of body force loading on intensively broken rock, rock mass behavior in caving systems of mining, support during excavation, i.e., the mechanics of arching.

8. Problems of excavation and support in intensely fractured rock, and its relation to arching.

9. Investigation of the phenomenon of arching in relatively competent geologic materials.

10. Effect of elements such as water, heat, etc.

11. Dynamic effects such as cratering in rock, dynamic stress waves impinging on underground openings, gravity induced energy release, etc., comparison with cratering in sand.

12. Experimentation with other geologic structures where body forces (gravity) cause engineering problems.

Deficiencies of Numerical Modeling

While it is fundamental to geotechnical studies, mathematical modeling offers a means of solution for only relatively simple rock structures. Their capacity for solution of complex geologic structural design problems, especially coupled problems, is limited. Brady and St. John (1982) describe more than twenty-six interrelated factors which may cause critical limitations in the application of the computational methods of geotechnical problems:

(1) Numerical instability; (2) machine dependence of source code; (3) lack of quality input data; (4) results of unspecified quality;

(5) limitations of a given modeling activity not understood, except by originator; (6) problems of design not yet solved in use of technique include (a) scale effects, (b) difficulty of testing undisturbed specimens, (c) definition of ambient conditions, (d) mechanical properties of design, (e) in situ state of stress; (7) solutions limited to parameter studies of a particular model; (8) discontinuities not taken into account; (9) inelastic response not accounted for, or is acutely difficult to deal with; (10) pilot scale in situ studies limited to observation and reformation; (11) in the use of generalized codes--complexity does not lead to more significant analysis; (12) logical methodology--includes a scheme containing a large number of critically pertinent factors; (13) must ensure execution of all elements of logic, no assurance of this in existing programs.

Further, mathematical models: (14) must use reasonably small number of elements, otherwise computer costs are excessive; (15) required geometries for codes are symmetric; this is almost never found in nature and is a serious source of error; (16) non-linear behavior presents acute problems (creep, non-elasticity, etc.) as well as non-symmetry, isotropy, etc.; (17) field tests make no contribution to code verification, but present an extra level of complexity, (this will require special procedures for evaluation, such as physical modeling); (18) qualification of codes is limited to prediction of upper and lower bounds, and may be limited to simply showing that results are consistent with historical experience; (19) most analysis is limited to two dimensional geometry; (20) for elastic and non-linear problems, plane and antiplane problems are coupled, which may create computational difficulties; (21) zones of complex behavior are small and localized requiring extra costly computational versatility, resolution questionable; (22) the large scale or small models of nuclear waste repositories may readily lead to absurd computational models; (23) use of hybrid schemes is recommended for salt repositories; (24) most existing BE and FE codes can model slip only of elastic order; (25) FE slip requires large concentration of elements near a plane of weakness; (26) site characterization now requires determination of response of mass specified load and application of an analytical method, usually with the assumption of isotropic, elastic behavior.

On the other hand, in the centrifugal modeling of bedded geologic structures, Sutherland, Schuler, and Benzley (1983) state, "...we have demonstrated that a relatively simple centrifuge model can provide a wealth of experimental data which demonstrates the complexities of geotechnical behavior...." Physical modeling in a centrifuge will not immediately provide a means to solve all complex problems in geotechnical rock mechanics modeling, it is apparent that most of the above mathematical limitations do not exist in physical modeling, and the two methods should complement each other. This type of mutually supportive planning will be required for meaningful progress.

Relevant factors are: (1) most mathematical models require isotropy or symmetry, while physical models can be of various irregular shapes and anisotropic constitution; (2) physical models are not limited within a practical range by the number of elemental blocks, their shape, or properties; (3) physical properties may be modeled according to in situ conditions, and parameters of natural materials measured; (4) boundary conditions may be designed and adjusted in the physical model to simulate many practical field conditions; (5) discontinuities can be designed into a physical model according to the ingenuity of the model fabricator; and (6) loading can be varied over a reasonable range with good simulation, less so in mathematical model, while loading adjustments in situ are usually not possible.

Modeling of Models

Strong natural rock with a high modulus of elasticity can be used currently for body force model testing only for very small models in centrifuges developing gravity fields well over 1000 g's. For other types of rock model testing, it is necessary to use simulant materials which have low strength and low moduli, particularly where the scale factor is large. Where large models are used to demonstrate body force effects on deformation and failure processes in the earth's gravity field, very low strength materials are required, the model usually being formed of uniform blocks to demonstrate the effect of joints and the degree of cementing between the blocks. Higher strength materials have been used where external loads are applied, which are at the same level of loading as that to which a model is subjected in a centrifuge such as that at Ames, i.e., where gravity loads to 300 g's may be possible.

For investigations of the behavior of full scale engineering rock masses, it has been found expedient to use physical as well as mathematical models to study critical factors in the response of rock structures to loading, the models being loaded (1) by applied loads, (2) by earth's gravity, or (3) by multiple gravity fields in geotechnical centrifuges. Much effective material modeling with very weak materials has been done in modeling large scale tectonic masses, and fairly large models of dams and open pit mines have been built and tested in the earth's gravity field. Much information is available for this type of modeling from European laboratories (Fumagalli, 1968).

However, a major current need is for the fabrication of models made of rock-like materials to simulate rock for testing of models in a centrifuge which has a maximum g-load capacity of 300 g's, and dead loads up to several tons. For example, if 600 g's is needed to test a given strong rock then that will be modeled with a simulated material with a Young's modulus and strength of, say, one-fourth of that of the prototype rock the latter can be tested at 150 g's to determine critical test parameters. These types of tests are needed

for parametric studies to correlate test results with mathematical model analysis.

While exact similitude requires compliance with the Buckingham pi theorem, which may include a large number of possible variables, the problem of material property scaling for rock mechanics investigations may be simplified, first by the assumption of elastic behavior. Where the failure of the material in the prototype is of concern, then the strengths should scale with Young's modulus. Poisson's ratio and strain are dimensionless, and, hence, automatically scale, but Poisson's ratio must be kept nearly the same in the model and the prototype only if it has an effect on critical model behavior (Clark, 1981).

Thus, if λ is the geometric scaling factor and ζ the stress ratio, then (Fumagalli, 1968)

$$\lambda = \frac{L}{L'} \tag{1}$$

and

$$\zeta = \frac{\sigma}{\sigma'} = \frac{E}{E'} = \frac{\sigma_{yield}}{\sigma'_{yield}} = \frac{\sigma_{uc}}{\sigma'_{uc}} \tag{2}$$

where the primes for the prototype, and

E = Young's modulus

σ = stress

σ_{yield} = yield stress

σ_{uc} = ultimate compressive strength

For specific gravity

$$\gamma = \sigma L^{-1} \tag{3}$$

and the specific gravity ratio

$$\rho = \frac{\nu}{\nu'} = \frac{\sigma L^{-1}}{\sigma L'^{-1}} = \zeta \lambda^{-1} \tag{4}$$

for a concentrated force

$$P = L^2 \tag{5}$$

and the scale ratio

$$\psi = \frac{P}{P'} = \frac{\sigma L^2}{\sigma L'^2} = \zeta\lambda^2 \tag{6}$$

giving two basic relations for static problems

$$\zeta = \lambda\rho \tag{7}$$

$$\gamma = \rho\lambda^2 \tag{8}$$

the stress-strain relations must follow

$$\sigma = \zeta\sigma' \tag{9}$$

$$\varepsilon = \varepsilon' \tag{10}$$

and for Mohr's diagram

$$\tau = \rho\lambda^2 \tag{11}$$

Many tests have been conducted with scaled property materials in the earth's gravity field in which case

$$G = \frac{g}{g'} = \frac{LT^{-2}}{L'T'^{-2}} = \lambda\tau^{-2} = 1 \tag{12}$$

However, in a multiple g field the relationship between Young's modulus or the stress, and the density and gravity are

$$\frac{\sigma}{\sigma'} = \frac{L}{L'} = \frac{E}{E'}\frac{\rho}{\rho'}\frac{g}{g'} \tag{13}$$

If the prototype material is used in the model and the gravity ratio is increased inversely with the length ratio, then the stresses are ideally the same at corresponding points in the model and prototype. However, if a centrifuge is not available with a large enough capacity to provide the necessary loading for a strong rock, then the moduli and strength must be reduced and if the density is changed, adjustments made for this change in the

$$\frac{p'g'}{pg} \tag{14}$$

ratio. Or, rewriting gives

$$\frac{\rho_m g_m L_m}{E_m} = \frac{\rho_p g_p L_p}{E_p} \tag{15}$$

That is, for a constant geometric scaling factor, i.e., for a model of

a desired size and shape, and simulation of a strong rock of, say, one-half the strength of Young's modulus, with reduced stress of one-half in the model, the material properties must be modeled accordingly for similitude. If fracture or yield strength are not critical within the testing range then only E need be modeled.

Although it is desirable to consider other properties of modeled materials, the first interest is in modeling rock of a higher modulus of elasticity with materials of modulus of about one-half to one-fourth that of such prototypes so that they may be used to make models to be tested in a large centrifuge at the g-levels currently available, i.e., from 100 to 300 g's. This will provide for a large number of parametric studies to fill the present gap for data for input in mathematical modeling programs.

Past research in the modeling of rock properties has been directed at (1) the fabrication of models which can be subjected to the forces on a model scale such as dams in the earth's gravity field where the moduli and strengths must be very low, and (2) the fabrication of models of higher moduli and strength for simulation of a given rock not weak enough to fail under gravity loads, but of the ratio of about 1/20 to 1/30th of the moduli and strength of the given rock (Rosenblad, 1968). The latter "rocks" are designed to be subjected to applied loads in testing machines, the models being much smaller than those designed for gravity loading in the earth's field.

Very low strength materials are usually composed of celluloid, and a variety of resins such as the epoxies, phenolic and acrylic resins. The higher strength models have been made of materials such as sand, plaster, Portland cement, kaolinite, and gypsum cements, and those have been subjected to applied loads in attempts to demonstrate the effects of loading on models made up of blocks of the material (Table 1).

In the prospective use of modeled materials for centrifugal testing rock-like materials of Class III - Moderately Strong will be needed. Those in Class II appear to have been fabricated and tested (Rosenblad, 1968, Saucier, 1967), while representative rock simulants of reasonably high strength and moduli were developed very recently by Lindberg (1982) to model granite.

The procedures described by Rosenblad (1968) were used by Haas and Clark (1970) in the fabrication of models for circular tunnels for tests of applied loading in plane stress and plane strain, as well as a test in a centrifuge. Although such modeling on a one-time basis offered some difficulties, obtaining the necessary compositions and establishing procedures was not difficult, produced the desired results, and was not difficult to repeat.

Rosenblad (1968) desired a rock-like material for a block model in simulation of a jointed schist whose physical properties were known.

Table 1

Model Material Properties

Class	Stress and Moduli	Type of Load	Materials
I.	Weak 1/1000 ratio	Earth's gravity	Sand and chemicals resins, etc.
II.	Moderately weak 1/100 to 1/20	Applied loads small models	Sand, cement, plaster
III.	Moderately strong 1/20 to 1/2	Applied loads or low-g centrifuge	Sand, cement, plaster, strong cementing materials

Although such modeling on a one-time basis offered some difficulties, obtaining the necessary compositions and establishing procedures was not difficult, produced the desired results, and was not difficult to repeat.

Rosenblad (1968) desired a rock-like material for a block model in simulation of a jointed schist whose physical properties were known. This included that the material should be economical, easily obtainable, and reproducible. It was to have an upper compressive strength of 1000 psi, a ratio of compressive to tensile strength of 20:1, and a corresponding Young's modulus. Jointed structure was provided by the block construction. Cementing agents tested in an extensive research program included Portland cement, plaster, pottery clay, and gypsum cements. For filler materials, sand was the best, although hydrated lime, kaolinite, and crushed glass were tested. Procedural factors included storage methods, types of specimens, mold release agents, batching and mixing, vibrating (a critical factor), curing, shrinkage, and procedures for specimen preparation. Plotting of results included stress-strain curves, Mohr envelopes, and tabulation and analysis of results. After considerable experimentation a material was designed which compared within reasonable limits of unconfined compressive strength, direct tensile strength, Young's modulus, cohesion, unit weight, and Poisson's ratio.

Although most small scale physical property tests of rock are conducted with cores of intact homogeneous specimens of rock, assumed to be elastic in character, the properties of rock masses are governed more by geologic structure than by the intact strength of the rock itself. Here standard engineering practice involves distorted modeling, which is used consistently in engineering application. Large scale engineering rock mechanics, therefore, is concerned with the mechanical behavior of a discontinuum. The mass strength is the residual strength,

in relation to anisotropy, determined by the bonding of the interlocking irregular blocks, and its deformability, elasticity, and Poisson's ratio result from internal displacement of the constituent blocks within the mass.

Concern is with not only the intact strength of the rock, but also the effects of microfractures, and of close to widely spaced joint systems. That is, rock mechanics deals with the behavior of small blocks and how these affect the rock mass behavior under applied loads and body forces. The density, spacing, and orientation of fractures and joints are of primary concern in the characterization of the rock mass. Thus, modeling the geologic structure of rock is of vital importance along with the details of material fabrication in all physical modeling.

The strength and other physical properties of cemented aggregate materials depend upon a number of factors which include the following:

1. Strength and moduli of fillers.
2. Strength and moduli of cements.
3. Orientation of filler grains.
4. Cohesion of materials.
5. Adhesion of materials.
6. Percent of filler cement.
7. Grain size distribution.
8. Additives.
9. Shape of grains, round, angular, etc.
10. Density of components.
11. Percent of voids.
12. Density of cemented aggregate.
13. Properties of cemented aggregate.
14. Sonic properties.

While much innovation will be required to obtain results beyond the present state-of-the-art, the problems of rock material property modeling and the modeling of geologic structure can be solved in the future as similar problems have in the past.

Rotor and Model Holder Design

Hoek (1965) presented the design equations for a small rotor for a high-g centrifuge with a constant cross-section where the radius is small and the bending moment is neglected. The arms may be constructed of bars, rods, or tubes, preferably of a light, strong metal. The total force due to the rotor mass is:

$$F_s = \int_0^{r_t} \frac{bwn^2 r}{35232}\, dr \qquad (16)$$

where

r = the radius of the rotor, in.

F_s = the total centrifugal force in the rotor, lb.

n = revolutions per minute

b = the cross sectional area of the rotor, $in.^2$

2 = the weight of the metal, $lb./in.^2$

or

$$F_s = \frac{bwn^2r^2}{2 \times 35323} = 1/2\ bwAr = b\sigma_s \tag{17}$$

and

$$\sigma_s = 1/2wAr \tag{18}$$

where

$$A = \frac{4\pi^2rn^2}{g}\text{ , number of g's at radius r} \tag{19}$$

and

g = acceleration of gravity

If the effective weight of the model and model holder are W_m and W_h, respectively, then the centrifugal force generated by them at r_t is

$$F_w = (W_h + W_m)A \tag{20}$$

where, also

$$A = \frac{rn^2}{35232} = \frac{g_m}{g} \tag{21}$$

where

g_m = gravitational acceleration at r_1 in the model

If this load is evenly distributed over the cross-sectional area b, then the stress due to F_μ is

$$\sigma_\mu = (W_h + W_m)A/b \tag{22}$$

and the total stress is

$$\sigma_t = \sigma_s + \sigma_\mu = (A\ 1/2\ wr + \frac{W_h + W_m}{b}) \tag{23}$$

For a yield stress of the metal σ_e, a stress concentration factor of 3, and a safety factor of 2, then

$$b = \frac{(W_h + W_m)}{(\sigma_e/6A - 1/2wr_t)} \tag{24}$$

For example, if a model weighs 100 lb (45.36 kg), the model holder 60 lb (27.22 kg), and with an acceleration of 1,000 g's, then

$$b = \frac{96 \times 10^4}{\sigma_e - 3{,}000wr} \tag{25}$$

and for a light metal with σ_e = 76,000 psi and 2 = 0.102, b = 15.5 in^2 for r_t = 46 in.

These design procedures may be modified for a rotor for a large centrifuge, which must be designed to take into account the bending stresses. Also an arm may be designed with a tapering cross section which increases in cross-sectional area toward the shaft to oppose the centrifugal force due to the increasing mass of that portion of the arm outward.

It may be advantageous to taper the rotor because the centrifugal force is a function of the radius. Tapering gives the least total weight, which may be desirable for large rotors.

The equation for the total force sustained by the arm may be written (Davis, 1971):

$$F_s = F_{rt} + \int_0^{r_t} \frac{bwn^2 r}{32532}\, dr \tag{26}$$

where

F_s = total force at r = 0
F_{rt} = effective weight of model and holder at r_t
b = b(r), a function of r

For a constant working stress σ_w:

$$F_s = \frac{w_T r\omega^2}{g} + \int_0^x \omega^2 w(r_t - x)b(r)dx \tag{27}$$

But

$$b(r) = \frac{F_s}{\sigma_w} \tag{28}$$

and hence

$$b(r) = \frac{w_T t_t \omega^2}{\sigma_w g} + \int_0^x \frac{\omega^2 b(r) w}{\sigma_w} (1 - x)dx \qquad (29)$$

Thus,

$$\frac{db}{dx} = \frac{w\omega^2}{\sigma_w} (r_t - x)b \qquad (30)$$

or

$$\frac{db}{b} = \frac{w\omega^2}{\sigma_w} (r_t - x)dx \qquad (31)$$

which is integrated to yield

$$\ln b = \frac{w\omega^2}{\sigma_w} (r_t x - \frac{x^2}{x}) + C_o \qquad (32)$$

At $x = 0$, with a payload w_t and acceleration A at r_t

$$\ln b_{x=o} = \ln \frac{Aw_T}{\sigma_w} = C_o \qquad (33)$$

and

$$b = C_1 \, e \, \frac{w\omega^2}{\sigma_w} (r_t x - \frac{x^2}{x}) \qquad (34)$$

but

$$r = r_t - x; \; x = r_t - r \qquad (35)$$

and

$$b = \frac{Aw_T}{\sigma_w} \exp[\frac{w\omega^2}{2\sigma_w} (r_t^2 - r^2)] \qquad (36)$$

Thus the weight of the rotor arms may be decreased by a factor of about 10 percent if the arm is tapered, and the cost of fabrication of a tapered arm should be considered.

Stress Fields in Large Centrifuged Models

The model rock beams tested in centrifuges at Columbia University, U.S. Bureau of Mines, Upsalla University, and the University of Missouri

at Rolla, were placed in centrifuges with the long dimensions of the beams parallel to the axis of rotation of the centrifuge. Hence, the curvature of the path of rotation had a negligible effect on the force field in the beam. However, in the testing at Sandia by Sutherland and in South Africa by Hoek, the axes of the models were perpendicular to the axes of rotation of the centrifuges. Further, the rotor itself in the very high-g centrifuge (20,000) at Queen's University is a rotating disk. The centrifugal field is, of course, the same in each case, and the force at a radial distance r is defined by $\rho\omega^2 r$. The stresses in bodies of various shapes is of interest, particularly in the case of large rock models where the g forces will be greater than those usually used for testing soil models.

Timoshenko and Goodier (1951) have analyzed the stresses due to centrifugal force in thin and thick rotating disks, which analyses serve as bases for evaluating the stresses in rotating bodies with other shapes and boundary conditions. Where the thickness of a disk is constant and is small compared to the radius the equation of equilibrium and the body force is equal to

$$\frac{\partial \sigma_r}{\partial r} + \frac{\sigma_r - \sigma_\theta}{r} + R = 0 \tag{37}$$

$$R = \rho\omega^2 r \tag{38}$$

which gives

$$\frac{d}{dr}(r\sigma_r) - \sigma_\theta + \rho\omega^2 r^2 = 0 \tag{39}$$

For a stress function F

$$r\sigma_r = F, \quad \sigma_\theta = \frac{dF}{dr} + \rho\omega^2 r^2 \tag{40}$$

The strain components are

$$\varepsilon_r = \frac{du}{dr}, \quad \varepsilon_\theta = \frac{u}{r} \tag{41}$$

or

$$\varepsilon_\theta - \varepsilon_r + r\frac{d\varepsilon_\theta}{dr} = 0 \tag{42}$$

and

$$r^2\frac{d^2F}{dr^2} + r\frac{dF}{dr} - F + (3 + \nu)\rho\omega^2 r^3 = 0 \tag{43}$$

whose

$$F = Cr + C_1 \frac{1}{r} - \frac{3 + \nu}{8} \rho\omega^2 r^3 \tag{44}$$

and

$$\sigma_r = C + C_1 \frac{1}{r^2} - \frac{3 + \nu}{8} \rho\omega^2 r^2 \tag{45}$$

$$\sigma_\theta = C - C_1 \frac{1}{r^2} - \frac{1 + 3\nu}{8} \rho\omega^2 r^2 \tag{46}$$

where the constants C and C_1 are determined from the boundary conditions. For a <u>solid disk</u> $C_1 = 0(g)$ and $r = b$ with no applied forces

$$C = \frac{3 + \nu}{8} \rho\omega^2 b^2 \tag{47}$$

$$\sigma_r = \frac{3 + \nu}{8} \rho\omega^2 (b^2 - r^2) \tag{48}$$

$$\sigma_\theta = \frac{3 + \nu}{8} \rho\omega^2 b^2 - \frac{1 + 3\nu}{8} \rho\omega^2 r^2 \tag{49}$$

These stresses are greatest at the center of the disk, where

$$\sigma_r = \sigma_\theta = \frac{3 + \nu}{8} \rho\omega^2 b^2 \tag{50}$$

For a disk with a <u>circular hole</u> of radius a at the center and no forces acting on the boundaries,

$$\sigma_r = \frac{3 + \nu}{8} \rho\omega^2 \left(b^2 + a^2 - \frac{a^2 b^2}{r^2} - r^2\right) \tag{51}$$

$$\sigma_\theta = \frac{3 + \nu}{8} \rho\omega^2 \left(b^2 + a^2 + \frac{a^2 b^2}{r^2} - \frac{1 + 3\nu}{3 + \nu} r^2\right) \tag{52}$$

The maximum radial stress is at $r = \sqrt{ab}$, where

$$(\sigma_r)_{max.} = \frac{3 + \nu}{8} \rho\omega^2 (b - a)^2 \tag{53}$$

the maximum tangential stress is at $r = a$

$$(\sigma_\theta)_{max.} = \frac{3 + \nu}{4} \rho\omega^2 \left(b^2 + \frac{1 - \nu}{3 + \nu} a^2\right) \tag{54}$$

and is larger than $(\sigma_r)_{max}$.

For a stress distribution symmetrical with respect to the axis of rotation, but a disk of greater thickness, the differential equations of equilibrium are

$$\frac{\partial \sigma_r}{\partial r} + \frac{\partial \tau_{rz}}{\partial z} + \frac{\sigma_r - \sigma_\theta}{r} + \rho\omega^2 r = 0 \tag{55}$$

$$\frac{\partial \tau_{rt}}{\partial r} + \frac{\partial \sigma_z}{\partial z} + \frac{\tau_{rz}}{r} = 0 \tag{56}$$

and the compatibility equations become

$$X = \rho\omega^2 y, \quad Y = \rho\omega^2 y, \quad Z = 0 \tag{57}$$

This gives

$$\nabla^2 \sigma_r - \frac{2}{r^2}(\sigma_r - \sigma\theta) + \frac{1}{1+\nu}\frac{\partial^2 \Theta}{\partial r^2} = -\frac{2\rho\omega^2}{1-\nu} \tag{58}$$

$$\nabla^2 \sigma\theta + \frac{2}{r^2}(\sigma_r - \sigma\theta) + \frac{1}{1+\nu}\frac{1}{r}\frac{\partial \Theta}{\partial r} = \frac{2\rho\omega^2}{1-\nu} \tag{59}$$

$$\nabla^2 \sigma_z + \frac{1}{1+\nu}\frac{\partial^2 \Theta}{\partial z^2} = -\frac{2\nu\rho\omega^2}{1-\nu} \tag{60}$$

And finally the stresses for a disk of uniform thickness are found to be

$$\sigma_r = \rho\omega^2\left[\frac{3+\nu}{8}(a^2 - r^2) + \frac{\nu(1+\nu)}{6(1-\nu)}(c^2 - 3z^2)\right] \tag{61}$$

$$\sigma\theta = \rho\omega\left[\frac{3+\nu}{8}a^2 - \frac{1+3\nu}{8}r^2 + \frac{\nu(1+\nu)}{6(1-\nu)}(c^2 - 3z^2)\right] \tag{62}$$

Compared with the solution for this disk there are additional terms $(c^2 - 3z^2)$. The stresses are small for a thin disk and their resultant is zero. If the rim of the disk is free from external forces, the solutions (62) give the state of stress in the disk some distance from the edge.

Radial Columns

For a thin slab shaped model in a holder, the tangential stresses usually play a minor part, and the radial stresses are counteracted by the holder. The same procedure may be used to determine the radial stresses in the model, the rotor, and the model holder, as was done by both Hoek (1965) and by Davis (1971).

The following assumptions are made for the mathematical evaluation of radial stresses in the model (and rotor):

1. The rock is homogeneous in density, uniform in composition, etc.

2. It is of intact structure, i.e., has no faults, joints, etc., which will affect the radial stress distribution.

3. It is of uniform thickness but is thin relative to the length of the radius of the rotor.

4. Lateral effects in the direction of rotation very near the axis of rotation are ignored, those at greater radii are negligible.

5. If the plane of the model is normal to the axis the tangential stresses may affect the overall stress distribution.

6. The thickness of the model will determine conditions of plane stress or strain.

7. For the purposes of the following analysis the curvature of the centrifugal field may be neglected.

8. As a result the tangential stress which are normal to the radial stresses may be neglected.

The radial stresses in a model, or in the rotor, may be determined for either a model of height $r_2 - r_1$ or of the model extending to the axis of the centrifuge, although the latter never occurs in practice (Figure 2). The centrifugal force acting on an element of unit width and thickness, and depth dr, results in a stress $d\sigma_r$, or

$$(d\sigma_r + \frac{\partial \sigma_r}{\partial r} dr) - d\sigma_r = \rho\omega^2 r dr \qquad (63)$$

which reduces to

$$d\sigma_r = \rho\omega^2 r dr \qquad (64)$$

and upon integration

$$\sigma_r = \rho\omega^2 \int_{r_1}^{1} r\,dr = \frac{\rho\omega^2}{2}(r^2 - r_1^2) \qquad (65)$$

and at the bottom of the model:

$$\sigma_r = \frac{\rho\omega^2}{2}(r_2^2 - r_1^2) = \rho\omega^2\left(\frac{r_2 + r_1}{2}\right)(r_2 - r_1) \qquad (66)$$

The effective average gravity in the model is $\rho\omega^2(r_2 + r_1)/2$ acting at the geometric center of $(r_2 - r_1)$. Hoek (1965) showed that the relationship between the stress in rock in situ due to the earth's gravity and that in a model in a 53 inch diameter centrifuge, and that the difference between the two is quite small.

If a model is rotated with a large dimension normal to the axis then the lateral (tangential) stress must be taken into account, and also if the model is parallel to the axis but is thick relative to its height. In the model holder the radial stress is opposed by the stresses in the rotor (see rotor design). For the radial stresses in a rotating disk with internal and external radii a and b the maximum radial stress is at $r = \sqrt{ab}$ and the maximum stress is smaller than that in a column. This principle was probably used in the design of the Queen's University centrifuge rotor.

For the determination of the radial (tensile) stresses in the arm of uniform cross section, and the (compressive) stresses in a model which extends the complete length of the radius its value is given by

$$\sigma_r = \pm \frac{1}{2}\rho\omega^2 r^2 \qquad (67)$$

where

n = rpm

ρ = density of arm or model

w = unit weight of material, lb/cu in.

r_t = radius of rotation, inches

r = radial stress, psi

The stress equation may also be written

$$\sigma_r = \pm \frac{1}{2} wAr_t \qquad (68)$$

where

A = number of g's acceleration at r_t.

For a model of (radial) depth $(r_2 - r_1) = h$ the radial stress is

$$\sigma_r = \frac{1}{2} \frac{wn^2}{35323} (r_2^2 - r_1^2) \qquad (69)$$

An example of the variation of stresses in a 5 foot model in a large centrifuge with a 35 foot arm is given in Table 2.

Table 2

Radial Stress in Centrifuged Model

h = 5 ft r_1 = 30 ft r_2 = 35 ft

rpm	r's at r_2	$r_1\sigma_r+1/2h$	σr_2
100	119	319	664
125	185	498	1037
150	268	718	1495
175	364	978	2035
200	476	1278	2658
225	602	1620	3364
250	743	1993	4150
275	890	2412	5021
300	1071	2871	5976

Or for the smaller centrifuge dimensions but with the same model height, the stresses are given in Table 3.

Table 3

Radial Stresses in Centrifuged Model

h = 5 ft r_1 = 10 ft r_2 = 15 ft

rpm	r's at r_2	$r_1+1/2h$	r_2
100	51	141	255
125	79	218	398
150	115	315	573
175	156	428	780
200	204	560	1020
225	258	708	1290
250	318	875	1593
275	385	1058	1928
300	659	1260	2295

That is, if the model height and the radial stresses are kept at a constant value, and the rotor radius is decreased then the rpm must be increased (Figures 4 and 5) as well as the g-level.

In the radial stress equation for a model if the size of the centrifuge is increased and the stress at the bottom of the model is to be kept constant, and all dimensions are scaled, both of the centrifuge and model, then

$$\frac{\sigma_r}{\sigma'_r} = 1 = \frac{n^2(r_2^2 - r_1^2)}{n'^2(r'^2_2 - r'^2_1)} \tag{70}$$

or

$$\frac{n'^2}{n^2} = \frac{(r_2^2 - r_1^2)}{r'^2_2 - r'^2_1} \tag{71}$$

and required rpm varies inversely with the radius.

As given elsewhere, the stress in the rotor due to the weight of the rotor itself is

$$\sigma_a = \frac{1}{2} wAr_t \tag{72}$$

or the stress increases directly with the number of g's and with the length of the arm (see also rotor design).

A basic factor is that if the height of a rock model is to be scaled with the same linear scaling factor γ as the rotor radius for constant maximum stress at a representative point in the model, then

$$\gamma^2 = n^2/n'^2 \tag{73}$$

at a radius r_2,

$$g = \frac{n^2 r_2}{35232} \tag{74}$$

and at r'_2

$$g' = \frac{n^2 r'_2}{35232} \tag{75}$$

or

$$\frac{g}{g'} = \frac{n^2 r_2}{n'^2 r'_2} = \gamma \tag{76}$$

Thus, if the model and rotor are both linearly increased in dimension for the same stress at r_2 the number of g's required at this radius is smaller by the inverse of the scaling factor. This same loading principle, i.e., decrease of required body force required to stress a model also holds for beams as described earlier.

Beam Scaling Factors

In both of the gravitational fields in the earth's crust and in models loaded in a centrifuge the stresses in geologic rock structures may be caused by two mechanisms:

1. Those due to the direct body force loading in a member of the structure, such as an isolated beam loaded by its own weight, and

2. Those induced by the stress field created by the whole mass, such as the stresses caused by the weight of the overburden, including the horizontal stresses caused by Poisson's ratio effects.

A separated stratum of an in situ horizontal lying mine roof is subject to a direct body force which is uniformly distributed throughout the beam and acts in a vertical direction. The restrained ends are held vertically by the weight (body force stress field) of the overburden, constituted of a load acting downward and an upward reaction. In addition there may be a horizontal component to the accompanying induced pressure (stress). Tectonic forces would also add components, but these are not usually directly gravity induced in the same sense as the other stress fields.

The beam above the first, which is in contact with the stratum above it, is acted on by the same stresses due to the beam's own weight plus a distributed load on its top surface due to the interaction there.

The body force loading of simple and restrained beams either by gravity or by a body force in a geotechnical centrifuge is of engineering interest because sections of competent stratified mine roofs can in many cases be represented by elastic beams. The assumption of elasticity is necessary to the mathematical solution of the equations of equilibrium, etc., for restrained beams. The elastic constant, Poisson's ratio, enters only in the equations for horizontal stress for restrained beams and a simple beam loaded in a centrifuge. The plane stress distribution may be obtained mathematically by use of the Airy stress function, equations for equilibrium, etc. (Caudle and Clark, 1955). It was noted in this analysis that in order to obtain a comparison of the magnitude of stresses in (a) beams with a uniform load, (b) beams loaded by their own weight, and (c) beams loaded in a centrifuge, that the uniform load q had to be set equal to $2 c\rho g$ for a beam loaded by its own weight and $wc\rho r_o\omega^2$ for a beam loaded in a centrifuge. (Tables 4 and 5.)

Table 4

Compilation of Stress Equations for Simple Beam Loaded by Three Type Loads

No.	Total Load	σ_x	σ_y	τ_{xy}
1A	Uniform Load	$\sigma_x=\frac{3qy}{4c^3}(l^2-x^2)+\frac{qy}{2c^3}\left(y^2-\frac{3c^2}{5}\right)$	$\sigma_y=\frac{qy}{4c^3}(3c^2-y^2)-\frac{q}{2}$	$\tau_{xy}=-\frac{3qx}{4c^3}(c^2-y^2)$
1B	Loaded by Own Weight	$\sigma_x=\frac{3\rho gy}{2c^3}(l^2-x^2)+\frac{\rho gy}{c^3}\left(y^2-\frac{3c^2}{5}\right)$	$\sigma_y=\frac{\rho gy}{2c^3}(c^2-y^2)$	$\tau_{xy}=-\frac{3\rho gx}{2c^2}(c^2-y^2)$
1C	Centrifugal Loading	$\sigma_x=\frac{3\rho\omega^2r_oy}{2c^3}(l^2-x^2)+\frac{\rho\omega^2r_oy}{c^3}\left(y^2-\frac{3c^2}{5}\right)+\frac{\nu\rho\omega^2}{2}\left(\frac{c^2}{3}-y^2\right)$	$\sigma_y=\frac{\rho\omega^2}{2}(c^2-y^2)\left(\frac{r_oy}{c^2}+1\right)$	$\tau_{xy}=-\frac{3\rho\omega^2r_ox}{2c^2}(c^2-y^2)$

Table 5

Compilation of Stress Equations for Restrained Beam Loaded by Three Type Loads

No.	Total Load	σ_x	σ_y	τ_{xy}
11A	Uniform Load	$\sigma_x=\frac{3qy}{4c^3}(l^2-x^2)+\frac{qy}{2c^3}\left(y^2-\frac{3c^2}{5}\right)-\frac{qy}{2c}\left(\frac{l^2}{c^2}-\frac{3}{5}-\frac{3\nu}{2}\right)$	$\sigma_y=\frac{qy}{4c^3}(3c^2-y^2)-\frac{q}{2}$	$\tau_{xy}=-\frac{3qx}{4c^3}(c^2-y^2)$
11B	Loaded by Own Weight	$\sigma_x=\frac{3\rho gy}{2c^3}(l^2-x^2)+\frac{\rho gy}{c^3}\left(y^2-\frac{3c^2}{5}\right)-\rho gy\left(\frac{l^2}{c^2}-\frac{3}{5}-\frac{\nu}{2}\right)$	$\sigma_y=\frac{\rho gy}{2c^3}(c^2-y^2)$	$\tau_{xy}=-\frac{3\rho gx}{2c^3}(c^2-y^2)$
11C	Centrifugal Loading	$\sigma_x=\frac{3\rho\omega^2r_oy}{2c^3}(l^2-x^2)+\frac{\rho\omega^2r_oy}{c^3}\left(y^2-\frac{3c^2}{5}\right)+\frac{\nu\rho\omega^2}{2}\left(\frac{c^2}{3}-y^2\right)-\rho r_o\omega^2y\left(\frac{l^2}{c^2}-\frac{3}{5}-\frac{\nu}{2}\right)$	$\sigma_y=\frac{\rho\omega^2}{2}(c^2-y^2)\left(\frac{r_oy}{c^2}+1\right)$	$\tau_{xy}=-\frac{3\rho\omega^2r_ox}{2c^2}(c^2-y^2)$

These factors contain a linear dimension of the beam c. Thus, while the stress equations for a uniformly loaded beam are dimensionless for a normalized stress $\sigma_x/2$, the terms for normalized stresses $\sigma_x/\rho g$ and $\sigma_x/\rho\omega^2 r_o$ caused by body forces are not. That is, for geometrically similar beams where the dimensions ℓ and c of a unit beam are increased, the stress at corresponding points in similar beams is the same for a uniform load q. As the dimensions of beams are increased in proportion, in the beams loaded by (b) or (c), however, the maximum stresses all increase with the increase of linear dimensions for which the loading parameters are held constant. For constant stress the body force load is decreased directly with increase of model dimension.

Of particular interest are the critical stresses which may cause fracture initiation (Figure 6). The stress in the bottom fiber at the center is proportional to ℓ^2/c, which mean that the beam stresses increase with the dimensions at a constant body force load. The same types of increase of stresses occur for the vertical and shear stresses, although all do not increase in direct proportion to the scale factor of the beam size. In practice for very large beams with conventional applied loads, it would become necessary to consider the stresses due to gravity.

Arching of Incompetent Geological Materials

The arching of roofs of underground excavations in broken rock such as mines and underground power stations, etc., illustrates the well known phenomenon of the transfer of stresses in sands, soils, and broken rock when they are excavated and contain foreign structures. The loads in the rock and on the structures are due entirely to gravity body forces. The mechanical action of the materials is also related to the occurrence of hang up of fine and coarse materials in bins and chutes which cause well-known engineering problems. Such phenomena are all controlled by material properties, but flow and stability are ultimately determined by the force of gravity.

Quantitative experimental arching studies have been made (1) with fine sands with three types of material-structure interaction, as well as (2) centrifugal studies of the arching of competent rock, both massive and layered, and (3) qualitative studies of the behavior of weak, incompetent geologic structures around tunnels. This behavior of coarse broken ore in mine chutes is closely associated, as is the flow and instability of broken ore in caving methods of mining.

Arching tests with fine sand have used the following mechanisms to evaluate the transfer of load of the material overlying an excavation or included structure by: (1) dropping of a trap door under a sand column in a box, (2) raising of a trap door, and (3) the inclusion of movable structures in the sand. The pressure on the door or structure or the pressure in the sand indicates the load transfer, and while early experiments used

only the weight of the sand column, later research included the effects of applied surface pressure. These conditions have two deficiencies, (1) the pressure distribution as with similar soil mechanics situations, are inadequate to demonstrate the effects of gravity, and (2) applied pressures likewise do not simulate the effects of body force loads.

With the exception of the simple trap door experiment the effects of gravity are not simulated. This can be effectively done in a centrifuge where the important factors affecting the material behavior can be modeled. In a current military engineering problem in deep basing and egress through fractured and rubble rock materials, the detailed mechanics of stability of flow of either heterogeneous or relatively uniform broken materials are not known. A large centrifuge would provide a means of determining their important behavioral parameters during and after excavation. Specific parameters which require simulation to give representative engineering data include body force loading and resultant pressure distribution, pressure magnitudes, comparable internal friction, structure interaction, means for instrumentation, and general observable results of large model similitude studies.

Rock Mechanics Centrifuge Facility

Of the large (greater than 8 ft diameter) geotechnical centrifuges currently in operation none have a body-force capacity above 300 g's. However, the principles which have been learned in the successful design of these machines have established a foundation of engineering information for the effective design of centrifuges of larger diameters for critical machine elements for higher g loads needed for rock mechanics, particularly the rotor and bearings. The methods of analysis of power source and power drive problems are well established, and electric, gear box, and hydraulic drives have all been employed.

The construction of a centrifuge chamber to provide both safety and a low pressure, partial vacuum for low-power operation can economically utilize a sealed underground chamber excavated in competent rock. Design features will include rock support problems, sealing the rock and design of air-tight doors, and defiladed entrance ways to prevent flight of high velocity objects, etc. An adequate vacuum pump system may be designed of moderate capacity. The chamber will probably be excavated by drill and blast, supported with roof bolts, sealed with liquid grout, shotcreted, and provided with air scoops to assist the rotor in the air evacuation process. Instrumentation systems may be made and installed for model observation and instrumentation. Existing types of sensors and instruments employed in soil mechanics centrifugal testing may be utilized where applicable, catalogued for potential use, and the proven techniques used in rock mechanics research.

The special innovative requirements for a support model shop for the effective design and fabrication of models must be planned to include the preparation of artificial and natural rock models, photoelastic models, use of stress-coat, sensor installation and testing, debugging, and all related fabrication and model mounting operation. A method is needed for checking out instrumentation and sensors on an experimental setup can be designed which will not occupy the centrifuge itself during the debugging process.

Recommendations may be formulated from the information similar to that given in this paper for sizes of machines that will serve for the foundation of a phased program in the development of a rock mechanics facility. This can be initiated with a relatively small machine for which the components are more easily proved out. Then a larger machine may be constructed, its design based upon research findings and well defined requirements. A cost analysis will be needed for the design, construction and operation phases of an effective facility for possible machine sizes and capacities which are found to be best adapted for rock mechanics research.

Rock model design is rapidly developing as an art and science, and two decades of experience in geotechnical mathematical modeling can be integrated into a combined, fruitful program of study.

References

Brady, G. H. G., and St. John, C. M., (1982), The role and credibility of computational methods in engineering rock mechanics, 23rd Symposium on Rock Mechanics, University of California.

Caudle, R. D., and Clark, G. B., (1955), Stresses around mine openings in some simple geologic structures: University of Illinois Engineering Experimental Standard Bulletin 430.

Clark, G. B., (1980), Geotechnical centrifuges for model studies and physical property testing of rock and rock structures: Quarterly, volume 76, number 4, Colorado School of Mines.

Davis, J. O., (April 1971), Development of large, high-performance centrifuges, SC-DR-710164, Sandia Laboratories, 62 pp.

Fumagalli, E., (1968), Model simulation in rock mechanics problems: Rock Mechanics in Engineering Practices, chapter 11, Wiley.

Haas, C. J., and Clark, G. B., (July 1970), Experimental investigation of small scale lined and unlined cylindrical cavities in rock-like materials, University of Missouri School of Mining, Rolla, Missouri, Technical Report Number AFWL-TR-70-58, 191 pp.

Hoek, E., (1965), The design of a centrifuge for the simulation of gravitational force fields in mine models: Journal of South African Institute of Mining and Metallurgy, volume 65, number 9.

Lindberg, H. E., (August 1982), Tunnel response in jointed rock: 23rd Symposium on Rock Mechanics, Berkeley, California.

Rosenblad, J. L., (May 1968), Development of a rock-like material: 10th Symposium on Rock Mechanics, Austin, Texas.

Saucier, K. L., (1967), Development of material for modeling rock: USAE WES Miscellaneous Paper 6-934.

Sutherland, H. H., Schuler, K. W., and Benzley, S. E., (1983), Numerical and physical simulations of strata movement, In Situ, volume 7, number 1, pp. 87-113.

Timoshenko, S., and Goodier, J. N., (1951), Theory of elasticity: McGraw-Hill, New York.

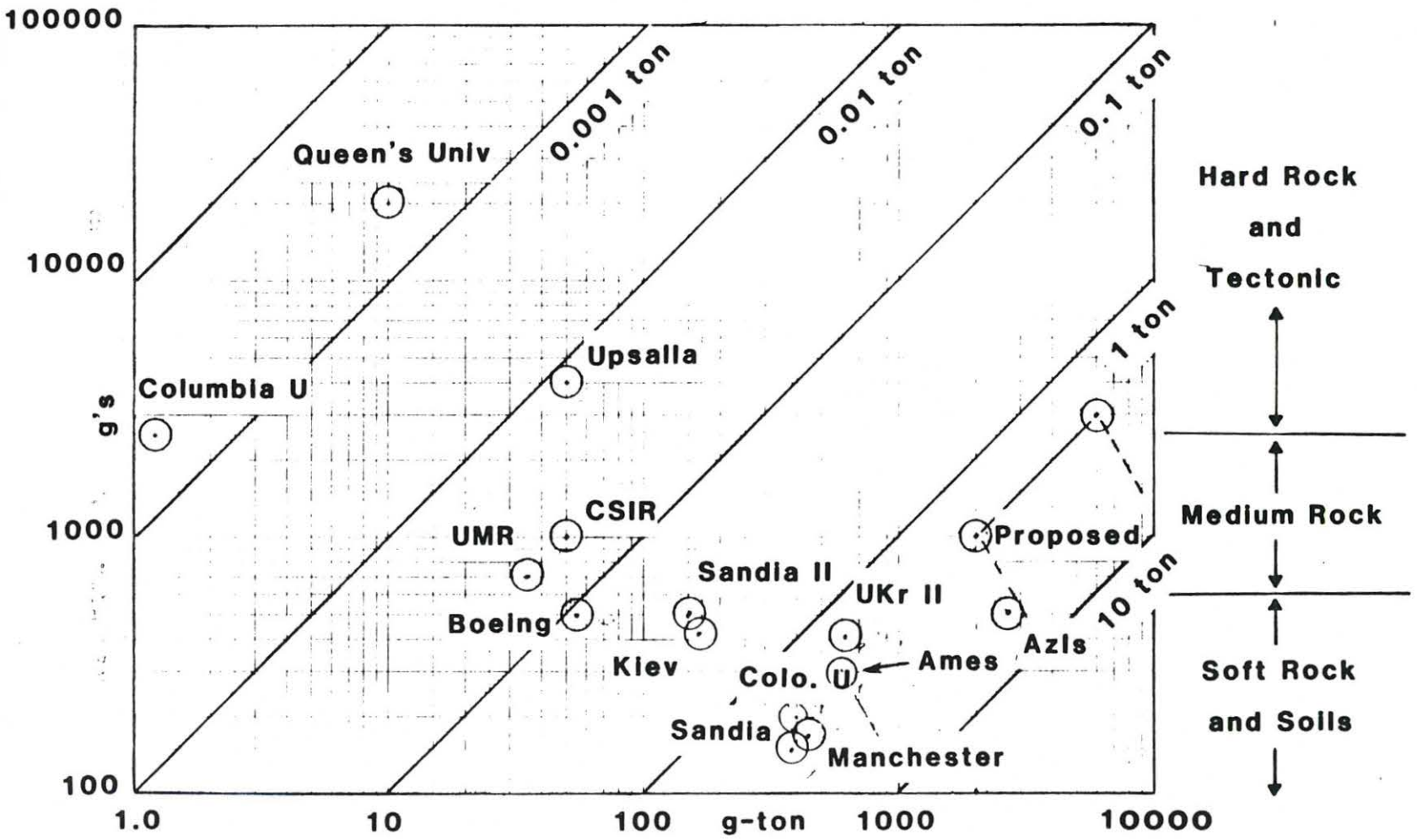

Figure 1. Capacities of known centrifuges and proposed rock mechanics centrifuge

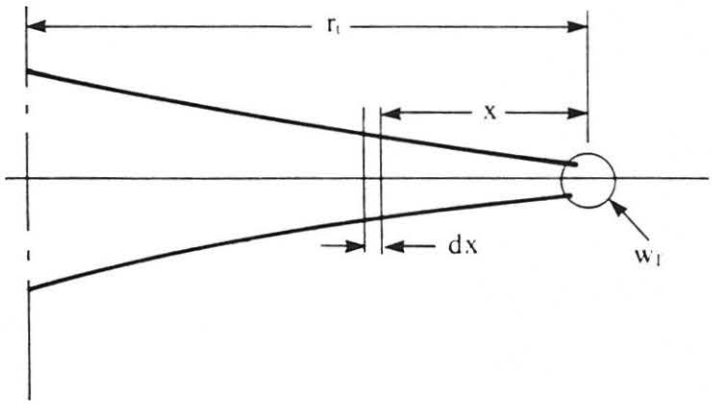

Figure 2 .--Tapered arm schematic

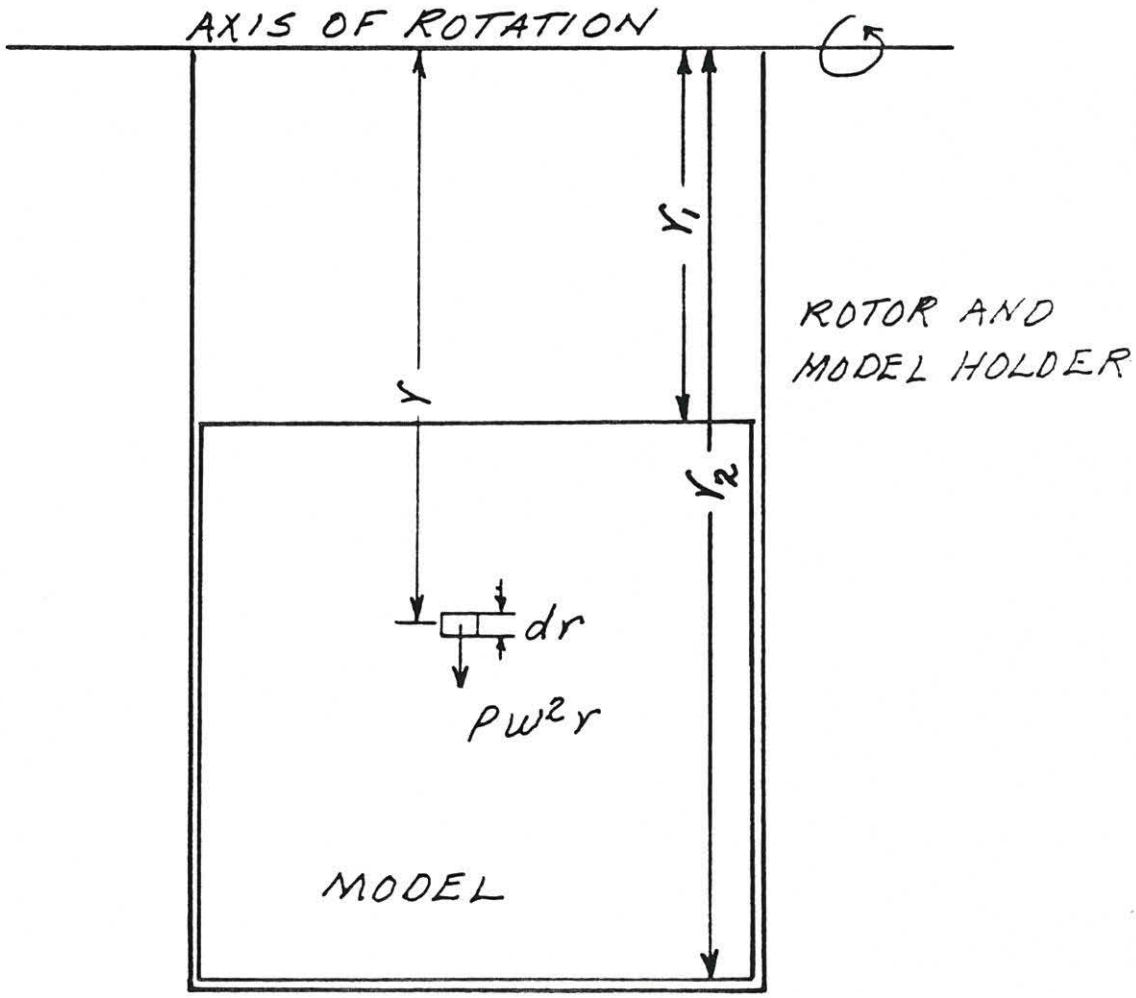

Figure 3.--Diagramatic sketch of rotor with model mounted parallel to axis of rotation.

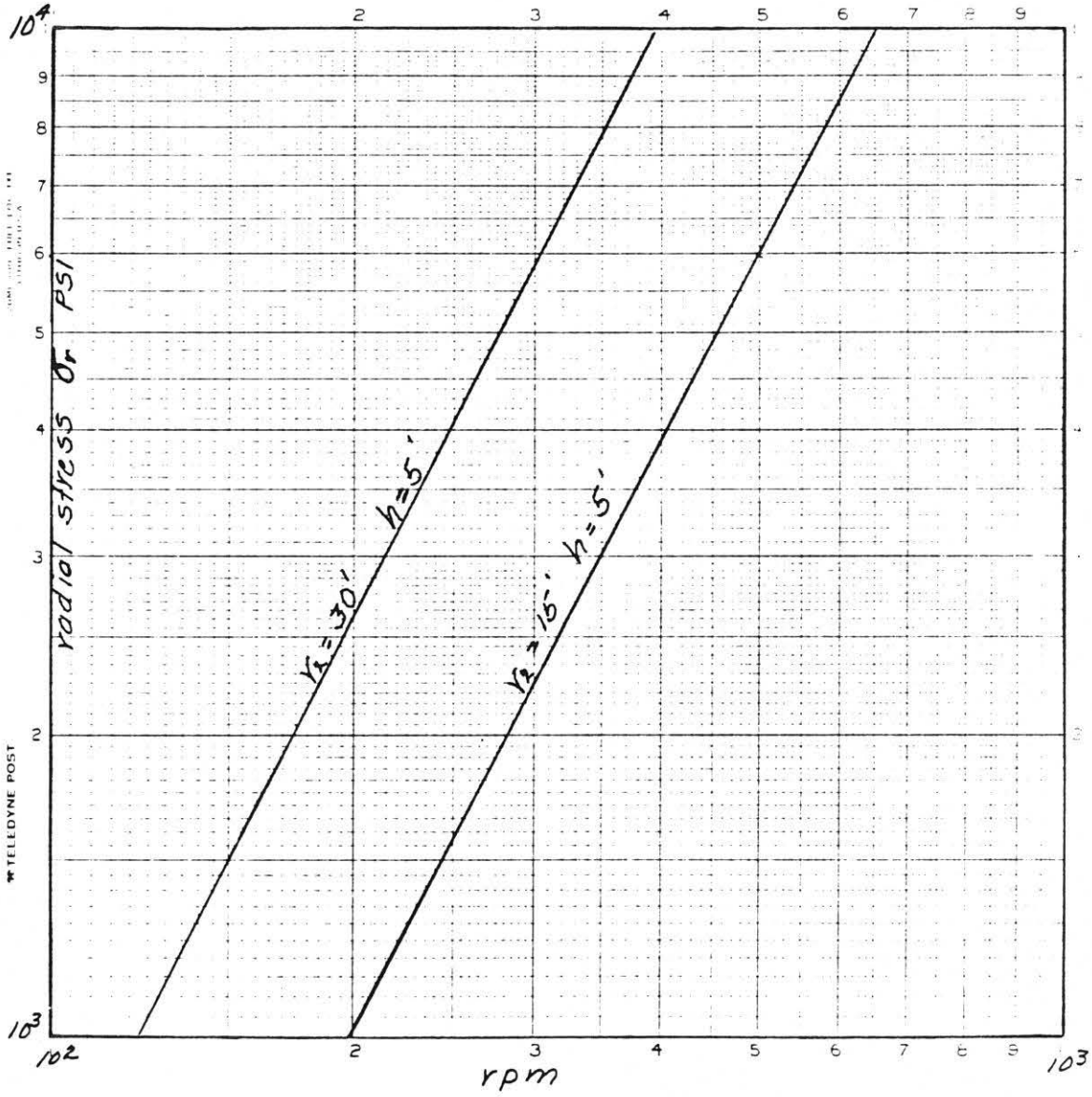

Figure 4 --Example Vertical Stresses in Model Slab,
h = 5' two large rotor radii.

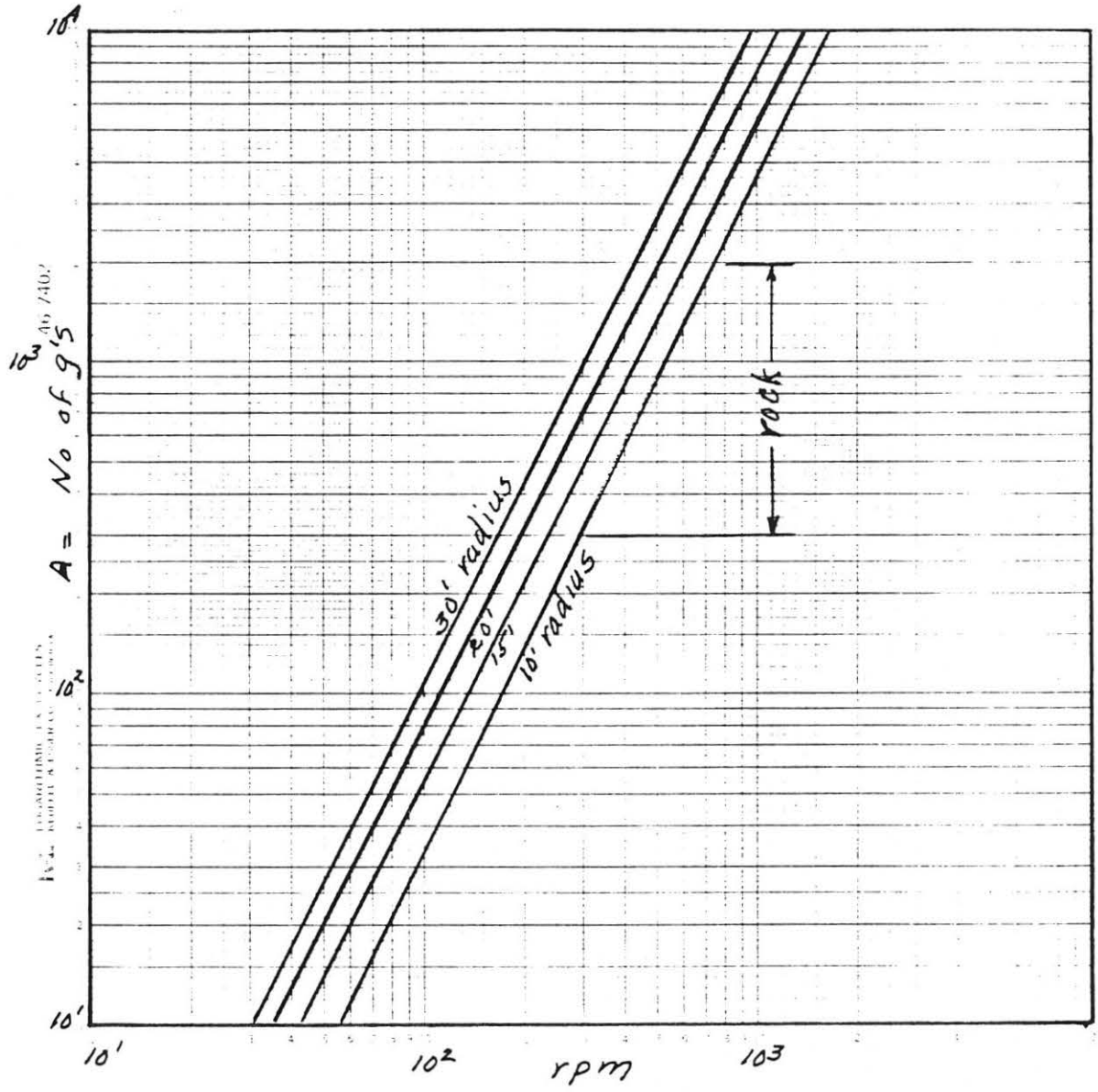

Figure 5.--G's developed by a large centrifuge for large radii rotors at given rpm.

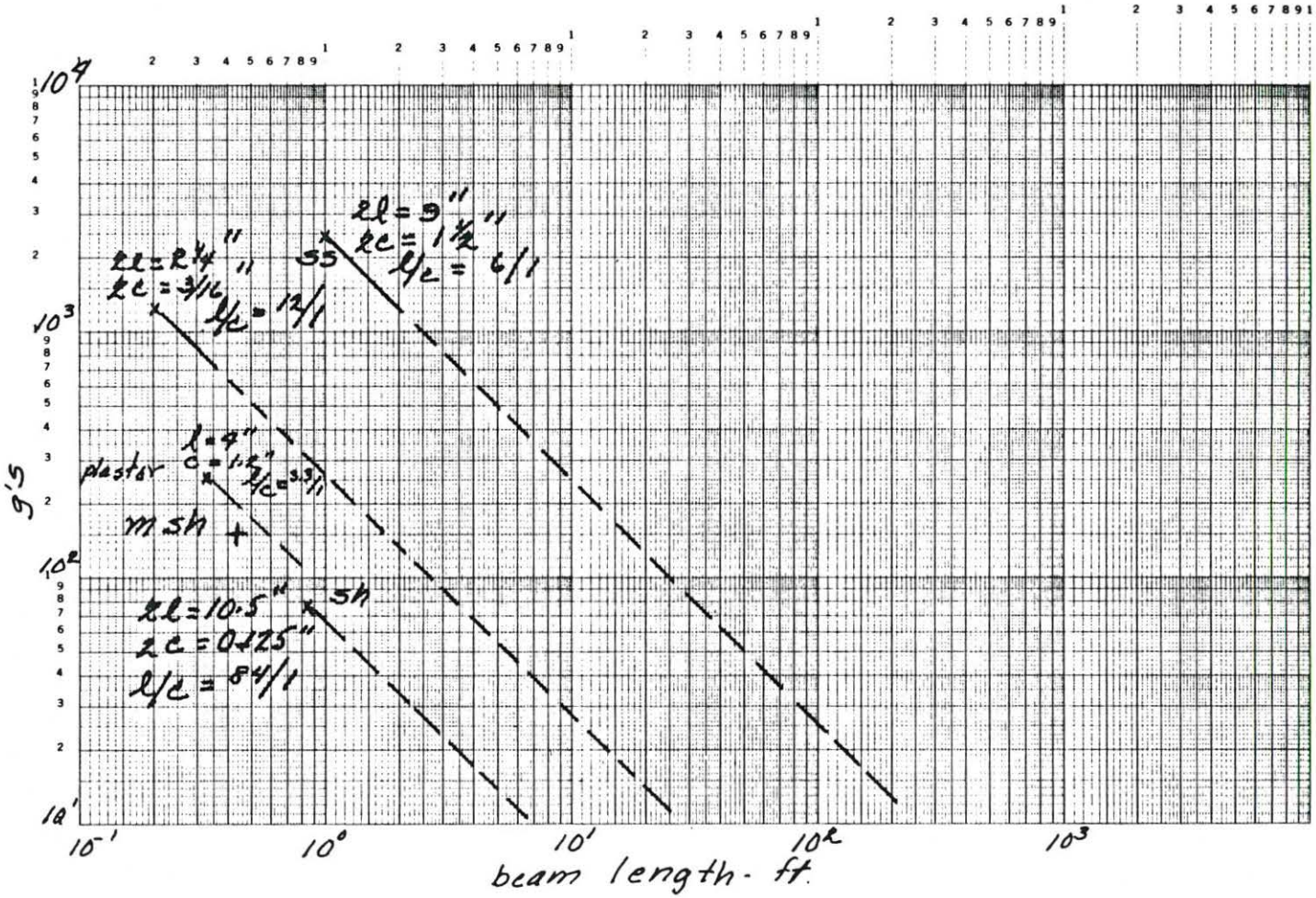

Figure 6 -- G-loads for Model Beams at Different Strengths and Dimensions